UNIVERSITY OF SOUTHAMPTON

FACULTY OF ENGINEERING AND THE ENVIRONMENT

Water and Environmental Engineering Group

Investigating the performance of paddlewheels used in microalgae raceways for the production of biomass

by

Ed Musgrove

Thesis for the degree of Doctor of Philosophy

June 2017

UNIVERSITY OF SOUTHAMPTON

ABSTRACT

FACULTY OF ENGINEERING AND THE ENVIRONEMENT
Water and Environmental Engineering Group

Doctor of Philosophy

Investigating the performance of paddlewheels used in microalgae raceways for the production of biomass

Ed Musgrove

It has been suggested that biofuels produced from microalgae may be a more sustainable alternative to other types currently produced, although currently the production of microalgae for this purpose has the potential for the overall energy balance to be negative. Microalgae are today cultivated in oval ponds of up to 10 m width and 500 m length, with water depths of 200 to 300 mm. The water must be kept in motion to avoid sedimentation. This is usually done with paddlewheels which have 6 to 8 blades, and a typical diameter of around 1.20 m. The energy demand for the continuously running wheels is one of the main cost factors, whilst the wheel efficiency is typically estimated as only 10 %. Very little is known about the effect of blade number or rotational speed on wheel efficiency. This research aimed to improve the paddlewheel as a propulsion mechanism in order to reduce the energy required.

Theoretical work and 1:5 scale physical model tests were conducted to analyse the parameters affecting paddlewheel performance, to develop a consistent and improved model of the hydraulics of algae ponds, to define optimum configurations and to develop appropriate design tools. The results indicate that the number of blades, rpm and immersion depth have a great effect on the efficiency, with optimum values of over 60 % being achieved with higher blade numbers and lower rpm. Using an insert to reduce the backflow around the blades increased the efficiency and discharge of a 12-bladed wheel especially for the lower rotational speeds tested.

A new theoretical equation to calculate the efficiency of the wheel was derived and validated against the physical model. It was found that the leakage of the fluid beneath the blades was the main loss factor in the efficiency of the wheel and should be minimised by using the insert where possible.

Contents

List of figures

List of tables

Declaration of authorship

I, Ed Musgrove declare that this thesis entitled Investigating the performance of paddlewheels used in microalgae raceways for the production of biomass and the work presented in it are my own and has been generated by me as the result of my own original research.

I confirm that:

1. This work was done wholly or mainly while in candidature for a research degree at this University;
2. Where any part of this thesis has previously been submitted for a degree or any other qualification at this University or any other institution, this has been clearly stated;
3. Where I have consulted the published work of others, this is always clearly attributed;
4. Where I have quoted from the work of others, the source is always given. With the exception of such quotations, this thesis is entirely my own work;
5. I have acknowledged all main sources of help;
6. Where the thesis is based on work done by myself jointly with others, I have made clear exactly what was done by others and what I have contributed myself;
7. Parts of this work have been published as Musgrove and Heaven, 2015.

Signed: …….

Date: ……

Acknowledgments

I would like to thank my supervisor Dr Sonia Heaven for the support over the last few years and more recently Dr Gerald Muller and also The FP7 ALL-GAS project (208268, www.all-gas.eu), for funding my research. With the oversight of my main supervisor, editorial advice has been sought. No changes of intellectual content were made as a result of this advice.

Thanks to Toru Tsuzaki for his help and patience in constructing the paddlewheel model. I would also like to thank Jose-Luis Mendoza for his knowledge on raceways which he has always been happy to share with me and also his help in collecting the validating data.

Most of all I would like to thank the staff of Southampton General Hospital, my family and wife for all the care and kindness they have given me.

List of variables

Symbol	Description	Unit
a	Acceleration	m s^{-2}
A	Cross sectional area	m^2
A_b	Wetted area of blade	m^2
A_g	Area of the gap around the blade	m^2
AR	Aspect ratio	-
B	Channel width	m
b_c	Width of weir opening	m
b_e	Effective breadth of the weir opening	m
C_a	Algal concentration	mg dry weight L^{-1}
C_c	Contraction coefficient	-
C_d	Discharge coefficient	-
C_D	Coefficient of drag	-
$C_{D\theta}$	Coefficient of drag at an angle of attack of θ	-
c_g	Group velocity of a wave	m s^{-1}
C_v	Velocity coefficient	-
d	Fluid depth	m
d_1	Upstream fluid depth	m
d_2	Downstream fluid depth	m
d_{b2}	Fluid depth halfway around the bend as if the channel was straight	m
D_m	Molecular diffusivity	m^2 s^{-1}
d_p	Light penetration depth	m
E_W	Energy density of a wave per unit width	J m^{-1}
F	Force	N
F_1	Upstream hydrostatic force	N
F_2	Downstream hydrostatic force	N
F_D	Drag force	N

Fr	Froude number	-
g	Gravitational acceleration	m s^{-2}
H	Head gained from paddlewheel	m
h_3	Head of fluid above the crest of the weir	m
h_e	Effective height of the weir	m
h_g	Gap clearance	m
$\overline{h_g}$	Average gap clearance	m
h_{gb}	Gap clearance around the bottom of the blades	m
$h_{g,max}$	Maximum gap clearance when blade is halfway through the stroke	m
$h_{g,min}$	Minimum gap clearance when blade is perpendicular	m
h_{gS}	Gap clearance around the side of the blades	m
H_L	Head loss from an obstacle	m
h_N	Normalised head loss	m
H_W	Wave height	m
K	Minor head loss coefficient	-
k	Turbulence kinetic energy per unit mass	m^2 s^{-2}
k_b	Weir width adjustment factor	m
k_h	Weir height adjustment factor	m
K_L	Gas transfer coefficient	-
k_{Slip}	Slip factor	-
K_{Turb}	Turbulent loss coefficient	-
L	Raceway channel length	m
L_M	Model characteristic length	m
L_N	Normalised raceway channel length	-
L_P	Prototype characteristic length	m
L_W	Wave length	m
m	Mass	kg m^{-3}
M_R	Resultant moment acting on the wheel	N m
M_{T1}	Upstream moment acting on the wheel	N m
M_{T2}	Downstream moment acting on the wheel	N m

n	Manning's roughness coefficient	-
P	Height of the weir crest	m
P_1	Pressure acting on the upstream side of a blade	N m^{-2}
P_2	Pressure acting on the downstream side of a blade	N m^{-2}
P_b	Power of a single blade	W
P_{clear}	Power to drive the paddlewheel with no fluid	W
P_{hyd}	Hydraulic power	W
P_{hyd_T}	Theoretical hydraulic power	W
$P_{hyd_{Turb}}$	Hydraulic power with the turbulent losses taken into account	W
P_{in}	Power into the system	W
$P_{operational}$	Power to drive the paddlewheel with fluid	W
P_{out}	Power measured in the system	W
P_S	Shaft power	W
P_{S_R}	Shaft power per unit surface area	W m^{-2}
P_{S_T}	Theoretical shaft power	W
P_W	Power of a wave per unit length of crest	W m^{-1}
Q	Fluid discharge	m^3 s^{-1}
Q_L	Leakage discharge	m^3 s^{-1}
Q_R	Relative discharge	m^3 s^{-1} W^{-1}
Q_T	Theoretical discharge	m^3 s^{-1}
Q_{T_L}	Theoretical discharge accounting for leakage	m^3 s^{-1}
R	Radius of blade	m
R^*	Shear Reynolds number	-
r_0	Exterior bend radius	m
r_1	Interior bend radius	m
r_c	Centreline bend radius	m
Re	Reynolds number	-
R_H	Hydraulic radius	m
R_m	Model blade radius	m
R_P	Prototype blade radius	m

R_s	Shaft radius	m
S_c	Schmidt number	-
SR	Shape ratio	-
t	Control time	s
T	Time period of a wave	s
U	Velocity magnitude	m s^{-1}
u^*	Shear velocity	-
v	Fluid velocity	m^2 s^{-1}
V	Volume	m^3
$\bar{v}$	Cross sectional average velocity	m s^{-1}
v_0	Velocity at time 0	m s^{-1}
v_1	Upstream fluid velocity	m s^{-1}
$v_{1_{max}}$	Maximum upstream fluid velocity	m s^{-1}
$v_{1_{min}}$	Minimum upstream fluid velocity	m s^{-1}
v_2	Downstream fluid velocity	m s^{-1}
v_b	Velocity of the blade	m s^{-1}
v_m	Average fluid velocity halfway around the bend	m s^{-1}
v_M	Model velocity	m s^{-1}
v_p	Prototype velocity	m s^{-1}
v_t	Velocity at time t	m s^{-1}
$V_{v<0.1}$	Volume of fluid with a velocity less than 0.1 m s^{-1}	m^3
v_w	Velocity of water	m s^{-1}
W	Work done to move a volume of fluid	J
α	Kinetic energy correction factor	-
η	Pump efficiency	-
θ	Bend angle	degrees
λ	Scale factor	-
μ	Dynamic viscosity	N s m^{-2}
ν	Kinematic viscosity	m^2 s^{-1}
ρ	Density of fluid	kg m^{-3}

ρ_w	Density of water	kg m^{-3}
σ_ε	K-E turbulence model constant	-
σ_k	Turbulence model constant for the k equation	-
τ	Shear stress	N m^{-2}
τ_R	Resultant torque	N m
τ_S	Shaft torque	N m
φ	Angle between blades	rad
ω	Paddlewheel rotational speed	rad s^{-1}
ω_M	Model rotational velocity	rad s^{-1}
ω_P	Prototype rotational velocity	rad s^{-1}

List of abbreviations

Abbreviation	Meaning
ADV	Acoustic Doppler Velocimeter
ARID	Algae Raceway Integrated Design
BOD	Biological Oxygen Demand
CFD	Computational Fluid Dynamics
CO2	Carbon dioxide
DTMD	Direct Torque Measurement Device
GHG	Greenhouse Gases
HRAP	High Rate Algal Pond
LEAR	Low Energy microalgae Reactor

1 Introduction

1.1 Concern with current energy mix

Burning of fossil fuels is currently the dominant form of energy generation used across the world and accounted for 85 % of primary energy consumption in 2015 (BP Global, 2017). The combustion of fossil fuels releases significant quantities of carbon dioxide and other greenhouse gases (GHG) into the atmosphere, which has been linked to rising average temperatures across the world (Hill et al., 2012).

Global primary energy demand is set to rise by over half from 2004 to 2030, with 70 % of this increase concentrated in developing countries. The demand will primarily be met by the use of fossil fuels, which is forecast to rise by 83 % between 2004 and 2030. As a result, it is suggested that there will be a 55 % increase in CO_2 equivalent emissions in the same time period (IEA, 2006).

This projected increase from 2004 requirements has so far been matched in reality, with total primary energy demand increasing 17 % between 2004 and 2012, and with a 32 % rise in developing countries. Coal consumption increased 25 %, mainly due to a 42 % rise in China (BP, 2013).

It has been suggested that fossil fuel reserves are nearing an end and that there are only 53 years of oil, 56 years of gas and 109 years of coal reserves at current production rates, as of 2012 (BP, 2013). Others consider that this is an over-estimate and there are only 27 years of oil reserves left as of 2007 (EWG, 2007; Owen et al., 2010). While predictions vary, and are periodically updated in the light of new discoveries, it is clear that these reserves are finite and the fossil fuel period in human history will therefore come to an end in the not too distant future.

The price of energy is an ever-increasing concern for world governments as the overall performance of global markets is closely linked to it (IEA, 2006). Prices of fossil fuels are fairly volatile, as the majority of production occurs outside the main economically developed countries. Prices of crude oil have seen a 40 % fluctuation between maximum and minimum prices during the period 2008 to 2012 and natural gas prices have seen even greater fluctuations of nearly 70 % in the same period (BP, 2013). Costs for refined oil are expected to rise in real terms through to 2030 (IEA, 2006). Some estimates

suggest that the price of oil may double by 2030 (Owen et al., 2010); although this is perhaps unlikely, as the pressure this would apply to economic markets would probably lead to a global recession and a consequent fall in demand for oil.

As a result of concerns about global warming, many countries and organisations around the world have set mandatory targets for the reduction of GHG emissions. The EU has set a wide-ranging target to cut GHG emissions by 2020, by 20 % compared to 1990 levels (European Commission, 2013). It has also set out plans to decrease its emissions by 80 % compared to 1990 by 2050 (European Commission, 2011). This target was specifically adopted by the UK government through the Climate Change Act 2008 (Great Britain, 2008).

1.2 Renewable energy sources and biofuels

In response to rising concerns over GHG emissions, fuel security and limited resources there has been increased interest in the development of renewable technologies. Solar, wind, tidal and hydropower along with fuels derived from biomass are currently widely deployed, and accounted for around 13 % of the total world energy consumption in 2011 (World Energy Council, 2013). National and international bodies are trying to increase the use of renewables through the application of directives, incentives and subsidies to make renewable energy available and cost-competitive with fossil fuel derived energy.

Fuels from biomass currently provide around 10 % of the total world energy demand. In non-industrially developed countries this source accounts for around 22 % of demand, mainly through direct combustion of biomass for cooking and heating (World Energy Council, 2013). In developed countries, however, the use of biofuels is much lower at around 3 % of energy demand; but interest is growing as these are the only renewables that can be used as a liquid fuel in transport (World Energy Council, 2013; BP, 2013). The EU's Renewable Energy directive (2009/28/EC) requires member states to have a minimum biofuel mix in transport fuels of 10 % by 2020 (European Union, 2009).

Biofuels are often classed into three distinct categories. First generation biofuels are derived from sugar, starches and vegetable oils which are extracted from terrestrial plants that are usually grown specifically for the purpose of biofuel production. Second generation biofuels are made from agricultural and forestry residues and other wastes,

and are mainly lignocellulosic in nature. Third generation biofuels come from novel biomass sources that do not compete directly with current agricultural food and feed production. Of these, microalgae have been receiving considerable interest as a possible source of biomass for biofuel production.

1.2.1 First generation biofuels

First generation biofuels have become more economically viable in recent years but are still not generally competitive with conventional diesel without government subsidies (FOA, 2008).

Biofuels derived from purpose-grown energy crops are in direct competition with food crops and, while the cost of producing biomass for biofuels may fall, this will indirectly affect the cost of food and feed by introducing competition for land and other resources.

The use of biofuels accounted for only 0.9 % of world transport fuel requirement in 2005 (FOA, 2008), In 2004, however, 1 % of arable farmland was given over to biofuel production (IEA, 2006). It is therefore clear that to supply all the global transport fuel demand from biofuels would be unrealistic.

The view that major and indeed unfeasible changes in land use would be required is supported by Hill et al. (2006) who reported that in 2005 14.3 % of the US corn harvest was used to make ethanol which accounted for only 1.72 % of US gasoline usage, and 1.5 % soybean production was refined into biodiesel making up only 0.09 % of US demand (Hill et al., 2006).

In the United Kingdom, as of 2014/2015, only 3.73 % of the fuel for road traffic and non-road mobile machinery was biofuels (Transport, 2014). Of the biofuels used in the UK only 30 % is domestically produced and of that only 55 % was produced from first generation fuels; therefore only 0.6 % of transport fuel used was produced by domestically grown first generation biofuel crops. In the same period 1.3 % of arable land was used to produce biofuels (Department for Environment, 2015).

If biofuels were to meet 50 % of the transport fuel requirements of the United States, extensive land use changes would have to occur. If soybeans, the crop most commonly used to produce biodiesel, were to be grown then 594 million hectares of cropping land would be needed or 326 % of the total US cropping area. Even if oil palm, the most

productive first generation biofuel which can produce 5950 L ha^{-1}, were to be used 24 % of US cropping land would need to be reallocated for production of biodiesel crops (Chisti, 2007).

Projections for the use of biofuels as a transport fuel suggest this will remain limited at around 3 - 3.5 % by 2030 (FOA, 2008), due to the high land requirements and cost of converting land.

The main driving factor behind the investment and implementation of biofuel production was to reduce GHG emissions from the direct combustion of fossil fuels. For this purpose it is often assumed that any carbon released in burning the biofuels can be ignored, since it is captured from the atmosphere through photosynthesis, i.e. is part of the short term carbon cycle. This is true so long as the amount of CO_2 released in the production of the fuel is less than or equal to the amount absorbed by the plant. Depending on the methods used in the cultivation of the feedstock, however, there can be large emissions of other GHGs. Nitrogen fertilizers, for example, may produce nitrogen oxide which is 300 times more powerful as a GHG than CO_2 (FOA, 2008).

Other indirect factors are normally excluded from the carbon balance when estimating net CO_2 equivalent GHG emissions. One of the largest releases of carbon into the atmosphere is through the conversion of non-agricultural land to crops. Converting grassland can release up to 300 tonnes of carbon per hectare and converting forest land can be double or triple this (Searchinger et al., 2008).

At the same time it is estimated that the production of ethanol derived from maize can save up to 1.8 tonnes of CO_2 per hectare per year compared to fossil fuels. This means that, if the GHGs released during conversion of the land from grassland are taken into consideration, it could take 167 years for the benefits to mitigate the negative impacts and achieve a net positive CO_2 equivalent balance. If Brazilian sugarcane from current cropland is used for the production of ethanol, a cumulative reduction in GHG emissions could be achieved in as little as four years: but if a change from forestland to cropland is required it could take up to 45 years to achieve a positive impact (Searchinger et al., 2008).

According to one study the GHG emission savings of using biodiesel derived from soybean are 59 % and these rise to 88 % if ethanol from corn is produced; but only if

current cropland is used (Hill et al., 2006). Other studies have also suggested that there can be GHG emission savings of up to 80 - 90 % compared to fossil fuels for ethanol from sugar cane, and a 50 - 85 % reduction using biodiesel from palm oil (IEA, 2006). These estimates do not give a complete picture, however, as conversion of any agricultural land to grow feedstock for biofuels will most probably lead to the indirect impact of non-agricultural land being converted into cropland for food production.

Intensive farming practices will be needed if the production cost of biofuels is to become competitive with traditional fossil fuels, but these practices too have significant impacts. Water requirements are likely to become an important issue as many of the crops used in commercial scale production of biofuels are very water intensive, requiring between 857 - 1333 L water/L fuel (FOA, 2008). Currently 70 % of fresh water usage is for agricultural purposes, and an increase in the quantity of biofuel crops could cause this to become higher still (International Water Management Institute, 2008). This is seen to be a key factor especially in water deprived areas where there is already large investment into the biofuel industry (IEA, 2006). Most of the crops currently used as biofuel feedstocks are rain fed, however, including 76 % of Brazilian sugarcane and 70 % of American maize, and only an estimated 2 % of irrigation water was used for biofuel production worldwide in 2007 (FOA, 2008).

1.2.2 Third generation microalgal biofuels

There has been growing interest in microalgae as a source of biomass for biofuel production with the aim of minimising impacts on the environment and on arable land usage.

Microalgae are reportedly capable of producing a biomass yield between 2 and 10 times that of 1st generation crops (Schenk et al., 2008; Chisti, 2007). These higher yields are due to the fact that microalgae are more efficient converters of solar energy than terrestrial plants. Their efficiencies are up to 5 %, five times higher than traditional crops (Posten and Schaub, 2009). The higher conversion efficiencies are a result of the simple single-cell structure of the biomass (James and Boriah, 2010). If these high yields can be achieved in practice, microalgae could potentially produce larger amounts of biomass from smaller land areas than traditional first generation energy crops.

In appropriate growth conditions, certain species of microalgae can have much higher oil content than that of terrestrial plants, ranging between 20 - 50 % of dry weight (Chisti, 2007; Metting Jr, 1996; Spolaore et al., 2006). These oil contents have been recorded under laboratory conditions, and may be more difficult to achieve in large-scale production systems; but they account for much of the recent interest in microalgae as a source of biofuel. To meet 50 % of the transport fuel needs in the US in 2007 using microalgae with an estimated oil content of 30 % would require 4.5 million hectares of land or 2.5 % of US cropping land (Chisti, 2007). A more conservative estimate of 10 % oil content would require 7.5 % of US cropping land to achieve the same quantity of fuel. Unlike traditional biofuel feedstocks, it could thus be physically possible to achieve a switch from fossil fuels to an algal biofuel mix; however it would not be socially or economically possible at the current technology level.

Microalgae can potentially be grown in saline water on non-arable land minimising the GHG emission impacts of land conversion, the competition with food or feed production, and the need for additional fresh water resources (Searchinger et al., 2008; Chisti, 2008). The marginal land for this in China alone is 130 million ha, and this far exceeds the 9.65 million ha needed to satisfy the 2030 demand for fuel of China (Zhang et al., 2012). There could, however, be other far-reaching environmental and ecological impacts on the land converted, especially in sensitive coastal regions. These include but are not limited to: loss of habitats, GHG emissions from land conversion, rainfall runoff, water pollution. The procedures for converting land and the logistical issues surrounding production may also be challenging. For marginal land to be suitable it would need access to large amounts of saline or fresh water, a CO_2 source if required, and suitable infrastructure to transport the biomass or fuel to the required locations for processing. These requirements are likely to reduce the available land for cultivation considerably.

Microalgae can potentially also be fed with waste water as a nutrient source (Delrue et al., 2016; Craggs et al., 2012; Abdel-Raouf et al., 2012). This may reduce the energy need to treat the wastewater and create a useful by-product that can be turned into a biofuel.

Energy from microalgae can be extracted in multiple ways. Direct combustion of dry algal biomass is seen as the most energetically efficient way of extracting the energy, as the total algae biomass being converted into energy. It does, however, have the most

disadvantages and fewest applications (Sturm and Lamer, 2011; Milledge and Heaven, 2014).

Transesterification is another option whereby the parent oil from micro-algal lipids, is mixed with an alcohol, usually methanol, to produce biodiesel and glycerol. This process has many drawbacks and can be very costly (Fukuda et al., 2001). The by-product, glycerol, can be used as a carbon source for microalgal production, which has been shown to produce an almost seven-fold increase in biomass production compared to unsupplemented growth and a nearly four-fold increase in lipid production (Li et al., 2011). The process of oil extraction also leaves a significant amount of residual biomass available for other purposes.

It is claimed that the cost of biodiesel produced from microalgae is more expensive than from terrestrial crops (Chisti, 2007) and although it maybe technologically possible it is still not economically feasible to use microalgae to produce biodiesel unsubsidised (Shen et al., 2009; Singh and Olsen, 2011). A comprehensive techno-economic analysis of biodiesel cost from algae put the price at around $13.4 /gallon in 2012 compared to terrestrial biodiesel prices of $4.3 /gallon and $3.5 /gallon of fossil fuel diesel (Richardson et al., 2012; Alternative Fuels Data Center, 2017).

This is It may be possible to couple multiple sources of renewable energy to bio-refine microalgae into both high-quantity low-value products, such as biofuel, and high-value low-quantity products, such as cosmetics and food supplements. This could mitigate the high capital costs of setting up a production plant (Subhadra, 2010); although if large-scale production of microalgal biomass becomes widespread, the costs of these high value products could fall rapidly.

Methane production from microalgae has been described as the only energetically profitable process (Posten and Schaub, 2009), and can be carried out on either whole biomass or biomass after lipid extraction. It has also been suggested that the methane generated from the anaerobic digestion of the biomass residual after extraction is greater than the electrical and heat needs of the biomass production plant (Stephenson et al., 2010; Milledge and Heaven, 2015)

Whatever the biofuel to be produced, there is the potential for a negative energy balance in the production process because of energy requirements in water pumping,

CO_2 diffusion and biomass extraction (Hirano et al., 1998; Doucha et al., 2005). Only limited research has been carried out on the energy requirements for microalgae production. The most comprehensive study was conducted by the Solar Energy Research Institute who calculated that the mixing and propulsion of the fluid in raceways can account for 69 % of the energy cost (Neenan et al., 1986). More recently theoretical life cycle analysis studies have suggested that the propulsion of water requires 74 % of the cultivation energy and can account for just over half of the total energy requirement of the biodiesel (Stephenson et al., 2010). This result conflicts with the work of Chisti (2008) who concluded that 28 % of energy input for algal production is for cultivation, mainly in the form of propulsion and mixing processes (Chisti, 2008). The importance of energy consumption in the algal cultivation process to the net energy balance, and the lack of consensus on this, indicates that further research is required to improve it.

1.1 Conclusion

The combustion of non-renewable fossil fuels is the most common form of energy supply in the world accounting for 85% of world energy demand in 2015. There are two main concerns with the use of fossil fuels: fuel security and environmental impacts of GHG emissions. Fuel security has become a key issue for governments as the price of it is closely linked to the overall performance of global markets. As the majority of fossil fuel production occurs outside the main economically developed countries prices can be very volatile. GHG emissions have been linked to global warming and as a result of many countries and multilateral organisations have set mandatory targets to reduce the production of GHG emissions.

There is a there is a growing interest in alternative renewable fuels to combat both issues. Of these, plant derived biofuels have become increasingly popular as they can be mixed with current fossil fuels used in the transport sector. To promote this the European Union have set a mandatory target of 10 % biofuel mix in transport fuels by 2020. The primary production of biofuels has been conducted with first generation biofuels. These are fuels from terrestrial plants specifically grown to produce fuels. It has been shown that first generation fuels cannot replace fossil fuel usage at the current production efficiency. This is due to the impact that the production will have on the food production.

Third generation biofuels produced from microalgae are reported to give a yield of at least twice that of first generation fuels. Alongside this the microalgae biomass can be grown in non-arable land on saline water to limit its impact on food production. If it is grown specifically for the production of biofuels there is the possibility for there to be a negative energy balance and also economically unfeasible. Techno-economic analysis of biodiesel put the cost of microalgae derived biodiesel as $13.4 /gallon in 2012 this was three times that of terrestrial biodiesel at around $4.3 /gallon. To mitigate this, the biomass can be fed with wastewater to supply a nutrient source and also act as a wastewater treatment process.

1.2 Structure of the report

Chapter 1

This chapter details the principles of renewable energy and the problems traditional 1st generation feedstocks face in regard to their economic and environmental performance. It gives the basic background to micro-algal biofuels.

Chapter 2

This section begins with some background information on microalgae. It then evaluates the different cultivation methods used to grow microalgae biomass. These are split into two main categories:

- Closed systems
- Open systems

From these algal raceways and photobioreactors systems are compared against each other.

Chapter 3

This focuses on different aspects in the cultivation of microalgae and the design and operation of algal raceways. It goes on to evaluate the efficiency and energy costs in the production of algal biomass in detail. Other parameters that may affect the biomass productivity are also discussed. The end of chapter 2 reviews the use of computational models to model the hydrodynamics of the raceways and also growth models that have been constructed thus far. From this review the aims and objectives are designed and presented.

Chapter 3

Here the current hydrodynamic theory behind paddlewheels is assessed. Beginning with how a paddlewheel works at a fundamental level by lifting and not pushing the fluid. The chapter then goes on to explain the current paddlewheel numerical models and the issues with these. A new theory is then developed to take into account the head difference across the wheel and the leakage of fluid beneath and around the sides of the blades. At the end of the chapter the insert design is introduced and it is theoretically shown how this should be a much improved design.

Chapter 4

This chapter focusses on the experimental evaluation of the paddlewheel and how different parameters affect it. These parameters are:

- The rotational speed of the wheel
- The number of blades in the wheel
- The fluid discharge
- The downstream fluid depth and head difference
- The length of the raceway

The chapter describes in detail the methodology used to evaluate these. The results are then described and analysed in respect to other published work and the theory proposed in chapter 3. Both the experimental and theoretical models are validated firstly against each other and then against a 500 m^2 prototype raceway channel with an 8-bladed paddlewheel located in Chiclana de la Frontera, Spain.

Chapter 5

Chapter 5 applies the experimental results to four different case studies. Each of these is currently an operation paddlewheel driven raceway pond system. The energetic and financial savings that could be made with changes to the paddlewheel construction and operation are estimated.

Chapter 6

Concludes the work done and summates the results from chapters 4, 5 and 6. New work is also proposed that could be carried out further to extend the understanding of the propulsion mechanism.

2 Microalgae cultivation

A literature review was conducted into the different cultivation techniques and aspects of algal raceway design in regards to the energy costs and production of biomass. Further to this, a review of the current computational fluid dynamic and growth models designed to investigate the different aspects of the raceway has been carried out. From these reviews the aims and objectives of this work were conceived and are presented at the end of this chapter.

2.1 Cultivation conditions

There are several main categories of microalgae:

1. Green (*Chlorophyta*)
2. Red (*Rhodophyta*)
3. Diatoms (*Bacillariothyta*)
4. Cyanobacteria (*Chloroxybacteria*)

Within these the algae can either be heterotrophic or autotrophic. Heterotrophic are non-photosynthetic therefore require an organic compounds and nutrients for growth. Whereas autotrophic algae are photosynthetic therefore can use inorganic compounds, such as CO_2, salts and light as an energy source for growth. Photosynthesis enables the conversion of light and CO_2 into adenosine triphosphate and O_2. These are used produce cellular energy and support growth (Brennan and Owende, 2010).

The majority of algae used for biomass production are autotrophic. The optimal conditions for the algae depend upon the strain of algae and also the required composition. A general set of conditions are set out below in Table 2.1.

Table 2.1. General growth conditions required for autotrophic microalgae (FAO, 1996).

Parameters	Range	Optimal
Temperature (°C)	16-27	18-24
Salinity (g L^{-1})	12-40	20-24
Light intensity (lux)	1,000-10,000	2,500-5,000
Photoperiod (light: dark, hours)		16:8 (minimum) 24:0 (maximum)
pH (-)	7-9	8.2-8.7

2.2 Cultivation techniques

Microalgae can be grown in closed systems known as photobioreactors (PBRs) or in open systems. There are advantages and disadvantages to each type of system which are discussed in the following sections.

2.2.1 Closed systems - Photobioreactors

Photobioreactors (PBRs) can be classed as either tubular reactors, which are usually constructed from pipes with diameters of up to 0.1 m (Figure 2.1 a) through which the culture medium flows; or as flat plate reactors (Figure 2.1 b) in which the culture is generally kept in motion by gas bubbling and which can also include bag-type systems constructed of lightweight disposable plastic (Pruvost et al., 2016; Chisti, 2007). Both types are more commonly operated as closed reactors where the algal culture is not exposed to the atmosphere at any time during the cultivation period. This is to ensure that the major problems of contamination and predation are reduced.

Figure 2.1. Photographs of two different types of photobioreactors. a) Horizontal tubular reactor. b) Flat plate reactor (Bitog et al., 2011).

The fluid in tubular PBRs is normally circulated by a mechanical or an airlift pump. The use of mechanical pumps is believed to be more efficient in energy terms, but may result in damage to the algal cells due to the high shear stresses applied while the culture passes through the pump (Pruvost et al., 2016; Chisti, 2007). This is further discussed in Section 3.4.2.1.

2.2.2 Open systems

Contamination of open systems can easily occur and can be from a variety of sources such as (Chisti, 2016):

- Local algae and other organisms such as zooplankton
- Leaves and other biological material
- Dust particles and other airborne materials
- Insects and other animals which feed on the biomass such as birds

If a single microalgae species is required, open pond systems can be made into a very selective environment to ensure there is minimal contamination of the preferred species by other microalgae and protozoa. This can be achieved by increasing the salinity, alkalinity or nutrient content of the water (Borowitzka, 1999). Further to this the raceway can be flushed every two weeks to reduce the build-up of toxins and prevent contamination (Lardon et al., 2009). This is usually done for the production of high value products. For production of biomass for anaerobic digestion, especially using

wastewater as a nutrient supply, the environment is unlikely to be as selective, as the main aim is normally to maximise biomass production rather than ensuring strain selectivity.

2.2.2.1 Ponds systems

Waste stabilisation ponds have been in use from as early as the 1900s in the United States and can provide a simple but effective wastewater treatment system (Figure 2.2). These ponds normally have a very large surface area to depth ratio. The first reported system was constructed in 1901 and covered 275 hectares with an average depth of only 1.4 m (Milledge, 2013; Gloyna and WHO, 1971). Due to the relatively simple technology needed to run these algal treatment plants they are frequently implemented in developing countries to provide a simple wastewater treatment system, with the microalgae as a potential by-product (Pittman et al., 2011).

Figure 2.2. Image of a waste stabilisation pond system (GreenerLifes, 2010).

Algae in the pond consume CO_2 to produce oxygen via their natural photosynthesis process. The oxygen is used by bacteria to break down the organic waste matter in the wastewater. This release of oxygen can remove the need for aerators in the ponds and thus reduce the overall power demand, which is often the most energetically costly part

of the wastewater treatment process (Mallick, 2002; Buhr and Miller, 1983; Milledge, 2013).

Waste stabilisation ponds have thus far not been designed and utilised to maximise the production of microalgae. Investigations into the use of waste stabilisation ponds in conjunction with wastewater treatment have shown it is possible to provide the nitrogen and phosphorus needed for algal growth (Cantrell et al., 2008). Some studies, however, have shown that the microalgae may become nitrogen, rather than phosphorus, limited when grown in wastewater (Sturm and Lamer, 2011); while others suspect the growth to be carbon limited due to the low carbon to nitrogen ratios of wastewater at roughly 3:1 compared to that of biomass at 6:1 (Benemann, 2003)

2.2.2.2 Raceway

Raceway systems have for some time been the most common method for microalgal biomass cultivation (Ben-Amotz, 2008; Becker, 1994; Weissman et al., 1989; Dodd, 1986). This is mainly due to the lower level of technology and capital costs needed for implementation compared to other systems.

A raceway can be characterised as a large recirculating loop (Figure 2.3). They are typically relatively shallow with high surface to depth ratios to ensure adequate light penetration into the culture and prevent the microalgae from experiencing long periods of exposure to intense light or to darkness (Sompech et al., 2012; Chiaramonti et al., 2012).

Figure 2.3. Operational raceways located in Israel (Ben-Amotz, 2008). The red arrow indicates the direction of fluid flow from the paddlewheel (Ben-Amotz, 2008).

Raceway designs are fairly standard and normally consist of two long straight channels divided by a central barrier with 180° end bends. The fluid is propelled by a paddlewheel with 6 or 8 blades and a carbonation sump is sometimes used to pump carbon dioxide into the fluid to increase the gas transfer (Figure 2.4).

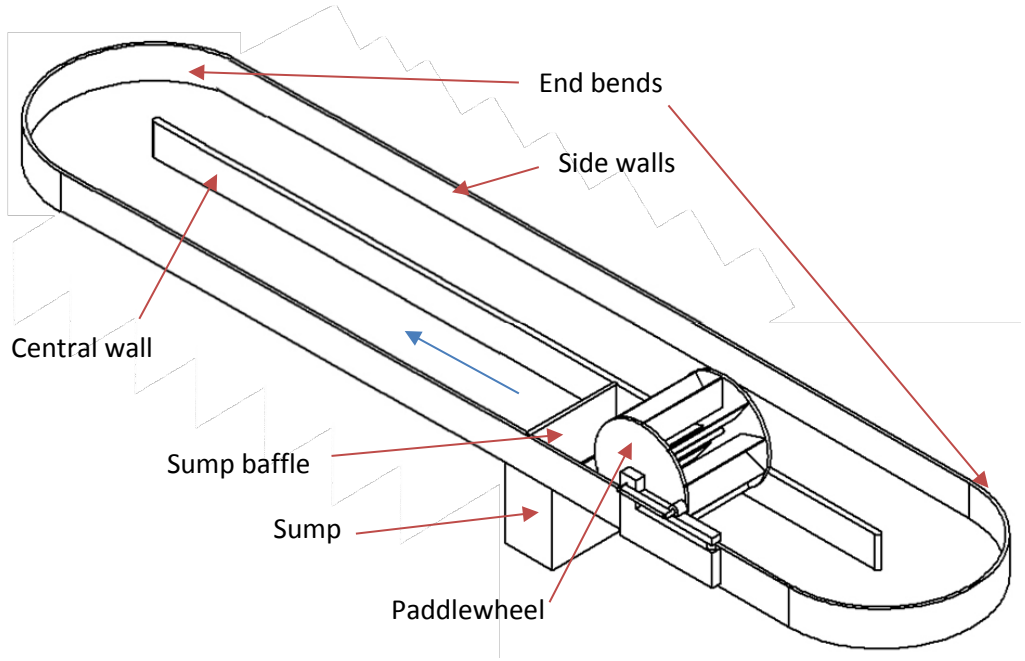

Figure 2.4. Conceptual raceway showing the different aspects. The blue arrow indicates the motion of fluid.

2.2.2.3 Other open systems

Figure 2.5. Model ARID system in use (Waller et al., 2012).

Several other innovative redesigns of algal ponds have been implemented in recent years. The ARID (Algae Raceway Integrated Design) concept focuses on reducing diurnal temperature changes in the culture. This is done by the use of multiple shallow ponds

that are active during the day to increase the surface area and light penetration. These ponds are then drained into a central deep pond at night to reduce heat loss and degassing. Using this approach it is possible to reduce diurnal temperature changes from 12°C for standard configurations to 3°C (Waller et al., 2012). This study, however, did not address other implications of the new design, such as an increase in pumping costs due to the need for drainage at night or the increased frictional losses around the system.

Investigations are now being undertaken into advanced systems which use high rate algal ponds to treat wastewater. These can require 50 times more land than a traditional activated sludge plant; however the capital costs can be 50 % lower and the running costs 20 % lower than those of an equivalent activated sludge plant (Park et al., 2011). The FP7 ALL-GAS consortium project is investigating the feasibility of using algal biomass to treat wastewater and produce algal biofuels in order to make the wastewater treatment process energy self-sufficient or even energy positive (ALL-GAS, 2017). The project is currently in the process of upscaling from 500 m^2 to 5000 m^2 raceways and has made significant steps to showing that the treatment process can be a net energy producer (ALL-GAS, 2015).

2.2.3 Photobioreactors vs raceways

There have been many investigations into the advantages and disadvantages of each type of algal growth system. Closed loop reactors offer more control over the algal cultivation process and can achieve higher production rates.

Chisti (2007) suggested that PBRs can be 13 times more productive than raceways and can achieve 30 times higher biomass concentrations (Chisti, 2007). This view is broadly supported by others claiming that production rates 5 to 8 times higher can be achieved with PBRs compared to open raceways (Narala et al., 2016; Raes et al., 2014; Brennan and Owende, 2010; Stephenson et al., 2010). The lower productivity of raceways can be attributed to several factors which will affect growth, such as the temperature, light intensity, CO_2 limitation, poor nutrient mixing and contamination (Pruvost et al., 2016; Brennan and Owende, 2010).

The higher concentration of biomass in PBRs compared to raceways results in lower biomass and bio-oil extraction costs. According to Chisti (2007) if the biomass capacity of

a plant was increased to 10,000 tonnes per year then the cost per litre of bio-oil produced using PBRs would be roughly 75 % less than if it was produced using raceways. This study, however, did not include the capital costs and the finance charges arising from them and it is not stated which operational costs are also included in the cost calculation. It has been suggested these are nearly three times higher for PBRs than raceways (Richardson et al., 2012). Other studies on the relative costs of PBRs and raceways have indicated that PBRs are 2 to 3 times more expensive per unit of biodiesel than raceways (Richardson et al., 2014; Davis et al., 2011). This is again mainly due to the capital costs, but also to the operational energy required, which is reported as being 13 to 28 times higher for PBRs (Stephenson et al., 2010; Rodolfi et al., 2009; Scott et al., 2010).

2.3 Conclusion

Microalgae can be either heterotrophic or autotrophic. The former is grown in the absent of light and the latter with light. The majority of algae used for biomass production are autotrophic which are grown in either closed or open systems. Closed systems are known as photobioreactors (PBRs) and the biomass is not exposed to the open air. This allows for very selective microalgae to be produced with little contamination which can be used to grow high value products.

Open systems allow the microalgae to be exposed to the atmosphere which means there is likely to be more contamination in the system. The opens systems can be split into two main categories: raceways and open pond systems. The latter is a large shallow pond with no mechanical circulation and requires very large surface areas with low productivity. The raceway systems are typically consist of a long channel with a central dividing wall, and a paddlewheel to drive the cultivation medium around the system.

Large-scale open raceways have been designed to produce microalgae in large volumes and are seen as the most feasible option for mass production of microalgae. They are, however, unlikely to be economically feasible at the current state.

3 Raceway design and parameters

The following section describes the different aspects and features of the raceway used in the production of biomass. Further to this the operating parameters of the system are discussed. The main aspects of the raceway to be discussed are:

- The size
- Then end bends
- The gas transfer methods
- Fluid operating parameters
- Propulsion methods

Further to this a review of current CFD investigations and growth models done so far into raceway designs has been completed.

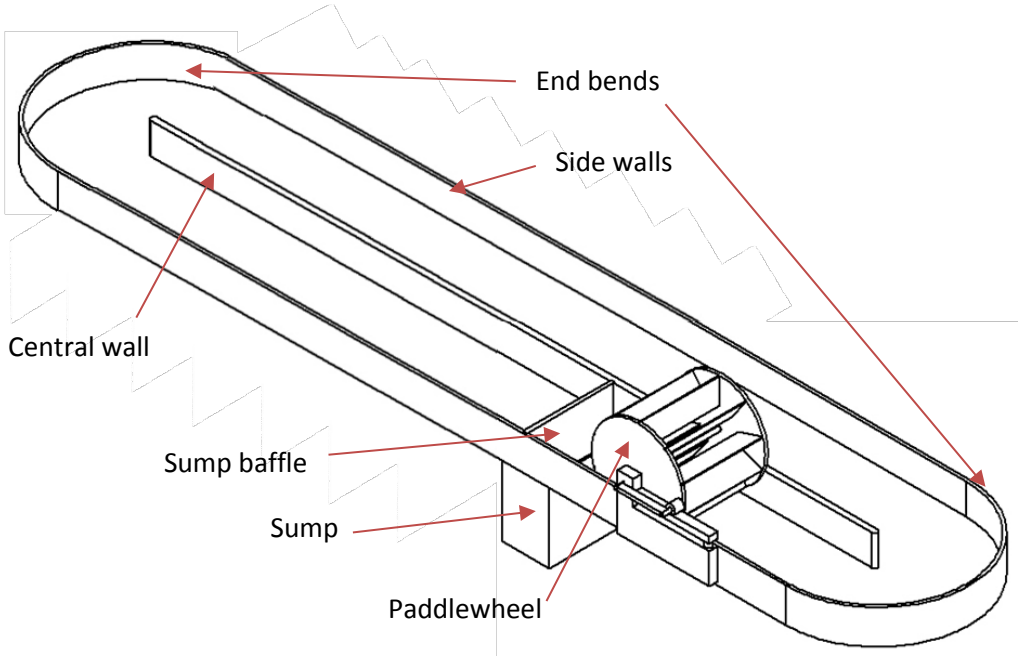

Figure 3.1. Conceptual raceway showing the different aspects

3.1 Size

3.1.1 Depth

The depth of the fluid in the raceway is significant both for the growth of the microalgae and for the propulsion energy needed in the system. It is normally between 0.1 - 0.3 m deep to allow for adequate light penetration for the biomass to utilise (Amini et al., 2016;

Jiménez et al., 2003; James and Boriah, 2010; Chisti, 2007). Experimental testing by Mendoza et al. (2013) in a fibreglass raceway system with a width of 1 m and a surface area of 100 m^2 powered by a conventional 8-blade paddlewheel showed that the optimal depth in terms of propulsion energy requirement was 0.2 m; however this will be specific to the setup of the raceway and the propulsion mechanism used. It has been suggested that the depth of the culture can be increased up to 0.5 m (Brennan and Owende, 2010), but this is likely to lead to adverse growth conditions. If the depth of the fluid is greater than this it can lead to the microalgae spending prolonged periods in the dark thus reducing overall productivity (James and Boriah, 2010).

The concentration of the microalgae in the fluid is another important factor when determining an optimal depth as the light is absorbed by the microalgae in the upper layers of the pond (Grobbelaar et al., 1990) as well as by the water itself. The light penetration depth, the depth which the light is absorbed, has been empirically linked to the concentration of microalgae by Oswald (Oswald, 1988):

$$d_p = \frac{60000}{C_a} \qquad \text{Equation 3.1}$$

where d_p is the light penetration depth (m) and C_a is the algal concentration (mg dry weight L^{-1})

Typical algal concentrations are between 0.025 % (250 mg VS L^{-1}) and 0.25 % (2500 mg VS L^{-1}) (Chisti, 2016) which result in a light penetration depth between 0.24 cm and 0.024 cm (Milledge, 2013).

Through observations of large-scale culturing systems (Borowitzka, 2005) suggested that the light penetration depth can be linked to the fluid depth by the following relationships:

$$d_p = \frac{2}{3}d \qquad \text{Equation 3.2}$$

Or:

$$C_a = \frac{90000}{d_p} \qquad \text{Equation 3.3}$$

where d is the fluid depth (m) and C_a is the algal concentration (mg dry weight L^{-1})

Borowitzka did not stipulate any constraints on Equation 3.2; however it must be limited by a minimum and maximum fluid depth. In very shallow channels the light would penetrate the entire depth and in extremely deep channels the light is unlikely to penetrate the full 2/3 of the depth. Therefore a sliding ratio is more likely to exist as a function of the depth and microalgae concentration with a minimum depth where full light penetration occurs

The highest possible algal concentrations occur at extremely low depths and growth in these conditions can reduce the downstream processing costs. Any optimisation should, however, take into account the power required for fluid mixing which increases at lower depths (Weissman and Goebel, 1987; Park et al., 2014). The productivity per unit of pond surface area is another key factor as a reduced fluid depth may lead to higher algal concentrations. If taken, however, to extremely shallow depths, less than the light penetration depth, there is the potentially lower total biomass volume and production as there would be less effective volume for biomass to grow. Where the effective volume is the top surface region where light penetration occurs.

The aspect ratio is an important design parameter that relates the depth and the width of the raceway. The aspect ratio can be calculated from:

$$AR = \frac{B}{d} \qquad \text{Equation 3.4}$$

where AR is the aspect ratio (-), B the channel width (m).

Raceways with a lower aspect ratio (deeper narrower sections) have a lower power requirement than broader narrower sections. A CFD modelling study by Ali et al. (2014) found that reducing the aspect ratio from 15 to 5 resulted in a 50 % saving in the hydraulic power requirement per unit surface area. This can be attributed to the lower hydraulic radius which would result in a lower proportion of the fluid being in contact with the bed of the raceway; reducing the frictional losses. An aspect ratio of 1.0 would be a square channel which would have the lowest hydraulic radius and should result in the lowest power requirements; however this configuration would be unrealistic due to the large depths required per unit of surface area as the light penetration would not be sufficiently deep for the biomass to photosynthesise at the bottom of the fluid.

To investigate the effect of depth on power consumption, Ali et al. (2014) conducted a CFD analysis on a raceway 23 m long and 2.25 m wide. It was predicted that when the bulk fluid velocity was kept constant and the depth of the fluid was reduced from 0.3 m to 0.15 m then the hydraulic power requirement would be reduced by around 40 %. Experimental testing by Mendoza et al. (2013) showed that the total power for an 8-bladed paddlewheel increased if the fluid depth was reduced from 0.3 m to 0.15 m across a range of paddlewheel speeds. The power requirement did, however, drop to a minimum at a depth of 0.2 m. This could be a result of the efficiency of the paddlewheel falling as the depth decreased, which is consistent with results from other studies investigating paddlewheels (Park et al., 2014; Li et al., 2014).

3.1.2 Width

There has been little investigation into the effects of the width of the raceway channel and how this may affect the pumping energy requirement and algal growth. The shape ratio of a raceway links the length to the width of the raceway. The shape ratio can be calculated as:

$$SR = \frac{L}{B} \qquad \text{Equation 3.5}$$

where SR is the shape ratio (-), L is the channel length (m).

Hadiyanto et al. (2013) carried out CFD modelling of raceways with a constant width of 0.7 m and different lengths of 3.5 m, 7 m and 10.5 m, giving different shape ratios of 5, 10 and 15, to see the effect on the energy requirement. It was found that if the surface area is kept constant an increase in the ratio led to a decrease in the power requirement per unit surface area, but the velocity and depth had a greater impact on the power requirement than the shape ratio. Other CFD investigations into the shape ratio have come to similar conclusions that the larger the shape ratio the lower the power requirement per unit surface area. Above a ratio of around 15, however, there was little or no change in the power requirement (Ali et al., 2014).

No explanation has been given for the reduction in power requirement with an increased shape ratio. It can be suggested, however, that longer raceways will have a greater proportion of their length in straight sections than in bend sections in which more energy loss will occur. At very high shape ratios there will be little change, as the energy lost in the bends is relatively small compared to the straight sections. Therefore

the shape ratio is likely to have little significance in full-scale raceway systems where the length will generally be more than 15 times the width; but may be an issue for laboratory or pilot-scale models.

It has been reported that the increase in the shape ratio also leads to an increase in the microeddy length (Ali et al., 2014; Hadiyanto et al., 2013). The microeddy length is the rate of turbulence energy dissipation in respect to the viscosity of the fluid. It has been suggested that microeddies may reduce the growth rate of the biomass and damage the cells as the size of the eddies approach the dimension of the diameter of the microalgae cells (Grima et al., 2010). There has been no explanation given to why the length scale would increase with increasing shape ratio. It may be linked to the turbulence being created in the bend sections having a reduced impact to the overall volume of fluid.

One CFD investigation into the shape ratio predicted that the percentage area of dead zones, or areas of stagnation in the raceway, halved as the ratio was increased from 5 to 15 (Hadiyanto et al., 2013). Ali et al. (2014) have proposed similar values of a 60 - 70 % reduction in the dead zone volume with a rise in the shape ratio from 5 to 15.

3.1.3 Surface area

The size of raceways can vary considerably, from small inoculation ponds to full-scale industrial plants. It has been stated that the theoretical maximum surface area of a raceway can be as large as 1500 m^2 (Ben-Amotz, 2008); however this is incorrect as sizes of 5000 m^2 have been used commercially (Becker, 1994; Earthrise Nutritional, 2014), and raceways of this size are currently under construction in the FP7 ALL-GAS project (ALL-GAS, 2015). The large size to depth ratio is to ensure that there is maximum light input per unit volume of culture.

The maximum size of the raceway is related to the head loss per unit length, or the energy slope; the smaller the energy slope the larger the pond can be. Work on this was carried out by Oswald (1988) who concluded that depth may be a limiting factor when considering the maximum total size of a raceway. He considered that to ensure uniform mixing of nutrients and light penetration a maximum head drop of half the depth was permissible. Using this it was calculated that a maximum surface area of 32,500 m^2 was possible for a 6 m wide and 0.3 m deep raceway operating at a fluid velocity of 0.15 $m\ s^{-1}$ (Oswald, 1988). A similar type of investigation into the maximum permissible size was

also carried out by Weissman et al. (1988) who declared that sizes could be up to 50,000 m^2 for raceways with a shape ratio of 1:20 and a head difference across the paddlewheel of 30 cm (Weissman et al., 1988). These investigations, however, did not take into account the physical limitations applied to the propulsion mechanism. Based on discussions with a paddlewheel manufacturer, Milledge (2013) suggested that the maximum allowable head difference across a paddlewheel is 0.076 m. Using this value the maximum length would be half that calculated by Oswald (Milledge, 2013).

A solution to increase the maximum length achievable is to use two or more paddlewheels. This would effective double the maximum possible length that can be achieved. This would, however, have an increase operational risk associated with it. If one of the paddlewheels brakes down or the raceway is closed down for cleaning or maintenance then there would be a greater operational impact than if there was two separate raceway systems.

In these calculations only the major head loss associated with frictional losses was considered and no head loss was calculated for the bends or any other features; these are therefore likely to over-estimate the maximum size achievable.

3.2 Bends

Simple bend designs are not optimised for the purpose of biomass growth as they lead to large areas of stagnant flow and high energy loss. Sompech et al. (2012) carried out a theoretical CFD investigation into a raceway system with a length of 630 m, a width of 4 m and depth of 0.3 m powered by a conventional 8-blade paddlewheel with a fluid velocity of 0.14 m s^{-1}. The authors found that the percentage area of dead zones around the bends was as high as 14.2 % of the total area (Sompech et al., 2012). Another CFD investigation by Liffman et al. (2012) into a 5 m wide by 96 m long and 0.3 m deep raceway with a fluid velocity of 0.3 m s^{-1} found similar results, at 18 % of the total area (Liffman et al., 2012). These stagnant areas are usually located behind the central barrier (Location 1, Figure 3.2) and around the outside of the bend (Location 2, Figure 3.2).

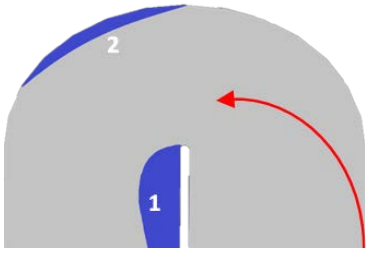

Figure 3.2. Diagram of a basic end bend design. The areas of stagnation or dead zone areas are marked in dark blue. The direction of flow is indicated by the red arrow.

Dead zones appear around the barrier as flow separation occurs at this point. Flow separation is a result of the formation of an adverse pressure gradient. In the case of the raceway end bends the turn is too sharp and the boundary layer is unable to follow the turn as this would require too rapid acceleration. Thus the main area of flow breaks away from the side wall around the bend and reattaches later on further down the channel (Sompech et al., 2012; Hreiz et al., 2014). This phenomenon is apparent in 90° bends as well, where the separation length has been linked to the width to the channel, with a smaller separation zone occurring in narrower channels (Han et al., 2011).

Around the outside of the bend there is an increase in the fluid depth. This increase in depth is called superelevation (Blanckaert, 2003). It is a result of the fluid wanting to continue in a straight line and the wall exerting a force on it to prevent it. This leads to a pressure difference across the section of the channel, which in turn leads to the formation of flows transversely to the main flow (Figure 3.3) (Bonakdari et al., 2011; Blanckaert and De Vriend, 2004). These transverse flows are called secondary flows and when combined with the main forward flow result in a helicoidal flow pattern (Naji-Abhari et al., 2010).

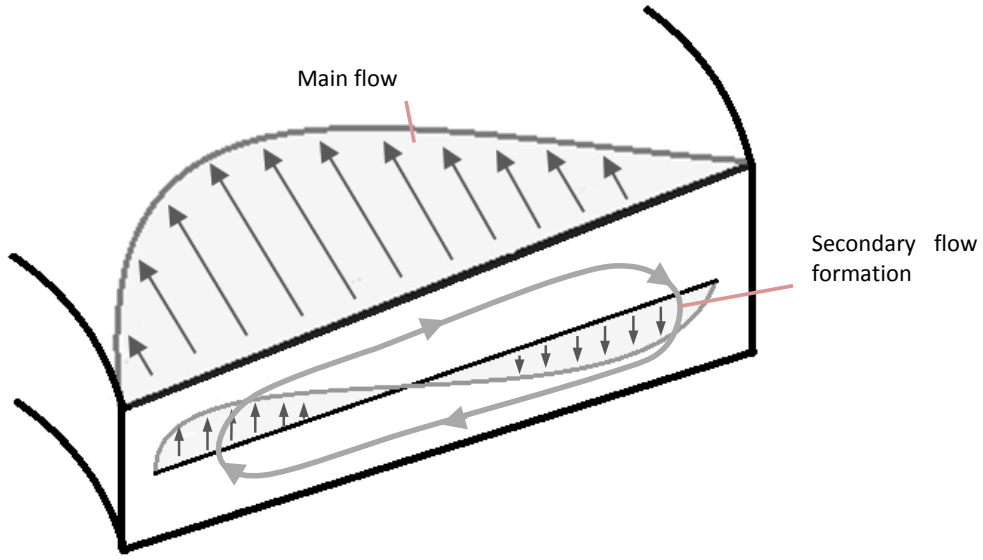

Figure 3.3. Diagram of main and secondary flows in a curved open channel. Adapted from Blanckaert and De Vriend, 2004.

Sompech et al. (2012) linked the decrease in local velocity around the outside of the bend to the superelevation of the water by means of continuity. It was suggested that the greater fluid depth would result in a lower total velocity if the discharge per unit area was constant across the width of the channel. This theory takes into account the formation of secondary flows acting transversely to the main forward velocity, as the results were for the absolute velocity values of each cell in the model; but the assumption that there is a constant forward discharge per unit area across the width of the channel is incorrect due to the momentum of the fluid and also the likely turbulence in the bend. Other studies have theorised that there is a constant total head across the width of the channel, and as a result of the increased depth there must be a reduction in the velocity head (Shams Ghahfarokhi et al., 2008).

3.2.1 Flow deflectors

Pacheco-Ceballos (1983) devised a set of equations to calculate the energy loss in a bend. These showed that the energy losses increased with a rise in the ratio of the radius of the bend (r_c) to the channel width (B) of the bend (r_c/B) (Pacheco-Ceballos, 1983). Flow deflectors reduce the channel width at the bend and in doing so increase the value of r_c/B. This in turn results in a reduction in the superelevation of the water, and there is therefore less head difference between the outside and inside of the bend. Reducing this difference leads to a reduced secondary flow; therefore less energy is lost

through the movement of water traveling transversely to the main direction of flow (Pacheco-Ceballos, 1983).

Flow deflectors have been employed in raceways to reduce the head loss that occurs at the end bends (Figure 3.4). Deflectors have been shown to reduce secondary flows and separation zones in 90° bends, resulting in lower head loss. Experimental investigations by Han et al. (2011) using a 0.61 m wide channel with an inlet fluid velocity of 0.24 m s^{-1} and depth of 0.09 m into 90° bends with an inner radius of 0.15 m, showed that there were large separation zones and secondary flows occurred with no flow deflectors in the channel. With the implantation of one flow deflector in the centre of the channel there was a 52 % reduction in the average separation length; when three flow deflectors are used there was a further 19 % reduction. This reduction in separation has been associated with more uniform flow and reduced secondary flows. Due to the reduction in separation, the head loss around the bend was reduced from 0.16 cm with no flow deflectors to 0.13 cm for both the one and three deflector systems (Han et al., 2011).

Figure 3.4. Image of flow deflectors in operation (Schwartz, 2012).

As fluid travels around a sharp bend there is a localised increase in the velocity at the inner wall. This localised increase in velocity leads to greater energy dissipation through turbulence and wall friction in these areas. Deflectors reduce the magnitude of this increase as the flow pattern becomes more uniform across the width of the bend (Han

et al., 2011). They will however increase the wall length in contact with the fluid and thus has the possibility to increase the friction.

In addition to reducing the head loss, the implementation of bend deflectors in raceways has been shown to increase the bulk fluid velocity for a given paddlewheel rotational speed. Mendoza et al. (2013a) using a standard flat 8-bladed paddlewheel, found that at the paddlewheel's maximum rotational speed, adding one deflector increased the fluid velocity from less than 0.3 m s^{-1} to over 0.4 m s^{-1}. Increasing the number of deflectors led to further smaller increases in fluid velocity to a maximum of 0.47 m s^{-1} with three deflectors installed (Mendoza et al., 2013a). The increase in velocity was recorded when the paddlewheel was operating at the maximum rotational speed, and thus at much higher fluid velocities than those which are required to keep the microalgae in suspension. At lower velocities of around 0.2 m s^{-1} the introduction of flow deflectors had a reduced impact (Mendoza et al., 2013a). This is as a result of the energy losses being proportional to the square of the velocity.

A number of CFD investigations have been conducted into the implementation of flow deflectors in raceways. Sompech et al. (2012) conducted a CFD analysis on the power requirement of a 630 m long and 4 m wide raceway with one, two and three end bend flow deflectors. It was reported that when any number of the deflectors were used the power requirement was reduced by 16 % at a fluid velocity of 0.14 m s^{-1}. The flow deflectors also reduced the area of dead zones. When one deflector was used the area fell from 14 % to 3.4 %. As in the work of Mendoza et al. (2013a) it was suggested that there was relatively little further decrease in power with increasing number of deflectors, but additional deflectors did reduce the percentage area of dead zones from 3.4 to 0.9 % (Sompech et al., 2012). These results are also supported by the work of Liffman et al. (2012) where it was suggested that the use of deflectors can reduce the power requirement by around 20 %.

These changes in head loss will affect the performance efficiency of the paddlewheel. When no deflector is used there will be a greater upstream depth as a result of the greater head required to overcome the obstacle (Figure 3.5). This greater depth will have a higher hydrostatic pressure which will push back against the section of the paddlewheel in the water, requiring more power to turn the wheel. In addition there will be a greater head difference either side of the wheel resulting in more water being

forced beneath and around the sides of the paddlewheel. When a deflector is introduced the head loss is reduced, therefore there is less depth upstream adversely affecting the paddlewheel.

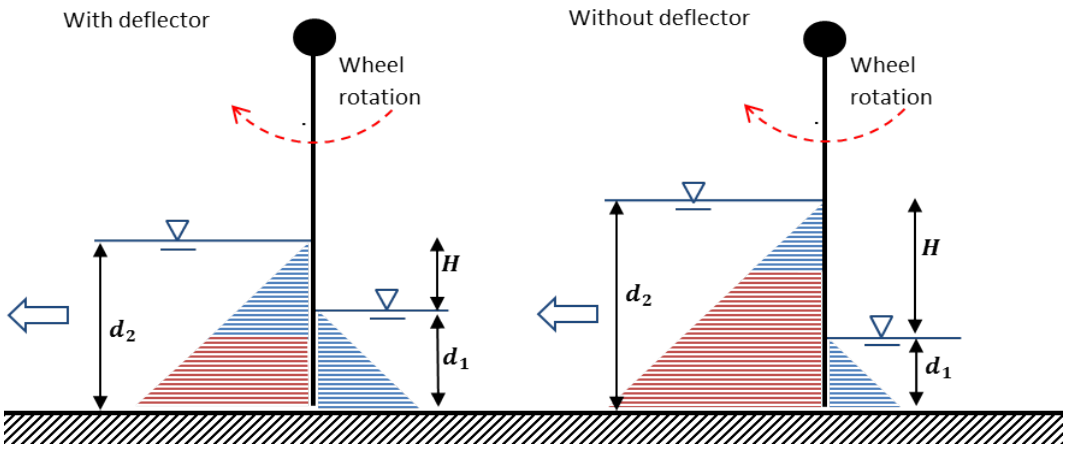

Figure 3.5. Diagram of the hydrostatic pressures acting on the paddlewheel with and without a flow deflector in the end bends. The red area indicates the pressure gradient that the wheel must overcome.

Other CFD work by Hadiyanto et al. (2013) investigating a 7 m long, 0.7 m wide and 0.25 m deep raceway with a velocity of 0.3 m s^{-1}, contradicts the finding that the implementation of deflectors will lead to a decrease in the power requirement: when three deflectors were modelled it led to an increase in power requirement of 20 % but did reduce dead zones by 90 %. This could potentially be explained by the extra wall lengths increasing the friction applied to the fluid in the channel. For a smooth wall this increase would be minimal, however, and is unlikely to have such a marked effect on the head loss as calculated, leading to uncertainty around the reliability of the model.

If the start of the deflector is located after the start of the bend then the fluid circulates behind the deflector (Figure 3.6 a). This results from the flow entering the deflector region at an angle relative to the start of the deflectors. Consequently there will be an increase in the head loss around the bend. To eliminate this, deflectors should start before and end after before the bend section ensuring that the fluid enters and exits parallel to the deflector. Additionally if deflector is wider at the tip for any reason, such as caught debris, then a bow wave forms in front of the deflector which would further increase the head loss (Figure 3.6 b).

Figure 3.6. a) Wrongly positioned deflector. b) End deflectors with debris caught at the start causing a bow wave in front of the deflector. Both deflectors are part of a 20m^2 raceway on the FP7 ALL-GAS demonstration site located in Chiclana de la Frontera, Spain. The red lines indicate the direction of fluid flow.

3.2.2 Islands

CFD has been used extensively to investigate the use of 'islands', the term used for an increase in the internal radii of the bend in a raceway (Figure 3.7).

Figure 3.7. Asymmetric island bend design in use in a large-scale algal pond system (Tribal Energy and Environmental Information Clearinghouse, 2016). The red arrow indicates the motion of the fluid.

Some work has focussed on the use of asymmetric islands (Figure 3.8a). It has been suggested that a decrease in the power requirement of around 16 % compared to the standard configuration is possible when an asymmetric island is introduced (Sompech et

al., 2012). Results from other investigators support this, with reported savings of around 10 % (Liffman et al., 2012). From the fluid velocity images produced for these designs it is clear that there was a reduction in localised areas of increased velocity which were causing higher energy losses due to more turbulence and wall friction. The results of Hadiyanto et al. (2013) were in conflict with this, indicating that the implementation of asymmetrical islands will lead to an increase in power requirement of 10 %. This seems unlikely, however, as increases in the bend radius should reduce separation and secondary flow effects which can account for a high proportion of energy loss in bends; and therefore raises further questions about the validity of some of the results from this modelling.

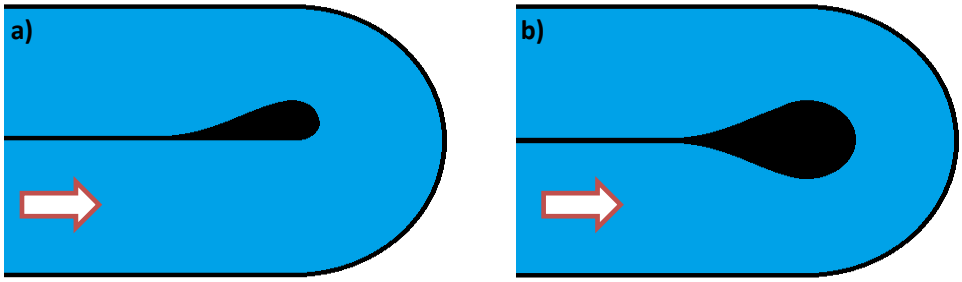

Figure 3.8. Diagram of the different "island" end bend designs. A) An asymmetric island bend design. b) A symmetrical island bend design. The red arrow indicates the fluid flow direction.

Other island designs have been studied which are symmetrical (Figure 3.8b) and have narrower channel widths with increased channel depth. These are reported to achieve much higher energy savings of 78 % of the total pumping power of the basic design (Liffman et al., 2012). This is supported by other investigations where a wider central divider was used in the model, with savings of 50 % being reported from more uniform flow around the bends (Hadiyanto et al., 2013). These latter claims appear to be disproportionately high, however, and are unlikely to be reliable as these results are expressed in terms of the total energy including the straight sections of the raceway.

The head loss in the bend will reduce as the radius of the island bend is increased as there will be a reduction in the size of the separation zone occurring after the bend (Sompech et al., 2012; Malone and Parr, 2008). Further to this, both types of island design reduce the ratio of the bend radius to the channel width (r_c/B) which will have similar effects to those seen when flow deflectors are introduced. In addition the narrower shape of the raceway bend results in a reduced wetted perimeter in the

channel, which would result in lower frictional losses. If the depth is not increased then there must be an increase in fluid velocity to ensure continuity is maintained, leading to higher localised losses. If the channel is deepened then the new cross-section will have smoother flow, as the wall friction has a reduced effect, and therefore less energy will be dissipated through turbulence.

The major drawback of all island designs is the reduction in productive surface area of the raceways due to the unusable space created by the island. The more complex geometry of an island raceway may also be associated with higher construction costs.

3.2.3 Other designs

Sompech et al. (2012) investigated other bend designs which combined flow deflectors and island configurations. This option was the best of those simulated as it gave the lowest total power requirement, with a reduction of 18 % compared to the standard configuration, and the complete elimination of dead zones in the raceway. This design, however, reduces the power by only 1.5 % compared to the design with three deflectors, but requires much more complex construction which may result in higher capital costs.

It has been reported that increasing the channel depth towards the outside of the bend as a quadratic profile (Figure 3.9) can reduce the total power requirement by 60 % compared to the standard cross-section (Liffman et al., 2012). The greater saving for the quadratic profile is due to it forming a deeper more uniform section and thus replicating the effects of the narrow but deeper channel cross sections. In addition the water is forced into the outer part of the bend, thus reducing the effects of the sharp end. Another advantage of this design is that the secondary flows that set up in the bend will be reduced by the sloping bank. The reported energy reduction again appears to be unrealistically high as it is expressed in terms of the total energy in the raceway. The idea, however, is a very clever way to decrease the head loss that occurs in the bend while still maintaining the maximum surface area for sunlight penetration.

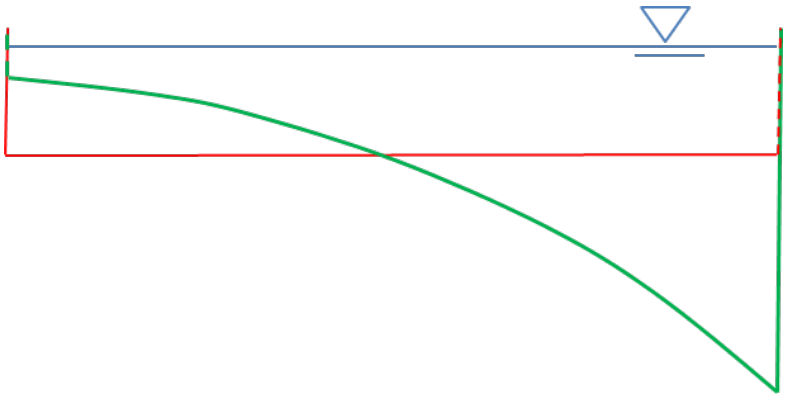

Figure 3.9. Vertical cross-section of a quadratic channel section (green) and standard box channel section (red) used by Liffman et al. (2012) in CFD modelling of raceway bends.

3.2.4 Head loss

The head loss in a channel between any two locations can be calculated using experimental data and by applying Bernoulli's Equation:

$$H_L = \alpha \frac{{v_1}^2}{2g} + d_1 - \left(\alpha \frac{{v_2}^2}{2g} + d_2\right) \quad \text{Equation 3.6}$$

where

$$\alpha = \frac{1}{\mathrm{A}} \int \left(\frac{v}{\bar{v}}\right)^3 dA \quad \text{Equation 3.7}$$

where H_L is the head loss (m), v is the average velocity of the section (m s^{-1}), d is the depth of the fluid (m), g is the gravitational acceleration (m s^{-2}), α is the kinetic energy correction coefficient (-) and A is the cross sectional area (m^3), $\bar{v}$ is the cross sectional average velocity (m s^{-1}). The subscript number 1 indicates the upstream location and 2 the downstream location. In turbulent flows the kinetic energy correction coefficient is generally considered to be close to 1.0 (Bright Hub Engineering, 2016).

To be able to apply Bernoulli's Equation a large amount of experimental data is needed; however due to the paucity of empirical data from large-scale plants this is not realistic. If the head loss in the system can be estimated theoretically, this avoids the need for gathering of experimental data.

The head loss in the system can be split into two main parts. The first and commonly the most prominent is the major head losses. The second main loss of energy can be expressed as the minor losses in the system, which is more important in bend sections.

The minor head losses occur as a result of obstacles in the fluid flow and in smaller channels can actually account for the majority of the total energy losses. Minor losses occur due to the energy dissipation from increased local turbulence and flow separation (Pacheco-Ceballos, 1983). They may also arise due to localised increases in velocity across the section leading to higher frictional losses.

The minor head loss resulting from a bends can be calculated using the formula:

$$H_L = K\frac{v^2}{2g} \qquad \text{Equation 3.8}$$

where H_L is the head loss (m), K is the minor head loss coefficient (-), v the fluid velocity (m s^{-1}) and g is the gravitational acceleration (m s^{-2}).

Values for the minor head loss coefficient have been empirically measured for standard bends and sections. There are also numerous design codes and investigations which attempt to calculate the minor head loss in open channels. The first of these were formulated by Raju (1937) and followed up by Shukry (1950) who worked out multiple mathematical curves in order easily to obtain the minor head loss coefficient. These curves were related to multiple parameters including the Reynolds number and the angle of curvature of the bend (Raju, 1937; Shukry, 1950).

Pacheco-Ceballos (1983) devised a set of empirical equations to calculate the value of the minor head loss coefficient:

$$K = \left(d_1 - d_b + \frac{v_m^2}{2g} - N\frac{y_1^2}{y_m^2}\frac{v^2}{2g}\right)\frac{2.50}{\frac{V^2}{2g}} \qquad \text{Equation 3.9}$$

in which

$$N = \frac{1}{\left(\ln\frac{r_0}{r_1}\right)^2\frac{r_0 r_1}{B^2}} \qquad \text{Equation 3.10}$$

and

$$\log(d_1 - d_b) = Av + \log B \qquad \text{Equation 3.11}$$

where coefficient A has a value of 2.11 for all bend designs and coefficient B can be found from:

$$\log B = -\Phi(\theta) - 0.07\frac{r_c}{B} + 0.06\left(\frac{r_c}{B}\right)^2 - d_{b2}$$ Equation 3.12

Where d_1 is the upstream depth (m), d_b is the average depth halfway around the bend (m), d_{b2} is the fluid depth halfway around the bend as if the channel was straight (m), v_m is the average channel velocity halfway around the bend (m s^{-2}), r_0 is the exterior bend radius (m), r_1 is the interior bend radius (m) r_c is the centreline bend radius (m), B is the channel width (m), θ is the bend angle (degrees). For bends of 45° to 180° the term $\Phi(\theta)$ varies from a value of 2.98 to 2.64 (Shukry, 1950).

This equation shows that the head loss around the bend rises with increases in the fluid velocity and depth; and that it would decrease with a rise in the radius of the bend, with both N and r_c/B terms increasing.

Experimental work has found the minor head loss coefficient to be between 3.2 to 3.5 for bends where the width of the channel is equal to the width of the bend (Kawamura, 2000; MacDonald and Streicher, 1977; Montgomery, 1985). Decreasing the bend to channel width ratio, using symmetrical bend designs, leads to a drop in the coefficient to 1.5, which will result in a lower head loss (Kawamura, 2000). This supports the work done by Liffman et al. (2012) which showed that the narrow bend channels had a lower power requirement.

If flow deflectors are introduced the head loss drops significantly and the coefficient can be taken as 2.0 (Lundquist et al., 2010). This supports the majority of the experimental and computational results discussed previously, and also the work of Pacheco-Ceballos, 1983.

3.3 Gas transfer

CO_2 is transferred into the raceway culture medium through equilibration with atmospheric CO_2, but if microalgae are carbon limited they may benefit from the provision of additional CO_2. Microalgae can utilise CO_2 if it is pumped into the culture (Hsueh et al., 2007; Vunjak-Novakovic et al., 2005; Kadam, 2002). In a study in which CO_2 was injected into a 1 m deep carbonation sump it was found that 66 % of carbon supplied was taken up by biomass (de Godos et al., 2013); the majority of the rest left the raceway in the liquid phase as carbonate. Ketheesan and Nirmalakhandan (2012) found that increasing the concentration of CO_2 in a CO_2-enriched gas stream for

injection into the culture from 0.25 % to 1 % led to much higher biomass yields. Enrichment higher than 1 % however led to no significant increase in biomass production.

These and other investigations indicate that microalgae are likely to be carbon limited if they depend on natural mass transfer of CO_2 from the atmosphere and no supplementary carbonation takes place (Gouveia, 2011; McGinn et al., 2011). This is due to the fact that for every 1 kg of microalgae biomass grown in the reactor 1.65 - 2.2 kg of CO_2 is needed (Berg-Nilsen, 2006; Weissman and Goebel, 1987).

As a result of photosynthesis, oxygen starts to build up in the raceway system and can inhibit the growth of the algal biomass (Molina et al., 2001; Jiménez et al., 2003; Mendoza et al., 2013b). Jiménez et al. (2003) investigated the effects of dissolved oxygen concentrations ranging from 10 mg O_2 L^{-1} to 30 mg O_2 L^{-1} on algal biomass growth in a 450 m^2 outdoor raceway. It was found that there was a decrease in biomass concentration when the dissolved oxygen concentration was higher than 25 mg O_2 L^{-1}. Another direct impact of photosynthesis is that as CO_2 is consumed by the biomass there is a rise in the pH of the culture (Craggs, 2005), and high values may adversely affect algal growth (Hsueh et al., 2007). Similarly if too much CO_2 is absorbed by the fluid the pH will start to drop, and low values will again affect the algal growth (Azov et al., 1982; Jiménez et al., 2003).

3.3.1 Gas type

A simple approach to carbon supplementation is to bubble CO_2-enriched gas through the culture, thus increasing the gas transfer of CO_2 into the system and O_2 out of it (Craggs et al., 2012; Heubeck et al., 2007). In one study by Olaizola et al. (1991) using a 5.9 m^2 raceway with a depth of 0.2 m, pure CO_2 was bubbled through at 150 L min^{-1} and the results were compared to those for a 5 % carbon-enriched air mixture bubbled in at 3000 L min^{-1}. It was found that the pure CO_2 was more readily absorbed into the fluid than the same carbon supplied at 5 % with air (Olaizola et al., 1991). When de Godos et al. (2013) investigated a 1 m deep carbonation sump it was found that when the gas flow rate was increased from 50 L min^{-1} to 280 L min^{-1} the carbon transfer efficiency dropped from 98 % to 73 %. There was, however, a fourfold increase in the amount of CO_2 transferred to the liquid at the higher gas flow rate; therefore it was unclear whether the higher gas flow rate or increased CO_2 affected the transfer efficiency. These

studies indicated that the greater flow rate will result in larger bubbles forming, which will rise more quickly to the surface, reducing the contact time. Further to this the larger bubbles have a smaller surface to volume ratio which will reduce gas transfer into the fluid.

These conclusions are supported by the results of Mendoza et al. (2013) who tested three diffuser types producing different sized bubbles in a 1 m deep carbonation sump. It was found that the diffuser creating small bubbles under a high pressure resulted in the highest mass transfer rate. This was, however, only slightly higher than for the diffuser which produced small bubbles at a relatively low pressure. It was further found that the diffuser which produced larger bubbles under low pressure had a much lower mass transfer coefficient of around half that of the other two (Mendoza et al., 2013b). It can therefore be concluded that bubble size can be a major determining factor in the gas transfer rate independent of pressure. This is supported by work done by Nock (2015) who investigated the rate of gas transfer from single bubbles compared to small bubble swarms. It was observed that the bubble swarms increased gas transfer, and this was more apparent at lower input concentrations of CO_2 (Nock, 2015). If a gas with a lower CO_2 content is used then bigger bubbles are more likely to form due to the greater gas flow rate required to deliver a given mass of CO_2 and the increased likelihood of bubble coalescence occurring.

Duarte-Santos et al. (2016) investigated the carbon uptake when CO_2 enriched gas at the same flow rate but with different CO_2 concentrations was passed through the culture in a 100 m^2 raceway with a 1 m deep sump. It was found that when the CO_2 concentration was 2 - 6 % the carbon transfer was greater than 95 %, with 85 % being transformed into biomass. When the concentration was increased to 14 % the transfer efficiency dropped to 67 % with only 32 % being fixed by the biomass (Duarte-Santos et al., 2016). This work indicates that the concentration of the gas not only affects the transfer efficiency, but also the biomass fixation efficiency.

An investigation using photobioreactors sparged with flue gases from a coke oven found that higher biomass concentrations are achievable than with CO_2 enriched air or just pure air (Kao et al., 2014). This was linked to the nitrous oxide compounds in the gas which may serve as a nitrogen source for the biomass. These findings are contradictory to those of an investigation by Doucha et al. (2005) using flue gas containing 6 - 8 % CO_2

in a 55 m^2 outdoor photobioreactor and pure CO_2 in a 224 m^2 unit. No difference was found in the daily net productivity of two different cultures using CO_2 or flue gas (Doucha et al., 2005). This investigation, however, used 100 % CO_2 instead of CO_2-enriched air and the two cultures were grown in different sized units. The culture saturated with pure CO_2 was in a unit four times bigger than that used for the flue gas culture. The larger units are likely to perform less well due to differences in the mixing characteristics, nutrient dispersion, general culture management and the ratio of sump volume to raceway volume (Fernandez, 2016).

Relatively few experiments have been conducted to compare the biomass yields when pure CO_2 and flue gases are used in raceways. Mendoza et al. (2013b) found that there was a higher biomass yield when flue gas with 10 % CO_2 was used as a carbonation source compared to pure CO_2 when these gases were bubbled in through a 1 m deep carbonation sump. The gas flow rate for the pure CO_2 was, however, an order of magnitude lower than that used with the flue gas, as the same amount of carbon was supplied. This led to the conclusion that the deoxygenation effect of the greater gas flow was more important than the carbonation effect (Mendoza et al., 2013b). These findings are supported by earlier investigations by Olaizola et al. (1991) who found that though the CO_2 was more readily dissolved when in its pure form, there was a slight increase in the biomass growth when it was supplied as 5 % CO_2 in air. There will, however, be greater costs associated with compressing a larger volume of gas to be released through the fluid. Optimisation of the CO_2 ratio may be needed to ensure that the best balance between uptake of the CO_2 and desorption of any excess oxygen. Where feasible the most cost effective method is likely to be the use of flue gases from industrial processes, which contain a mixture of CO_2 and other gases, as pure CO_2 would be very expensive especially in the quantities needed.

3.3.2 Effect of pH and alkalinity on gas transfer

A large number of experimental tests have been carried out to investigate the effect of alkalinity on the gas absorption efficiency. Putt et al. (2011) carried out a pilot-scale study on carbon transfer efficiencies using a 3.1 m high carbonation column connected to a 1.1 m^2 raceway with a fluid depth of 0.15 driven by a paddlewheel. The alkalinity was reduced using CO_2 in a carbonation column. It was found that alkalinity had little effect on CO_2 transfer efficiency across the range of pH values tested, from pH 10 to 8

(Putt et al., 2011). These findings are supported by Hsueh et al. (2007) who investigated the carbon uptake of a 15 % CO_2 enriched gas through an algal culture at various pH values which were varied using the CO_2. It was found that the carbon removal efficiency increased from 3 to 13 % when the pH was raised from 8.9 to 12.2. Above pH 12.2, the transfer efficiency increased dramatically reaching 78 % at a pH of 13.5. At these very high pH values, however, there was reduced microalgal growth, dropping from a peak growth rate of 2.5 day^{-1} at pH < 10 to 1.5 day^{-1} at a pH of 11 (Hsueh et al., 2007).

Other investigations have shown conflicting results and found a twofold increase in the absorption efficiency at a pH of 8 compared to that at pH 6 (de Godos et al., 2013). It is clear that the higher the pH the larger the amount of CO_2 that can be absorbed due to a greater driving force across the fluid boundary.

3.3.3 Surface transfer

Few studies have investigated the gas transfer at the surface of a fluid which is supersaturated with oxygen. There have, however, been studies of the oxygenation of fluids. These have shown that the gas transfer of oxygen into the fluid at the surface quickly saturates the boundary layer at the surface of the fluid. This saturated fluid is then transported away from the surface by turbulence and vertical velocity fluctuations in the body of the fluid. These fluctuations may not reach the surface of the fluid, thus the saturated zone may not become fully mixed (Moog and Jirka, 1999). This principle can be reversed when the unsaturated fluid is not moved away from the surface boundary (Figure 3.10).

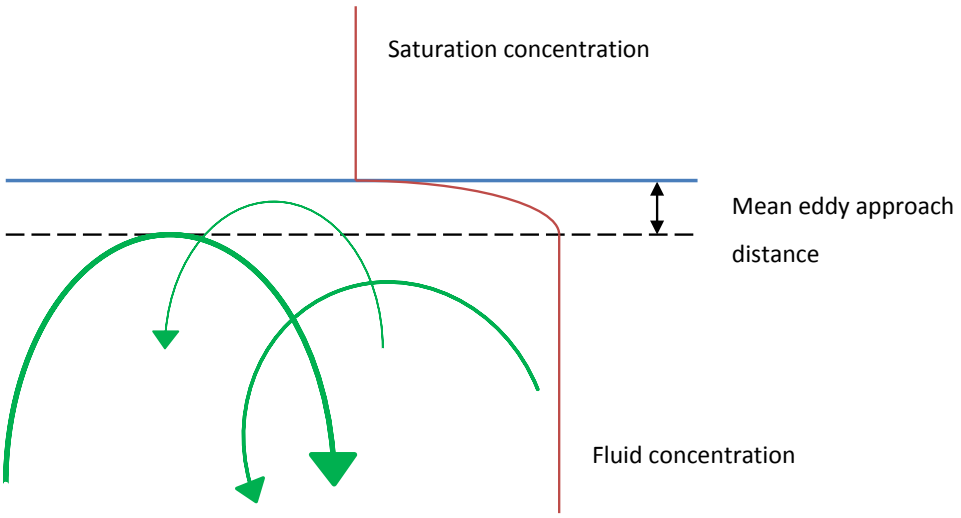

Figure 3.10. Diagram of oxygen levels in the fluid and eddy transport way from the surface.

Large and small eddy models have been formulated to try to calculate the gas transfer coefficient for a fluid (Moog and Jirka, 1999; Lamont and Scott, 1970). The large eddy model stipulates that:

$$\frac{K_L}{u_*} \propto Sc^{-\frac{1}{2}} R_*^{-\frac{1}{2}} \qquad \text{Equation 3.13}$$

And the small eddy model that:

$$\frac{K_L}{u_*} \propto Sc^{-\frac{1}{2}} R_*^{-\frac{1}{4}} \qquad \text{Equation 3.14}$$

where K_L is the gas transfer coefficient (-), u_* is shear velocity(-), R_* is the shear Reynolds number (-) and Sc is the Schmidt number (-).

The shear velocity can be found from:

$$u_* = \sqrt{\frac{\tau}{\rho}} \qquad \text{Equation 3.15}$$

where τ is the shear stress (N m^{-2}) and ρ the density of the fluid (kg m^{-3}). The shear stress in a fluid as a result of the interaction with a non-slip boundary layer can be calculated for a Newtonian fluid as:

$$\tau = \mu \frac{dv}{dy} \qquad \text{Equation 3.16}$$

where μ is the dynamic viscosity (N s m^{-2}), v is the velocity of the fluid (m s^{-1}) and y the distance to the boundary (m). The Shear velocity can then be used to calculate the shear Reynolds number:

$$R_* = \frac{u_* d}{\nu} \qquad \text{Equation 3.17}$$

where ν is kinematic viscosity (m^2 s^{-1}) and d the fluid depth (m). The shear Reynolds number is an approximation for the turbulent Reynolds number and it has been found that $\mathrm{R}_* \sim 1.2\mathrm{R}_\mathrm{L}$ when investigating the surface interactions in uniform flow (Nezu and Nakagawa, 1993).

The Schmidt number can be calculated as:

$$\mathrm{Sc} = \frac{\nu}{D_m} \qquad \text{Equation 3.18}$$

Where D_m is the molecular diffusivity of the gas in water (m^2 s^{-1}).

It is thought that at high Reynolds numbers there will be more smaller eddies in the system which will have a larger effect on the transport of the fluid away from the surface region. At low values of the turbulent Reynolds number, R_L<500, the large eddy model is expected to be true (Theofanous et al., 1976). From initial CFD investigations into a carbonation sump carried out in the current work, the shear Reynolds number was calculated being below 500. This threshold (R_L<500), however, has been formulated for the calculation of gas transfer of oxygen into the fluid from the atmosphere which is the opposite of the problem faced in the production of microalgae, and further investigations are needed to determine whether it still holds true in this case.

According to the model in Equation 3.13 and Equation 3.14, if the bulk fluid velocity increases then the surface gas transfer coefficient should also increase. This has been shown in experimental investigations by Mendoza et al. (2013) using a 100 m^2 raceway, which found that there was an increase in the mass transfer in all parts of the raceway as the liquid velocity was raised from 0.17 m s^{-1} to 0.39 m s^{-1}. There was, however, little oxygen absorption occurring in the straights and bends of the raceway. The straight sections contributed only 19 % and the bends only 4 % of total absorption that occurred in the whole system when a carbonation sump was present (Mendoza et al., 2013b).

The total surface area of the straights and bends can be very large and therefore even a small increase in the gas transfer coefficient would result in a large rise in the total gas transfer. Raising the velocity of the system will result in a much greater energy requirement. Therefore other methods of increasing the vertical velocity and eddies are needed to increase surface gas transfer and keep energy losses to a minimum. This is discussed further in Section 3.4.2.

3.3.4 Coverings

Weisman and Goebel first proposed covering part of a raceway to increase gas transfer, in 1987. These coverings would have to be transparent in order for there to be little or no effect on the photosynthesis of the biomass. It was considered that these coverings would increase the gas hold up. Along with this it was predicted that, if the coverings where in direct contact with the fluid beneath, then there would be an increase in the vertical mixing which would also increase the surface gas transfer. It was calculated that a 'rippled' cover design using a corrugated material to cover 26 % of the raceway would reduce the average mixing time from 50 s to less than 4 s in a 20 cm deep raceway with a velocity of 0.2 m s^{-1}. The calculated increase in head losses, however, led to an increase in power requirement of 5 to 10 % (Weissman and Goebel, 1987). This calculation was not validated against any experimental work. If this is correct, however, the increase in power required is much lower than if the same improvement in mixing were achieved using a higher velocity alone. This method of increasing vertical mixing is very crude and is likely to be less efficient than a purpose-built structure; however it does have the added benefit of increasing the gas to fluid contact time.

Few experimental investigations have been carried out with regard to enclosing the raceway. Li et al. (2013) investigated a 1.2 m long 0.25 m wide raceway with a fluid depth of 0.04 m which was completely enclosed with a transparent cover so that the fluid surface was touching the cover. The maximum CO_2 dissolution was 64 % when the raceways was aerated with 15 % CO_2-enriched air (Li et al., 2013). This CO_2 percentage is similar to that found in flue gases which usually contain between 2 and 25 % CO_2 (Packer, 2009). This investigation did not compare this result to performance in a control open channel raceway, but this efficiency is twice as great as the efficiencies found in other studies when bubbling gas through a 0.15 m deep raceway with a 5 % CO_2-air mixture

(Putt et al., 2011). It is likely that the efficiency in this latter study would have been higher with a more concentrated gas; therefore a direct comparison cannot be made.

The experiment conducted by Li et al. (2013) did not focus on using different coverings to increase the coefficient of friction and thus increase the mixing. It is therefore likely that higher gas transfer efficiency could be achieved if the scheme proposed by Weismann and Goebel (1987) of installing a corrugated material was used rather than a flat surface.

The carbon transfer efficiencies found when covering the raceway are much lower than those found in carbonation columns and carbonation sumps. Systems based on covers are expected to have lower running costs due to the reduced head losses around the channel but, depending on the cost of the plastic covering, may have higher capital costs relating to the construction of the raceways.

3.3.5 Carbonation columns

Putt et al. (2011) investigated CO_2 transfer efficiencies in a 3.1 m high carbonation column connected to a 1.1 m^2 raceway with a fluid depth of 0.15 driven by a paddlewheel. It was estimated that this column could theoretically achieve 90 % utilization, assuming a biomass productivity of 20 g m^{-1} day^{-1}. The experimental values were found to be lower than this at 83 % utilization when 10 % CO_2 enriched air was passed through the column. It was proposed that this was due to the coalescence of bubbles inside the column. This efficiency was still far greater than that of bubbling the same gas through the depth of the raceway, which resulted in only 37 % utilization. These experiments were conducted at pH values of 10 to 9 (Putt et al., 2011). No mention was made in this investigation of any associated pumping costs and gas compression costs with the carbonation column.

The carbon transfer in the column was less than that calculated for carbonation sumps (Weissman et al., 1989; de Godos et al., 2013). In addition the energy requirements are likely to be higher for the column than the sump, as there is a 3 m hydrostatic head to overcome for gas pressurisation and fluid pumping. Energy losses from the fluid friction and high levels of turbulence are also likely to be greater, due to the small diameter of the column. Other issues may arise from pumping of the fluid, as it is likely that a

centrifugal pump would be the most efficient means of raising the liquid to the required level, and this may cause damage to the algal cells as mentioned in Section 2.4.2.

3.3.6 Carbonation sumps

CO_2 is most commonly supplied through a carbonation sump, which is a deeper column of water within the raceway (Figure 3.11). This results in a greater contact time between the culture medium and the CO_2 thus increasing the gas transfer. Numerical models have shown greater CO_2 transfer occurring in larger fluid depths (Yang, 2011).

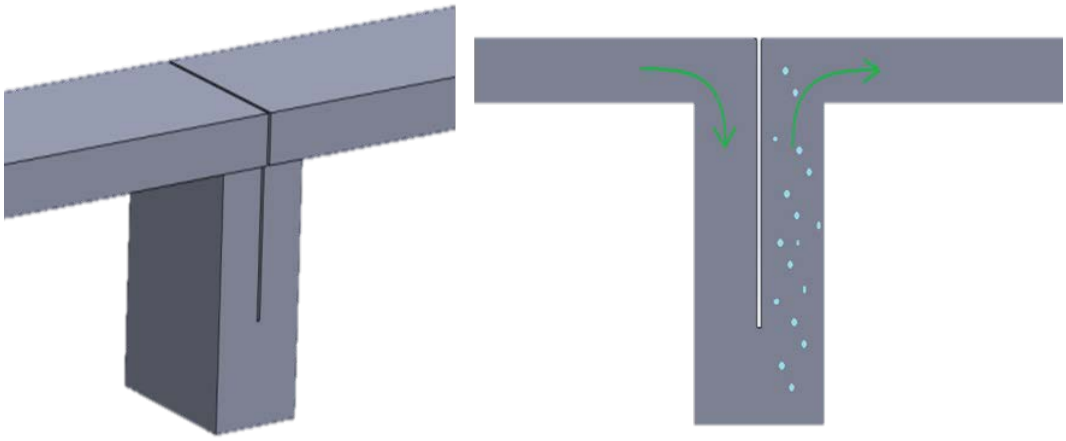

Figure 3.11. Example of carbonation sump. The green arrows indicating the direction of flow and the light blue circles signify the CO_2 gas in a co-current system.

3.3.6.1 Carbon transfer

The efficiency of the gas transfer is paramount to keeping the size of the carbonation sumps to a minimum. Some early investigations into gas uptake were carried out by Weissman et al. (1989) who reported that 80 - 90 % gas transfer was achieved using a 0.91 m deep sump with the diffuser located at 0.88 m in a co-current system and that increasing the depth further had little impact on the CO_2 transfer. It was further found that changing the depth of the sparger in the sump, from 0.88 m to 0.58 m deep did not have a large impact on the efficiency (Weissman et al., 1989). This indicates that a shallower sump would have sufficed, which might have a reduced head loss.

de Godos et al. (2013) found equally high gas absorption efficiencies for a raceway 50 m long, 1 m wide and 0.2 m deep with a 1 m deep carbonation sump without a baffle. When this was supplied with 100 L min^{-1} flue gas at 10.6 % CO_2 it was reported that a gas

absorption efficiency of 94 % was achieved at a pH of 8 with liquid velocities greater than 0.22 m s^{-1} (de Godos et al., 2013).

One source of concern with carbonation is the risk of outgassing, in which supplemented CO_2 is released back into the atmosphere due to the very low atmospheric concentrations (Putt et al., 2011). At the start of the experiment by de Godos et al. (2013) there was no outgassing and high rates of gas transfer occurred due to the concentration gradients between the gas and liquid phases. As the gas and liquid phases reached equilibrium all of the absorbed carbon in the liquid was released in the straight sections of the raceway. This experiment, however, was conducted without an algal culture in the system. If microalgae are being cultivated the culture will consume most of the CO_2 and equilibrium of CO_2 between the liquid and gas phase is unlikely to be reached. When an algal culture was introduced into the same system it was found that decarbonation accounted for only 6 % of total carbon supplied and 66 % was assimilated into the biomass. There was, however, a significant loss of carbon leaving in the liquid phase as inorganic carbon (de Godos et al., 2013).

When a baffle was introduced in the above system the transfer efficiency increased to over 94 % at a lower fluid velocity of 0.19 m s^{-1}. This small increase in CO_2 transfer efficiency with the addition of a baffle, however, required a six-fold increase in power (de Godos et al., 2013). The design of the baffle was not optimised in this study, but a significant improvement in hydrodynamic performance would be required to make the gain in gas transfer worthwhile.

Mendoza et al. (2013b) reported that for a 100 m^2 raceway operating at a depth of 0.2 m a 39 % increase in the rate of gas exchange in the entire raceway was achieved by increasing the liquid velocity from 0.17 to 0.39 m s^{-1} (Mendoza et al., 2013b). Other investigations in the same raceway system had similar findings which showed that the absorption efficiency dropped as the liquid velocity was reduced (de Godos et al., 2013). In a counter current system, where the gas flows against the direction of water, the gas is able to escape the water phase faster if there is a reduced velocity as there will be less force holding it in suspension in the water. To give the longest contact time and therefore the maximum gas transfer the velocity of the fluid would need to match the rise velocity of the gas so that it rises very slowly or remains stationary. This may mean that a smaller carbonation sump could be used to deoxygenate the fluid which could

result in a net decrease in energy required, but again the system would need to be optimised for the overall net energy balance.

3.3.6.2 Energy requirement

Inclusion of a carbonation sump is likely to lead to increased energy losses in a raceway system, especially in the presence of a sump baffle. This is due to the more complex and tight flow geometry the fluid is forced to flow through (Mendoza et al., 2013a).

The minor head loss in a sump can be calculated using Equation 3.8 in Section 3.2.4. Standard values for the minor head loss coefficient have been empirically calculated for uniform bend sections, but for the more complex geometry found in the sump these coefficients do not exist. Only one experimental data set has been recorded for the head loss through a 0.91 m deep sump with a baffle, which indicated a coefficient of 2.0 could be used (Weissman et al., 1989). This is likely to be an under-estimate, as large errors were recorded in this work with regards to the head loss across the sump at the lower velocities tested.

The carbonation sump accounts for a large proportion of total pumping energy requirements. This will ultimately depend on the size and configuration of the sump in comparison to the raceway, but for a 1000 m^2 raceway with a 0.91 m deep sump with a baffle it accounted for 17 to 25 % of the total pumping energy required (Weissman et al., 1989). If this information is combined with other literature data it can be calculated that the total energy lost in the sump can be up to 19 % of the total cultivation energy (Stephenson et al., 2010).

Stephenson et al. (2010) calculated that reducing the depth of a 3 m sump by half can lead to a decrease in the energy used of over 50 %. This work was very crude, using only basic numerical equations, however, and the value is most likely a gross over-estimate of energy loss. To date, it has not been shown either experimentally or computationally whether and to what degree the depth of the sump will affect the pumping energy required, and this area therefore needs further work.

Carbonation sumps are typically installed with a central baffle to force the fluid around the full depth of the sump and maximise the contact time between the gas and the fluid. This will affect the head loss in the sump and has been shown to increase the pumping power by up to six times in a non-optimised configuration (Mendoza et al., 2013a). The

design and location of the baffle in connection with the diffusers is likely to be of importance to reducing the energy loss while maintaining a high level of absorption of CO_2.

In a co-current system the fluid surrounding the bubbles will gain energy through the friction with the bubbles as the CO_2 rises in the column. Therefore the sump will act like an airlift pump, as explained in section 2.4.1. If the system is designed and operated to maximise gas transfer, however, it is unlikely to offer an efficient performance as an airlift pump. It may therefore be possible to optimise the performance of both aspects based on minimising the overall energy balance for raceway mixing and carbonation.

3.4 Fluid mixing

There should be sufficient vertical mixing in the culture to provide adequate mixing in order to prevent thermal stratification and photoinhibition of the microalgae and to ensure homogenous mixing of nutrients and the microalgae stay in suspension (Molina et al., 2001). Photoinhibition occurs when the photosynthetic apparatus of the microalgae is damaged by excessive light exposure, and can lead to reduced biomass yield (Chisti, 2007).

If the microalgae are treated similarly to suspended sediment then the profile of concentrations could easily be mapped using a number of different theories. The most appropriate theory would be the Rouse profile which relates the concertation of the suspended particle to its fall velocity and the fluid flow characteristics (Mofjeld and Lavelle, 1988). This cannot be applied to the situation of microalgae as there is no constant density and so the fall velocity cannot be applied. Some strains of microalgae will never settle and some even have the ability to move independently of the flow (Becker, 1994).

3.4.1 Fluid velocity

Traditionally the fluid velocity has been the metric used to ensure that the microalgae stay in suspension. A forward velocity in the range of 0.15 - 0.3 m s^{-1} is most commonly recommended due to the need to keep the microalgae in suspension while keeping pumping costs low (Craggs, 2005; Chiaramonti et al., 2012; Borowitzka, 2005).

Various minimum fluid velocities to keep microalgae in suspension have been stated, starting from a very low value of 0.05 m s^{-1} (Borowitzka, 2005). It has commonly been accepted, however, that the minimum fluid velocity should be above 0.1 m s^{-1}; if the fluid velocity drops below this critical value sedimentation of microalgae may take place (Weissman et al., 1988; Dodd, 1986). In general settlement behaviour is dependent on the strain of microalgae as some microalgae can swim and others can adjust their buoyancy. Even at relatively high fluid velocities of 0.32 m s^{-1} significant deposition of microalgae has been reported (Weissman et al., 1989). Anaerobic conditions will occur in the areas of deposition, which will create adverse conditions for algal growth.

James and Boriah (2010) simulated algal growth in a 43 m long, 3 m wide and 0.3 m deep raceway. They calculated that at very low velocities of 0.0007 m s^{-1} there was a 13 % drop in the biomass concentration, and suggested that this was a result of incomplete mixing. The modelling indicated, however, that increasing the fluid velocity past 0.007 m s^{-1} led to no increase in biomass concentration as complete mixing had been achieved (James and Boriah, 2010). This value for velocity is far too low when compared to reports from experimental work as large amounts of deposition would be expected to occur; therefore it can be concluded that the deposition of algal biomass was not accurately modelled, leading to unrealistic results.

3.4.2 Turbulence

Using the forward velocity as the measure of mixing may not be the most appropriate metric. A more suitable metric may be the turbulence diffusion or the shear stress that occurs in the system. Both of these variables are a related to the turbulence, which is the chaotic movement of fluids and can be described using the Reynolds number:

$$R_e = \frac{\rho v R}{\mu} \qquad \text{Equation 3.19}$$

where R_e is the Reynolds number (-), ρ is the density of fluid (kg m^{-3}), v is the fluid velocity (m s^{-1}), R_H is the hydraulic radius (m) and μ is the dynamic viscosity (N s m^{-2}). The hydraulic radius of an open channel is given by:

$$R_H = \frac{Bd}{B+2d} \qquad \text{Equation 3.20}$$

where B is the width (m) and d the depth of the channel (m). The hydraulic radius can be defined as the flow efficiency as it is the ratio of the fluid in contact with the channel to the cross sectional area of the fluid.

The Reynolds number is defined as the ratio of inertial forces to viscous forces and helps in the estimation of flow characteristics. At low Reynolds numbers (Re <500) the viscous forces control the fluid and the flow can be described as laminar. This is defined as uniform fluid motion with little or no reverse or vertical flow. At high Reynolds numbers (Re >2000) the fluid is dominated by the inertial forces and the flow becomes turbulent. Turbulent flow is where circulating microeddies occur in the flow, resulting in areas of reverse and vertical flow (Crowe et al., 2008).

Using Equation 3.19 to calculate the Reynolds number, the flow in algal raceways can normally be described as turbulent. In studies on a pilot-scale system, however, it has been reported that very little vertical or horizontal mixing occurs and there is strong plug flow in the raceway with little fluctuation in velocity across the width of the straight channels (Mendoza et al., 2013a). CFD studies have also shown that very little vertical mixing occurs in the straight sections of raceways even in very turbulent flow conditions, and microalgae tend to settle out towards the bottom of the raceways (Chiaramonti et al., 2012; Prussi et al., 2014).

It has been proposed that the Reynolds number is not a useful indicator of vertical mixing in raceway systems and that the main mechanisms for mixing are achieved through larger vortex structures (Prussi et al., 2014). These vortex structures are achieved with use of the paddlewheel, the wall effects, the carbonation sump, air lift mixing and vortex inducing structures (James and Boriah, 2010; Mendoza et al., 2013a; Voleti, 2012).

A better method to evaluate the vertical mixing in the system is to evaluate the diffusion coefficient which is related to turbulent mixing created by the shear velocity in the fluid. There are models that predict the diffusion coefficient in each direction of flow. In fully developed turbulent open channel flows in a straight channel it has been shown the vertical mixing coefficient can be expressed as (Sonin, 2002):

$$D = \frac{1}{15} du^* \qquad \text{Equation 3.21}$$

where D is the diffusion coefficient (m^2 s^{-1}), d is the fluid depth (m) and u^* the shear velocity. Using the above equation the diffusion coefficient can be calculated for any fluid shear velocity. A higher diffusion coefficient will lead to greater vertical mixing. To calculate the diffusivity in the channel the fluid depth and friction velocity must be measured. While the former is easy to measure the latter is often more difficult. To do this accurately detailed velocity profiles need to be recorded from which the friction velocity can be calculated. This is one of the major drawbacks of this system and why the more simple idea of a minimum forward velocity is adopted.

3.4.2.1 Shear stress and microeddy damage

Turbulent flow will experience shear stresses as the flow is not uniform and different particles of the fluid are travelling at different velocities. The interaction of these particles with each other results in shear forces in the fluid. It has been shown that the relationship of shear stress to paddlewheel rotational speed is linear until very high rotational speeds (>23 rpm) are reached (Ali et al., 2014). At this point there is a dramatic rise in shear stress. It is suggested that this is a result of the high rotational speeds creating high velocity gradients (Ali et al., 2014). The greater the velocity gradient the more particle interaction occurs in the fluid, leading to high strain rates. Damage to the biomass can occur from the shear stress in the fluid. Thomas and Gibson (1990) showed that for a *dinoflagellate* species biomass growth rates started to decline at shear stress rates of 0.002 N m^{-2}.

Another more common parameter to compare biomass growth rates and fluid flows is the turbulence dissipation rate. Like the shear strain, this also increases with increased agitation and is a measure of the rate at which turbulence kinetic energy is transformed into thermal energy. As the turbulence length scales tend towards the size of the biomass cell diameter, cell damage starts to occur (Grima et al., 2010). This has been reported in many different experimental studies where cell death rates are greatest when the agitation is highest and the length of the smallest eddies is lowest (Camacho et al., 2000; Sullivan et al., 2003). This could theoretically be used to benefit the growth of some species or control predators: if the required species of microalgae is very small then turbulence vortices could be used to damage any foreign bodies larger than this. The energy costs are likely to be significant, however, and control of eddy size may be problematic.

From Table 3.1 it can be seen that the level of turbulence dissipation which starts to damage biomass varies widely depending on the processes used to create the turbulence and also on the species of biomass used. Thomas and Gibson (1990) proposed a scale of inhibition due to turbulence which followed the order *green microalgae < blue-green microalgae < diatoms < dinoflagellates*. This was also demonstrated in experiments carried out by Berdalet who concluded that the biomass growth rate response depends primarily upon the species selected and the experimental methodology imposed (Berdalet et al., 2007).

Table 3.1. Table showing the effects varying levels of turbulence have on different biomass species.

Effect at differing levels of turbulence dissipation rate (m^2 s^{-3})	**Biomass species**	**Turbulence generation method**	**Reference**
Twofold increase growth rates at 10^{-7} m^2 s^{-3} compared to static fluid	*Green microalgae*	Speakers	(Warnaars and Hondzo, 2006)
Decreased growth rate at 1.80 x 10^{-5} m^2 s^{-3}	*Dinoflagellates*	Rotating cylinder	(Thomas and Gibson, 1990)
Decreased growth rate at 1.4 x 10^{-4} m^2 s^{-3} to 1.9 x10^{-5} m^2 s^{-3}	*Green microalgae*	Oscillating grid	(Hondzo and Lyn, 1999)
Ten species tested at 10^{-4} m^2 s^{-3}. Four showed no effect, three decreased and three increased growth rates.	*Dinoflagellates*	Vertically oscillating rods	(Sullivan and Swift, 2003)
Increase linearly with log of dissipation rate up to 10^{-4} m^2 s^{-3}. Sharp decrease in growth rate at 10^{-3} m^2 s^{-3}	*Dinoflagellates*	Vertically oscillating rods	(Sullivan et al., 2003)
No effect at 1 x 10^{-3} m^2 s^{-3}	*Dinoflagellates*	Vertically oscillating rods	(Sullivan et al., 2003)

It can be concluded from this that there is no set value at which damage to algal biomass occurs but increasing the turbulence dissipation rate beyond 10^{-3} m^2 s^{-3} is likely to lead to the onset of decreased growth rates.

3.4.3 Raceway mixing

There are three main areas of the raceway where vertical mixing can occur. These are:

1. The end bends
2. The paddlewheel
3. The carbonation sump

Additionally to this structures can be incorporated into the raceway channels to induce more mixing, such as delta wings.

3.4.3.1 Bends

CFD investigations have shown that the 180° end bends provide a necessary increase in vertical velocity for mixing, increasing it fivefold compared to the straight sections (Hreiz et al., 2014). Additionally other experimental work has shown that the end bends increase the dispersion coefficient (Bodenstein number), which is a measure of the fluid mixing, two-fold (Mendoza et al., 2013a).

CFD modelling has been carried out to investigate the effect of flow deflectors on vertical mixing in the channel. In one study which used streamline tracking to estimate the amount of vertical movement that occurs across the bend, where 180° movement is when a particle moves from the base of the raceway to the surface, found that the use of deflectors increased the vertical movement from 10° to 200° (Liffman et al., 2012). This is plausible as, instead of only one large rotating cell where vertical mixing occurs at the edges of the bends (Figure 3.3, Section 3.2), there will be multiple rotating cells set up by each of the deflectors as well. The CFD simulation by Liffman et al. (2012) however, used a mesh which had a minimum of four elements in the vertical direction. This could introduce large errors in the calculation of the amount of vertical mixing that is occurring due to over-simplification.

The 'Island' design of end bends has a smaller capacity to increase vertical mixing of the fluid when compared to the use of deflectors. CFD investigations into vertical mixing have suggested there is a limited increase when asymmetrical islands are introduced. When symmetrical islands were introduced this did lead to a 13-fold increase in vertical mixing (Liffman et al., 2012).

3.4.3.2 Paddlewheels

Mendoza et al. (2013a) reported that in a 100 m^2 raceway a standard 8-bladed paddlewheel increased the dispersion three-fold without a baffle in the sump and six-fold with a baffle (Mendoza et al., 2013a). When a baffle is introduced the upstream depth increases as there is a greater head loss in the sump. The greater depth of fluid interacts with the paddlewheel, since in this design the wheel was located only a short distance upstream of the sump; therefore more dispersion can occur within a given time period. CFD investigations into the vertical mixing in raceways have suggested that the vertical velocity of the fluid particles immediately after leaving the wheel is twice as

great as the vertical velocity found in the bends and ten times that in the straights (Hreiz et al., 2014).

3.4.3.3 Aeration mixing – Carbonation sump

A common method for mixing is through aeration of the fluid. This is more applicable in PBR systems than in open channel raceways, but a carbonation sump would act in a similar way.

Early investigations into the specific growth rates of microalgae when mixed using aeration systems investigated the differences in optical density between continuous, discontinuous (30 minutes of aeration followed by no aeration for 30 minutes) and static systems. All experiments were carried out simultaneously using *Chlorella* sp., which is single cell green algae, in a 100 L indoor test system over a two week period. The continuously and discontinuously mixed systems showed a 37 % and 27 % increase in optical density compared to the static case (Persoone et al., 1980).

It was further found that the intensity of aeration rates was important. Experiments were run in a 1.0 m x 1.3 m x 0.5 m container split into three sections with aeration rates of 7.5, 10.5 and 14 L min^{-1}. The lowest aeration intensity of 7 L min^{-1} showed a 20 % lower yield and slower growth curves than 10.5 L min^{-1}. Further increases to 14 L min^{-1} led to no significant changes in the biomass yield or growth. When an aeration of 14 L min^{-1} was applied there was very little difference between continuous and semi-continuous half-time mixing. It was suggested that these increases in yield with more intense aeration were linked to the decrease in the light cycle times, which is the time the microalgae spend in the dark areas. At very high aeration intensities there are further decreases in light cycle times but the cycle becomes so short that the microalgae are not spending a long time in the dark areas (Persoone et al., 1980).

These findings are supported by more recent experiments conducted on the effect of aeration velocity in a bubble column. It was found that there was a significant increase in biomass concentration with initial increases in the aeration velocity. Further increases, however, gave no further advantages in the yield (Mirón et al., 2003). This is likely to be explained by the fact that after a certain velocity or intensity has been reached the culture has become fully mixed.

Figure 3.12. 3m long carbonation bubble columns with a total volume of 50 L each (Kao et al., 2014).

Other investigations using 10 cm diameter cylindrical culture flasks have also found that at low levels of agitation and aeration the cell death rate was correspondingly low, as the microalgae and nutrients are more homogenously mixed, meaning that the access to light and carbon is optimised. Contrary to the previous work, however, further increases in the aeration and agitation intensity resulted in a higher specific death rates of the algal cells (Camacho et al., 2000). The specific cell death rate rises as physical cell damage occurs in the system, and it is proposed that this damage occurs through two hydrodynamic mechanisms. The first occurs at low levels of agitation in a two phase system where gas bubble entrainment and rupture leads to cell damage. The second mechanism occurs at higher levels of agitation and is linked to the formation of microeddies. The second mechanism is widely accepted and is discussed in Section 0.

It is accepted that algal cells can be damaged by bubbles in the system, but the mechanism by which this damage occurs is not conclusively known. Camacho et al. (2000) believed that the damage was caused by the rupture of the bubbles at the surface of the fluid. The reasoning behind this was that as the depth of the fluid increased there was a rise in the specific cell death rate in the systems. This hypothesis was thought to be credible as the deeper the culture the more cells can attach to the rising gas bubble and thus are damaged by its rupture at the surface (Camacho et al., 2000).

Barbosa et al. (2003) used laboratory-scale bubble columns with a diameter of 0.0358 m and a height of 0.725 m sparged through a single 0.8 mm injector with an entrance gas velocity of 78.3 m s^{-1} to measure specific cell death rates when the culture was at a depth of 0.25, 0.35 and 0.5 m. The results contradict the findings of Camacho et al. (2000) as they found that the specific death rate reduced linearly with increasing culture depth (Barbosa et al., 2003; Suzuki et al., 1995). Barbosa et al. (2003) proposed that the damage to the cells was caused at the sparger and not at the surface. It was established that there was a rise in the death rate with an increase in the gas velocity from the sparger. Two possible mechanisms were suggested as causes for this damage. Firstly there is a local spike in fluid velocity around the bubble that occurs when it detaches from the sparger; and secondly high pressures are applied to the cells in the fluid while the bubble is forming. Another potential reason for the damage which was overlooked by Barbosa is that the greater gas flows at the sparger will result in very high turbulence, which is likely to damage the cells through the creation of a large number of very small microeddies.

Both mechanisms, bubble rupture and formation, are likely to have some impact on the specific cell death rate in the system and only a limited degree of mitigation is possible. The size of the gas bubble can be controlled and it was reported that a smaller nozzle size in the sparger lead to higher death rates (Barbosa et al., 2003). It is unknown, however, whether this higher death rate was linked to the smaller bubbles or the higher frequency of bubble formation. The reduced dependence on bubbles may be an advantage of paddlewheel mixing systems over gas-lift systems, as these use a very high gas flow.

The dispersion coefficient in carbonation sumps with internal baffles (Figure 3.11, Section 3.3.6) have been shown to be three times greater than that of the straight sections. If the baffle is removed, however, the dispersion coefficient increases threefold (Mendoza et al., 2013a). The reduced mixing with a baffle compared to without is a result of the fluid in the sump acting in a similar way to that in pipe flow.

3.4.3.4 Delta wings

Several studies have been conducted into the use of delta wings, triangular metal plates, to increase vertical mixing in the straight sections of raceways (Figure 3.13). The idea was first conceived by Laws et al in 1983 where arrays of wings or foils were used to

generate vortices that increased the vertical movement of the biomass. It was reported that use of the foils in a 48 m^2 raceway increased biomass yield twofold. This was attributed to the reduction in the dark light cycle times and also the better dispersion of nutrients and microalgae (Laws et al., 1983). This work however did not investigate the changes in the power requirement and head loss in the system.

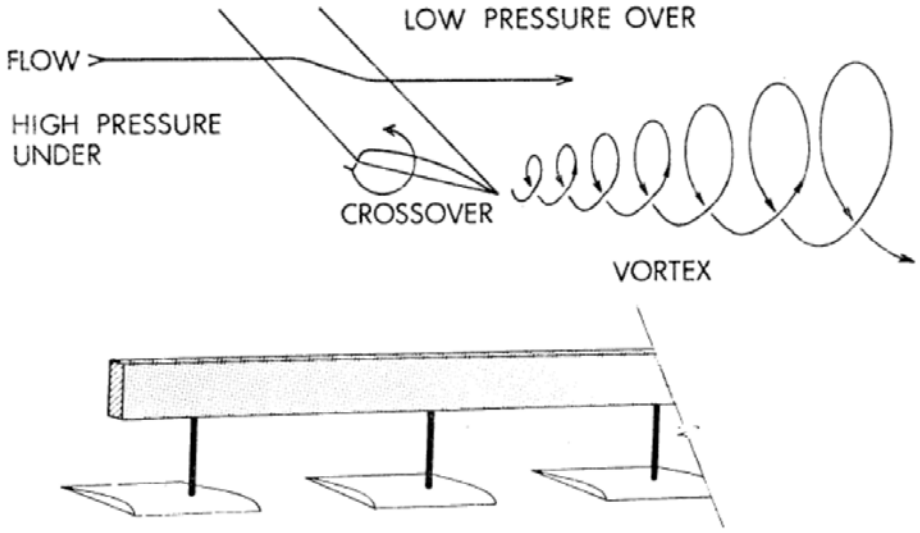

Figure 3.13. Conceptual design of an array of delta wings and the vortices that are produced as a result (Laws et al., 1983).

More recently work has been conducted at Utah State University into the use of foils in a 2.7 m^2 raceway. Voleti (2012) experimented on the use of a single delta wing in different positions around the raceway. The vertical velocity in the channel was measured at specific points upstream and downstream with the use of an Acoustic Doppler Velocimeter (ADV). The amount of vertical mixing was dependent upon the position of the wing, with the lowest increases in vertical velocity experienced when the wing is positioned directly after the end bend. When the wing is located in the centre of the long straight section the vertical velocity increases from almost zero to above 0.1 m s^{-1} immediately after the wing. This velocity decreases with distance downstream for up to 3 m after which the vortices have dissipated (Voleti, 2012). It was concluded that an array of wings at 3 m intervals would be required in the straight sections to maximise the mixing. This study did not accurately evaluate the power lost due to the wings.

A follow-up study by Vaughan (2013) using the same equipment investigated the effect of delta wings on biomass growth. Three 12-day algal growth experiments were conducted, all of which showed a peak-to-peak improvement of 25 - 30 % in the biomass dry weight yield when delta wings were used. Further investigations followed into the use of two smaller delta wings located next to each other (Figure 3.14). This investigation showed that there was a reduced vertical cycle time for delta wings placed in this way, and that stagnation areas occurred between the wing vortices. An increase in power consumption of around 5 % was also found when delta wings were installed (Vaughan, 2013). In a study by Zhang et al. (2015) the introduction of delta wings in a 4 m^2 experimental raceway reduced the duration of the light/dark cycle time from 14.05 s to 4.42 s. This led to a 30 % increase in the dry weight of *Chlorella sp.* produced over an 8-day period (Zhang et al., 2015). A larger-scale experiment in a 20 m^2 raceway using delta wings showed similar productivity increases of 35 %; however, it has been shown that the use of the delta wings led to a slight increase in the power requirement (Huang et al., 2015). This experiment was conducted with a paddlewheel speed of 20 rpm, however, which is much greater than those normally used, and results in a much lower wheel efficiencies(Musgrove et al., In Preparation).

Figure 3.14. Photograph of the two delta wings position side by side in the experiment carried out by Vaughan, 2013.

3.5 Propulsion

3.5.1 Airlift pumps

Airlift pumps, like co-current carbonation sumps (Figure 3.11), are more commonly installed in photobioreactors (PBRs) than in raceways, but some studies have suggested that airlift riser pumps require much less power than a conventional paddlewheel (Ketheesan and Nirmalakhandan, 2011). This study investigated two reactors: one was a

20 L raceway with a 0.48 m riser and the other a 23 L reactor with a 0.72 m riser. Only the second reactor was able to reach velocities over 0.1 m s^{-1}. For a 5000 L reactor the riser would have to be around 10 m deep which would have major effects on the power required to compress the gas. The power calculation for the paddlewheel was for a wheel with 4 or 6 blades which is less than the optimum number (Musgrove et al., in preparation). In contrast other investigations into the use of airlift pumps using a 0.91 m deep sump in a 5000 m^2 raceway have suggested that they will have lower operational efficiencies than paddlewheels (Weissman and Goebel, 1987).

It has been noted by several authors that not only the propulsion of the culture but also the transfer of CO_2, which can account for almost a third of cultivation costs, can be much more easily achieved if CO_2 is used in the airlift riser (Ketheesan and Nirmalakhandan, 2011; Weissman and Goebel, 1987; Benemann and Oswald, 1996). The dual function of gas lift pumping systems is less of a consideration in systems where carbon comes from other sources, e.g. wastewater, and CO_2 supplementation is not required; but may still have a role to play in deoxygenation.

3.5.2 Centrifugal and other pumps

Centrifugal pumps can have very high efficiencies of up to 70 % (Weissman and Goebel, 1987), but they have not been widely implemented in algal cultivation systems due to the potential for damage to the biomass as a result of the high shear stresses applied in the pump (Sobczuk et al., 2006; Vandanjon et al., 1999). Other studies investigating different types of pumps have found high algal mortality with centrifugal pumps and other more gentle pumps, such as rotary vane pumps, are better suited to this application (Jaouen et al., 1999).

Work done by the FP7 ALL-GAS project compared the use of a standard 8-blade paddlewheel in a 80 m long and 3 m wide raceways and Low Energy microalgae Reactor (LEAR) with a shrouded impeller pump (Figure 3.15) in a similar raceway with end island and baffles in place. It was found that the LEAR design reduced the power requirement by 85 % in comparison with the paddlewheel system (Aqualia, 2014). It is unknown which savings were achieved from the use of flow deflectors and islands and which were a result of the propulsion mechanism (ALL-GAS Meeting, 2016). Further studies comparing the two setups, however, did find that the microalgae productivity was lower

in the LEAR design compared to that of the paddlewheel driven design. It is thought that this is mainly due to the deoxygenation effect the paddlewheel has on the fluid.

Figure 3.15. LEAR design used in the FP7 ALL-GAS project (Aqualia, 2014).

Other investigations in raceways which used shrouded impeller pumps found no damage to the algal cells (Chiaramonti et al., 2012) and these pumps have been implemented in PBR systems with no damage being caused to the biomass (Chisti, 2007).

3.5.3 Archimedes screws

Archimedes screw pumps have been shown to be more efficient than other types of pump at greater head differences, but this is not so at the low head differences found in raceways. They also have much higher initial capital costs than other propulsion methods (Weissman and Goebel, 1987). For this reason, they are not favoured in raceway systems.

3.5.4 Paddlewheels

Paddlewheels have become the preferred method for propulsion in raceways (Figure 3.16) (Benemann and Oswald, 1996; Borowitzka, 2005). This is mainly because they are very well suited to the high volume and low head difference requirements found in raceway applications. Secondly there is less possibility of damage to algal biomass due to the lower shear stresses applied to the fluid. Finally they are mechanically very simple and can be installed at a relatively low capital cost. They are,

however, less efficient than some other types of propulsion system. The efficiency of the paddlewheel is determined by the ratio of useful power output, i.e. hydraulic power, to mechanical electrical power input. To calculate the efficiency of the paddlewheel alone the power input is the mechanical shaft power; however if the total efficiency is calculated then the total electrical power input must be used which includes the motor and gearbox efficiency values. Reported efficiencies for paddlewheels vary from 10 - 40 %, although the basis of the value (mechanical or electrical) is not always given (Weissman and Goebel, 1987; Weissman et al., 1988; Chiaramonti et al., 2012; Wray and Starrett, 1970). Additionally there is a maximum head difference that can be applied in each design, which will limit the maximum size of the raceway.

Weissman et al. (1988) collected data from a 23 m long and 4.5 m wide raceway built from wood with a sand base and mixed using a 6-bladed paddlewheel. The power was measured by the electrical input to the motor. The calculation of the shaft power was done by subtracting the 'no load' (empty pond) power from the working (full pond) power. It was calculated that the wheel efficiency increased as the mixing velocity was increased, which contradicts the majority of other work and theory on paddlewheels. This contradiction is due to the unreliable measurement method for shaft power, as the efficiency of the motor and gearbox will change depending on the torque which will change with changes in resistance. Later work by Weissman in a larger 1000 m^2 raceway using the same method to calculate the shaft power found the paddlewheel efficiency ranged from 183 % to 40 % across a range of velocities of 0.15 to 0.40 m s^{-1} (Weissman et al., 1989). Efficiencies over 100 % are impossible, and were attributed to errors in the recording of the forward velocity in the raceway. For values of 183 % these errors are unlikely to be due only to the velocity measurement as the efficiency values are 4.5 times higher than the maximum found by others; therefore the shaft power measurement method must also part of the error. Although these two studies by Weissman are widely cited, more credible work on efficiencies is clearly needed.

Figure 3.16. Standard flat 8-blade paddlewheel design (Cellana Inc., 2015). Notice the fluid lifted from the surface of the raceway falling away from the blade.

In addition to providing the forward velocity for the culture medium, paddlewheels provide high levels of vertical mixing in the raceway and can lead to degassing of the oxygen that can build up as a result of photosynthesis (Mendoza et al., 2013a). It was found that the gas transfer achieved in the paddlewheel was fourfold higher than that in the channel and nine-fold higher compared to the bends (Mendoza et al., 2013b). This, however, was for a 100 m^2 raceway: larger raceways are likely to have a greater proportion of gas transfer occurring over the total area, the majority of which is likely to be in channel sections. This improved vertical mixing is supported by CFD models of raceways with simulated paddlewheels, which have shown that they produce twice as much vertical velocity as the bends and ten times that in the straight sections (Hreiz et al., 2014).

3.5.4.1 Wave creation

One drawback of using paddlewheels is wave production downstream of the wheel (Figure 3.7). Waves do not contribute any energy towards the forward motion of the fluid, but move it in a circular motion as the wave crest rises and falls. As well as not contributing to forward velocity, waves do not induce any mixing. As the wave approaches a section of water the particles move backwards and upwards, then

forwards to the crest of the wave directly above its starting position (Figure 3.17). The particle then continues moving forward but downward, then backwards to its original starting position. If the wave breaks, however, then the energy stored in the wave is transferred into the forward velocity. In addition there is likely to be an increase in the gas transfer potential as a large amount of turbulence occurs (Semat and Katz, 1958).

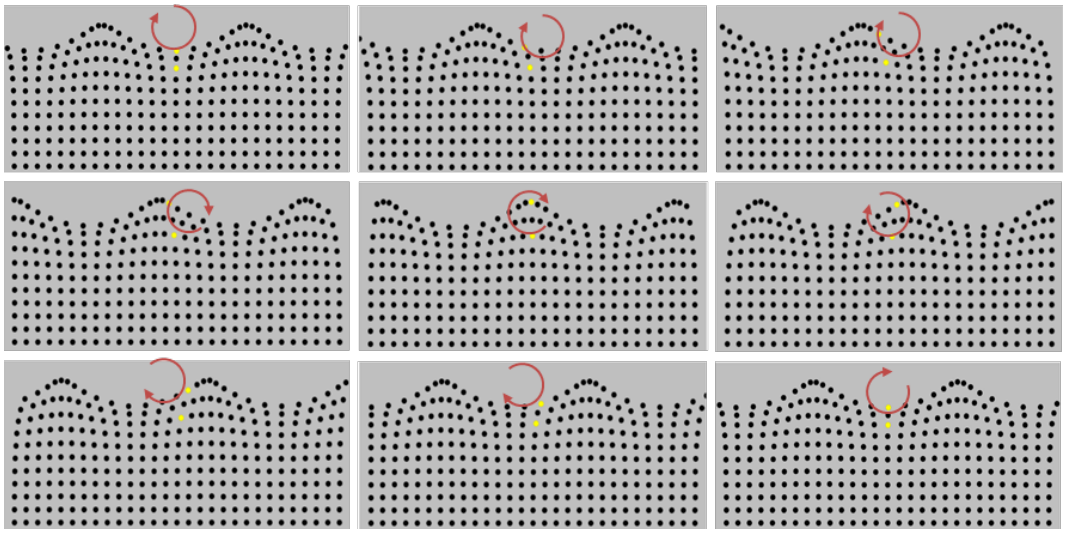

Figure 3.17. Motion tracking of a water particle indicated in yellow as waves pass through its location. Sequence goes from left to right.

The waves will continue to propagate until the energy is dissipated through friction with the side walls of the raceway. If the waves break then the energy is immediately dissipated into forward velocity and turbulence. The criteria for the waves to break are again dependent on whether the fluid depth is classed as deep or shallow.

In shallow water the breaking of the waves is dependent upon the depth of the fluid and height of the wave (McCowan, 1891). The height must not exceed:

$$H_W \leq 0.78d \qquad \text{Equation 3.22}$$

where H_W is the water wave height (m) and d the fluid depth (m).

In deep water the breaking of the wave is determined by the wave length and height as the depth does not affect the waves (Michell, 1893). The height must not exceed:

$$H_W \leq \frac{L_w}{7} \qquad \text{Equation 3.23}$$

where L_W is the dep water wavelength (m).

If the waves can be induced to break then the energy can be transferred to the motion and mixing of the fluid. Induced breaking of waves may therefore offer an opportunity for improving degassing. In shallow water this can be done by decreasing the fluid depth through raising the base of the raceway (Figure 3.18)

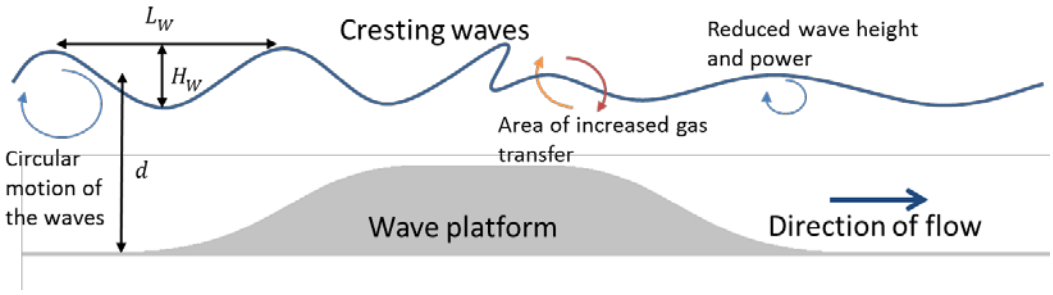

Figure 3.18. Longitudinal cross section of the raceway channel with an idea of how to induce the wave to crest by raising the channel floor to reduce the depth of the fluid.

3.5.4.2 Rotational speed

CFD investigations into a 10.2 m long, 1.9 m wide and 0.4 m deep raceway with a 0.65 m diameter 5-bladed paddlewheel predicted a linear relationship between paddlewheel rotational speed and liquid bulk velocity between 0 - 14 rpm (Hreiz et al., 2014). This is supported by the results of a small-scale test in a 2.2 m long and 1 m wide raceway with a 4-bladed wheel, which also showed a linear relationship between rotational speeds of 7 - 15 rpm (Li et al., 2014). Paddlewheel trials in split-pond systems for the production of catfish have similarly found linear correlations between paddle rotational speed and measured flow rate downstream of the wheel (Park et al., 2014; Brown and Tucker, 2013). Larger experimental studies using a 100 m^2 raceway and a standard 8-bladed wheel, however, have shown that at rotational speeds beyond 30 rpm the fluid velocity started to taper off (Mendoza et al., 2013a).

At the higher rotational speeds there is a greater head difference between the upstream and downstream side of the wheel. This difference in head results in more backflow around the immersed blade to the downstream side (Figure 3.5, Section 3.2.1). This backflow reduces the net forward flow, thus reducing the bulk liquid velocity. It has also been observed that the power consumption of the wheel starts to increase dramatically once a certain rotational speed has been exceeded (Mendoza et al., 2013a). This can be linked directly to the motor efficiency as the motors generally have specific operating parameters and if they are run outside the standard speeds then the efficiencies can

become very low. Other numerical investigations found a cubic relationship between rotational speed and power consumption (Park et al., 2014). This could be expected as the power of the blade is a function of the cube of the blade velocity:

$$P_b = C_D \, \rho_w \, A_b \, v_b^3 \qquad \text{Equation 3.24}$$

where P_b is the power of a single blade (W), C_D is the coefficient of drag (-), ρ_w is the density of water (kg m^{-3}), A_b is the wetted area of a blade (m^2) and v_b is the velocity of a blade (m s^{-1}). The velocity of the blade can be expressed as $v_b = \omega R$ where ω is the rotational velocity (rad s^{-1}) and R is the radial distance of the blade (m).

3.5.4.3 Blade design

There have been very few investigations into the wheel configuration or the blade designs for paddlewheels used as stationary or mobile propulsion mechanisms.

3.5.4.3.1 Curved blades

There are two distinct types of curved blade designs: forward and backward curved. The forward curved blades should enter the fluid surface at an angle which is closer to the perpendicular than a flat blade (Figure 3.19 b) and the backward curved blade should exit at this angle (Figure 3.19 c).

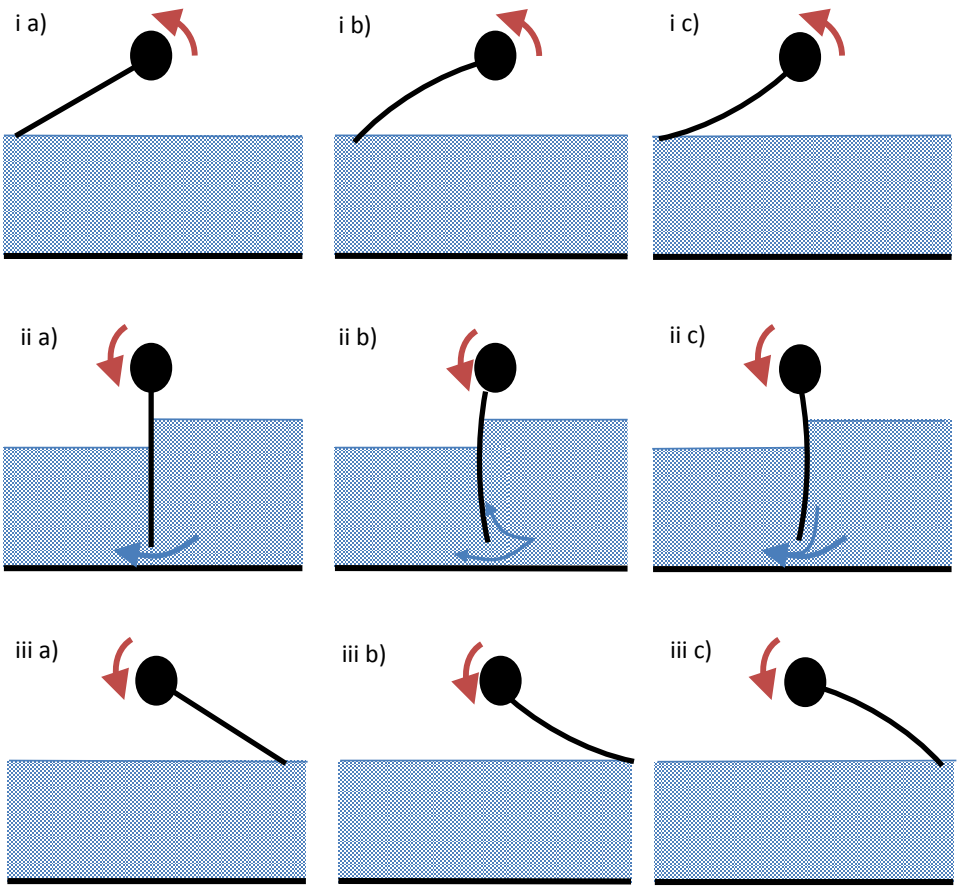

Figure 3.19. Blade designs: a) flat, b) forward curved blade and c) backward curved blade, at i) entry, ii) mid-stroke and iii) exit. Red arrow indicates the motion of the blade and blue arrows the backflow beneath the blade at mid-stroke.

Four different blade designs were experimentally evaluated by Li et al. (2014) in a 2.2 m^2 raceway at range of depths between 5 to 15 cm with a rotational velocities of between 7 and 15 rpm. These blade designs were standard flat blades, zigzagged blades and forward and backward curved blades. All of the designs gave very similar bulk flow velocities across the whole range of depths tested across the range of rotational speeds simulated except the backwards curved blades which forward velocities were consistently lower than the rest. The power requirement was lower for the flat and zigzag blades giving maximum efficiency values of 0.5 (Li et al., 2014).

These results contradict those of other work which showed that curved blades increased efficiency by about 10 % (Volpich and Bridge, 1956). Unfortunately the study by Volpich and Bridge does not state in which direction the blades were curved relative to the direction of flow.

Forward curved blades (Figure 3.20) have the advantage of entering the fluid at an angle closer to the perpendicular, and therefore giving a smoother entry of the blade into the fluid with less blade coming in contact with the surface of the fluid (Figure 3.19 i b). This should increase the efficiency as there will be less impulse force is applied to the motor as the blade enters the fluid and less energy required for the blade to brake the surface tension of the fluid and enter the water. Further to this it can be predicted that there is likely to be less backflow beneath a forward-curved blade, as the water is forced towards the blade centre and not around the bottom (Figure 3.19 ii b). Forward curved blades will, however, result in the fluid being lifted from the surface since it is more likely to pool in the centre of blade (Figure 3.19 iii b). This will reduce the efficiency of the design as any fluid lifted from the surface will result in a larger shaft power requirement for no increase in useful power. This lifting effect also occurs in large-scale systems for the flat blade design, and should be minimised in order to improve the efficiency (Figure 3.16).

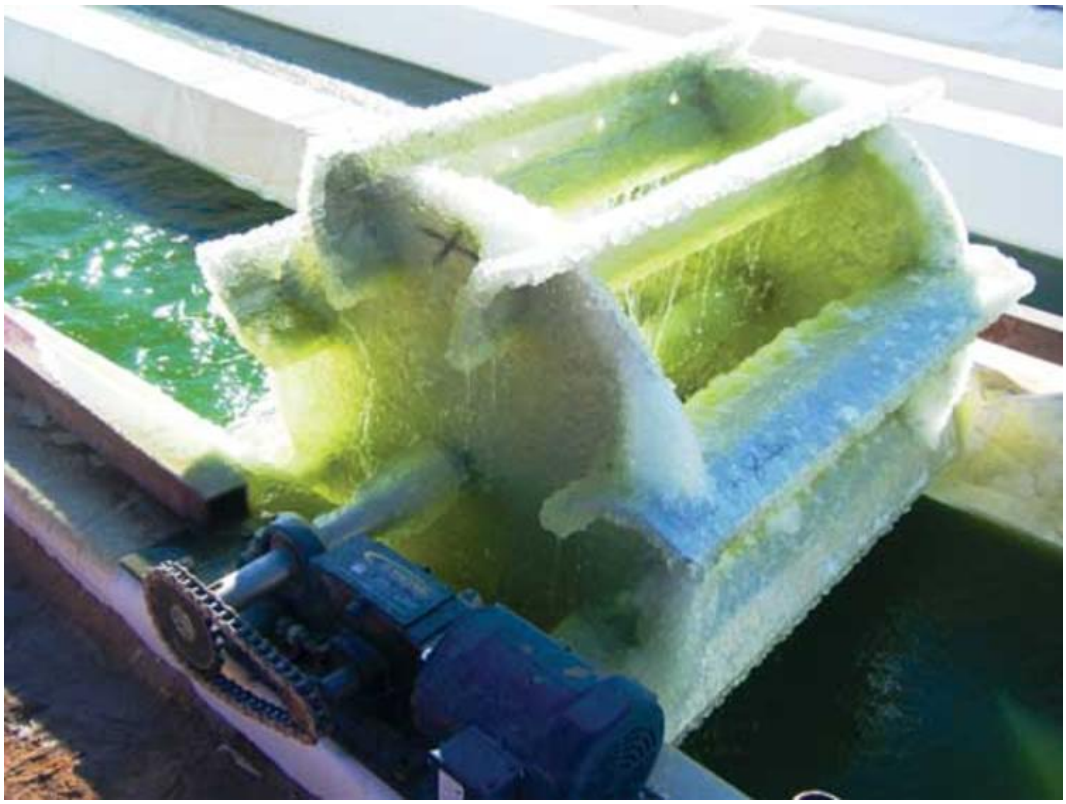

Figure 3.20. Forward curved 8-bladed wheel. Microalgae have been frozen to the wheel as a prototype extraction method (Sapphire Energy, 2009).

Backward curved blades will have a reduced efficiency when entering and passing through the fluid (Figure 3.19 i c, ii c). The fluid will flow more easily around the end of the blade, increasing the slippage which is the ratio between the velocity of the blade and velocity of the fluid immediately downstream. Conversely the exit of the blade will be greatly improved when the blade is curved in this way as the lifting effect will be reduced (Figure 3.19 iii c).

3.5.4.3.2 Non-aligned blades

Non-aligned blades (Figure 3.21, Figure 3.22) have a reduced total length of blade entering the fluid at any given time. The purpose of this is to reduce the impact force that is applied to the motor when the blade enters the fluid.

Figure 3.21. Non-aligned 8-bladed wheel in an open pond system (Doyle, 2013).

Initial CFD simulations have shown that wheels with aligned blades, i.e. standard full width blades, are far superior to non-aligned blade designs for mixing purposes, reducing the mixing times by half at the highest rotational speed of 12.5 rpm (Hreiz et al., 2014). This computational work is the only investigative work completed into blade alignment to date, and suggests that the non-aligned design has no benefit. This is probably due to the very low rotational speeds studied, and thus the relatively small impulse forces applied to the blade.

Non-aligned blades may be beneficial when the wheel spans a large raceway width, as they will have greater rigidity against lateral torsion from the motor and bending from the wheel's own weight. They may, however, have increased capital construction costs due to the increased complexity of the structure and greater material usage.

Figure 3.22. Non-aligned 8-bladed wheel in raceway system (Aquagy, 2010).

3.5.4.3.3 Angled blades

Angled blades are designed to act in a similar way to non-aligned blades by reducing the initial impulse force when the blade enters the fluid. As the blade rotates, more of it enters the fluid and the force on it gradually increases.

Angling the blade parallel to the direction of the axis of the wheel (Figure 3.23) has been numerically and experimentally tested in a 4.5 m long and 1.9 m wide raceway with a 6-bladed paddlewheel (Zeng et al., 2015). Changing the angle from 0° to 15° resulted in a 10 % reduction in power at a rotational velocity of 12 rpm. The fundamental design of the blade was flawed, however, as the depth of the water was greater than the length of the blade. This meant that water could flow over the top of the blade to the upstream section relatively easily. As a result of this, the outcome might have been different had the blade length been sufficiently long enough to protrude from the fluid surface.

Figure 3.23. Experimental 6-blade angled wheel in a small inoculation pond (Commercial Algae Professionals, 2015b).

Angled blades do not have a very close tolerance to the bed and channels of the raceway (Figure 3.23, Figure 3.24), allowing more fluid to flow around and beneath the blade. This will reduce the performance of the wheel, especially in large raceways where there is a greater head difference across the wheel.

Figure 3.24. Large-scale 6-blade angled wheel in a full size raceway (Commercial Algae Professionals, 2015a).

3.5.4.3.4 Feathered blades

Feathering blades, which rotate so that they are constantly perpendicular to the water surface, have been shown to have greater efficiencies in craft propulsion and may create fewer waves as the blade impact would be less severe (Figure 3.25) (Volpich and Bridge, 1956). It has been suggested that paddlewheels with feathering blades are 10 % more efficient than fixed radial blades however there has been little supporting experimental

evidence (Ghose, 2004). They should be more efficient as the blades enter and exit perpendicular to the surface of the fluid. At entry the motor will not experience such a large impact force and at exit the blade will not lift fluid from the surface. They are, however, more expensive, heavier and have higher maintenance costs due to the moving parts. They have never been investigated as a method of fluid propulsion in open channel systems.

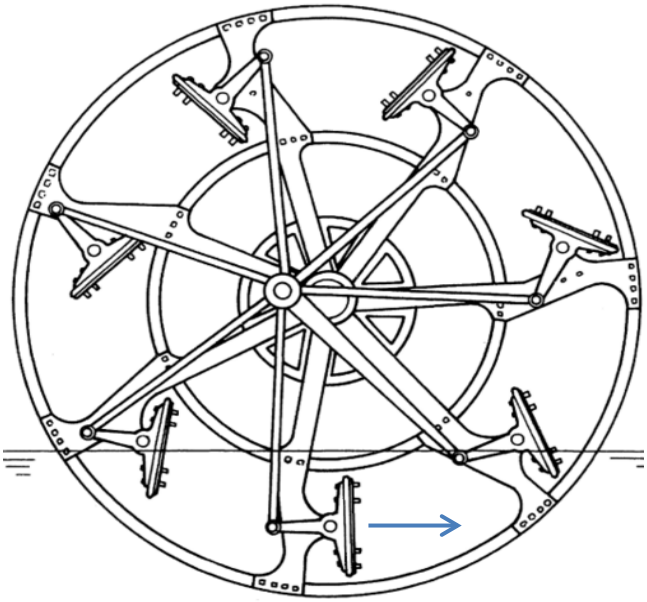

Figure 3.25. Diagram of a feathering blade wheel design (Carlton, 2007). The blue arrow indicates the motion of fluid.

3.5.4.3.5 Other Interesting designs

Short blades

The wheel design shown in Figure 3.26 is a 12-bladed paddlewheel located at Texas A&M's microalgae Research Facility. Its primary flaw is the lack of blade length. This means that when the blade is fully submerged, water can flow over the top of the blade as it passes through the fluid (Figure 3.27). Along with this there is a large gap between the blade and the bottom and side of the raceway. This gap will allow water easily to flow back around the blade to the upstream side, thus reducing the performance of the wheel.

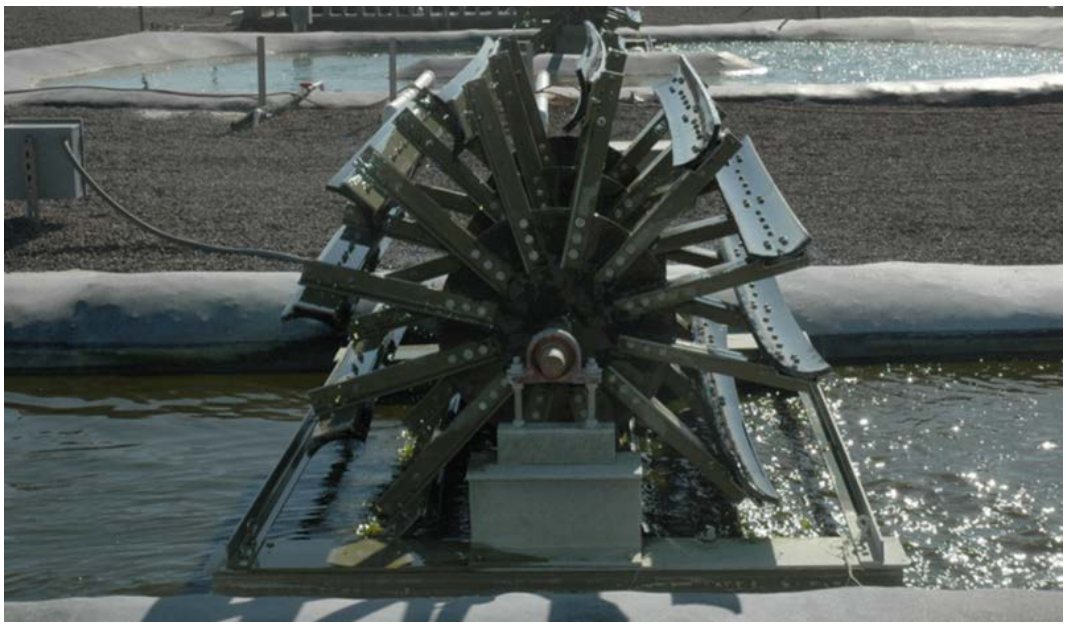

Figure 3.26. Full scale 12-blade wheel (Texas A&M AgriLife Research, 2016).

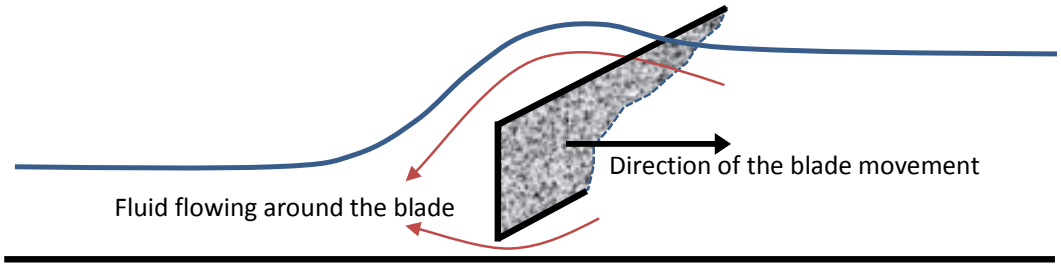

Figure 3.27. Schematic showing problems arising if the blade length is smaller than the fluid depth.

Scissor blade design

This angled or 'scissor' design by the Waterwheel Factory, Inc. is claimed to improve performance by 20 % when compared to standard wheel designs (Schwartz, 2012). Even though this design has backward curved blades, there appears to be a large amount of turbulence in the fluid downstream of the wheel, as shown by the white water and standing waves being produced (Figure 3.28, Figure 3.4). This turbulence and wave production will dissipate energy and which is unlikely to benefit in the wheel's performance. As in the previous design it appears the blade length is not sufficient as it does not protrude from the surface of the fluid.

Figure 3.28. Prototype angle 6-blade design (Fakhoorian, 2010).

Big gap design

The paddlewheel show in Figure 3.29 is a flat blade wheel with a 1.8 m diameter and was built in a 30 m long and 5 m wide raceway. This design has three major flaws. The first is the excessive gap around the sides of the blade leading to the potential for large backflows and leakage as previously described. The gap at each side of the wheel is around 0.15 m, or approximately one eighth of the width of the wheel.

Figure 3.29. Prototype flat 4-blade paddlewheel in a small closed raceway (Vargas E Silva and Monteggia, 2015).

The second significant issue is the use of only four blades. When the blade is halfway through its stroke there will be a large gap beneath it for leakage to occur. The use of a small number of blades will also lead to a higher impulse force when entering the fluid; this is likely to result in poor performance. Further to this, fewer blades will have a lower frequency of entering the water for a given rotational velocity, leading to the possibility of more wave propagation.

The last observed design fault is the sharp narrowing and expansion of the channel before and after the wheel. This narrowing of the channel before the wheel is done in large-scale microalgae raceways to allow smaller paddlewheels to be fitted (Figure 3.7). In these cases, however, there is a slower rate of change in the width of the channel. The sharp expansion of the channel width here will lead to fluid recirculating around in the dead areas to the side of the wheel.

Envelope blade design

The design shown in Figure 3.30 was built for a small inoculation pond in a production system in Myanmar. It is likely to be very inefficient and will provide little forward velocity to the fluid. The fluid can easily pass around the blades no head difference can be maintained across the wheel. As the fluid is driven by the surface gradient under gravity this system would be very poor at maintain a constant flow around the raceway. To ensure that there is enough energy the rotational velocity of the wheels is around 30 – 35 rpm; this is very high for the wheel and is due to the inefficient design employed. There is a large amount of turbulence and standing wave production as a result of this high rotational speed, leading to further energy losses.

Figure 3.30. Paddlewheel design used in small inoculation ponds in Myanmar (Thein, 2011).

The second design shown in Figure 3.31 is located at a microalgae facility at Bharathidasan University, India. In this design four blades are used and each is bigger than in the previous design. It does, however, still have large gapes between the blade which would not allow the blades to maintain a head difference between the upstream and downstream sides of the blade.

Figure 3.31. Paddlewheel designs used in research raceway ponds at Bharathidasan University, India (Thajuddin, 2016).

The final envelope blade design is used at a commercial site called Boonsom Farm. It is a small scale spirulina farm located just outside Mae Wang, Thailand. It consists of 44 ponds, some of which are covered, each 90 m long and 5 m wide (Figure 3.32 a). The propulsion mechanism used is a series of backwards curved 6 envelope blade wheels, which run at a speed of 16 rpm (Green Diamond Co. Ltd, 2010). There are, however, very large gaps between each of the wheels, which will ultimately reduce the efficiency greatly (Figure 3.32 b). It is proposed that these wheels will not be able to maintain the head difference needed to drive the fluid around the raceways. It is unlikely the fluid will be able to travel all the way around the raceway unless the high rotational speeds are great enough to keep lifting the fluid lost to backflow.

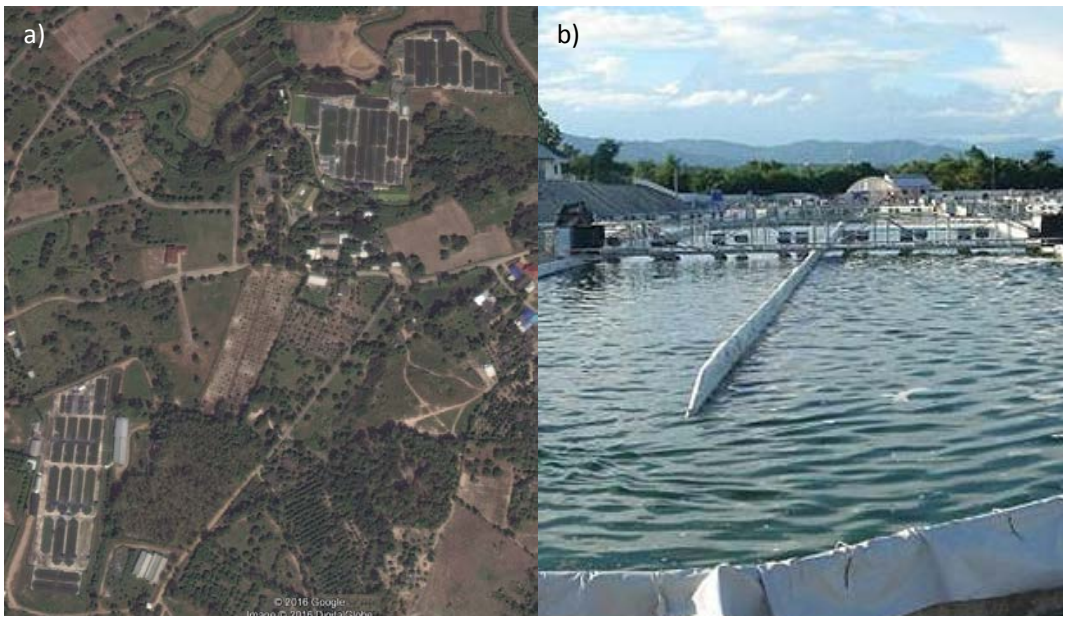

Figure 3.32. a) Satellite image of Boonsom Farm (Google Earth, 2015). b) Boonsom farm paddlewheel system (Thung Pi, 2016).

Part blade design

This paddlewheel is located in Guangzhou Institute of Energy Conversion, Guangdong province, China and is in a 260 m^2 raceway. Part of the width of the blade is missing. The reason for this is unknown, but one possibility is to create a wheel that acts in a similar way to a non-aligned blade wheels or are just poorly designed. This will greatly reduce the performance of the wheel, however, as there will be a very large amount of leakage, since the water will follow the path of least resistance and flow directly through the blade.

Figure 3.33. Part blade design from a 260 m^2 raceway located in Guangzhou Institute of Energy Conversion, Guangdong province, China.

3.6 Computational models

3.6.1 Computational Fluid Dynamic models

Computational Fluid Dynamic (CFD) models have recently been used to investigate the behaviour of fluids in open channel bends. Ramamurthy et al. (2012) reviewed the different approaches and techniques that could be used. It was concluded that the volume of fluid model is better than rigid lid and porous models, and that the rigid lid model did not simulate the separation zones correctly (Ramamurthy et al., 2012). Most early CFD investigations that have been completed focusing on the raceway bends have used rigid lid models (Sompech et al., 2012; Liffman et al., 2012; Hadiyanto et al., 2013).

Sompech et al. (2012) carried out a theoretical CFD investigation into a raceway system with a length of 630 m, a width of 4 m and depth of 0.3 m powered by a conventional 8-blade paddlewheel with a fluid velocity of 0.14 m s^{-1}. ANSYS CFX code was used in conjunction with the k-ε turbulence model. If the results from this investigation are compared to experimental data collected by Mendoza et al. (2013a) who used a in a 100 m^2 raceway with a carbonation the predicted power per unit area of raceway based on modelling is 10 to 12 times lower than experimental values when a conversion of 30 % is applied for the paddlewheel efficiency. This could in part be due to the fact that the raceway used for the experimental work had a carbonation sump. If the carbonation sump accounts for 25 % of the total head loss in the system (Weissman et al., 1989) then it is possible to estimate the energy lost in the sump and remove this from the experimental values. If this is done, then the modelled results are still just over 8 times lower than the experimental values. Further to this Sompech et al. (2012) estimated that a paddlewheel rotational speed of 30 rpm resulted in a fluid velocity of 0.11 m s^{-1}; however the experimental results of Mendoza et al. (2013a) gave much higher velocity readings of 0.39 m s^{-1} at 30 rpm. The modelling studies carried out by Sompech et al. (2012) have not been validated against any experimental data.

Hadiyanto et al. (2013) used CFD to investigate a smaller 7 m long, 0.7 m wide and 0.25 m deep raceway with a velocity of 0.3 m s^{-1} using the k-ε turbulence model. The power requirements per unit surface area calculated from simulations by Sompech et al. (2012) are 10 to 16 times lower than those from Hadiyanto et al. (2013) across the range of discharges investigated. Even though these investigations into raceway bends used very similar CFD boundary conditions, they have resulted in vastly different results. This could be due in part to the fact that the design modelled by Sompech et al. (2012) had a very large shape ratio of 158 compared to the ratio of 15 selected by Hadiyanto et al. (2013). As discussed in Section 2.1.2, however, the effect of the shape ratio on the power requirement starts to decrease beyond ratio values above 15.

The investigation by Hadiyanto et al. (2013) has been validated using data from Weissman et al. (1988) and appears to show good agreement between modelled and experimental results. The modelled data, however, has been manipulated by selecting an efficiency value of the paddlewheel to produce a good calibration with the hydraulic power requirement calculated by Weissman et al. (1988) which has been shown above

to be based on unreliable methods. If the total power requirement per unit of area is directly compared, instead of the hydraulic power requirement, the simulated results range from 50 to 150 % times those from Weissman's data (Figure 3.34).

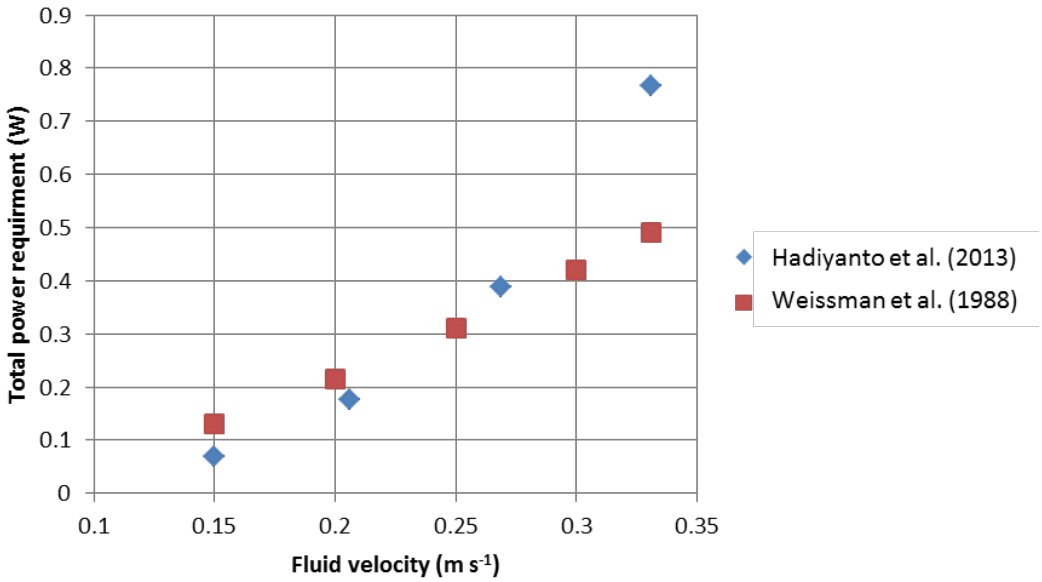

Figure 3.34. Comparison of the experimental results collected by Weissman et al. (1988) and the modelled results calculated by Hadiyanto et al. (2013).

More recent investigations have used the volume of fluid method to simulate the open surface of a raceway (Prussi et al., 2014; Zhang et al., 2015). Prussi et al. (2014) validated a numerical simulation against a 20 m^2 pilot-scale raceway. Once this validation was completed, a 500 m^2 industrial raceway was modelled. Validation is generally carried out using a smaller-scale system to limit the costs of the operation; however small errors in the numerical results at a small scale can lead to significant over- or under-estimation in the scaling process. In the work done by Zhang et al. (2015) the results were directly validated against a 4 m^2 raceway.

More advanced investigations have tried to simulate the paddlewheel, using a rotating domain for this purpose (Ali et al., 2014). Some researchers have gone further and have coupled the rotating domain of the paddlewheel with the volume of fluid model (Hreiz et al., 2014; Huang et al., 2015). This results in much greater computational requirements and run times, but has the potential to give better and more reliable results. A consequence of running the simulation with a rotating domain to model the paddlewheel is that it becomes a transient solution and not steady state. The use of a transient solution may increase errors in the results as they can oscillate out of control

and not towards a viable solution. This became apparent in one investigation where the size of the paddlewheel had to be altered to find a more reliable result, as a larger paddlewheel introduced too much instability in the model (Hreiz et al., 2014).

All these numerical simulations carried out with a rotating domain have been validated against experimental results. Hreiz et al. (2014) collected experimental data from a 56 m^2 raceway, while the numerical results of Huang et al. (2015) were validated against a 20 m^2 raceway. Both studies found that there was good numerical and experimental agreement once the paddlewheel dimensions had been adjusted. Work done by Ali et al. (2014) was validated against the experimental data collected by Weismann et al. (1988) and showed very good agreement across the whole range of mixing velocities investigated.

All numerical simulations conducted to date on the fluid dynamics of raceways have been completed using the Reynolds Averaged Navier–Stokes equations with the k-ε turbulence model.

3.6.2 Growth models

Many models have been created to simulate the growth of biomass and the production of lipids. To date only one of these has coupled a hydrodynamic model with a growth model (James and Boriah, 2010). This study used the freely available US Army Corps of Engineers' water quality code (CE-QUAL) for the growth model and the Environmental Fluid Dynamics Code (EFDC) for the hydrodynamic model. This coupled model was then used to simulate how different conditions affected the growth of microalgae and other biomass. It showed realistic values for the majority of conditions. The model accurately predicted growth rates at different temperatures and successfully modelled photoinhibition (James and Boriah, 2010).

The model predicted that a greater fluid depth resulted in higher biomass productivities. It was suggested that this was due to the greater depth of fluid acting as a natural buffer to dampen the effects of diurnal temperature fluctuations (James and Boriah, 2010). The model suggested, however, that the greatest depth simulated, of 0.6 m, resulted in the highest biomass productivity. This is a much greater depth than that found to be optimal in other studies and is not in agreement with fundamental theoretical considerations (Huisman et al., 2002). Even though the growth model accounted for solar irradiation

and self-shading something else appears to be wrong with the model. It was also reported that flow speed had no major effect on the growth rate except at very low velocities where there was a negative impact (James and Boriah, 2010). The velocity values tested, of 0.0007 - 0.07 m s^{-1}, were extremely low compared to data from other literature and would likely lead to large amounts of sedimentation which would affect the biomass productivity. This model was not validated against any experimental work and is likely to have major hydrodynamic flaws. The results do, however, suggest some interesting concepts such as using the depth as a buffer in climates where excessive temperature changes are likely to occur.

Other models have also simulated diurnal and seasonal changes. Quinn et al. (2011) created a biomass growth and lipid production model using temperature and light as the main driving factors. It predicted that lipid production would reach a maximum of 44 % of biomass in a nutrient depleted medium. This model was validated against experimental data and showed very good agreement with the experimental results for both growth and lipid production (Quinn et al., 2011).

Yang et al. (2011) investigated the growth and lipid production of *Chlorella minutissima* and its dependency on glycerine as a carbon source. It was found that higher glycerine concentration in the culture led to higher biomass growth rates and also to greater lipid production. This model further investigated the effects of different carbonation intensities on algal productivity. Based on the results it was proposed that if the percentage content of CO_2 in gas supply increased then higher levels of algal productivity were possible. It was predicted that the higher CO_2 concentrations would lead to a fall in carbon utilisation, and this result is similar to that seen in experiments on gas transfer (Section 3.3.1). Influent wastewater with high biological oxygen demand (BOD) was modelled as another carbon source instead of CO_2 gas. It was predicted that this source of carbon could significantly increase algal growth (Yang, 2011). It is unknown how robust these growth models are to changes in the parameters set, as validation has only been done for a small range of results.

3.7 Conclusion

There has been a large amount of experimental and numerical research into the production and use of microalgae as a feedstock for biofuels and an even larger number of comments and life cycle analysis reviews. There are, however, considerable omissions, in that the research has generally not focused on and sometimes not even considered the energetic inputs into the systems that have been designed, and their effect on the overall energy balance. Even when investigating the designs of new systems, such as carbonation columns, studies have not always measured or reported the real or estimated power required to implement the system.

There are a number of different design and operational conditions that need to be considered when designing the raceway. The main design aspects are:

- Length
- Width
- Depth
- End bend design
- Gas transfer technique and design
- Propulsion technique and design

There has not been a considerable amount of research done into the effects the length and width have on the system in terms of the energy demand. Only two CFD investigations have been conducted and have suggested that increasing the length to width ratio leads to a decrease in the power per unit surface area. These models were not validated and this has not been shown experimentally. There has been some investigations on the depth of the fluid and it has been suggested that the deeper the fluid the greater the power requirement. It is recommended that the fluid depth should be between 0.2 - 0.3 m, any deeper and the light is unlikely to penetrate through it so the microalgae cannot photosynthesise.

There has been a number of different CFD and experimental investigations in to the design of the end bend. The most common configurations are those with flow deflectors or islands. Both of these designs reduce the head loss and dead zone areas around the end bend. The island designs, however, do require more surface area which will be unproductive. There are a number of different end bend designs that have been tested

with the use of CFD and it is suggested that these could reduce the head loss further. They are, however, much more complex and would require a higher capital cost to construct.

The gas transfer systems used in the raceway are normally required to add additional CO_2 into the fluid and remove the build-up of the dissolved oxygen. Traditionally a carbonation sump has normally been used. This is a deep section of the raceway where CO_2 is pumped into the bottom. A baffle can be used to direct the fluid down to the bottom of the sump to increase its contact time with the CO_2. It has been shown that carbonation sumps are an affective gas transfer method with efficiencies of up 94 % being recorded. They have not, however, been investigated in terms of energy requirement. A few other designs to increase gas transfer have been investigated which include carbonation columns and coverings, but due to the higher implementation costs of these techniques and the high efficiency of the carbonation sump there has not been a great amount of work done on them.

Paddlewheels have become the preferred method for propulsion in raceways. This is mainly due to them being well suited to the requirements of moving a high volume of fluid with a low head difference.

The paddlewheels usually have a diameter of around 1 - 1.4 m. Their width depends on the raceway width, a narrowing of the raceway might be used to reduce the width if needed. The wheels have four to eight blades, which can be straight, curved, inclined, aligned, non-aligned, angled or a combination of such features. There is, however, very little experimental comparison between these designs.

Paddle wheels have several advantages compared with pumps as a means of propulsion for the fluid:

- There is reduced risk of damage to the algal biomass due to the low shear stresses applied to the fluid.
- Paddlewheels also provide high levels of vertical mixing in the raceway, and can lead to degassing of the oxygen that has built up as a result of photosynthesis. One study found that gas transfer from the paddlewheel was four times that in the channel and nine times greater than in the bends.

- Finally, paddlewheels are mechanically simple, easy to maintain and can be installed at a relatively low capital cost.

Their principal disadvantage is the low efficiency.

The energy demand for the paddlewheels constitutes an important aspect of the overall energy balance of algae ponds and can account for between a quarter and a half of the total energy required for the production of biomass in algal raceways. The range of reported efficiencies is wide, mainly due to the variation in the experimental procedure followed. The analysis of the literature indicates that an efficiency in the 10% range is most probable. A large amount of the literature on the efficiency of the paddlewheels makes reference to Weissman and Goebel (1987) who actually only suggested an efficiency value and did not test it. The literature review also indicated that there is very little in terms of design guidance for paddle wheels.

Further to these gaps identified in knowledge of the raceway design, the findings from computational and numerical models must be cautiously reviewed as a large amount of this work has not been validated experimentally, while some of the work that has been validated has used results that are now considered unreliable.

3.8 Aims

The main aim of this work is to improve our understanding of the methods of propulsion in raceway systems to provide design tools and concepts that will allow reduction of the energetic costs in large-scale cultivation of microalgae. Biomass growth is a strongly surface-driven process and due both to solar irradiance gas transfer, thus a key parameter of interest is the power per unit surface area of fluid (W m^{-2}). This is achieved by focusing on the main method currently employed for propulsion and investigating whether more optimal systems or set ups are possible. To the author's knowledge, no investigation has been published into how the number of blades affects paddlewheel efficiency and how the rotational speed impact is changed by the number of blades. Further to this there is very limited work done on how the head difference across the wheel affects its efficiency as a propulsion mechanism.

3.8.1 Objectives

Firstly, the main parameters that affect the efficiency of the paddlewheel as a method of propulsion will be experimentally investigated:

- Rotational speed
- Number of blades
- Fluid discharge
- Submersion depth
- Head difference across the wheel
- Channel length

Each experiment will use a flat bladed wheel with the same dimensions. Further to this, methods to reduce the backflow of water around and beneath the blades by employing the use of an insert will be empirically tested. In addition to the experimental work a theoretical model will be derived and validated against the data obtained.

4 Paddlewheel theory

This section of the chapter outlines the basic concept of how the paddlewheel works. It then sets out the current theory used to calculate the efficiency and discharge of a paddlewheel, and puts forward a new theory based on the hydrostatic pressures acting on the blade of the wheel as it lifts the fluid.

4.1 How a paddlewheel works

In order for fluid to travel around the raceway it must be given sufficient energy to overcome any frictional and turbulent losses that occur. The energy can be transmitted by increasing either the kinetic energy (velocity head) or the potential energy (hydraulic head) (Figure 4.2). If the paddlewheel "pushes" the water the energy gained would be the increase velocity head of the fluid. As the water travels around the raceway it will lose energy due to friction with the side walls. This loss of energy will result in a loss of fluid velocity and as a result the upstream fluid velocity will be higher than the downstream velocity. To maintain discharge continuity the downstream depth would have to be lower than the upstream depth. Figure 4.1 shows the discharge downstream of the paddlewheel, discretised into blocks of water. If the energy gained by the paddlewheel is in the form of velocity head which decreases as it flows around the raceway then for each discretised block to have the same area the depth would have to increase. As this is not the case, the paddlewheel must be increasing the hydraulic head by 'lifting' the fluid to give a higher depth upstream. The fluid is then driven by the surface gradient under gravity around the system to the downstream side of the paddlewheel where it is then lifted again

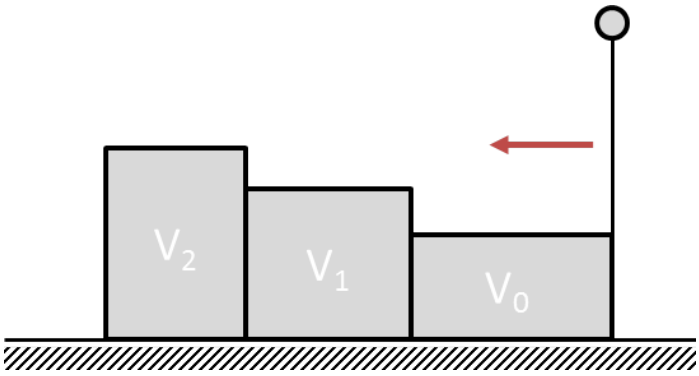

Figure 4.1. Conceptual sketch of the discharge if the paddlewheel "pushes" the water. The velocity scale is shown along the ground where $V_0 > V_1 > V_2$.

Figure 4.2 shows how the hydraulic head is increased by the wheel and then decreases as the water flows around the raceway and the energy is lost to friction and turbulence in the system. At the same time the opposite occurs for the velocity head as this will increase as the water travels around the raceway in order to maintain discharge continuity.

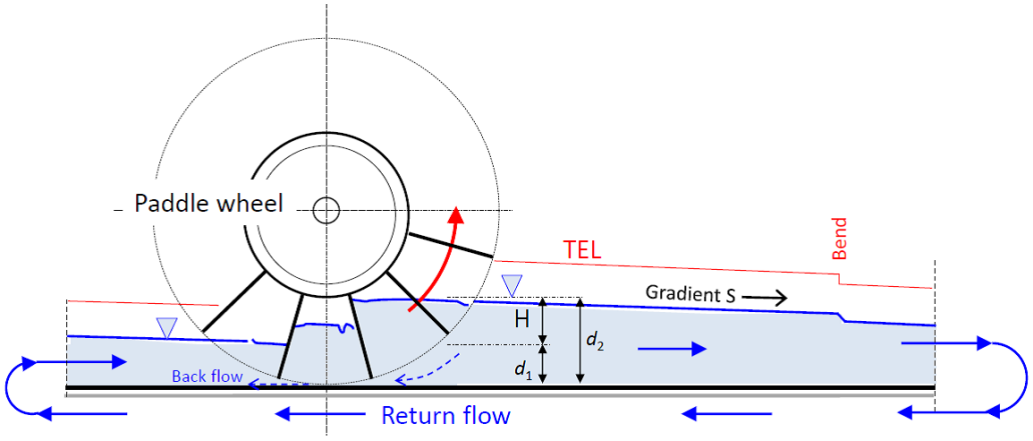

Figure 4.2. Conceptual diagram of the changes in velocity and hydraulic head as the fluid travels from the upstream to the downstream side of the wheel.

4.2 Previous theoretical models for paddlewheels

4.2.1 Discharge

To calculate the discharge of a paddlewheel, the first step is to consider a single blade passing through the fluid. Figure 4.3 shows a diagram of a blade halfway through its stroke and the different fluid parameters that may affect its motion.

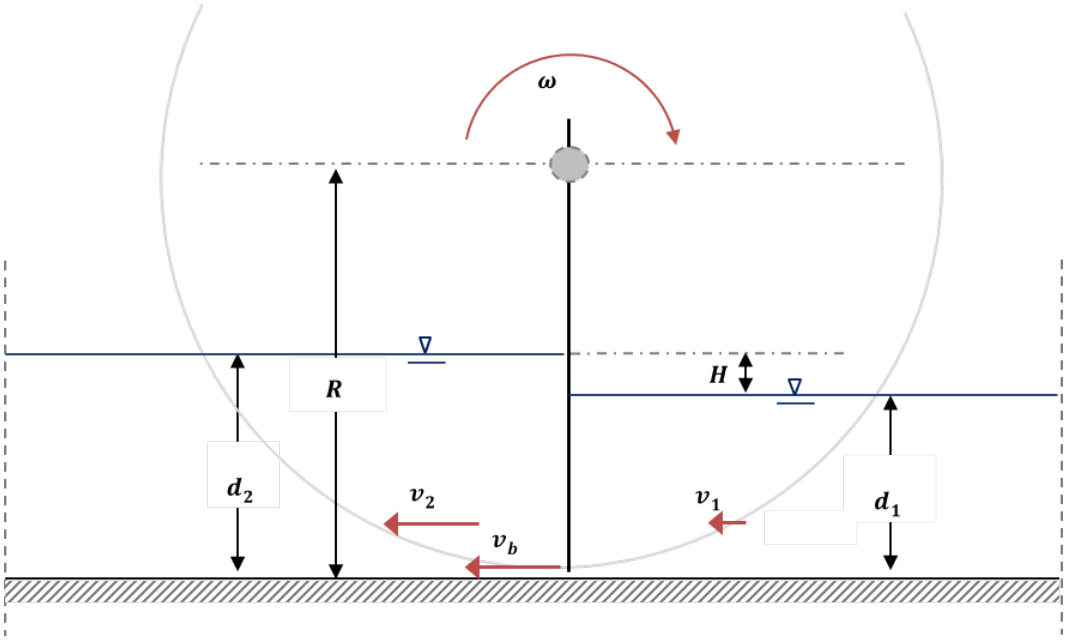

Figure 4.3. Cross section of the wheel and the different parameters which are used in the theory

There is very little information in the literature with regard to calculating the theoretical discharge or performance of a paddlewheel. One method proposed by Park et al. (2014) to calculate the theoretical discharge is to use Newton's second law:

$$F = ma \qquad \text{Equation 4.1}$$

where F is the force exerted on the fluid by the blade (N), m is the mass of water for a control volume (kg), a is the acceleration (m s^{-2}). If a control volume is considered which is accelerated by the blade across a control time (Δt) from a velocity at time 0 (v_0) to a velocity at time t (v_t) then the acceleration and mass of the fluid can be defined as:

$$a = \frac{v_t - v_0}{t} \qquad \text{Equation 4.2}$$

$$m = \rho V \qquad \text{Equation 4.3}$$

Then:

$$F = \rho V \frac{v_t - v_0}{\Delta t} \qquad \text{Equation 4.4}$$

where v_0 and v_t is the velocity at time *0* and *t* respectively (m s^{-1}), Δt is a change in time (s) and V is the control volume which is accelerated by the movement of the blade (m^3). In Figure 4.3 v_0 and v_t can be assumed to be v_1 and v_b respectively.

As discharge is unit volume per unit time ($V/\Delta t$), the force exerted on the blade travelling through the water can be given as:

$$F = \rho Q(v_t - v_0)$$ Equation 4.5

If the initial velocity (v_0) is zero then the equation can be reduced to:

$$F = \rho Q v$$ Equation 4.6

This can be arranged to give the discharge:

$$Q = \frac{F}{\rho v}$$ Equation 4.7

Park et al. (2014) stated that the force can be estimated theoretically by calculating the drag force acting on a blade:

$$F_D = \frac{1}{2} C_D \rho v_b^2 A_b$$ Equation 4.8

where F_D is the drag force (N), C_D is the coefficient of drag (-), v_b is the tangential velocity at the tip of the blade (m s^{-1}) and A_b is the wetted area of a blade (m^2).

The drag force acting on an object moving through a fluid is a function of the speed of the object relative to the fluid. The equation used by Park et al. (2014) assumes that there is no inflow velocity of the fluid and therefore is stationary as the blade moves through the fluid. This is incorrect as there is an inflow velocity and as a result this equation will lead to an over estimation of the force acting on the blade.

If there is a complete transfer of energy between the blade and fluid then the exit velocity of the fluid and the blade are the same, giving rise to:

$$Q_T = \frac{1}{2} C_D v_b d_1 B$$ Equation 4.9

where Q_T is the theoretical discharge (m^3 s^{-1}) and B is the width of the blade (m).

4.2.2 Losses

4.2.2.1 Blade Slip

Losses that occur in a paddlewheel are traditionally referred to as slip, which is the relationship between the velocity of the wheel and the fluid. Camp (1955) defined the slip factor when considering the power of a paddlewheel. This factor is the ratio of velocity of the water to the velocity of the paddlewheel:

$$v_2 = \left(1 - k_{Slip}\right)v_b \qquad \text{Equation 4.10}$$

where v_2 is the water velocity immediately downstream of the wheel (m s^{-1}) and k_{Slip} is the slippage factor (-).

The value of the slip factor was estimated to be between 0.24 and 0.32 (Camp, 1955). Others linked this factor to the blade velocity and found that there was a linear relationship (Hendricks, 2010), such that:

$$k_{Slip} = 0.074 + 0.007\ rpm \qquad \text{Equation 4.11}$$

This formula proposed by Hendricks implies there is a rise in the slip factor as the blade velocity rises, resulting in a fall in the efficiency as less of the blade velocity is transferred into water velocity.

4.2.2.2 Wave energy

The waves that are produced by the paddlewheel result from the backflow when the blade leaves the water. As the blade starts to leave the water the movement direction of the blade is more upwards and at the same time the water starts to flow beneath the blade: thus a circular fluid motion cell is created on each stroke which then moves downstream with the fluid bulk velocity (Figure 4.4). This has not before been investigated in relation to the paddlewheel; however the equations shown below are for linear wave theory and can be applied to the waves created by the wheel.

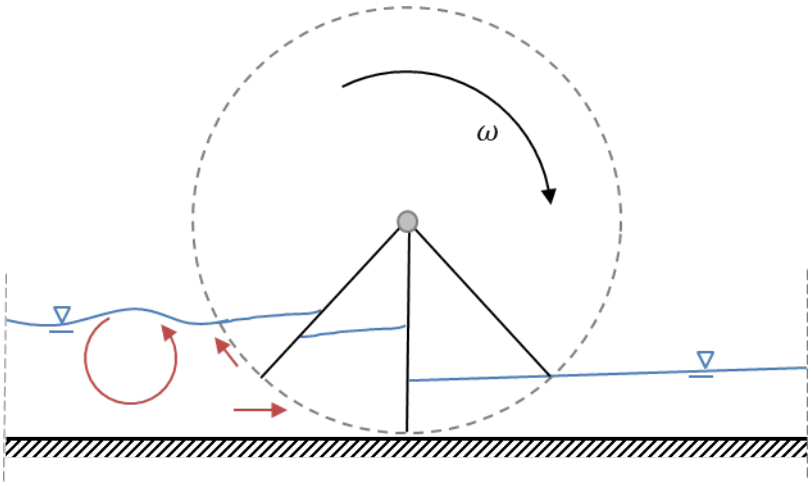

Figure 4.4. Conceptual sketch of how the waves are formed downstream of the paddlewheel. The red arrows located in the fluid indicate the movement of the fluid at different stages of the blades passage.

The energy in waves does not improve the fluid mixing or the forward velocity, but simply moves the water particles in a circular motion as shown in Figure 3.17, Section 3.5.4. Figure 3.18, Section 3.5.4, shows the parameters for a wave cross section.

For regular waves the energy in the wave is the sum of the kinetic and potential energy. If linear wave theory is assumed this can be calculated from (Waters, 2008):

$$E_W = \frac{1}{8}\rho g H_W^2 \qquad \text{Equation 4.12}$$

where E is the energy density of the wave (J m^{-2}) and H_W is the wave height (m).

As the waves propagate energy is transported and the power can be calculated from

$$P_W = E_W c_g \qquad \text{Equation 4.13}$$

where P_W is the power of the wave per unit width of crest (W m^{-1}) and c_g is the group velocity (m s^{-1})

The group velocity is different in shallow and deep water. In shallow water the wave is affected by the channel bottom, while in deep water the wave is independent of the depth (Waters, 2008).

Shallow water is defined as:

$$\frac{d}{L_W} < \frac{1}{20} \qquad \text{Equation 4.14}$$

where:

$$L = T\sqrt{gd}$$ Equation 4.15

$$T = \frac{60}{n_b \times rpm}$$ Equation 4.16

where d is the fluid depth (m), L_W is the wave length (m), T is the period of the wave (seconds) and n_b is the number of blades of the wheel (-).

In shallow water the wave height must not exceed the condition in Equation 4.17, or it will start to break and the energy will be dispersed (McCowan, 1891):

$$H_W \leq 0.78d$$ Equation 4.17

In shallow water the wave group velocity and wave power is given by:

$$c_g = \sqrt{gd}$$ Equation 4.18

Therefore the power per unit length of wave crest is:

$$P_W = \frac{1}{8}\rho g H_W^2 \sqrt{gd}$$ Equation 4.19

Deep water is defined as:

$$\frac{d}{L_W} > \frac{1}{2}$$ Equation 4.20

where:

$$L_W = \frac{gT^2}{2\pi}$$ Equation 4.21

In deep water the breaking of the wave is determined by the wave length (Michell, 1893). The height must not exceed the condition given in Equation 4.22:

$$H_W \leq \frac{L_W}{7}$$ Equation 4.22

In deep water the wave group velocity and wave power is given by:

$$c_g = \frac{gT}{4\pi}$$ Equation 4.23

and

$$P_W = \frac{1}{32\pi}\rho g^2 H_W^2 T$$ Equation 4.24

In practice most raceways are likely to be classified as intermediate rather than shallow or deep. This can be deduced from Figure 4.5 which shows the relationship between the time period of a wave and the depth to wave length ratio. Water bodies with ratios over

20 can be classed as shallow and those with ratios less than 2 as deep water. Those with wave time periods between 0.3 and 2.8 seconds are intermediate. This corresponds to a rotational speed of between 3 - 25 rpm and 2 - 16 rpm for an 8 and 12-bladed wheel respectively, and is where most raceway wave time periods lie (Green Diamond Co. Ltd, 2010; Parry Nutraceuticals, 2011).

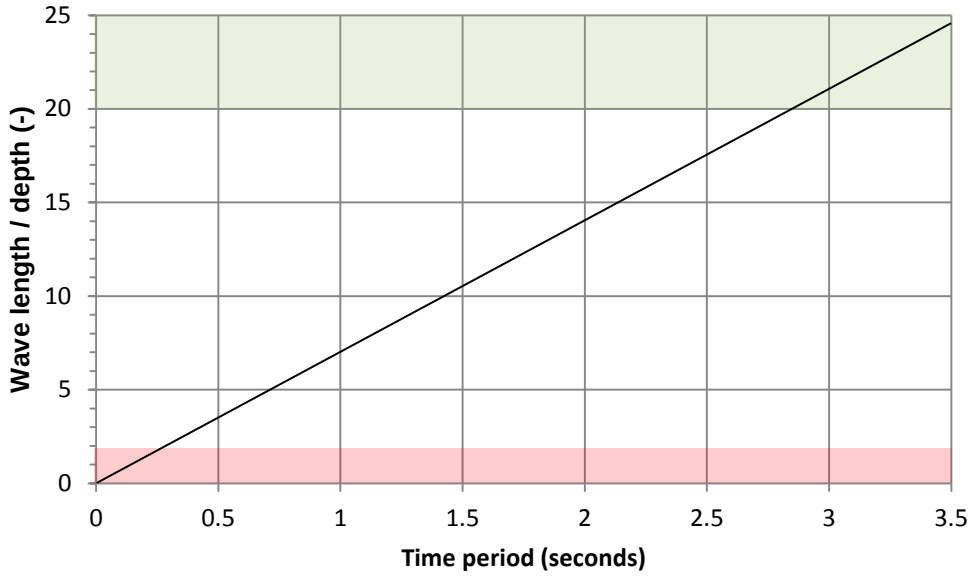

Figure 4.5. Comparison of the ratio of depth to wave length and the time period of the wave. The red area indicates that deep water wave theory applies and the green zone indicates that shallow water wave theory applies. The values where calculated using a depth of 0.2 m.

For intermediate waves, between the deep and shallow condition, the wave length can be calculated for any given time period from Equation 4.25 (Dingemans, 1997):

$$\left(\frac{2\pi}{T}\right)^2 = \frac{2\pi g \tanh\left(\frac{2\pi d}{L_W}\right)}{L_W} \qquad \text{Equation 4.25}$$

The group velocity can then be found using:

$$c_g = \frac{1}{2}\sqrt{\frac{g}{k_W}\tanh(k_w d)}\left(1 + \frac{2k_W d}{\sinh(2k_W d)}\right) \qquad \text{Equation 4.26}$$

where the wave number (k_W) is:

$$k_W = \frac{2\pi}{L_W} \qquad \text{Equation 4.27}$$

The power per unit width of crest can then be calculated using Equation 4.13 so that the power is given by:

$$P_W = \frac{1}{16}\rho g H_W^2 \sqrt{\frac{g}{k}\tanh(k_W d)}\left(1 + \frac{2k_W d}{\sinh(2k_W d)}\right)$$ Equation 4.28

The wave height, time period and depth are the three factors that determine the wave power for all depth conditions. In the case of a paddlewheel-driven raceway, the time period for each wave is the time between each stroke of the blade and it is therefore directly linked to the rotational speed and the number of blades (Equation 4.16). Figure 4.6 presents the relationship between the wave power and the time period of the wave, calculated for a depth of 0.2 m with a wave height set to 0.05 m. The ratio of L_W/d changes from deep to shallow as the time period increases, as shown by the red and green shaded areas. The difference between the results for the shallow water and deep water power equations is large, and it is thus very important to apply the correct wave power equation depending on the depth condition.

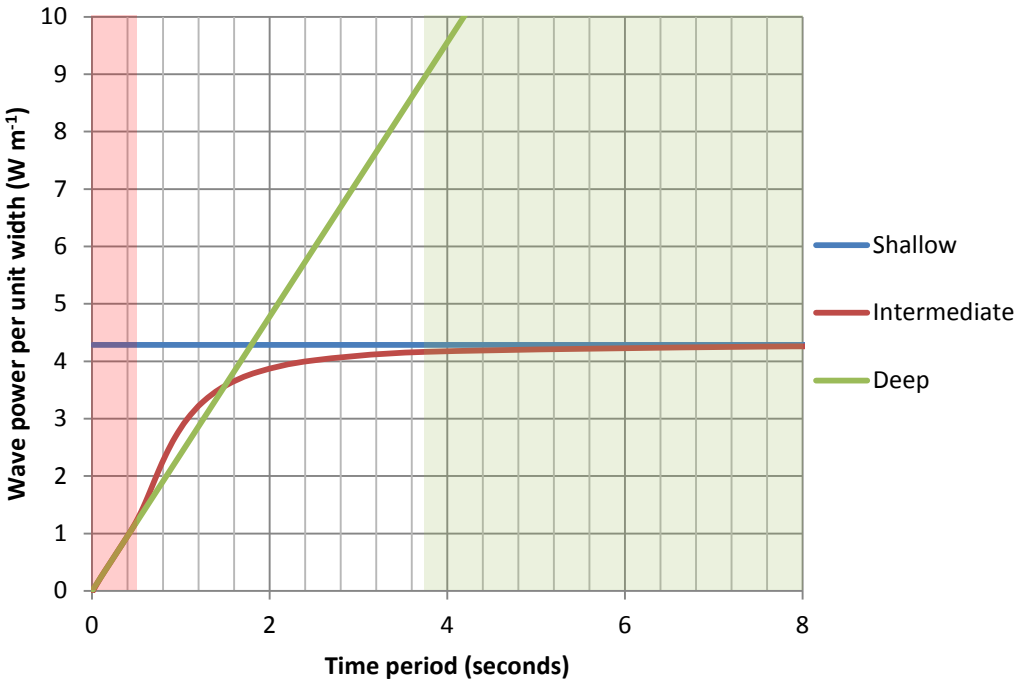

Figure 4.6. Relationship between the wave time period and the wave power per unit width per hour. The red area indicates that deep water wave theory applies and the green zone indicates that shallow water wave theory applies. The power values where calculated using a depth of 0.2 m and a wave height of 0.05 m. The legend indicates the method or formula used to calculate the power.

As the time period of the wave is linked to the number of blades and the rotational speed of the wheel, the wave power can be directly compared to the speed of the wheel. Figure 4.7 shows this for a range of wheels with a fluid depth of 0.2 m and wave height of 0.05 m, calculated using the intermediate depth equations. As the rotational speed is

inversely proportional to the time period of the wave the deep water condition is at high rotational speed and shallow water at low speed. The results show that to ensure the waves consume as little energy as possible the rotational speed should be very high. At higher rotational speeds, however, there are likely to be other energy losses as a result of greater turbulence and frictional losses. Increasing the number of blades further reduces the wave power, as this reduces the time period of the waves. The wave height used was fixed: however this may not be a valid assumption as the wave heights produced are likely to vary depending on the speed of the wheel. The wave height must reduce as the speed increases, otherwise the waves will start to crest and break as the wave length decreases, according to Equation 4.24.

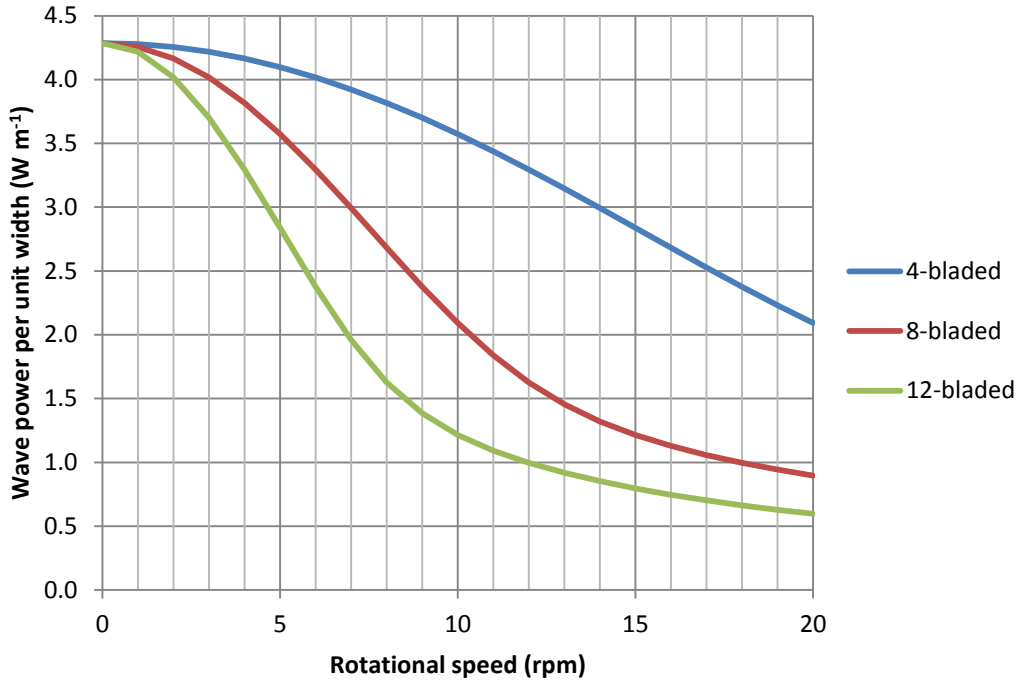

Figure 4.7. Comparison of the wave power per unit width per hour with the rotational speed and blade number of the wheel. The power values where calculated using a depth of 0.2 m and a wave height of 0.05 m. The legend indicates the number of blades that comprise the wheel. The intermediate depth equations were used to calculate the power.

The intermediate power calculated using Equation 4.28 gives a good estimate for the wave power in both the shallow and deep water conditions and therefore can be used for all cases.

To evaluate how wave height affects the wave power, depths of 0.05, 0.1 and 0.3 m were considered with a fixed wave time period of 1 second. This corresponds to a 12-bladed wheel at 5 rpm or an 8-bladed wheel at 7.5 rpm. It is clear from Figure 4.8 that as

the wave height increases the difference in the power rises quadratically in accordance with the power equations. The wave power is also slightly greater as the depth increases.

The energy in the waves could be utilised using the approach set out in Figure 3.18, Section 3.5.4.1. This idea involves raising the bed of the channel in order to reduce the depth and induce the wave to break. If this is done then the energy will be dispersed through the fluid, with a small gain in the forward bulk velocity and also in mixing and gas transfer. The deeper the fluid the higher the raised area needs to be for the waves to break.

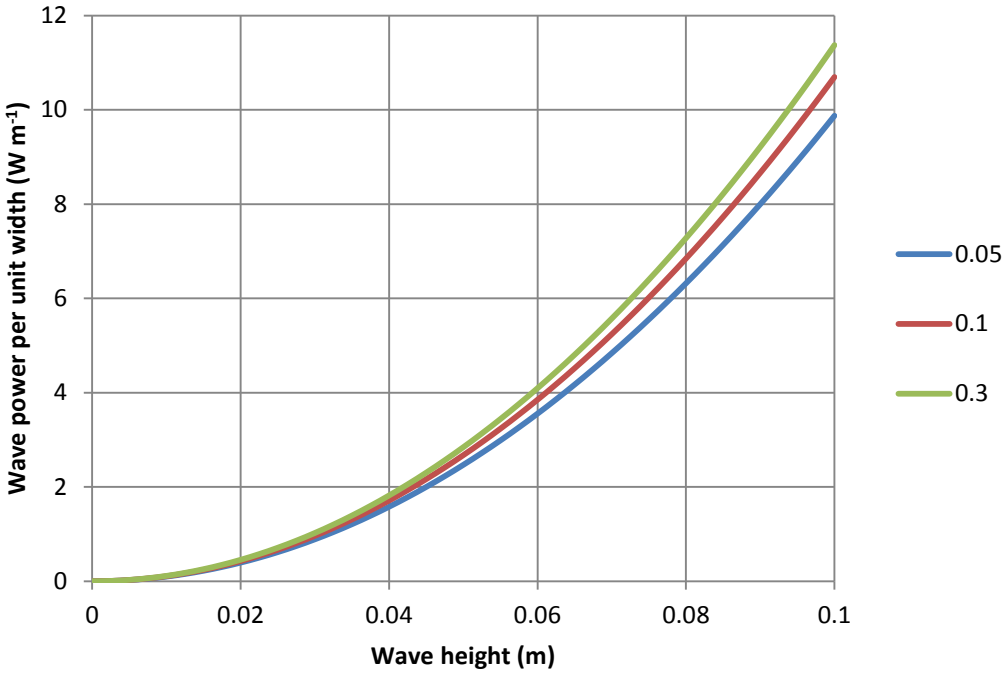

Figure 4.8. Comparison of the wave height and resultant wave power. The legend indicates the fluid depth. A wave period of 1 second has been used. The intermediate depth equations were used to calculate the power.

4.2.2.3 Turbulence

The theory described thus far only accounts for a single blade moving with the fluid at a constant velocity equal to that in the upstream section of the raceway. In practice multiple blades enter the upstream fluid at an angle with a velocity greater than that of the upstream fluid and rotate through the fluid to the downstream section at a greater speed than the fluid. This difference between the blade and fluid velocity together with the entry and exit of the blades is the main source of turbulence in the system.

The process described above is too complex for theoretical calculation without using some sort of computational modelling. Even if computational modelling is used there will be errors in the solution, these are quantified as a residual. If the solution has not converged to acceptable level then it may not accurately predict the behaviours of the fluid well enough to be used. It has therefore been proposed to calculate the turbulent losses from empirical data and assume that these are a function of the velocity squared (Linton, 2014), such that:

$$F_{Turb} = K_{Turb} {v_b}^2 \quad \text{Equation 4.29}$$

where F_{Turb} are the turbulent losses and K_{Turb} is the empirical turbulent loss value.

This value for loss can be applied directly to the hydraulic power such that:

$$P_{hyd_{Turb}} = P_{hyd} - F_{Turb} \quad \text{Equation 4.30}$$

where $P_{hyd_{Turb}}$ is the hydraulic power with the turbulent losses taken into account (W).

Values for these losses and for K_{Turb} were not calculated in the current work but can be found from the difference between the theoretical and experimental results where indicated.

4.2.3 Shaft power

As discussed at the start of this chapter the paddlewheel does not work by simply pushing the water forwards, but by raising the downstream depth. If the discharge and upstream and downstream depths can be measured then Bernoulli's equation can be applied to calculate the head loss (Equation 3.6, Section 3.2.4). This would, however, require empirical testing to be done. It is possible to estimate the power of the wheel by calculating the drag force of the fluid acting on each blade as it passes through (Park et al., 2014):

$$F_D = \frac{1}{2} C_D \rho v_b^2 A_b \quad \text{Equation 4.31}$$

As explained in Section 4.2.1 this equation used by Park et al. (2014) assumes that the fluid is stationary as the blade moves through it. This is incorrect as there is an inflow velocity and as a result this equation will lead to an over estimation of the force acting on the blade and as a result the shaft power calculation will also be greater.

From this the power per blade can be found by multiplying by the speed of the blade:

$$P_b = F_D v_b = \frac{1}{2} C_D \rho v_b^3 A_b$$ Equation 4.32

where P_b is the power of a single blade (W).

The tangential velocity at the tip of the blade velocity can be calculated from the linear blade velocity:

$$v_b = \omega R$$ Equation 4.33

where R is the radius of the blade (m) and ω the rotational velocity (rad s^{-1}). By substituting in Equation 4.33 into Equation 4.32:

$$P_b = \frac{1}{2} C_D \rho \omega^3 R^3 A_b$$ Equation 4.34

As the blades passes through the fluid the angle of attack changes, and this leads to a change in the drag coefficient of the blade. The maximum drag will occur when the blade is perpendicular to the fluid. Park et al. (2014) altered the drag coefficient accordingly allowing the total power of the paddlewheel to be calculated:

$$C_{D\theta} = C_D \cos\theta$$ Equation 4.35

$$P_{S_T} = \frac{1}{2} C_{D\theta} \rho \omega^3 \sum_0^{n_b} R^3 A_b$$ Equation 4.36

where P_{S_T} is the theoretical shaft power (W), $C_{D\theta}$ is the drag coefficient at an angle of attack of θ (-) and n_b is the number of blades (-).

The loss of power through leakage of fluid around and beneath the blades can be introduced as a slippage factor using Equation 4.10. This gives rise to:

$$P_{S_T} = \frac{1}{2} C_{D\theta} \rho \big((1-k)\omega\big)^3 \sum_0^{n_b} R^3 A_b$$ Equation 4.37

This theoretical derivation of the shaft power of a paddlewheel was first devised by Thomas Camp (1955) and has been investigated thoroughly by Hendrick, 2010 and Park et al. (2014). It takes no account, however, of the change in head across the wheel itself; the method is therefore unlikely to be accurate as the head across the wheel is one of the determining factors which affect the shaft power and hydraulic power. It also makes the assumption that the initial velocity $v_1 = 0$ which is not correct; and thus this equation can only be applied in very deep channels. This theory is tested in Section 5.3.1.

4.2.4 Efficiency

The efficiency of the wheel is the ratio of useful output power to total input power. If the useful output is taken as the hydraulic power gained which can be expressed by:

$$P_{hyd} = \rho g H Q \quad \text{Equation 4.38}$$

where

$$Q = dBv \quad \text{Equation 4.39}$$

where P_{hyd} is the hydraulic power (W), H the head gained (m), B is the channel width (m), v the fluid velocity (m s^{-1}).

The input power is the shaft power transferred from the motor to the wheel, the efficiency is:

$$\eta = \frac{P_{hyd}}{P_{S_T}} \quad \text{Equation 4.40}$$

where η is the wheel efficiency (-) and P_{hyd} is the hydraulic power (W).

The method derived by Thomas Camp (1955) for calculating the shaft power does not take into account the head difference and as a result cannot be used to calculate the hydraulic power and the traditional efficiency value as defined by Equation 4.40. The results can, however, be compared to the discharge (Equation 4.50) to give a relative discharge per power input:

$$Q_R = \frac{Q}{P_{S_T}} \quad \text{Equation 4.41}$$

where Q_R is the relative discharge (m^3 s^{-1} W^{-1})

Figure 4.9 shows the theoretical relative discharge calculated using Equation 4.37 across a range of rotational speeds. It can be seen that the flow rate per unit power decreases rapidly with rising rotational speeds. This is expected as there is a cubic increase in the shaft power requirement (Equation 4.37) and only a linear increase in the fluid discharge (Equation 4.9). This indicates that slower rotating wheels are more efficient in terms of discharge.

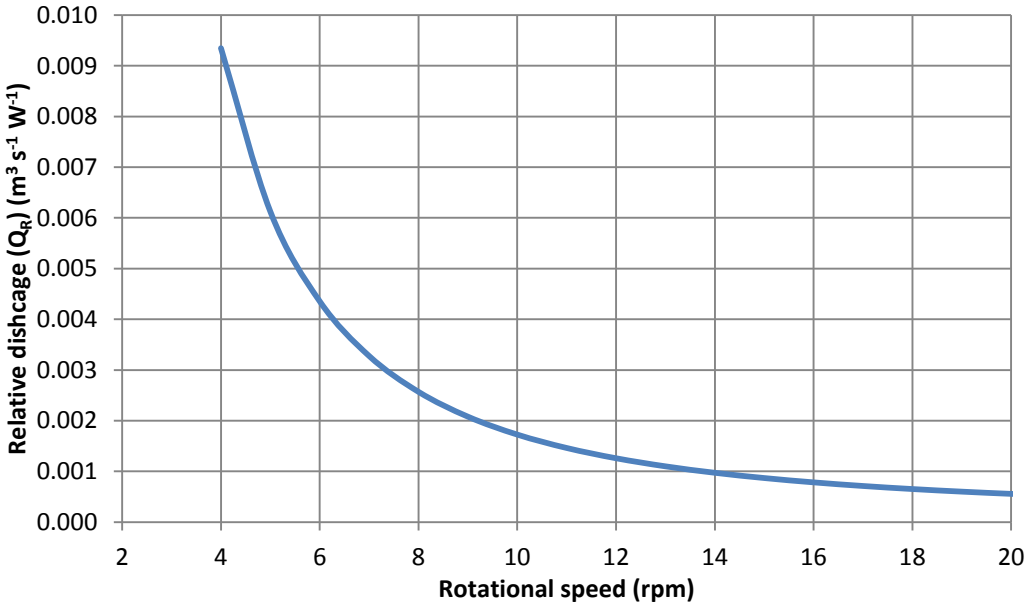

Figure 4.9. Theoretical relative discharge across a range of rotational speeds. Calculated using Equation 4.37 where h_2 = 0.13 m, h_2 = 0.2 m and R = 0.75 m.

4.3 Hydrostatic pressure lifting wheel

The theory of the hydrostatic pressure waterwheel was originally described by Senior (2009) for an undershot waterwheel to be used as a hydrostatic pressure converter; he then went on to further refine the model for middleshot waterwheels. The middleshot water wheel theory was further developed by Linton (2014) who went on to describe in detail the energy losses for these waterwheels. These theories have only been developed for middleshot waterwheels, however, and not for paddlewheels. In the current work a new theory has been developed for paddlewheels of finite radius.

4.3.1 Ideal theory

The ideal theory relates to a wheel with an infinite blade radius moving laterally through the fluid. Figure 4.10 shows an idealised paddlewheel which consists of a blade which separates a higher downstream from a lower upstream water level. The blade $B1$ moves forward from point 1 to 2 through a distance l, then the next blade $B2$ enters the water and $B1$ disappears. With a unit width, an upstream water depth d_1 and a downstream water depth d_2 the volume of water V lifted by a distance $d_1 - d_2$ per unit time is:

$$V = v_1 d_1 \qquad \text{Equation 4.42}$$

And the work required to lift the volume V is:

$$W = v_1 d_1 (d_2 - d_1)$$ Equation 4.43

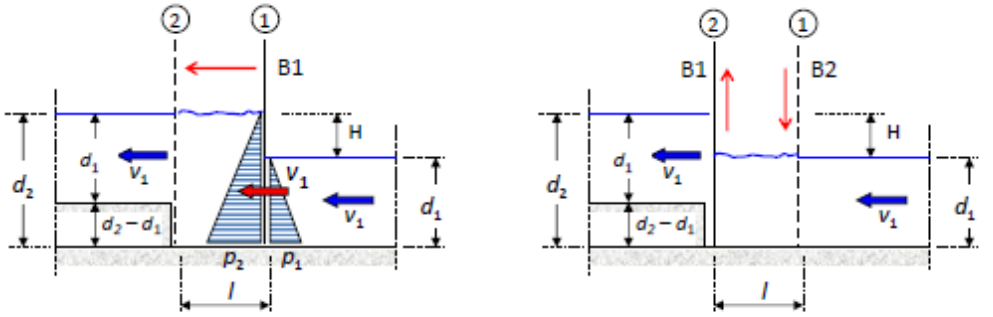

Blade moves forward

Blade B1 exits, new blade B2

Figure 4.10. The ideal Water Lifting Wheel with infinite radius.

The pressures acting on the blade $B1$ are $P_1 = \rho g d_1$ and $P_2 = \rho g d_2$; this gives a resultant force F:

$$F = \rho g \frac{d_2^2 - d_1^2}{2}$$ Equation 4.44

The power P required becomes:

$$P = F v_1 = \rho g \frac{d_2^2 - d_1^2}{2} v_1$$ Equation 4.45

With this, the efficiency η can be determined as *η = W/P:*

$$\eta = \frac{\rho g v_1 d_1 (d_2 - d_1)}{\rho g v_1 (d_2^2 - d_1^2)/2}$$ Equation 4.46

Figure 4.11 shows the hydraulic efficiency as a function of the water depth ratio d_1/d_2. It can be seen that the efficiency drops significantly for lower water depth ratios / higher head differences. Since the water volume is directly related to the upstream depth d_2, this means that the efficiency reduces for a smaller volume being pumped to a greater height. In other words: the paddlewheel performs best for situations where large volumes have to be lifted over small head differences.

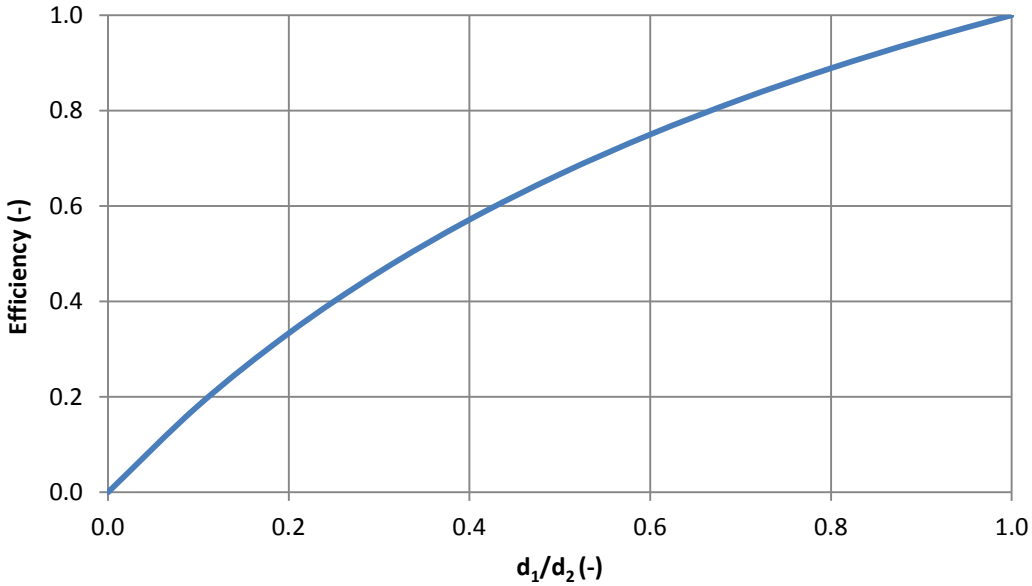

Figure 4.11 Theoretical efficiency as function of water depth ratio d_1/d_2.

4.3.2 Paddlewheels with finite radius

The theory considered above assumes an ideal paddlewheel of infinite radius, but in reality the radius of the wheel will be finite. This affects the torque created by the upstream and downstream acting forces. In addition, back flow and other losses occur. A new theory accommodating this is developed in the following sections, and is analysed and validated in Section 5.3.1.

4.3.2.1 Theoretical discharge calculation

In order to determine a theoretical efficiency for the wheel the hydraulic and shaft power must be calculated. For the hydraulic power to be calculated the discharge must first be known.

The discharge of the fluid from the motion of the blade can be calculated from the continuity equation

$$Q = v_1 A = v_1 d_1 B \qquad \text{Equation 4.47}$$

where A is the cross-sectional area of fluid (m^2) B is the channel width (m)

In order to calculate the velocity of the fluid the linear tangential velocity of a rotating blade must be known. This can be calculated from the rotational velocity and radius of a blade:

$$v_b = \omega R \qquad \text{Equation 4.48}$$

From this equation it can be seen that the linear velocity profile will increase from zero at the centre of the wheel to a maximum at the tip of the blade (Figure 4.12).

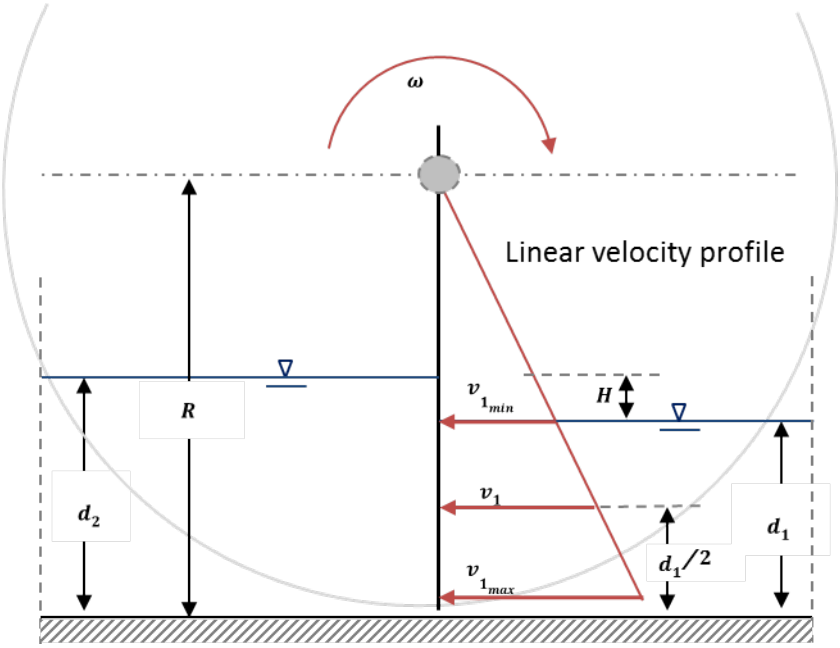

Figure 4.12. Cross section of the channel showing the linear velocity profile of a blade.

If the full radius of the wheel (R) is used this would result in the maximum linear velocity ($v_{1_{max}}$); however the fluid at the surface would be traveling much more slowly than this maximum value (Figure 4.12). For the average upstream fluid velocity the distance to half the depth of water must be used:

$$v_1 = \omega\left(R - \frac{d_1}{2}\right) \qquad \text{Equation 4.49}$$

where $\left(R - \frac{d_1}{2}\right)$ is the distance from the centre of the wheel to half the upstream fluid depth (m).

This gives the theoretical velocity immediately upstream of the wheel which can then be used to calculate the theoretical discharge:

$$Q_T = v_1 d_1 B = \omega \left(R - \frac{d_1}{2}\right) d_1 B \qquad \text{Equation 4.50}$$

where Q_T is the theoretical discharge ($m^3\ s^{-1}$)

Equation 4.9 and Equation 4.50 are fundamentally the same: however the first method uses the empirically derived coefficient of drag rather than a purely theoretical approach.

From Equation 4.50 it is clear that the maximum discharge for any given rotational speed is limited by downstream depth. Figure 4.13 shows how the maximum theoretical discharge increases with rotational speed and also increases with downstream depth.

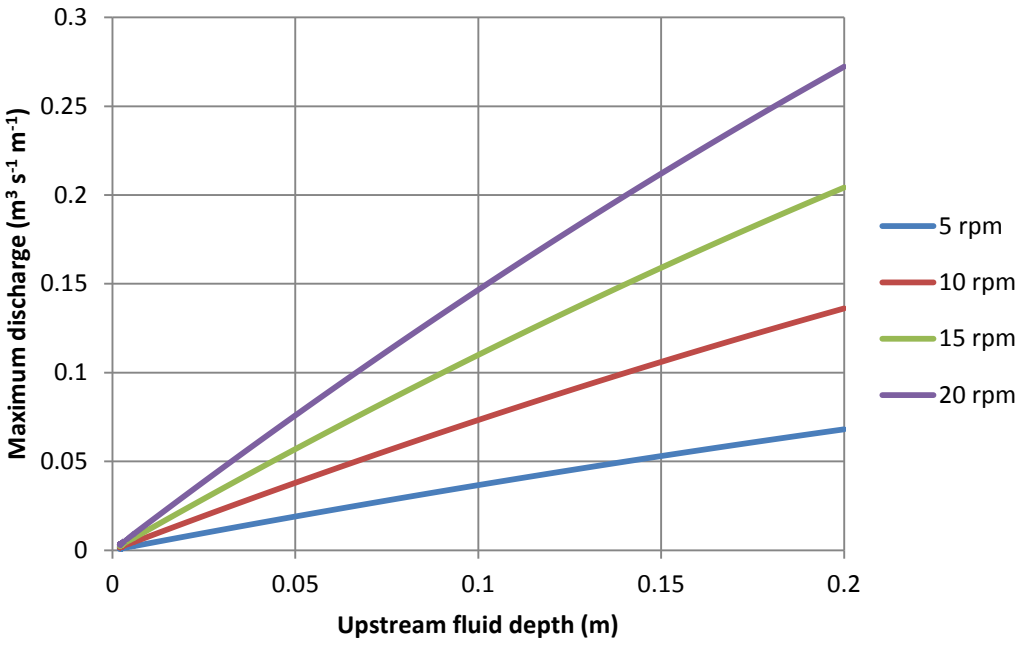

Figure 4.13. Comparison of the theoretical maximum discharge and the upstream depth. The legend indicates the rotational speed of the wheel. The blade length was fixed at 0.75 m.

As the wheel speed increases the head difference increases and the downstream depth decreases, if the volume of fluid in the system is kept constant. This will limit the maximum discharge, because as the upstream depth tends to 0 there is no more fluid to be pumped. This is shown graphically in Figure 4.14 where it can be seen that the upstream depth decreases as the speed of the wheel increases. This leads to a lower rate of increase in the discharge as the wheel speed increases. This is also linked to the leakage discharge, which is another limiting factor on the forward discharge. This occurs

where fluid flows 'backwards' from the higher downstream depth to the lower upstream side of the wheel. As the head difference rises more fluid is driven backwards to the upstream side, and at a certain rotational speed (shown as 'n' on Figure 4.14) any extra head gained is immediately lost to leakage. At this point there will be equilibrium between the forward and backward discharge and any further increase in wheel speed will just pump the fluid lost to leakage.

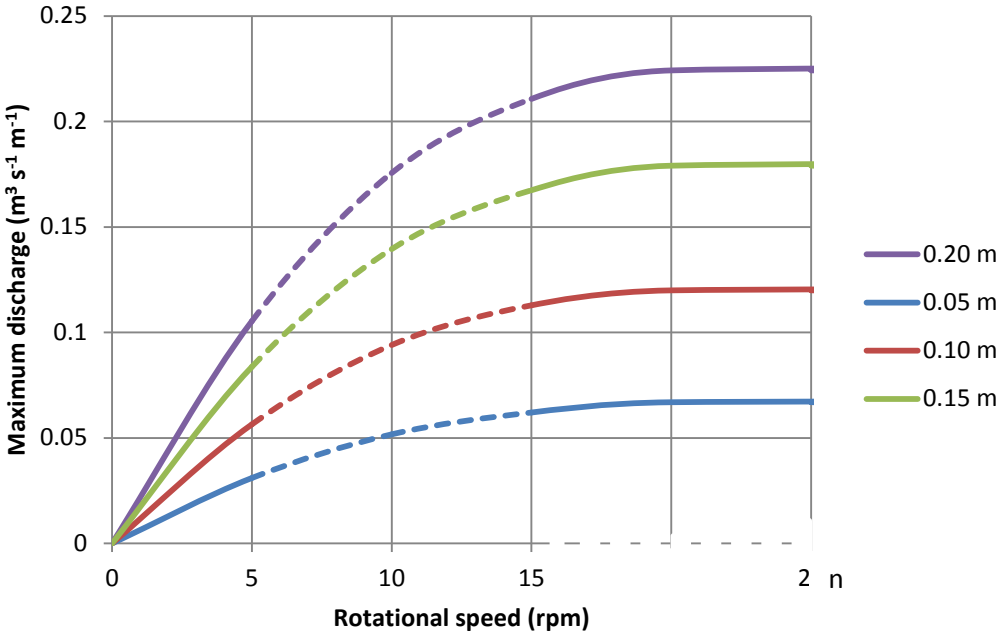

Figure 4.14. Conceptual comparison of the theoretical maximum discharge and the rotational speed of the wheel. The blade length was fixed at 0.75 m. The legend indicates the upstream depth when the paddlewheel is stationary.

4.3.2.2 Shaft power - hydrostatic principles method

The theoretical shaft power and hydraulic power can be calculated by considering a single blade in the vertical position lifting water from a depth of d_1 to d_2 (Figure 4.15).

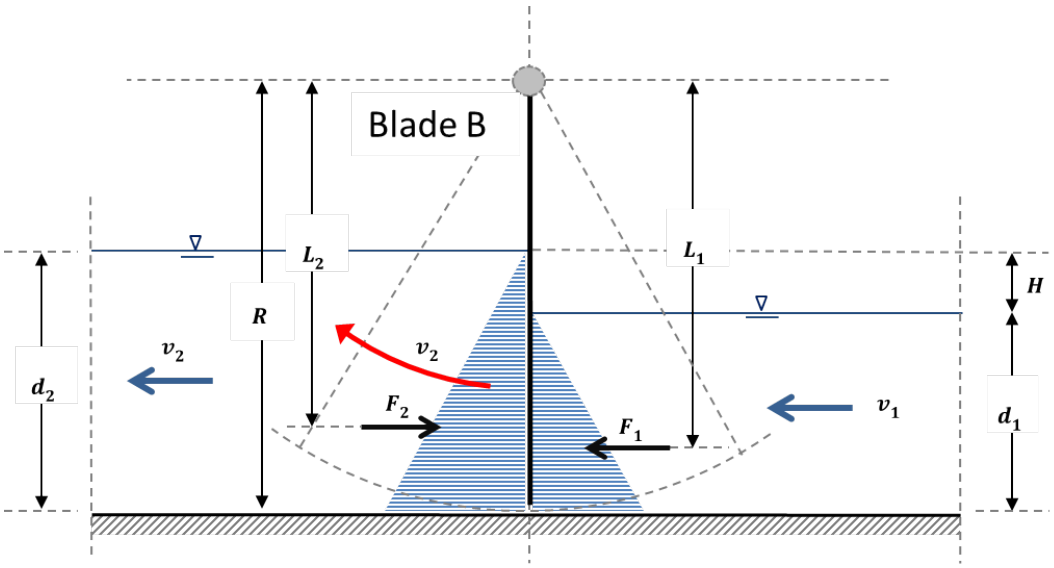

Figure 4.15. Water lifting wheel with finite radius.

The hydrostatic forces F_2 and F_1 are:

$$F_1 = \frac{1}{2}\rho g d_1^2 \qquad \text{Equation 4.51}$$

$$F_2 = \frac{1}{2}\rho g d_2^2 \qquad \text{Equation 4.52}$$

As the forces act at the centre of gravity of the hydrostatic pressure fields:

$$L_1 = R - \frac{1}{3}d_1 \qquad \text{Equation 4.53}$$

$$L_2 = R - \frac{1}{3}d_2 \qquad \text{Equation 4.54}$$

Taking moments about the centre of the wheel:

$$M_{T1} = F_1 L_1 = \frac{1}{2}\rho g d_1^2 \left(R - \frac{1}{3}d_1\right) \qquad \text{Equation 4.55}$$

$$M_{T2} = F_2 L_2 = \frac{1}{2}\rho g d_2^2 \left(R - \frac{1}{3}d_2\right) \qquad \text{Equation 4.56}$$

And the resultant moment per unit width acting on the centre of the wheel:

$$M_R = M_{T2} - M_{T1} = \frac{1}{2}\rho g \left[R(d_2^2 - d_1^2) - \frac{1}{3}(d_2^3 - d_1^3)\right] \qquad \text{Equation 4.57}$$

The shaft power per unit width can then be theoretically calculated from

$$P_{S_T} = \tau_R \omega \qquad \text{Equation 4.58}$$

Substituting in Equation 4.49:

$$P_{S_T} = M_R \omega = \frac{1}{2}\rho g \left[R(d_2^2 - d_1^2) - \frac{1}{3}(d_2^3 - d_1^3)\right] \frac{v_1}{R - \frac{1}{2}d_1} \qquad \text{Equation 4.59}$$

Figure 4.16 compares the relative discharge (Q_R), Equation 4.41, to the normalised head loss ($h_N = H/d_1$), this parameter is discussed further in Section 5.1.3.7.1. It produces very similar predictions to the relative discharge against rotational speed (Figure 4.9). This is to be expected as the normalised head is likely to increase with rotational speed. It is clear, however, that the relative discharge calculated from the traditional method (Section 4.2) is much greater than that obtained from the new hydrostatic method.

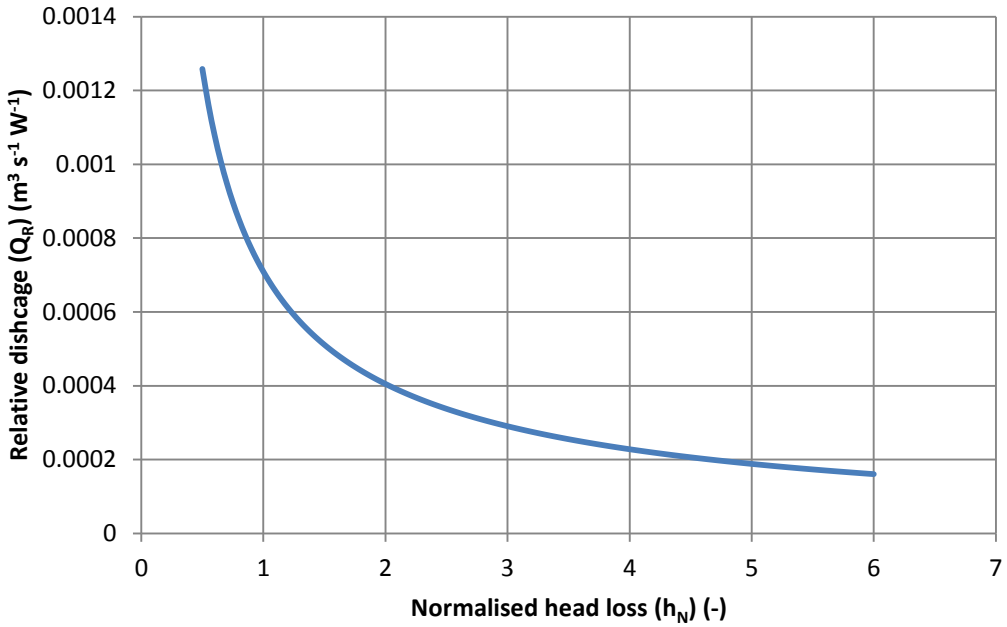

Figure 4.16. Predictions of the relative discharge at different normalised head losses, $h_N = H/d_1$. Where d_2/R = 0.26.

4.3.2.3 Efficiency

As noted above, the efficiency of a paddlewheel is normally taken as the ratio of output to input power (Equation 4.40). A value of 1.0 represents a perfect transfer of shaft to hydraulic power: in reality, however, this cannot be achieved due to losses in the transfer of power.

The hydrostatic principles method of calculating the shaft power as described above takes into account the head across the wheel. This head can then be used to calculate the theoretical hydraulic power per unit width:

$$P_{hyd_T} = \frac{\rho g H Q}{B} = \rho g (d_2 - d_1) d_1 v_1 \qquad \text{Equation 4.60}$$

where P_{hyd_T} is the theoretical hydraulic power per unit width (W m^{-1})

The theoretical efficiency of the wheel can be found from:

$$\eta = \frac{P_{hyd_T}}{P_{S_T}} = \frac{2\left(R-\frac{1}{2}d_1\right)d_1(d_2-d_1)}{R\left(d_2^2-d_1^2\right)-\frac{1}{3}(d_2^3-d_1^3)} \qquad \text{Equation 4.61}$$

If this efficiency is plotted against the normalised head loss (H/d_1) (Figure 4.17), it is clear that the head of fluid across the wheel has a significant effect on the efficiency of the wheel. A maximum efficiency of 1.0 occurs as the normalised head loss tends to 0; the opposite is also true, such that as the normalised head tends to infinity the efficiency drops to 0. This is expected because as the head loss increases the adverse pressure acting on the blade increases. This is shown by the rise in the required shaft power to a maximum at the highest normalised head calculated. The calculated hydraulic power begins to fall after a maximum has been reached at a normalised head loss of 1.0 as the shaft power rises to the maximum.

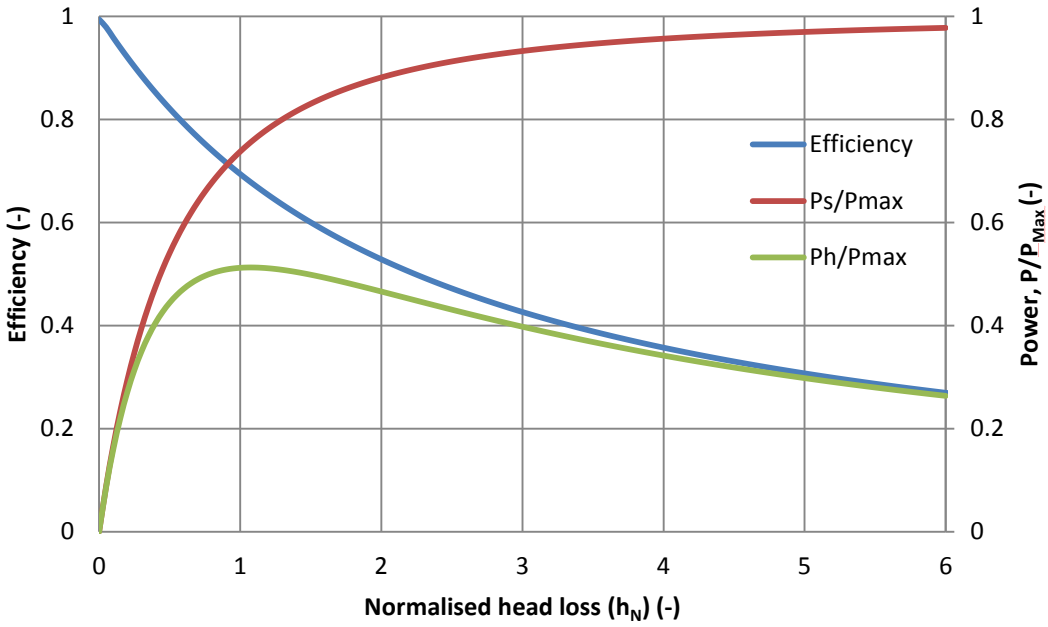

Figure 4.17. Hydrostatic pressure theory to calculate the shaft and hydraulic power and efficiency of the wheel at variable normalised head values ($h_N = H/d_1$). P_{Max} is the maximum shaft power calculated at the highest normalised head. The results have been calculated using d_2/R = 0.26.

As the efficiency of the wheel is a function of the radius of the blade and fluid depths, the ratio of blade radius to depth should be investigated. Figure 4.18 shows the efficiency as a function of the relative water depth d_1/d_2, for different ratios of downstream water depth d_2 and radius r_b, (d_2/r_b). It can be seen that the radius has little influence on the wheel efficiency, with maximum pumping efficiency always

reaching 100 % at a relative water depth of 1. The rate of increase in the efficiency at lower relative water depths is higher when the blade is fully submerged.

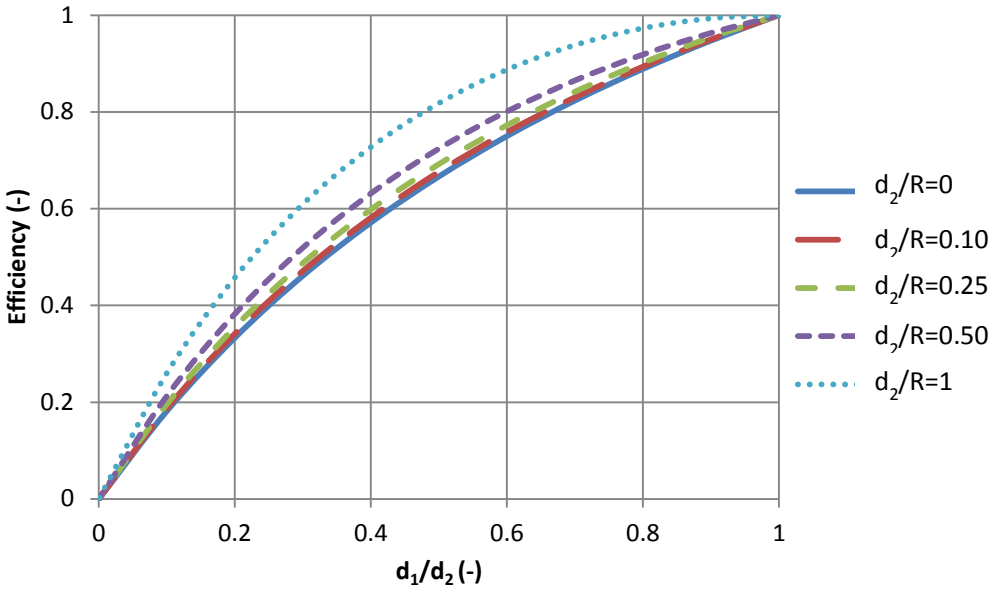

Figure 4.18. Theoretical efficiency as function of water depth ratio d_1/d_2 and different ratios d_2/R = 0.26.

Figure 4.19 shows how the efficiency, shaft and hydraulic power changes as the theoretical discharge increases to its maximum. Initially there is a rise in the hydraulic power as this is dependent on the discharge; however a maximum value for hydraulic power is reached when the discharge value is half of its maximum. The decline in hydraulic and shaft power with further increases in the discharge is a result of the decreasing head difference.

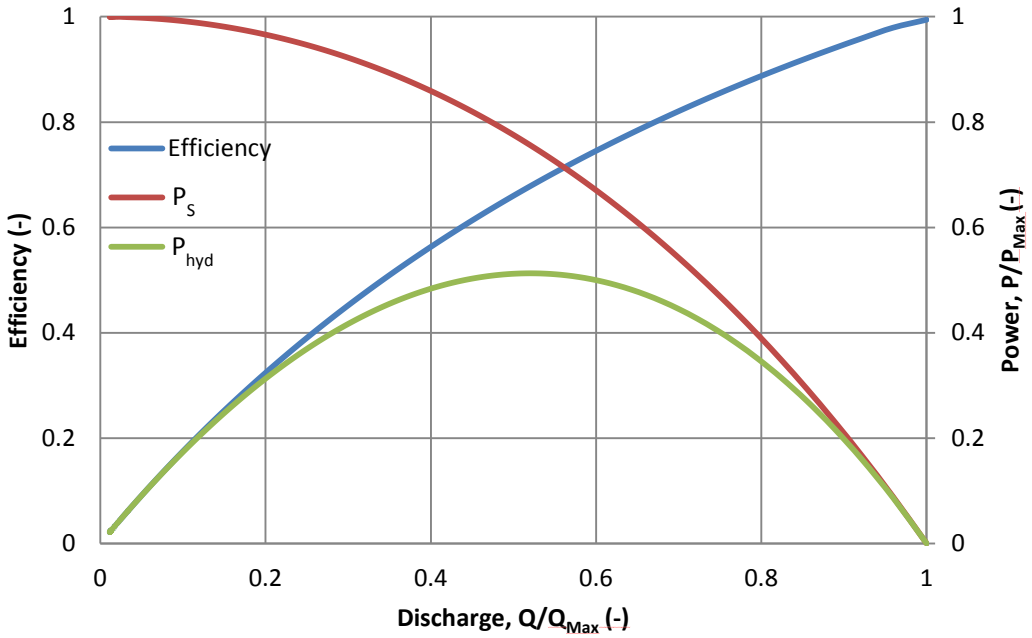

Figure 4.19. Hydrostatic pressure theory to calculate the shaft and hydraulic power and efficiency of the wheel at different flow rates. Q_{Max} is the maximum discharge value calculated. The results have been calculated using *d_2/R= 0.26.*

4.3.2.4 Losses - leakage

Almost all raceways have horizontal beds and this means that a gap exists between the bed and the blades of the paddlewheel, which varies in height as the blades rotate. The head difference created during operation of the wheel drives a backward flow through the gap, thereby reducing the wheel's efficiency.

Using the Torricelli formula, the leakage flow beneath the blades Q_l can be calculated:

$$Q_L = C_d A_g\left(\sqrt{2g(d_2 - d_1)}\right) \quad \text{Equation 4.62}$$

where:

$$A_g = h_{gB}B + 2h_{gS}d_2 \quad \text{Equation 4.63}$$

where A_g is the area around and beneath the blade (m^2), h_{gB} is the bottom clearance gap (m) h_{gS} is the clearance gap around the sides of the blade (m) and C_d is the discharge coefficient.

The discharge coefficient is an empirical value to adjust the flow measured for the fluid depth downstream of the gap. It is normally taken to be around 0.6 to 0.65 for very small openings.

As the clearance gap at the sides of the paddlewheel is much smaller than the gap beneath the blade and the bed, and the depth d_2 is small in comparison with the width, it can be argued that any backflow around the sides can be ignored. Thus the area around the blade can be simplified to:

$$A_g = h_{gB}\mathrm{B} \qquad \text{Equation 4.64}$$

The minimum gap occurs when the blade is vertical and the maximum when it is half way between strokes (Figure 4.20). The higher the number of blades the smaller the distance between strokes, and therefore a smaller the amount of backflow should occur.

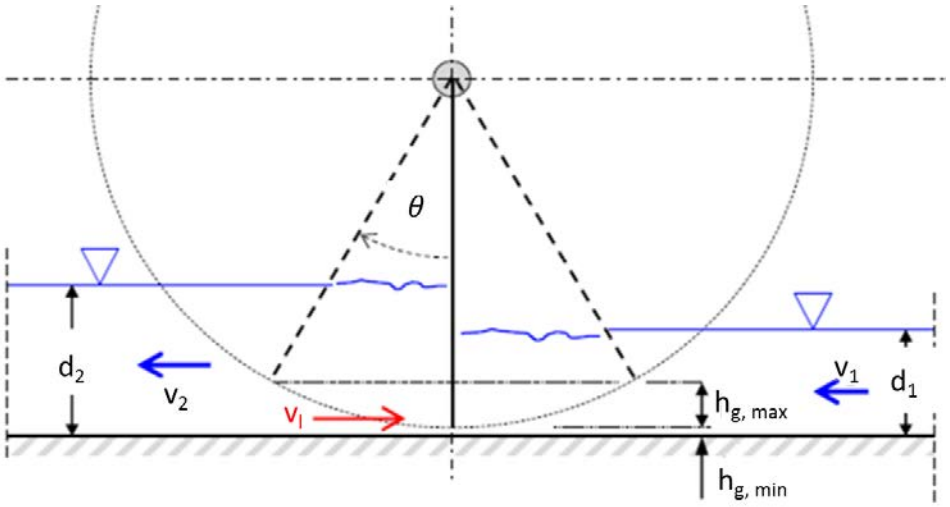

Figure 4.20. Diagram of a single blade and how the gap beneath changes over time. The solid black blades indicate when the wheel is in a position where there is a minimum gap beneath the wheel and the dashed black lines indicate when there is a maximum gap.

The gap beneath the blade as it rotates can be estimated by taking an average of the gap beneath the blade at three equal points between the maximum and minimum gap.

If at $t = 1$ the gap is at a maximum ($\mathrm{h_{g,max}}$) and at $t = 0$ the gap is at a minimum ($\mathrm{h_{g,min}}$). An average of the gaps at $t = 1/4$, $t = 1/2$ and $t = 3/4$ would give the average gap beneath the blade as it rotates.

At:

$t = 1/4$ $\qquad h_g = \left(1 - cos\frac{\theta}{8}\right)$ $\qquad$ Equation 4.65

$t = 1/2$ $\qquad h_g = \left(1 - cos\frac{\theta}{4}\right)$ $\qquad$ Equation 4.66

$t = 3/4$ $\qquad h_g = R\left(1 - cos\frac{3\theta}{8}\right)$ $\qquad$ Equation 4.67

The average gap then is:

$$\overline{h_g} = R\left(1 - \frac{\cos\left(\frac{\theta}{8}\right)+\cos\left(\frac{\theta}{4}\right)+\cos\left(\frac{3\theta}{8}\right)}{3}\right) + \mathrm{h_{g,min}} \qquad \text{Equation 4.68}$$

where $\overline{h_g}$ is the average gap clearance (m), θ angle between the blades (rad).

The leakage discharge can be used to recalculate the theoretical discharge as:

$$Q_{T_L} = Q_T - Q_L \qquad \text{Equation 4.69}$$

where Q_{T_L} is the theoretical discharge accounting for leakage losses ($m^3\ s^{-1}$). This new discharge value can then be used to recalculate the hydraulic power and efficiency.

4.3.2.4.1 The paddlewheel with insert

Apart from reducing the number of blades, the gap losses can be reduced by providing a curved insert on the bed at the upstream side of the wheel. The insert closes off the wheel against the bed, thereby reducing the effective gap width to the clearance gap width $h_{g,min}$. In addition the water is lifted in two stages rather than in one (Figure 4.21); this reduces the effective head difference which cuts the leakage flow by half. If the insert is designed so that more than two blades are always in contact with it a further reduction in the head difference could be achieved.

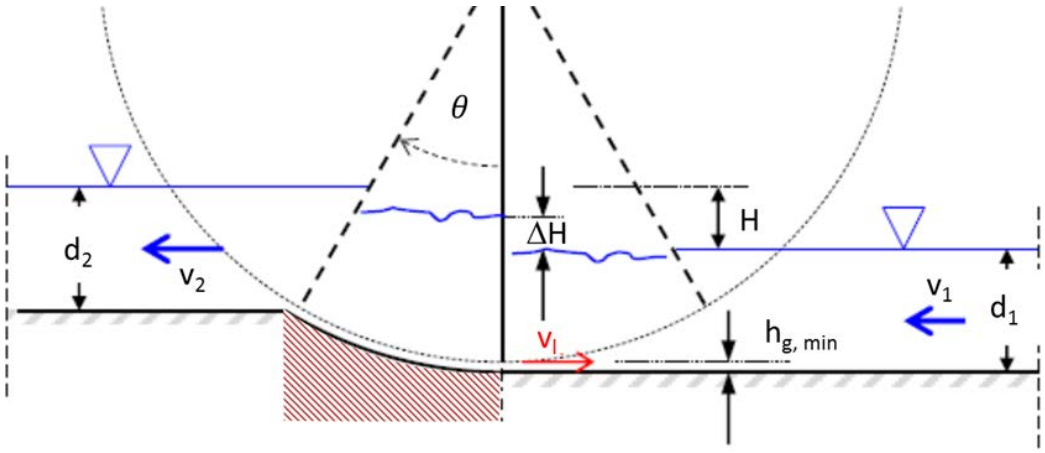

Figure 4.21. The paddlewheel with insert. The insert is shown by the red hashed area.

The insert raises the downstream bed level while allowing the blades to retain the water depth downstream of the wheel, so as to create a gravity drive flow without velocity changes.

This would result in lower energy losses throughout the system and especially at the second end bend of the raceway as velocities through these sections will be lower.

Table 1 shows the effective gap widths for 4, 8, 10, and 12 blades and for a 12-blade wheel with inset. The clearance gap width at the bottom is assumed to be 10 mm, the radius of the wheel r_b= 600 mm.

Table 4.1. Effect of different numbers of blades on the gap around the blades.

Number of blades	4	6	8	10	12	insert
Internal blade angle (rad)	1.57	1.05	0.79	0.63	0.52	
Average gap clearance ($\overline{hg}$) (mm)	0.028	0.018	0.014	0.013	0.012	0.010
Percentage difference of the total gaps to the 4-bladed wheel		-29 %	-43 %	-49 %	-52 %	-60 %

The lower number of blades results in increased gap widths (Table 4.1), which allow larger leakage flows to occur, and thereby reduce efficiencies. Blade numbers of 10 and more reduce the gap width and losses to a minimum, with further increases giving no real benefit.

Figure 4.22 shows the ratio of the theoretical leakage discharge to forward discharge against the normalised head loss. It is clear that there will be a point at which the leakage discharge is higher than the flow discharge and this will occur at the maximum head difference. At this point there will be a maximum forward discharge, as shown in Figure 4.14.

The maximum head difference will be lower when fewer blades are present. The insert is thus a marked improvement over the 12-blade solution as the head difference driving the leakage will be reduced since the water level acting on the following blade is lower.

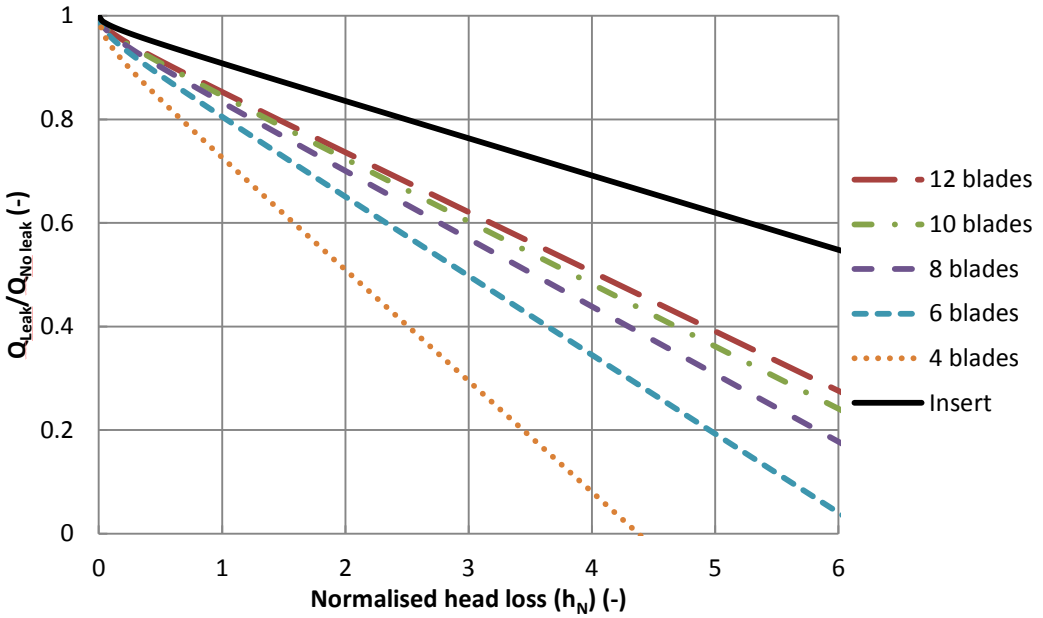

Figure 4.22. Ratio of the discharge of wheels with different blade numbers to the discharge with no leakage. The results have been calculated using d_2/R = 0.26.

If the leakage losses are included then the performance of the wheel is greatly reduced as the hydraulic power will reduce at lower discharge values (Figure 4.23). Even with the insert there is still a large loss in the efficiency of the wheel due to leakage. This loss increases with greater leakage so it is paramount that tolerances around between the blade and the insert are as tight as possible.

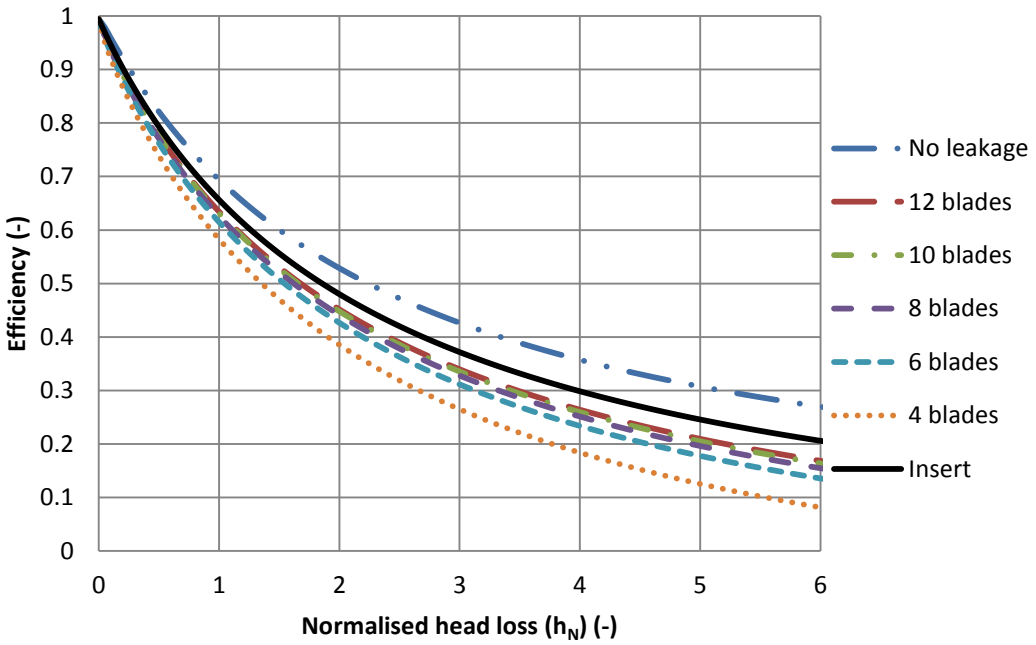

Figure 4.23. The theoretical efficiency of wheels with different blade numbers across a range of normalised heads. The results have been calculated using d_2/R = 0.26.

4.4 Conclusion

There has been little theoretical work done on the paddlewheel as a propulsion mechanism. The theory that has been proposed and used previously for paddlewheels was based on the calculation of the drag force that acts on the blade as it passes through the fluid. It has two major issues:

1. It did not take the head difference across the blade into consideration when calculating the shaft power requirements. This parameter is vital to power requirement as it is the mechanism by which the fluid gains energy from the wheel.
2. In the calculation of the drag force it assumed that the fluid was stationary and had no velocity. This will result in a much greater theoretical fluid drag force than the reality and thus overestimate the power requirement.

A new theory has been proposed based on the hydrostatic pressures acting on the blade with a finite length. The theoretical discharge is based on the rotational speed of the wheel passing through the fluid. This was further developed to include the leakage of the fluid beneath and around the blades as this was seen to be a major loss in the efficiency of the wheel.

The paddlewheel with the insert was theoretically explored. It was shown that by keeping a minimum gap between the tip of the blade and the bed of the raceway at all times the amount of fluid loss to leakage can be greatly reduced. This will lead to a higher forward discharge and thus efficiency of the wheel.

5 The paddlewheel as water propulsion technology

The propulsion of the fluid represents a significant fraction of the total energy required for the production of biomass in algal raceways. Some estimates suggest it can account for around a quarter of the total energy requirement, with others estimating as much as one half (Chisti, 2008; Stephenson et al., 2010). Paddlewheels are widely used as the propulsion mechanism in raceways; however their efficiencies are generally believed to be low and have not been widely studied. The range of reported efficiencies is wide, from 10 to 183 %, mainly due to variations in the experimental procedures used (Brown and Tucker, 2013; Chiaramonti et al., 2012; Betz, 1966; Tevata and Inprasit, 2011; Weissman et al., 1989).

This chapter investigates how different parameters affect the performance of the wheel. Further to this an insert for installation immediately downstream of the paddlewheel was designed and tested with the aim of improving its efficiency. This insert displaces water immediately downstream of the wheel and maintains a constant gap between the bed of the raceway and the bottom of the blade, thus reducing the backflow around the wheel blades.

5.1 Experimental methodology

This section sets out the method used to analyse the performance of the wheel. The same method was used to perform all experiments. The aim of this experimental work was to determine the efficiency of the paddlewheel system as reliably and accurately as possible, and then to improve this by altering its design. A numerical investigation into paddlewheels was deemed to be impractical as this would be a transient problem which would likely lead to large computational requirements and possibly non-converging and unreliable results. To investigate the paddlewheel a 1:5 scale model of a raceway and wheel was therefore constructed and used to measure the efficiency of the wheel (Figure 5.1).

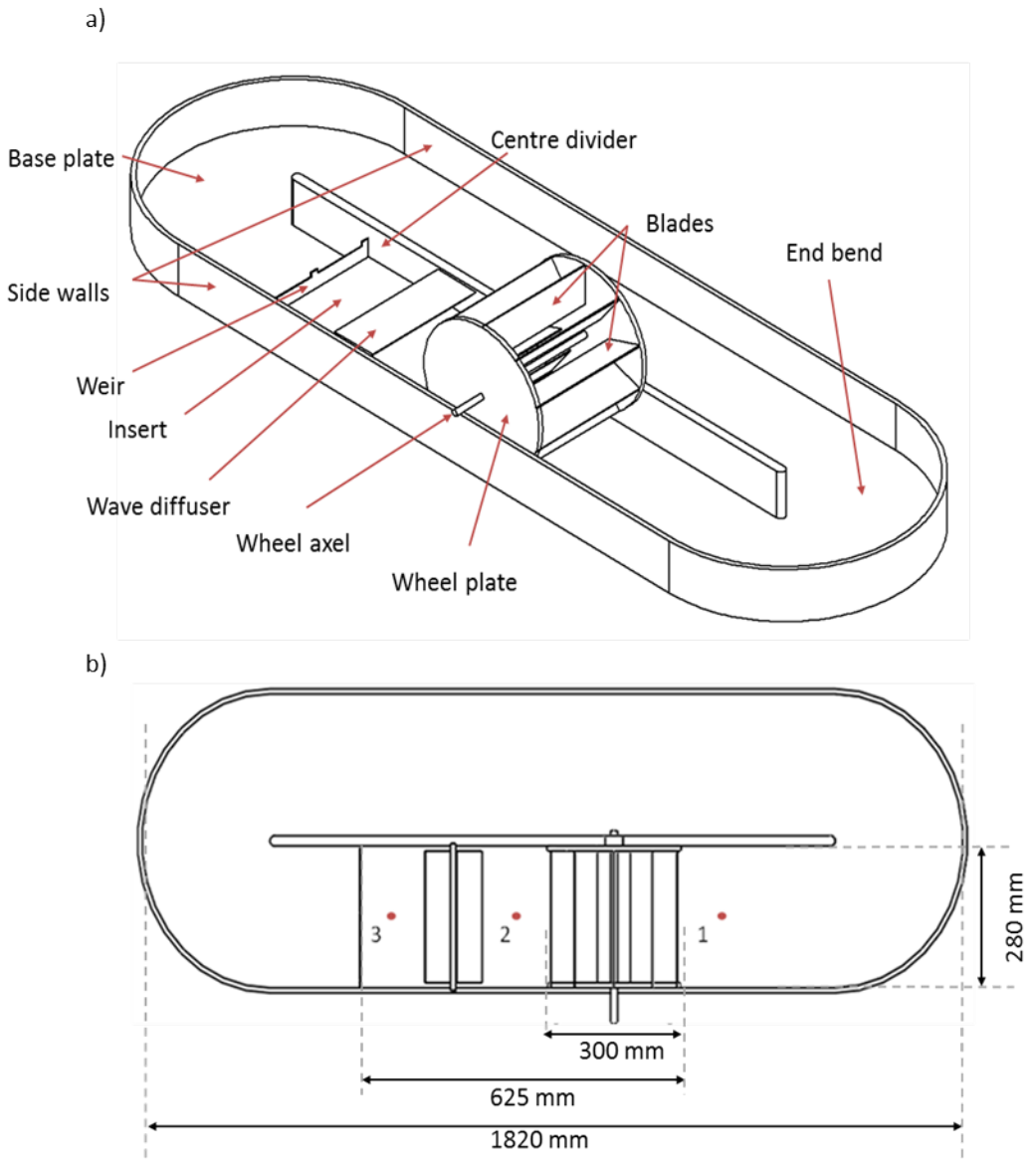

Figure 5.1. Schematic of the raceway model and location of the piezometer measurement locations.(a) principal components, (b) dimensions. The detailed designs and dimensions for each component are shown in Appendix B.

5.1.1 Measuring the paddlewheel efficiency

The paddlewheel efficiency can be found from the ratio of the output to input power of the paddlewheel (Equation 4.40).

5.1.1.1 Measuring the shaft power

To be able to calculate the paddlewheel efficiency correctly the power input must be reliably known. The power input to the motor can easily be measured as electrical power; as motor efficiencies depend on the speed at which they are run, however, the power transferred to the paddlewheel will vary considerably under different conditions.

Therefore the input power used to calculate the efficiency of the paddlewheel should be the input power to the paddlewheel or the output power of the motor. This power is known as the shaft power and is the amount of work that is done by the motor over a given time.

The shaft power of the motor can be determined by calculating the difference in electrical power when it is run operationally and in clear conditions:

$$P_S = P_{operational} - P_{clear} \quad \text{Equation 5.1}$$

where P_S is the shaft power (W). P_{clear} is the power required to drive the motor and wheel when the system is clear of fluid (W), which is the power required to overcome the inefficiencies in the motor and transfer system. $P_{operational}$ is the power required to drive the fluid and to overcome the inefficiencies in the system (W).

This method of measuring power is relatively simple and inexpensive; however it has led to large inaccuracies and unreliable data in previous work on paddlewheels. One of the major errors in this method is that the motor efficiency will change depending on the power requirement and rotational speed and this change may not be accounted for. This is shown in the work of Weissman et al. (1989) who used this method to calculate the paddlewheel efficiencies in a 1000 m^2 raceway and found that they ranged from 1.83 to 0.4 across a range of velocities of 0.15 to 0.40 m s^{-1}.

To calculate the shaft power more accurately the torque must be measured and used to calculate the power:

$$P_S = \tau_S \omega \quad \text{Equation 5.2}$$

where τ_S the torque of the shaft (N m) and ω the rotational speed (rad s^{-1}).

There are many methods of measuring the torque of a motor, of which the primary ones are the Prony brake (Linton, 2014; Senior, 2009) or more advanced torque readers (Helmizar, 2016). Each of these methods has advantages and disadvantages for accurate and reliable determination of the torque of the motor.

5.1.1.1.1 Torque reader

Torque readers can be very accurate and reliable and there are many forms of contactless readers which do not interfere with the performance of the motor. These types of readers could not be employed in this research, however, due to the small scale of the physical model used.

5.1.1.1.2 Prony brake

The Prony brake is a relatively simple mechanism for measuring the torque of a motor. It works by applying a frictional load to the shaft of the motor and measuring the force that is created. This is done by wrapping a cord over half the shaft and apply a fixed preload to both ends of the cord (Figure 5.2). When the motor turns the shaft the friction in the cord increases one of the readings and decreases the other. The torque can then be determined by:

$$\tau_S = R_S \times (F_1 - F_2) \qquad \text{Equation 5.3}$$

where R_S the radius of the shaft (m) and F_1 and F_2 are the force readings (N).

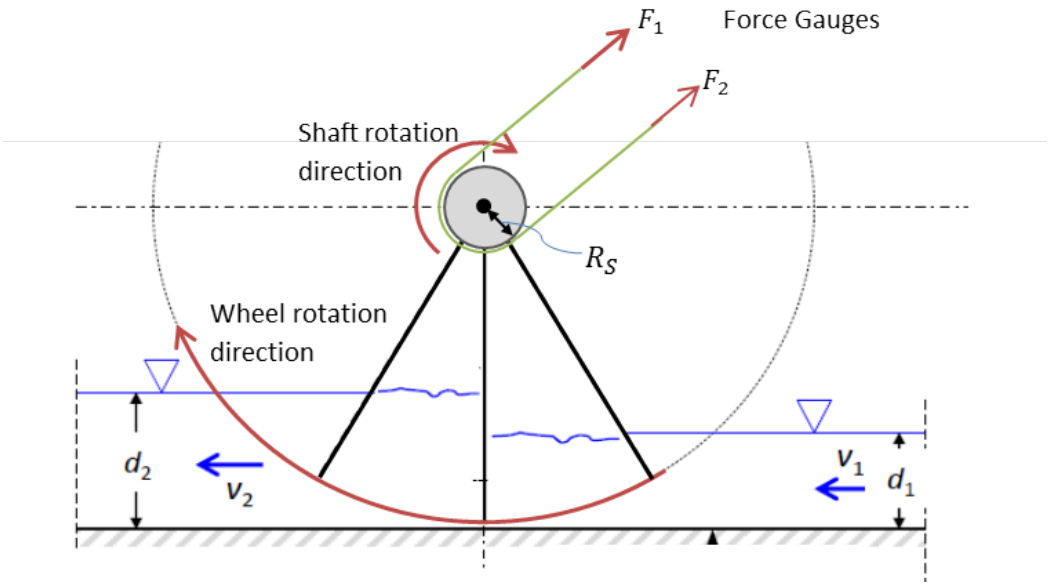

Figure 5.2. Conceptual diagram of a cord Prony brake. The black circle represents the shaft of the motor turning.

This method can lead to large errors resulting from the use of a cord which will have some degree of flex. If the cord expands and stretches the force readings will not be reliable and will give an underestimate of the torque. The work completed at University of Southampton has made it clear that large fluctuations occur as the friction is not

uniform and the cord slips around the shaft in discrete movements rather than a continuous movement (Helmizar, 2016).

5.1.1.1.3 Direct torque measurement device (DTMD)

The method used to measure the torque of the motor was developed specifically for this project and to the others knowledge this is the first time this method has been used to measure the torque of a motor. The motor is fixed in a block which is free to rotate (Figure 5.3). The block is attached to a lever arm which then applies a force at the opposite end similar to the Prony brake. This force will increase until it is equilibrium with the torque of the motor being transferred to the paddlewheel. The torque can then be calculated; the lever arm length, l, was set at 15 mm. This method is not affected by the efficiency of the motor as the shaft torque is directly measured.

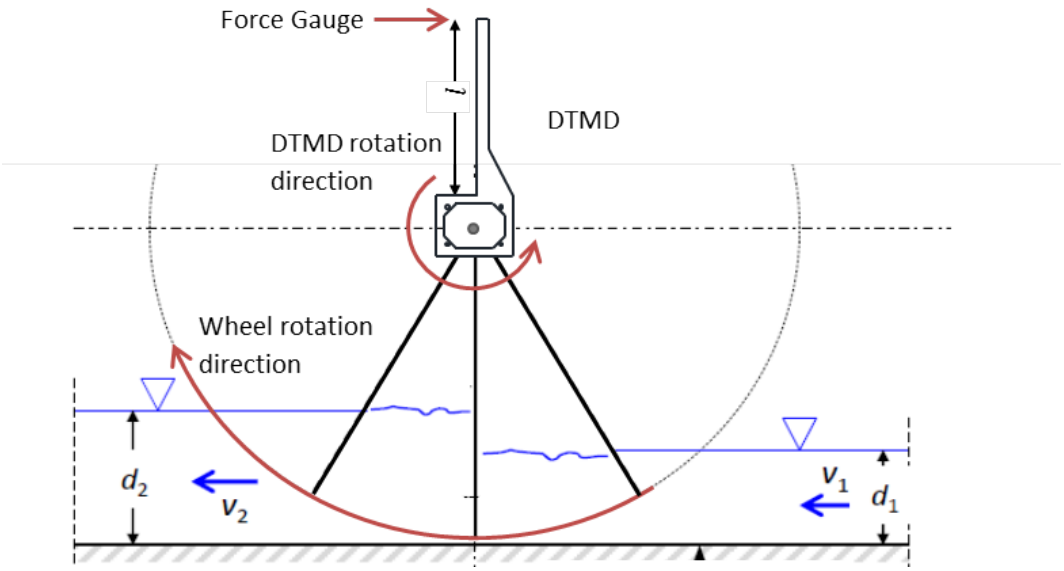

Figure 5.3. Diagram of the direct torque measurement device.

To ensure that the weight of the lever arm does not affect the readings by applying a moment from the centre of the motor it is placed vertically.

This method of measuring the torque has an advantage over the Prony brake as it will not affect the performance of the motor and does not rely on a friction force which may vary. The simplicity of the design avoids the issues associated with stretching of cords and moment losses if hinges are used in the setup.

5.1.1.2 Measuring the hydraulic power

The hydraulic power of the system is likened to the output power of the wheel. It can be calculated using Equation 4.38, Section 3.1.1.

The head difference can be measured using static drop-down gauges or piezometers. From initial experiments it was decided that piezometers would be more reliable and accurate due to the high levels of turbulence and waves created by the wheel when in use, as they have the advantage that water surface distortions are averaged. These were set upstream and downstream of the paddlewheel (Location 1 and 2 Figure 5.1 b). Another piezometer was required to measure the hydrostatic head used in calculation of the flow over the weir (Location 3 Figure 5.1 b).

The head difference should also include the velocity head of the system. Traditionally either a Pitot tube or Venturi meter would be used find this. A Pitot tube is a small tube inserted parallel to the direction of flow which bends at 90°. It works by converting the kinetic energy of the flow to potential energy (Swan, 2011). A Venturi meter is commonly used in pipe networks to measure flow rates. It is a section of pipe which narrows and forces the flow to accelerate and by measuring the change in pressure the velocity can be calculated (Harris, 2011). A measuring weir can be employed to control and measure the flow rate of the fluid. More modern techniques would be to measure the velocity directly using an Acoustic Doppler Velocimeter (ADV). This device measures the three dimensional velocity components of the fluid by use of the Doppler shift effect on the travelling fluid. Although it is accepted as the most reliable and informative method, as the turbulence can also be calculated, this method was not applicable in this system due to the shallow water depths investigated.

A weir was chosen as it can be used simultaneously to measure the discharge and artificially to increase the head of water acting against the wheel. A partially contracted rectangular sharp-crested weir was employed. This was chosen due to the shallow working depths in the raceway, as V-notched or Cipoletti weirs require a greater head or wider channel to achieve the same discharge.

The shape of the weir was designed to ensure that there was full aeration between the nappe and the weir. If this is not done then air could become trapped and slowly

entrained into the water, leading to a collapsed nappe which clings to the weir. When this occurs accurate measurement of the discharge is not possible (Johnson, 2000).

Bos et al. (1984) stated that the static head measurement (Location 3, Figure 5.1 b) should be located between two and three times the maximum total head upstream of the weir, to ensure that the drawdown to the crest of the weir does not affect these measurements (Bos et al., 1984). Other values have also been quoted: Bos also suggested values of three to four times with others stating this should be at least six times the upstream head (Bos, 1976). For this experiment the measuring stations were located roughly two times the maximum head away from the weir. This position was chosen based on visual inspection indicating that the water surface was not dropping at this position, and the location of the wave diffuser would likely affect the results if a greater distance was employed. It is also imperative that the crest of the weir is sufficiently narrow, less than 2 mm, and that the tapered edge is at an adequately steep angle so as not to influence the flow over the crest (Figure 5.4).

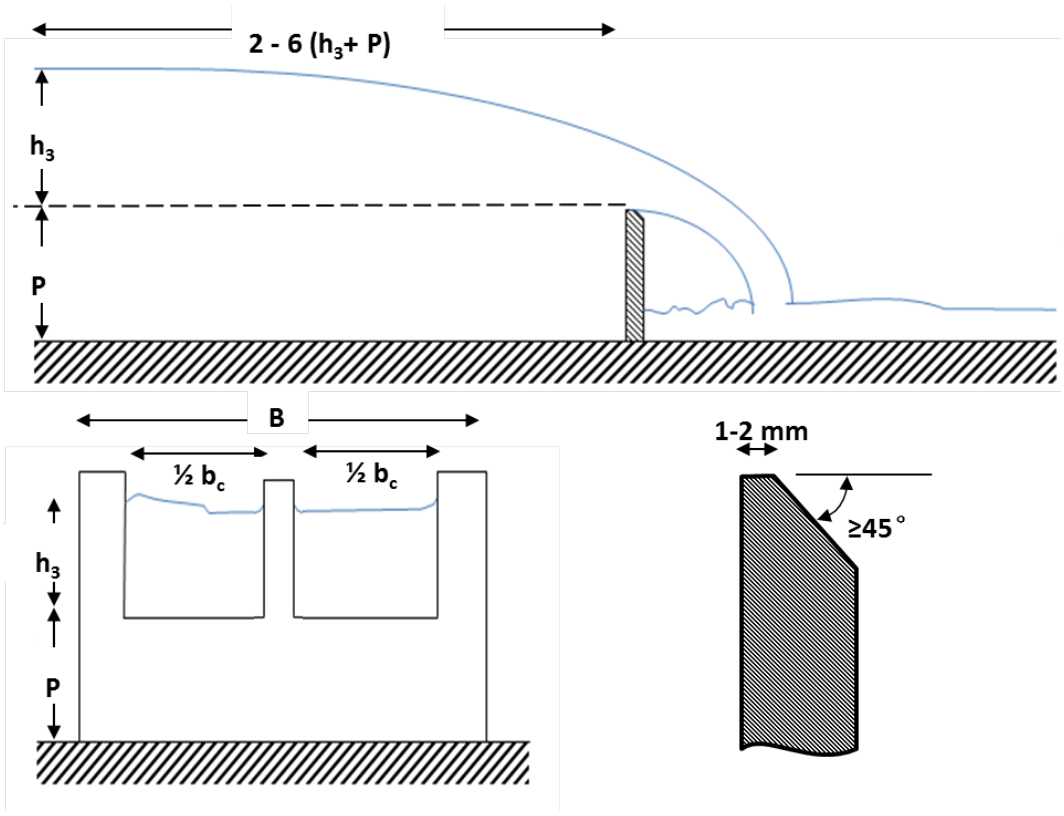

Figure 5.4. Schematic of a sharp crested rectangular weir.

In order to calculate the discharge the weir equation defined by experimental studies carried out by Kindsvater and Carter, 1957 is used:

$$Q = C_d \frac{2}{3}\sqrt{2g}\, b_e h_e^{\frac{3}{2}} \qquad \text{Equation 5.4}$$

Where:

$$b_e = b_c + K_b \qquad \text{Equation 5.5}$$

$$h_e = h_3 + K_h \qquad \text{Equation 5.6}$$

where Q is the discharge ($m^3\ s^{-1}$), C_d is the discharge coefficient (dimensionless), g is the gravitational constant ($m\ s^{-2}$), b_e the effective breadth of the weir opening (m), h_e is the effective upstream head above the crest of the weir (m) and b_c, P and h_3 are the physical width and height of the weir and crest (m), respectively (Figure 5.4). The terms K_b and K_h are empirically defined adjustment factors due to the effects of surface tension and viscosity (Kindsvater and Carter, 1957).

The value for K_b is dependent upon the ratio of channel to weir width (b_c:B), a value of 0.004 m has been used for the weir constructed with a ratio of 0.84 (Figure 5.5). For K_h, however, a constant value of 0.001 m was recommended for all ratios (Bos, 1976).

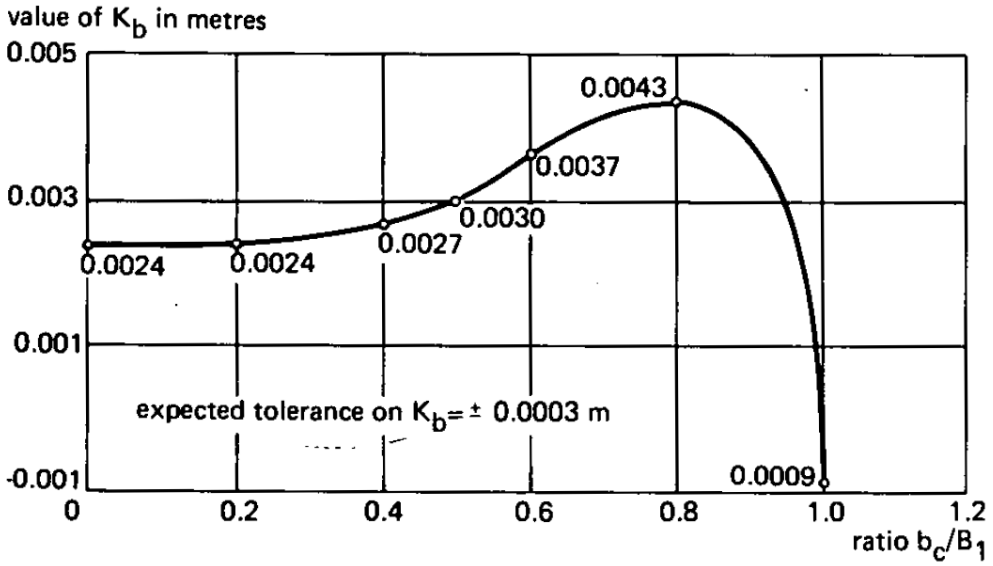

Figure 5.5. Graph showing the effects of the width ratio on the width adjustment factor (Bos, 1976).

In order to calculate the discharge, the discharge coefficient must be accurately determined. The coefficient is a function of the ratio of the channel to weir width and

the ratio of the crest to weir head. For a channel to weir width ratio (b_c:B) of 0.84 the coefficient can be found from (Bos, 1976):

$$C_e = 0.598 + 0.50\ \frac{h_3}{P}$$ Equation 5.7

Others (Arvanaghi and Oskuei, 2011) have found that the discharge coefficient can be determined by:

$$C_e = 0.611 + 0.08\ \frac{h_3}{P}$$ Equation 5.8

where $\frac{h_3}{P}$ is the ratio of the crest to weir head.

Both of these coefficients were used and compared to see if there was any large effect on the discharge and calculated hydraulic power as a result. From the preliminary experiments conducted it was decided that the latter (Equation 5.8) gave more realistic results.

Using a weir for measuring the discharge can give very accurate and reliable results for a whole range of discharges. Some estimates put the measuring error as low as 1 % (Bos, 1976); however this is only a theoretical estimate. Others have calculated greater errors in experimental work, of less than 4 % at a 98 % significance (Johnson, 2000). To ensure that there is as little error a possible a few design aspects must be considered as mentioned previously.

The discharge can then be used to calculate the average velocity at any point in the channel using the continuity equation:

$$v = \frac{Q}{A}$$ Equation 5.9

where v is the velocity (m s^{-1}), Q is the discharge (m^3 s^{-1}) and A is the crossectional area (m^2).

With these measurements the head gained can be calculated from:

$$H = \frac{{v_1}^2}{2g} + d_1 - \left(\frac{{v_2}^2}{2g} + d_2\right)$$ Equation 5.10

where H is the head gained (m), d is the depth of the fluid (m), g is the gravitational acceleration (m s^{-2}), locations 1 and 2 are shown on Figure 5.1 b.

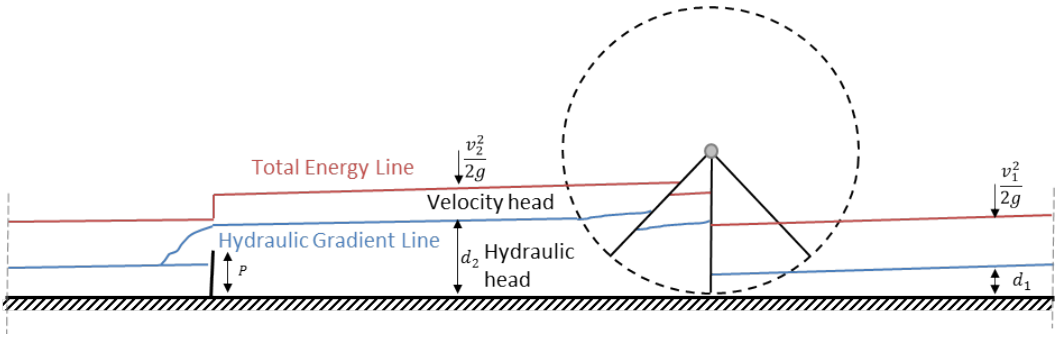

Figure 5.6. Conceptual idea of how the fluid depth and total energy is affected by the paddlewheel and downstream weir.

The weir will hold up fluid to create a greater head difference acting on the wheel (Figure 5.6). The amount of fluid backed up behind the weir (d_2) is dependent upon its height (P), the wheel rotational speed (ω) and the total fluid in the system. If any one of these changes it will affect both the downstream (d_2) and upstream head (d_1) which in turn will affect the discharge, shaft power and hydraulic power.

5.1.2 Model construction, materials and equipment

The model was based on the pilot-scale raceways described by Mendoza et al. (2013) (Mendoza et al., 2013a), and was built at a scale of 1:5 with an area of 0.98 m^2. It went through multiple design modifications due to the scaling down procedure, as the length of a full scale raceway had to be scaled greater than the width due to size and cost restraints. In order to achieve this; a weir was installed after the wheel to increase the head difference across it (Figure 5.1 a). The model had an internal channel width of 280 mm and a total internal length of 1820 mm. A weir was constructed and located 625 mm downstream of the wheel (Figure 5.1 b). All drawing specifications and exact dimensions can be viewed in Appendix B.

5.1.2.1 Raceway

The bed of the raceway was constructed out of 12 mm thick Polymethyl acrylic glass with the side walls of 10 mm thick clear Polymethyl acrylic glass. The centre divider consisted of two side wall pieces glued together for increased rigidity. The walls were 1280 mm long with the centre walls being rounded at each end. The side and centre walls were glued into place and then sealed with silicone on both sides to ensure water tightness. The two end bends and insert were fabricated from foam and laser cut to the

correct shape; these had a radius of 290 mm. These were also glued and siliconed into place to prevent leaks.

5.1.2.2 Paddlewheel

The wheel was in total 277 mm wide and consisted of two 10 mm thick clear Polymethyl acrylic glass side plates with a diameter of 300 mm (Figure 5.7). These side plates had notches for eight, ten and twelve blades which allowed multiple configurations to be tested. The side plates were attached to a central axle with the use of two taper locks and collars which attached to the wheel plates. The axle shaft was made from a 12 mm diameter aluminium shaft and was supported by bearing blocks to allow free rotation. The shaft ran to the centre of the raceway into a counter-bored bearing block which was supported by a bearing support block 20 mm wide to ensure it fitted flush with the central divider.

The blades were constructed from 2 mm thick aluminium sheet and were 267 mm long and 85 mm wide. The ends of the blades were recessed 5 mm into the wheel plates to ensure they were water tight and to increase rigidity of the wheel. When the blade slots were not in use they were filled with a waterproof putty to reduce the impact of these groves. The smallest achievable tolerance was 2 mm beneath the wheel and 1 mm at each side: when scaled up this is equivalent to 10 mm and 5 mm gap which was deemed to be within acceptable tolerances and similar to tolerances in real-scale systems.

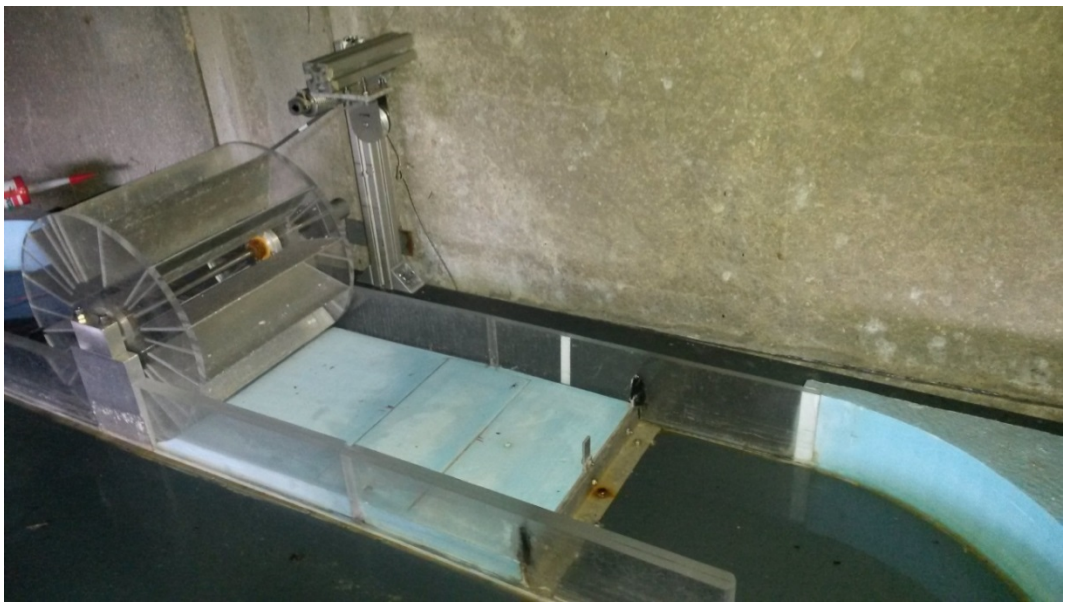

Figure 5.7. Image of the paddlewheel with 12 blades and the blue insert located immediately to the right of the wheel.

5.1.2.3 Insert

The insert used was specifically designed for this wheel diameter and for 12 blades as it is essential that at least one blade is present on the curvature of the insert at any one time (Figure 5.8). The use of an insert located downstream of the wheel to increase the efficiency has not previously been systematically investigated for the use in improving paddlewheel efficiencies.

The insert was constructed from foam and glued into place when needed. Foam was chosen as it could be laser cut to specific dimensions within a very tight tolerance (Figure 5.7).

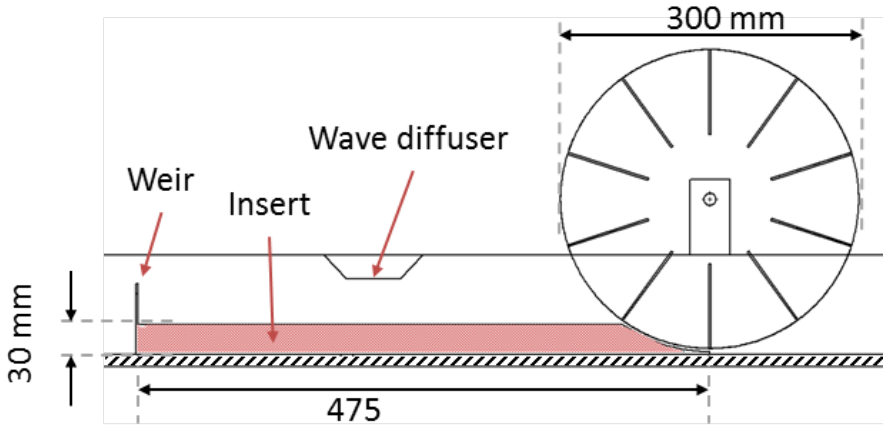

Figure 5.8. Cross section of the insert shown in red.

5.1.2.4 Weir

The weir was constructed from 2 mm thick aluminium sheet with the crest filed down to 1 mm and was 238 mm wide. It was built in two parts: the bottom piece which was screwed into the base of the raceway and the top piece which had an elongated bolt hole to bolt into the base part so it could be raised or lowered from 35 mm to 63 mm. It was located at the end of the insert to allow accurate measurement of the discharge (Figure 5.9). To imitate a longer raceway the weir could be raised, and therefore a greater water head difference would be acting adversely on the wheel. The weir had a central section that was raised above water height to ensure that there was adequate aeration beneath the nap to prevent it collapsing.

Figure 5.9. The weir in use.

5.1.2.5 Wave diffuser

From the preliminary tests it became apparent that the wheel started to create waves at certain rotational speeds. These waves made the use of the weir to record the discharge unreliable. The waves were more notable when the wheel had a smaller number of blades or a lower rotational speed, to the point that the water would pulse over the weir when eight or fewer blades were used or at very low blade velocities.

In order to eliminate these waves a wave diffuser was used (Figure 5.10). This consisted of a piece of foam located in the channel held in place using 5 mm groves cut into the

side walls. This diffuser was raised to the water level height for each run to stop the pulsating occurring.

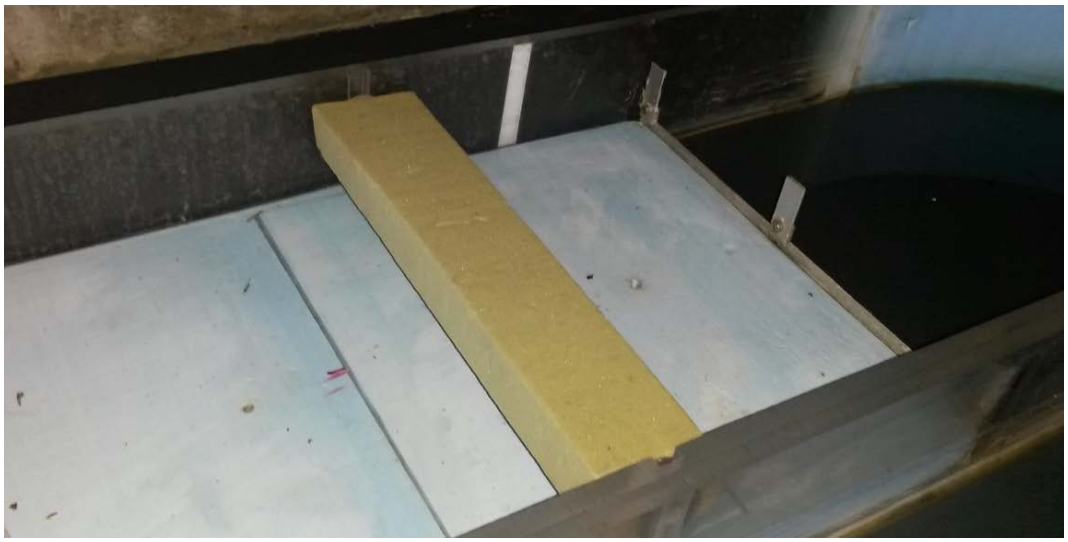

Figure 5.10. The wave diffuser. Note the grooves cut into the channel wall to hold the diffuser in place.

5.1.2.6 Piezometers

The piezometers were used to measure the water depth at the locations specified in Figure 5.1 b. These were constructed from 40 mm diameter clear plastic tubes with small self-adhesive scales applied (Figure 5.11). The piezometers were attached to the raceways by small diameter PVC tubes.

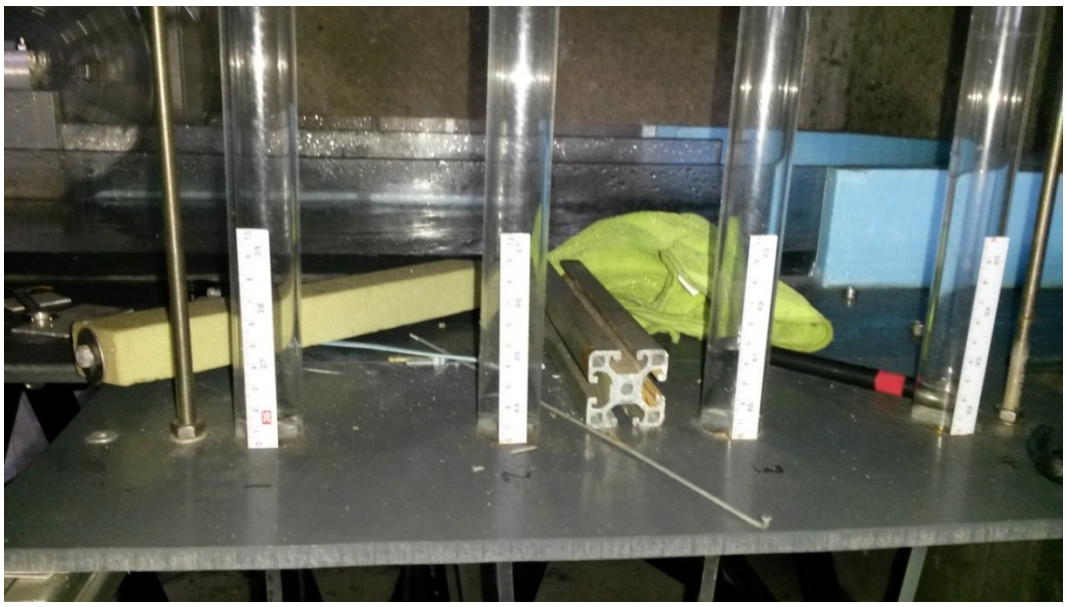

Figure 5.11. Piezometers used in the experiment.

5.1.2.7 Motor

The motor was a Philips 12 V DC motor with an internal gearing system to reduce the rotational speed to 60 rpm and increase the torque to 30 N cm and power output to 5 W (Figure 5.12 a). This was attached directly to the shaft of the motor with the use of a machined sleeve. This was done to mitigate any errors that might arise due to the stretching, misalignment and slippage of the drive train. This did, however, give rise to other problems such as alignment, as it was paramount that the two shafts were in perfect alignment to ensure that the energy was efficiently transferred between them. The speed of the motor was controlled by adjusting the direct voltage with an adjustable voltage regulator (Figure 5.12 b).

Figure 5.12. a) The motor used in the experiment with the direct transfer sleeve and b) the adjustable voltage regulator.

5.1.2.8 DTMD

The DTMD was attached to the motor with the end of the lever arm against the load cell (Figure 5.13). The motor is able to rotate freely and was set up with the top of the lever arm against the force transducer.

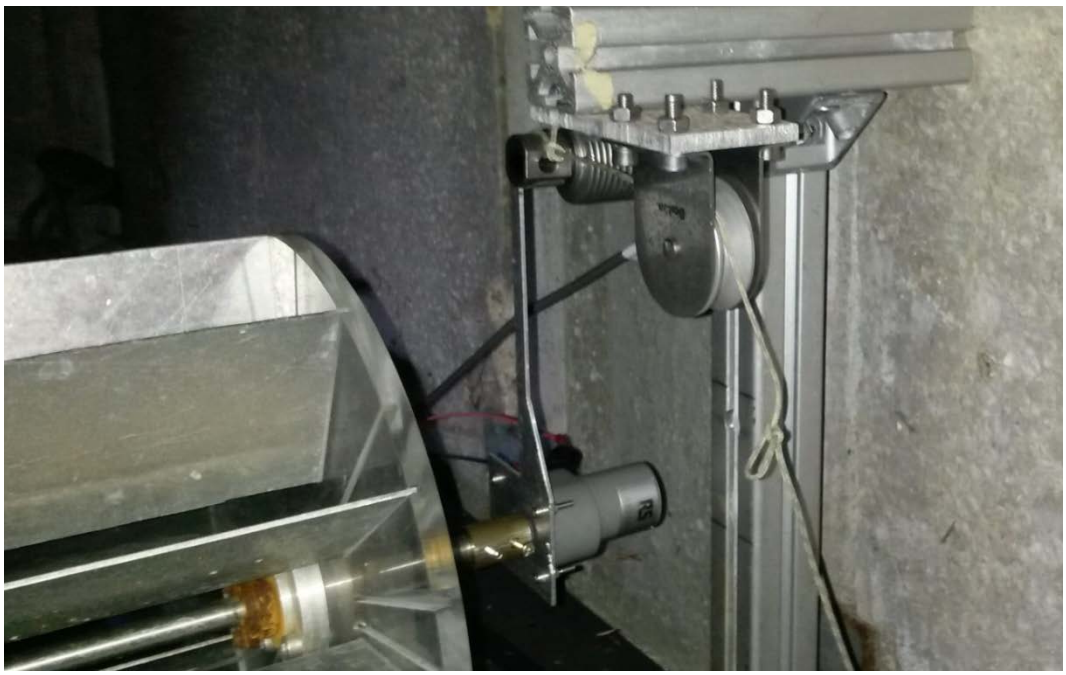

Figure 5.13. The load cell DTMD in use.

5.1.2.9 Load cell

The load cell was a Tedea-Huntleigh Model 355 Bending Beam Load Cell. It had a capacity range of 5 kg with an accuracy to 0.1 %. It was located at the end of the lever arm of the DTMD and fixed in place using item bars so that it was vertical of the motor.

The load cell was affected by changes in atmospheric pressure and temperature and needed to be calibrated to ensure reliable readings for each setup. The calibration of the load cell was done every time the weir height was adjusted. It was completed using two 20 N weights hanging vertically around a pulley to apply the load in the same direction as the wheel (Figure 5.14).

Figure 5.14. Image of the calibration weights in use.

5.1.2.10 Data acquisition

The data was sampled at a rate of 50 Hz over a range of 15 seconds using a LABVIEW control box. At the fastest wheel speed the frequency of the blade entering the fluid would only be 8 Hz, so this sampling rate should pick up every blade entry and exit. The sampling time is at least two full rotations of the wheel at the slowest rotational speed thus allowing any movements in the wheel to be taken into account in the calculation of the average force. For each setup the shaft power was calculated by taking an average of all force recordings recorded at 50 Hz.

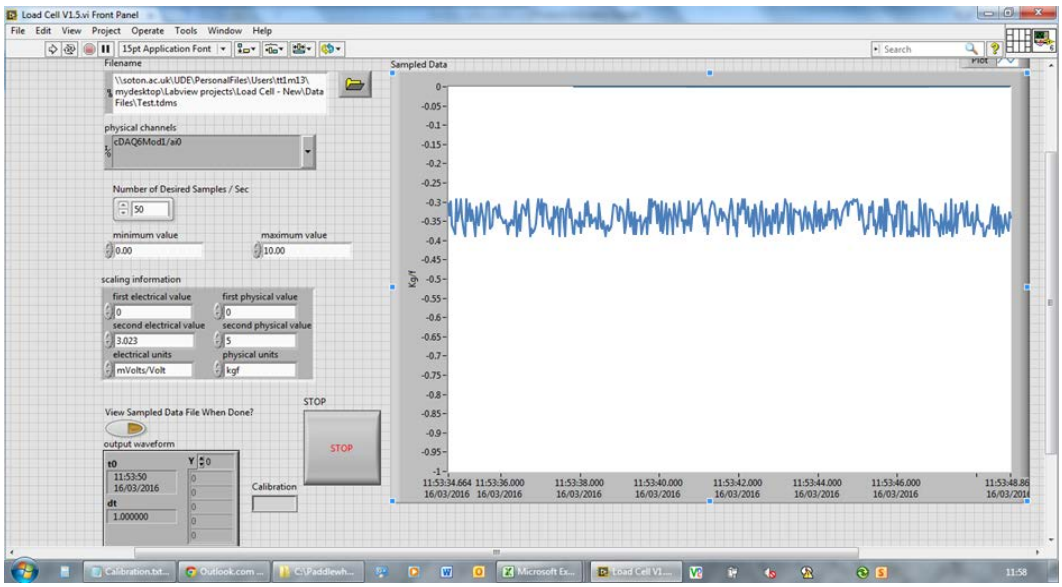

Figure 5.15. Screen print of the load cell data acquisition software interface during the experiment. The fluctuation in the force reading is due to the blade entry into the fluid.

5.1.3 Parameters investigated

The below is a list of the parameters that were investigated. The results and discussion are then displayed investigating how each individual parameter affects the wheels performance. The parameters are normalised as set out in Section 5.1.3.7.

5.1.3.1 Speed of the wheel

The rotational velocity of the wheel has been shown to have a major effect on the efficiency of the paddlewheel, as discussed in Section 3.5.3. Previous investigations to date have however only measured the power input into the motor, and not the power transferred to the fluid. With the used of the torque measurement device the actual efficiency of the wheel can be calculated.

The wheel ran at a range of different speeds from 10 to 40 rpm which corresponds to full scaled speeds of 4 to 18 rpm resulting in a full scaled fluid forward velocity of almost 0 to 0.6 m s^{-1}. Standard fluid velocities used in large-scale raceways lie well within this range (Section 3.4.1).

5.1.3.2 Number of blades

The number of blades should affect the efficiency of the wheel as a smaller number of blades results in a greater maximum gap beneath the blade ($h_{g_{max}}$) (Section 4.3.2.4). Currently there has been no investigations into how the number of blades affects the

efficiency of paddlewheels and wheels with 6 or 8 blades appear to be the standard in use in raceways (Vitale, 2012; Ben-Amotz, 2008).

The wheel was tested with 4, 6, 8, 10, and 12 blades.

5.1.3.3 Fluid discharge

The fluid discharge from the wheel is directly related to the efficiency of the wheel and therefore must be analysed. Furthermore it is also an import factor in algal raceways as it must be great enough to ensure that the algae are maintained in suspension. During the experiments the range of discharges recorded started at zero increasing to a maximum which differed depending on the number of blades and rotational speed of the wheel. All wheel speeds and blade numbers analysed reached the required range for algal cultivation of a velocity of 0.2 m s^{-1}.

5.1.3.4 Fluid depth and head difference

It has been shown numerically and physically that the depth of the fluid in the raceway has an impact on the power requirement as discussed in Section 3.1.1. Increasing the discharge of a wheel through a greater submersion depth has been shown to be more efficient than changing the speed of the wheel, as shown in Section 3.5.4. These investigations into the efficiency were only numerical calculations and this has not been physically tested.

The average full scaled depth of the fluid was between 0.12 and 0.33 m. The full scaled depth needs to be less than 0.3 m for reasons explained in Section 3.1.1. Table 5.1 shows the maximum and minimum upstream and downstream depth values either side of the wheel.

The head difference has been theoretically shown to affect the performance of the wheel and was investigated alongside the fluid depth due to them being linked. The range of measured head differences is shown in Table 5.1.

Table 5.1. The maximum and minimum head values around the wheel.

Number of blades	Downstream water depth (m)		Upstream water depth (m)		Head difference (m)	
	Minimum	Maximum	Minimum	Maximum	Minimum	Maximum
4	0.08	0.205	0.09	0.35	0.0375	0.21
8	0.0725	0.2	0.085	0.38	0.0625	0.255
12	0.05	0.235	0.07	0.47	0.0625	0.31

5.1.3.5 Length of the raceway

It has been reported that raceways with a greater shape ratio, SR, (length: width) have a reduced power requirement per unit surface area (Section 3.1.2). This has not been physically tested, however, but only numerically simulated. As discussed previously in Section 5.1.2.4 the weir can be used to imitate a longer raceway by increasing the head of water downstream of the wheel.

The full scaled length (L) can then be calculated applying Manning's equation:

$$L = \frac{H_L R_H^{4/3}}{v^2 n^2} \qquad \text{Equation 5.11}$$

where H_L is the head loss (m) which is calculated from Equation 5.10 (Section 5.1.1.2), v is the average velocity of the section (m s^{-1}) which is calculated from Equation 5.9 (Section 5.1.1.2), R_H is the hydraulic radius (m) which is calculated using Equation 3.20 (Section 3.4.2) and n is the Manning's roughness coefficient (-).

The Manning's roughness coefficient was taken as 0.01. This was selected due to the very smooth surfaces of the materials used in building the raceway channels.

5.1.3.6 Insert

The use of an insert located downstream of the wheel to increase the efficiency has never been systematically investigated. Some work was done at a larger scale by Mendoza (2016) but on a purely ad hoc and empirical basis without consideration of right size of device, scale effects or limitations of equipment. Mendoza (2016) highlighted this as an area which needed further consideration. The insert was only investigated for the 12-bladed wheel due to it having to be specifically designed for each number of blades

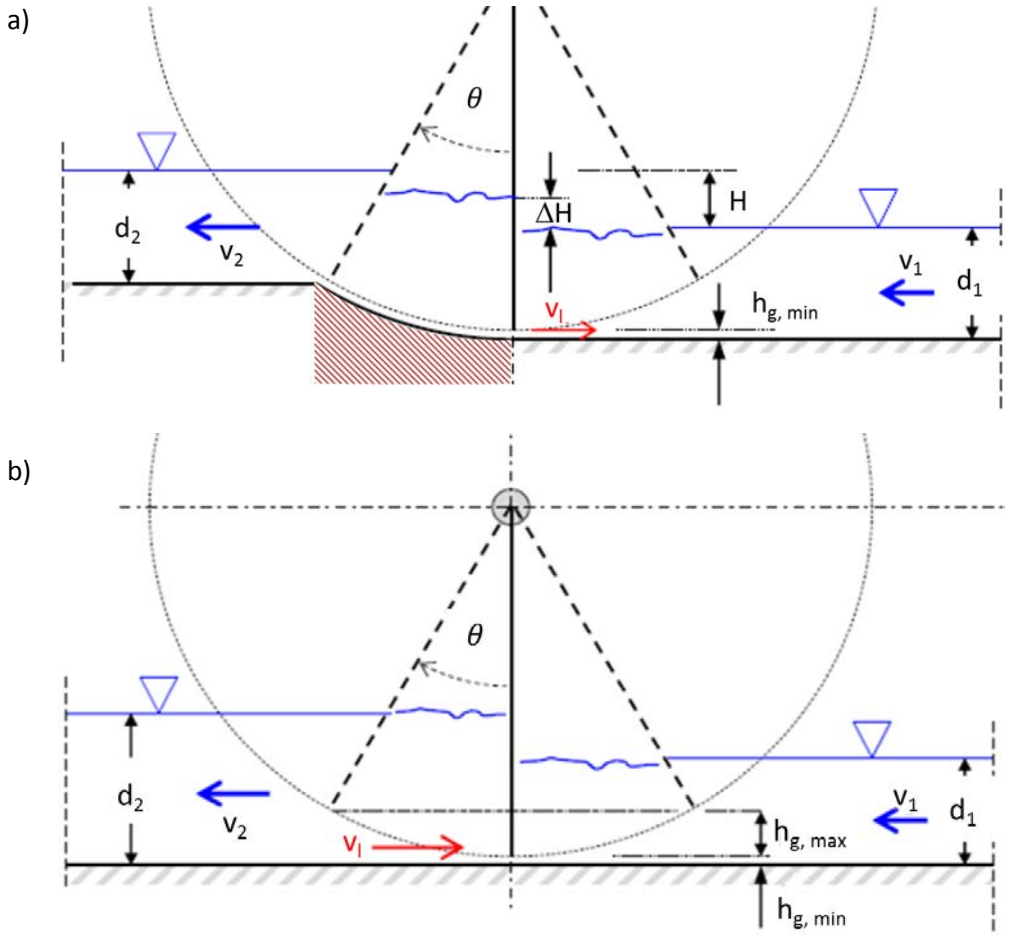

Figure 5.16. Conceptual diagram showing the effects an insert has on the leakage around the blade. a) With insert, indicated in red hatching, b) Without insert.

There may be higher channel losses, however, due to the shallower fluid depth which resulting in a higher velocity head in the system. This will need to be assessed to determine whether it has a major impact on the efficiency of the whole system and not just the wheel in isolation.

5.1.3.7 Normalised values

The continuous configuration of raceways means that if any parameter changes this affects all the others, i.e. if the downstream fluid depth is reduced then the upstream fluid depth must increase for the same amount of fluid in the system. To ensure that the results for different situations can be compared reliably to one another some of the values must be normalised in such a way as to reduce any bias that may affect the results.

5.1.3.7.1 Normalised head

Previous studies have suggested that the efficiency of the wheel is linked to the upstream depth (Park et al., 2014). The normalised head can be used to compare a range of different head conditions relative to the upstream head:

$$h_N = \frac{H}{d_1}$$ Equation 5.12

where h_N is the normalised head loss, H is the head gained from the wheel (m) and d_1 is the upstream fluid depth (m)

A normalised head of zero would mean that there is no head loss and the water depths either side of the wheel were equal. When the downstream depth is greater than the upstream depth values above zero would occur. The head loss was chosen for normalisation instead of the ratio of depths as this is a more appropriate parameter when discussing the efficiency of the wheel.

5.1.3.7.2 Normalised Length

Similarly to the depth the length must also be normalised in order to allow comparison of the data. Other researchers have normalised the width of the channel with the depth of fluid (Ali et al., 2014). In this experiment the width is constant but the length is normalised against the depth:

$$L_N = \frac{L}{d_1}$$ Equation 5.13

where L_N is the normalised length, L is the channel length (m).

5.1.3.7.3 Normalised wheel speed

The actual wheel speed can be normalised with the theoretical maximum fluid velocity if it was to flow freely under gravity. This normalised wheel speed should group the different speeds tested assuming that the velocity of the fluid is much led than the gradational head:

$$v_{b_N} = \frac{v_b}{\sqrt{2gH}}$$ Equation 5.14

where v_{b_N} is the normalised rotational speed, v_b is the tangential velocity at the tip of the blade (m s^{-1}) and $\sqrt{2gH}$ is the maximum possible flow velocity for a given head driven by gravity (m s^{-1}).

5.1.4 Scaling

A physical model is used to test features of a real life prototype at a fraction of the cost. The scale is defined as the ratio between the length of the model and real life prototype:

$$\lambda = \frac{L_P}{L_M} \qquad \text{Equation 5.15}$$

where λ is the scale ratio (-), L_P is the characteristic length of the prototype (m), L_M is the characteristic length of the model (m). For the model designed and constructed in the current work the scale ratio was 1:5.

Knowing how scaling effects the physics of the model is thus key to understand if the results gained are an under or over representation of the true system. A scaled model would produce exact results similar to the full scale prototype if it could fully satisfy three scaling conditions:

- Geometric similarity.
- Kinematic similarity.
- Dynamic similarity.

Problems arise when scaling down a hydrodynamic model as a result of the forces acting on the model not scaling correctly from the real life prototype. It is impossible to satisfy all of the scaling conditions fully and compromises must be made in regard to some of them. These errors are known as scale effects and can be significantly reduced by correct selection of the model design and parameters. If the model is design correctly these scaling effects will become negligible.

5.1.4.1 Geometric similarity

Geometric similarity entails having similar shapes and lengths, i.e. lengths, areas and volumes scale with λ, λ^2 and λ^3 respectively. It is the simplest condition to satisfy, although it is rare that is completely satisfied. There are normally some dimensions which are impossibly large or small to scale in relation to the other dimensions. The most common example of a non-scalable dimension is the surface roughness of smooth materials as this is usually very small in comparison to the other dimensions.

In this experiment the geometric scaling had to be distorted as the length was too large to scale and thus was artificially increased by using a weir downstream of the wheel to hold a greater head of fluid back to increase the head difference (Figure 5.6).

5.1.4.2 Kinematic similarity

Complete kinematic similarity ensures geometric similarity and also requires the motion of the fluid to be similar. For this to be satisfied the ratios of time, velocity, acceleration and discharge must be constant between the prototype and model in all situations. It is hard to fully achieve kinematic similarity as the turbulence length scales in the model do not fully scale from the prototype, and are greater in the model.

5.1.4.3 Dynamic similarity

Complete dynamic similarity not only requires geometric and kinematic similarity but also requires the force ratios between the structures to be equal. In slow open channel flow these primarily include the inertial forces, gravitational forces and sometimes the surface tension force. Other force ratios to be considered are the viscous forces, elastic compression forces and pressure forces.

Full dynamic similarity requires all these force ratios to be identical:

$$\frac{\text{Inertial force}_p}{\text{Inertial force}_m} = \frac{\text{Gravitational force }_p}{\text{Gravitational force}_m} \dots \frac{\text{Pressure force}_p}{\text{Pressure forcs}_m} = constant \qquad \text{Equation 5.16}$$

While it is possible to ensure that some of the ratios are constant, for there to be full dynamic similarity the gravity and atmospheric pressure would need to be scaled which is not realistically possible in most cases (Ettema et al., 2000).

5.1.4.3.1 Froude similarity – velocity and rotational speed

In open channels where frictional losses are negligible and there is a relatively high degree of turbulence, the flow is commonly governed by the ratio between the inertial and gravitational forces. In these instances Froude similarity is normally ensured. The Froude Number is:

$$Fr = \sqrt{\frac{Inertial\ force}{Gravitational\ force}} = \frac{v}{\sqrt{gL}} \qquad \text{Equation 5.17}$$

where Fr is the Froude number (-), v the characteristic velocity (m s^{-1}), L the characteristic length (m) and g is the gravitational acceleration (m s^{-2}).

If the viscous force dominates the flow then Reynolds similarity is a better choice to avoid scaling effects. Preliminary testing in the model raceway system used in the current experimental work showed that there appeared to be a high degree of turbulence in the system: this is independent of the Reynolds number and must be

scaled. At the lower rotational speeds there is less turbulence in the system and the scale effects are likely to have a larger effect on the results of the model.

Froude similarity of the model and prototype:

$$Fr_M = Fr_P = \frac{v_M}{\sqrt{gL_M}} = \frac{v_P}{\sqrt{gL_P}} \quad \text{Equation 5.18}$$

$$\frac{v_M}{v_P} = \sqrt{\frac{L_M}{L_P}} = \sqrt{\frac{1}{\lambda}} \quad \text{Equation 5.19}$$

$$v_M = v_P\sqrt{\frac{1}{\lambda}} \quad \text{Equation 5.20}$$

$$v_M = v_P\sqrt{\frac{1}{5}} = 0.45v_P \quad \text{Equation 5.21}$$

The subscript P indicates the prototype and M the model.

Therefore for a scale ratio of $\lambda = 5$ the scaled velocity is around 45 % that of the prototype.

The speed of the wheel must also be scaled according to the velocity and length scales. Where the top velocity of the prototype can be calculated from:

$$v_P = \omega_p r_{b\,P} \quad \text{Equation 5.22}$$

where ω is the rotational speed of the wheel (rad s^{-1}), v_P is the tip velocity (m s^{-1}) and r_b is the radius of the wheel (m).

This velocity is then scaled in accordance with Equation 5.20 so that:

$$v_M = \omega_p\, r_{b\,P}\sqrt{\frac{1}{\lambda}} \quad \text{Equation 5.23}$$

Then length can also be scaled so that:

$$r_{b\,M} = \frac{1}{\lambda} r_{b\,P} \quad \text{Equation 5.24}$$

The rotational speed of the model can thus be calculated from:

$$\omega_M = \frac{v_M}{r_{b\,M}} \quad \text{Equation 5.25}$$

Substituting Equation 5.24 and Equation 5.25 into Equation 5.23:

$$\omega_M = \frac{\omega_P\, r_{b\,P}\sqrt{\frac{1}{\lambda}}}{r_{b\,P}\frac{1}{\lambda}} = \omega_P\,\lambda\sqrt{\frac{1}{\lambda}} \quad \text{Equation 5.26}$$

$$\omega_M = 2.24\,\omega_P$$ Equation 5.27

Thus a scaled model wheel rotational speed is always faster than that of the real life prototype.

5.1.4.4 Scale effects

The effects of scaling will have an impact no matter how well designed the model is. A larger scale ratio, λ, leads to the errors in the modelled forces being compounded leading to greater deviation away from the real life prototype. The effects are not solely governed by the scaling ratio and are greatly influenced by the system being simulated and modelled.

Some forces in the prototype are less dominant than in the model such as gravity and intramolecular forces, which leads to certain aspects of the model being unrepresentative such as water tension. Phenomena such as wave height and solid transportation are normally smaller in the model (Heller, 2012).

The small nature of the model will have other errors associated with it such as human error is measuring and setup. The largest possible error would be if the model wasn't perfectly level as the fluid level will be distorted by the gradient. These distortions would affect the depth and velocity of the fluid and any slope will increased by a factor of five so it was important to take every possible precaution to ensure that this did not occur. These precautions included checking the level at six different points around the edge of the model and at four different points in the channels. There also will be some error in measuring the fluid depth as this was done physically. To overcome this each depth was checked twice with a 30 second delay between.

5.2 Model experimental results and discussion

In this section the results for each parameter are presented and discussed with respect to the literature and previous studies and the effects different variables have on the performance of the wheel. The different parameters were scaled, where appropriate, using the equations set out in Section 5.1.4.

5.2.1 Wheel rotational speed and blade number

The effect of the rotational speed of the wheel (ω) on paddlewheel efficiency and fluid velocity were investigated. The rotational speed has been shown in previous studies to

be a key factor determining the efficiency and fluid velocity of the wheel. In Section 4.3.2.3 the number of blades was shown theoretically to have a large impact on the performance of the wheel. The results were compared by keeping the weir height constant and using the same starting base fluid depth to focus on the wheel speed and blade number. Wheels with different numbers of blades were all tested with a full-scale equivalent base fluid depth of 0.175 m and full-scale weir height of 0.185 m. These values were chosen as they were representative of a high proportion of the total set of conditions studies, and were also typical of operating conditions used in full-scale systems.

5.2.1.1 Fluid velocity

The fluid velocity was determined from the discharge and downstream depth. It rose with increased rotational velocity, with the lowest fluid velocity being recorded at the lowest rotational speed. The fluid velocity was further affected by the number of blades on the wheel, with the greater number of blades resulting in the highest fluid velocities. For a speed of 4.5 rpm, flow velocities ranged from 0.02 m s^{-1} (4 blades) to 0.14 m s^{-1} (12 blades). At the higher wheel speed of 18 rpm, this difference increases and velocities of 0.25 m s^{-1} (4 blades) to 0.42 m s^{-1} (12 blades) were determined.

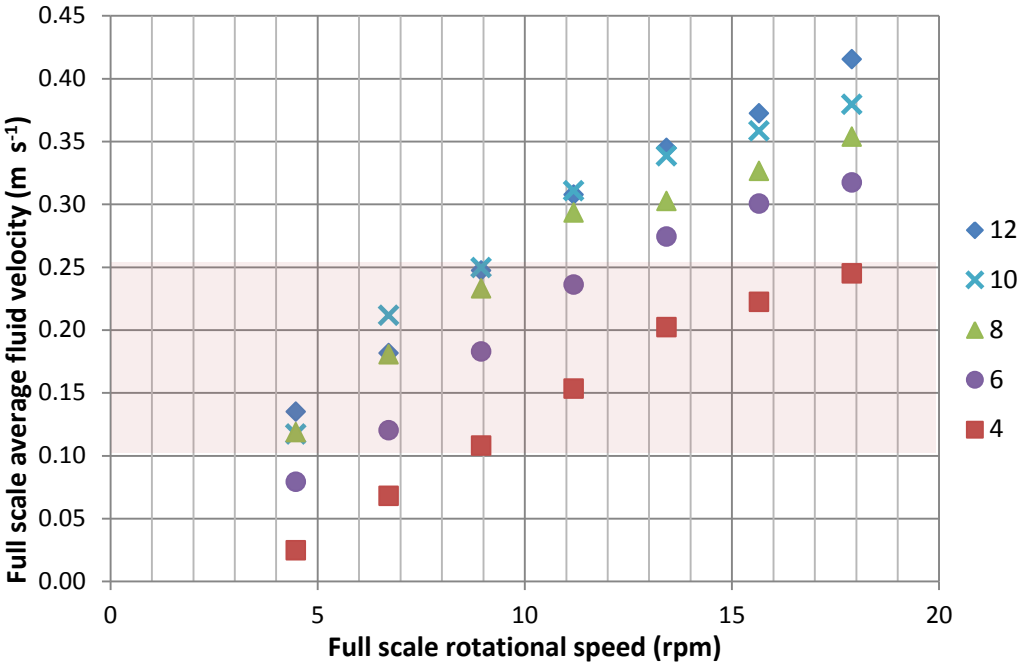

Figure 5.17. Variation in the average full scaled fluid velocity with different numbers of blades with rotational speeds. The legend indicates the no. of blades tested. The red square indicates the operating velocities applied in typical raceways.

Any changes made to the propulsion mechanism should aim to maintain or increase the fluid velocities in the channel while reducing the power requirement to achieve this. This is necessary to ensure that the microalgae remain in suspension around the whole of the raceway, as explained in Section 3.4.1.

The increase in fluid velocity as the blade number is increased is linked to the reduction in the leakage of fluid around and beneath the blades, as explained in Section 4.3.2.4. This explanation is supported by the larger increase in velocity accompanying an increase from 4 to 6 blades than from 8 through to 12 blades, as in the former case i.e. with lower blade numbers there is a greater change in the gap beneath the blades. To ensure that the microalgae are kept in suspension a minimum velocity of 0.1 m s^{-1} must be maintained throughout the raceway. For this to be met it is likely a fluid velocity of 0.2 m s^{-1} should be implemented by the paddlewheel. To achieve this with the 4-bladed wheel the rotational speed should be above 13 rpm while for the 8, 10 and 12-bladed wheels it should be above 7 rpm. For these wheels rotational speeds above 9 rpm result in excessive fluid velocities.

The fluid velocity was also affected by the rotational speed of the wheel. Initially there was a linear rise in velocity when the rotational speed was increased, which then started to level off at the very high rotational speeds. Experimental work by Mendoza et al. (2013) investigating the fluid velocity in a 50 m long and 1 m wide raceway driven by a standard flat 8-bladed paddlewheel found similar trends in fluid velocity as the rotational speed was increased. As the rotational speed increased the head difference rose, which leads to further leakage as explained in Section 4.3.2.4. The levelling off of the velocity can be attributed to this escalation in the leakage as the overall discharge is reduced. CFD simulations of a similar 8-bladed wheel by Sompech et al. (2012) found that only a linear relationship existed between the wheel rotational speed and fluid velocity. This study, however, was for wheel speeds from 30 to 45 rpm which lie well outside the range tested.

5.2.1.2 Wheel efficiency

There was a major improvement in the efficiency of the wheel when the number of blades was increased from 4 through to 12 blades (Figure 5.18). When the blade number was doubled from 4 to 8 there was a more than three-fold increase in the efficiency at the lowest wheel speed tested; this increase dropped to only 50 % at the highest speeds.

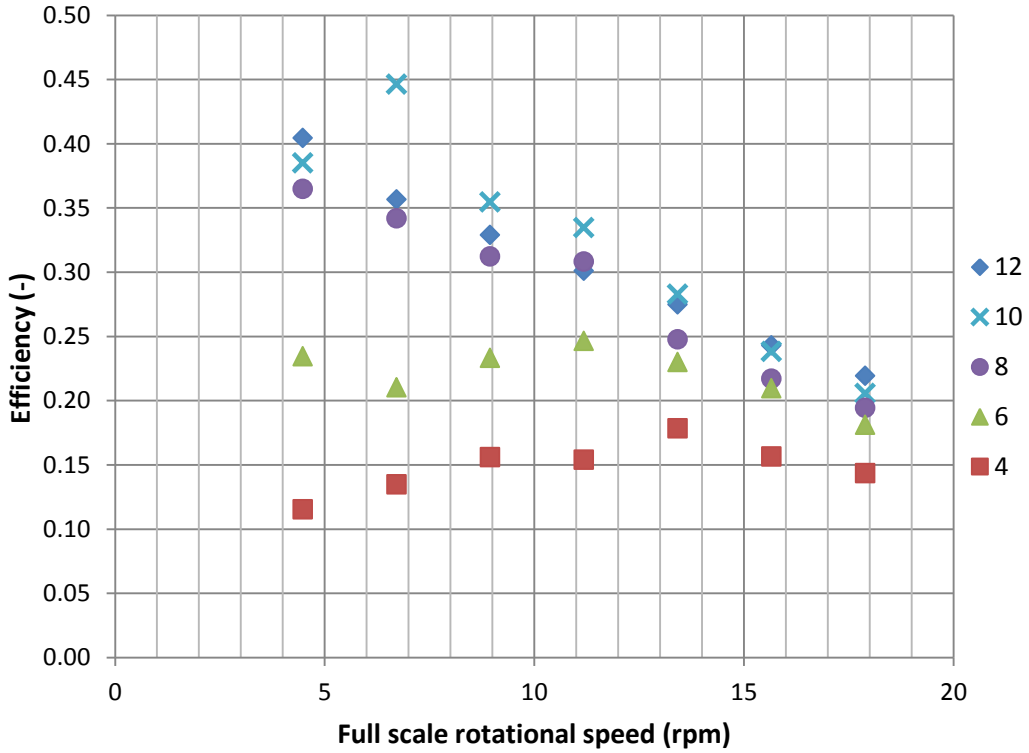

Figure 5.18. Variation in efficiency of paddlewheels with different numbers of blades with rotational speeds. The legend indicates the no. of blades tested.

The rise in the efficiency can again be attributed to the reduction in leakage when more blades are present, leading to a higher hydraulic power (Figure 4.22, Section 4.3.2.4). With a reduced number of blades more waves were also observed. Figure 4.7, Section 4.3.2.4.1, shows how the wave power increases for wheels with fewer blades as the time period of the wave increases. Waves are formed from the repeated oscillation caused by the blade entry and give no forward momentum to water particles but cause them to move vertically, thus providing no improvement to the system as explained in Section 4.3.2.4.1. The wave production and energy in the current system were not measured or quantified, however, as the waves were too transient and small.

Increasing the wheel speed reduced the efficiency for wheels with more than 6 blades for the entire range of rotational speeds tested. The 4 and 6-blade results showed an improvement in efficiency as the rotational velocity approaches 11 rpm where peak performance was achieved. Once the peak is past the results showed the same negative trend as for wheels with more blades, with all results grouping more closely together (Figure 5.18). The reduction in paddlewheel efficiency when rotational speed is increased has been shown numerous times for slow-rotating wheels (Park et al., 2014;

Brown and Tucker, 2013; Li et al., 2014; Mendoza et al., 2013a). This can be linked to the marked rise in the shaft power required at increased rotational speed (Figure 5.35). The shaft power increase is mainly caused by the greater head difference across the wheel at higher speeds. Mendoza et al. (2013) and Park et al. (2014) found a similar pattern in the power requirement when investigating the effects of paddlewheel frequencies. This effect was predicted by theory earlier on shown by Figure 4.17, Section 4.3.2.3.

Another reason for greater efficiency losses rising at higher rotational speeds is that more energy is being transferred into turbulence and wasted by the blades lifting the water into the air (Figure 5.20). Turbulence in the system increases as the wheel speed rises. This was not measured or estimated theoretically as it was taken into account by the empirical values. This rise can, however, be seen in the system as white water during the experiment. The rise in turbulence is beneficial for the biomass growth as it ensures homogenous mixing of nutrients and microalgae, as discussed previously in Section 3.4.2, and this rise should help increase that mixing. The turbulence reduces the energy in the system, however, as the eddies do not contribute to the linear fluid velocity but degrade in length eventually transforming into heat. Therefore there will need to be a compromise between the gain for the biomass growth and the loss of energy.

Under certain conditions loss of fluid from the raceway was observed during the experimental work. At very high rotational speeds the wheel starts to lift fluid out of the channel, significantly reducing its efficiency (Figure 5.20). This reduction is a result of using energy to move the fluid in an adverse direction. This has long been an issue for paddlewheels and waterwheels, and designs such as feathering or angled blades have sought to reduce this energy loss as explained in Section 3.5.4.3. Any improvements to the theoretical shaft power calculation would need to incorporate this phenomenon and also that of the dynamic motion of water.

As the wheel starts to lift fluid from the raceway into the air, the leakage and wave production losses become less critical. As a result the performances of the different wheels start to converge (Figure 5.18).

For the 4 and 6-bladed wheels peak efficiencies occurred at 13.5 and 11 rpm respectively, then efficiency decreased with falling rotational speed. The lower rotational speeds and blade numbers generated waves with a longer wave period and

height, leading to higher wave power and energy (Figure 4.6, Section 4.3.2.4.1). This higher wave power will reduce the overall useful hydraulic power produced by the wheel, thus reducing the performance. This was seen in the experimental results: if the lower wheel speed in Figure 5.19 is compared with higher speed in Figure 5.20 it is clear that waves are only present at the lower speeds.

Figure 5.19. An image of the paddlewheel at a model wheel rotational speed of 10 rpm (4.5 rpm full scale). Notice the large standing waves indicated on the image.

Figure 5.20. An image of the paddlewheel at a model wheel rotational speed of 30 rpm (13.4 rpm full scale). Notice the large extent of water lifting that occurs from the surface of the fluid.

5.2.2 Fluid discharge

The discharge is directly proportional to the hydraulic power and is an important factor to consider as it will have a large impact on the wheel efficiency. The discharge was calculated using the weir located downstream of the wheel. The discharge values recorded were then adapted from their raw format and grouped into distinct groups to the nearest 0.005 $m^3 s^{-1} m^{-1}$. This was done in order to make the large data sets more easily comparable. As the raceway is a closed system the depth parameters were constantly changing with the experimental conditions, and so lines of equal downstream depth and depth ratios were also superimposed on the results.

Figure 5.21 shows the discharge results for each wheel and their effect on the efficiency. The results clearly show a rise in the performance of the wheel as the discharge increased. For the lowest wheel speed of 4 rpm with 8 blades the efficiency increased from 0 % to a maximum of over 70 % at a discharge per unit width of around 0.05 $m^3 s^{-1} m^{-1}$. The performance was also dramatically affected by the wheel speed, with the highest wheel speed giving the lowest performance with a maximum of just below 30 % efficiency for all wheels tested. The higher wheel speeds, however, also showed a three-fold increase in discharge compared to the lowest speed. Discharge was also affected by the number of blades used, with maximum values of around 0.095, 0.135 and 0.165 $m^3 s^{-1} m^{-1}$ for the 4, 8 and 12-bladed wheels respectively.

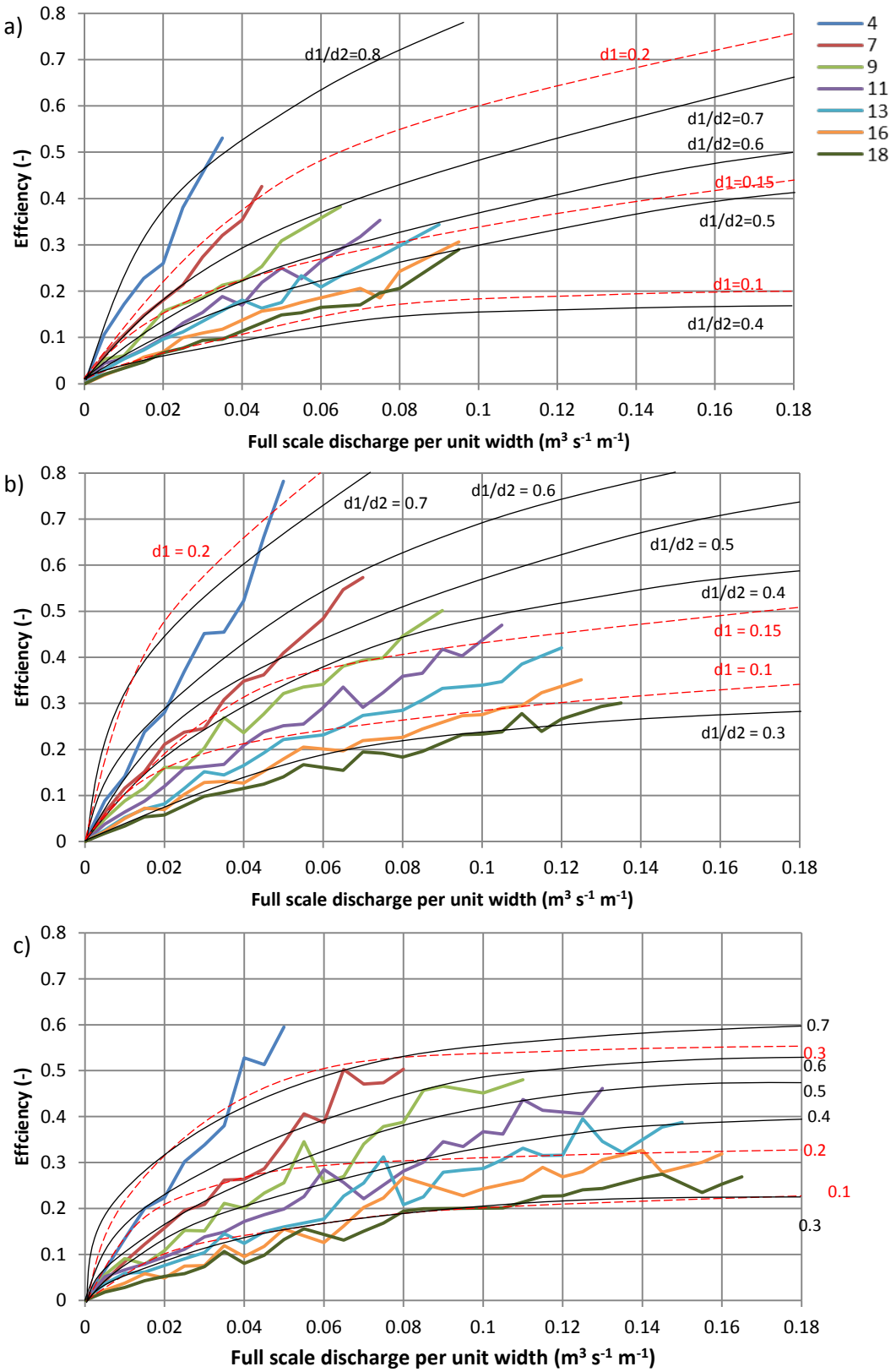

Figure 5.21. Relationship between the efficiency and discharge of the wheel with a) 4 blades, b) 8 blades, c) 12 blades. The legend indicates the rotational speed of the wheel. The black lines on the graph indicate lines of equal d_1/d_2 and the red dashed lines indicate lines of equal d_1. The values of these are indicated on the right of each graph.

The discharge achieved is an important factor as this needs to be great enough to ensure that the microalgae stay in suspension and pass around the raceway. The operating discharges of typical raceways are set within 0.03 to 0.08 $m^3 s^{-1} m^{-1}$. For the 4-bladed wheel it can be seen that the maximum discharge reached with the lowest rotational speed just about achieved the lower of these operating values. It is therefore likely that a higher rotational speed would need to be applied in practice. If more blades are added, however, the lowest speed is high enough to be applied in most circumstances resulting in an increase in efficiency from 35 to 50 %. If the upper end of the discharge range is required then the 8-bladed wheel would need to have an operating speed of at least 9 rpm; but the 12-bladed one would just about work at 7 rpm. This would increase the efficiency from 45 to 50 %.

Discharges greater than 0.08 $m^3 s^{-1} m^{-1}$ require much higher wheel speeds. These result in much lower efficiencies, as explained previously and shown in Figure 5.21. Therefore the discharge required must be matched specifically to the rotational speed and should be minimised if possible.

The number of blades affects the maximum discharge due to leakage in the system which reduces with higher blade numbers. It should be noted that there was a greater increase in the discharge with the move from 4 to 8 blades than from 8 to 12 blades: The average increase in the maximum discharge was 42 % when the number of blades rose from 4 to 8, but this fell to a 22 % increase when the blade number was increased from 8 to 12. The higher maximum discharges are a result of the gap beneath the blades being reduced when more blades are present, as shown in Equation 4.68. The greater discharges achieved with higher blade numbers mean that lower rotational speeds can be applied, thus increasing the efficiency.

The rise in the efficiency with discharge is a result of the higher hydraulic power output from the wheel. As the discharge increases towards the maximum, the efficiency increase begins to level off. This is due to the greater head difference across the wheel and thus the higher leakage which limits the maximum discharge and reduces the wheel efficiency.

In Figure 5.21 it can be seen that there was a slight reduction in performance when the number of blades was increased from 8 to 12. This is not purely caused by the change in

blade number, however, as the head difference also has an effect. As shown in the Section 4.3.2.3, for the same weir height increasing the blade number has a positive impact on the performance of the wheel (Figure 5.18).

When comparing the blade numbers directly (Figure 5.21 a, b and c) the ratio of upstream to downstream depths must be kept constant as well as the downstream depth. When this is done the efficiency for the 8-bladed wheel at 4 rpm with a depth ratio of 0.6 is around 30 % while for the 12-bladed wheel it is around 40 %. The maximum head difference achieved is also higher as the number of blades increases; this is discussed in Section 5.2.3 below.

5.2.3 Fluid depth and head difference

Fluid depth has been shown in the literature to affect the wheel performance, and the theory developed here also indicates head difference across the wheel should have an impact. The results in Figure 5.22 give an indication of the scale of this impact. In longer raceways the head difference across the wheel will naturally rise due to higher friction losses around the channel, however, in this experiment a weir was raised or lowered to increase the head difference acting on the wheel and thus simulate a greater channel length.

In order to evaluate the effect of the head difference on the wheel it is important to keep everything else constant. Figure 5.22 shows the effect of the head difference on the shaft power requirement across the range of wheel speeds and blade numbers investigated. Each set of results had the same upstream depth, from 0.125 m to 0.175 m. It has been shown previously in Section 5.2.1 that increasing the number of blades the efficiency of the wheel increases. This is also seen below, where for a constant head difference the shaft power requirement decreases when the number of blades increases from 4 to 12. For the shallowest depth with a head difference of 0.15 m, corresponding to a raceway length of around 600 m, the required power for the 4-bladed wheel is around 600 W; this was reduced to around 320 W for the 8 and 12-bladed wheels.

Increasing the downstream water level allows greater head differences to be achieved across the wheels, but has very little impact on the shaft power. It will, however, increase the discharge and thus the wheel efficiency.

Longer raceways will require a greater head difference to overcome the greater frictional losses that will occur. Therefore in very long channels it might be necessary to increase the fluid depth to achieve the required head. Increasing the number of blades, however, has a greater impact on the head difference realised. For example if a head difference of 0.2 m is required then the 4-bladed wheel could not be used even at its maximum rotational speed. Similarly the 8-bladed wheel would have to run at a faster rotational speed than the 12-balded one, leading to lower efficiency.

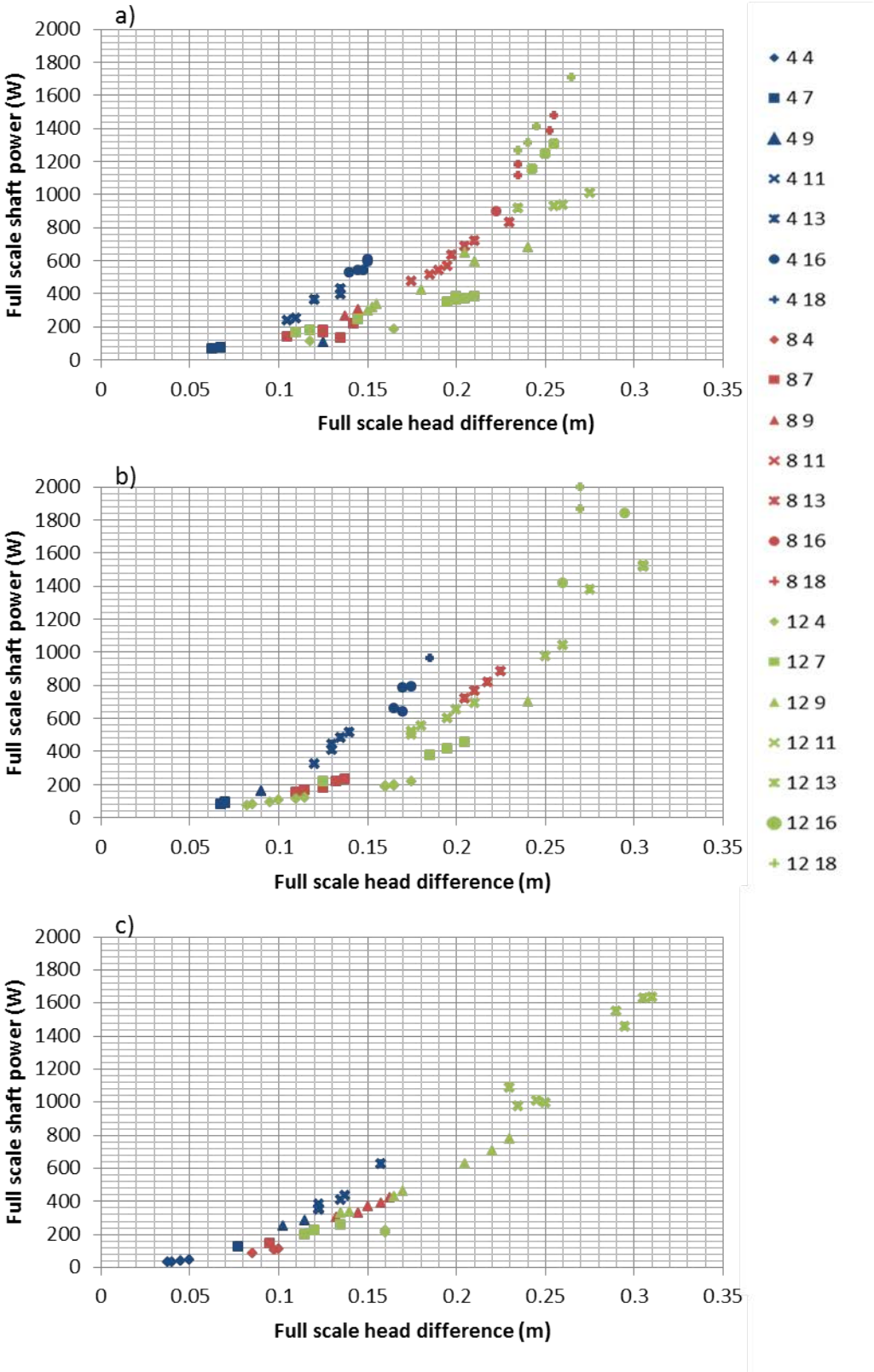

Figure 5.22. Relationship between the full scaled head difference and the full scaled shaft power with an upstream fluid depth of a) 0.125 m, b) 0.15 m, c) 0.175 m. In the legend the first number indicates no. of blades, and the second number gives the full scaled rpm.

Using a weir to increase the head difference has one major disadvantage in a closed system, as when the weir is raised the fluid depth upstream of the wheel drops as more fluid is held between the wheel and the weir. Therefore to allow comparison the whole data set the head difference results have to be normalised against the downstream fluid depth (5.1.3.7.1). Another consideration when using the weir is that the rotational speed of the wheel will also have an impact on the head difference and downstream fluid depth. For this reason it was not possible to compare the efficiencies of the different rotational speeds at regular head differences; therefore the rotational speed of the wheel was also normalised (Section 5.1.3.7.3).

The normalised head is affected by the wheel speed, with the highest normalised head values being reached at the maximum normalised wheel speed (Figure 5.23). At very high normalised wheel speeds further increases do not lead to any increase in the normalised head values. This is due once again to the leakage as the adverse pressure gradient is higher (Figure 5.24), and therefore more fluid flows back around the blades. Further increases in blade speed lead to equilibrium between the forward and backward changes in discharge and produce no meaningful increases in forward discharge.

As the normalised head was increased there was a drop in efficiency, with minimum efficiency occurring at the maximum normalised head (Figure 5.23). For any normalised wheel speed an increase in normalised head has a dramatic negative impact on the wheel performance. As the normalised head tended to 0.0 the efficiency of the wheel also tended to 100 %, as expected from theoretical considerations.

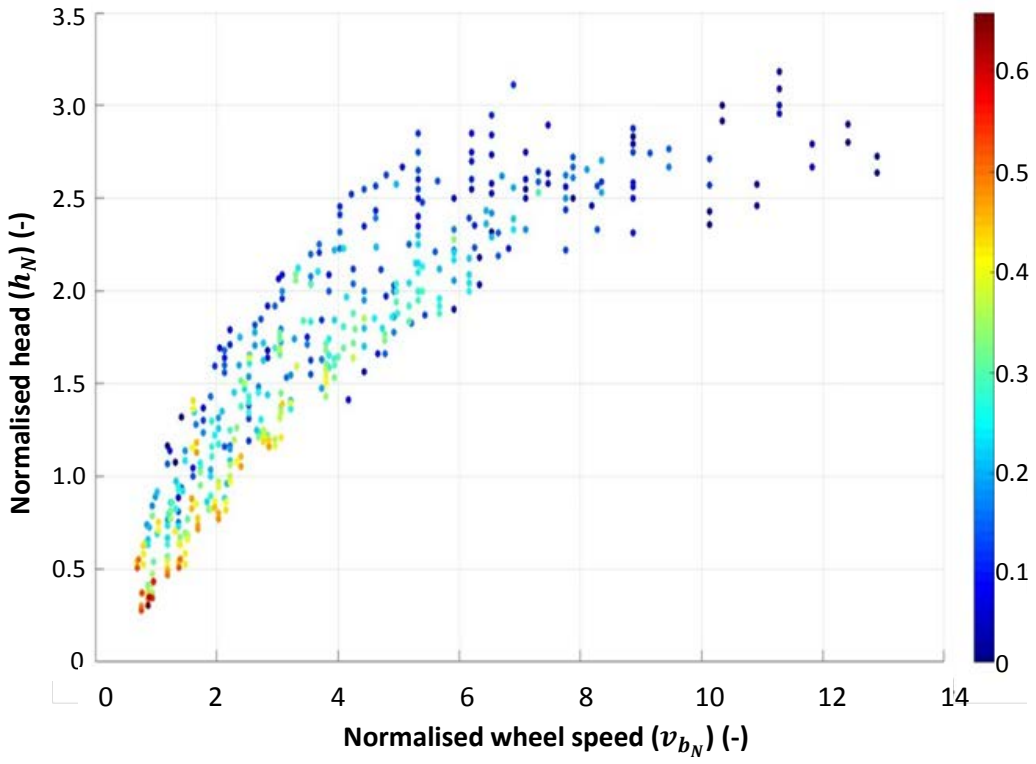

Figure 5.23. **Relationship between the normalised wheel speed, the normalised head, the efficiency and the discharge of the 12-bladed paddlewheel.** The colour legend indicates the efficiency of the wheel.

The increase in paddlewheel efficiency as the normalised head value (H/d_1) decreased is linked to the reduction in the adverse head acting against the motion of the blade (Figure 5.24). As the downstream depth tends to the upstream depth the efficiency of the wheel tends to 100 %. This can be deduced from the very small amount of shaft power needed to provide the hydraulic power to overcome this head difference. At this point there will be very little energy loss or leakage in the system as the adverse pressure gradient will also be very small. The theoretical calculations also show that as the depths begin to equalise the efficiency rapidly increases (Figure 4.17).

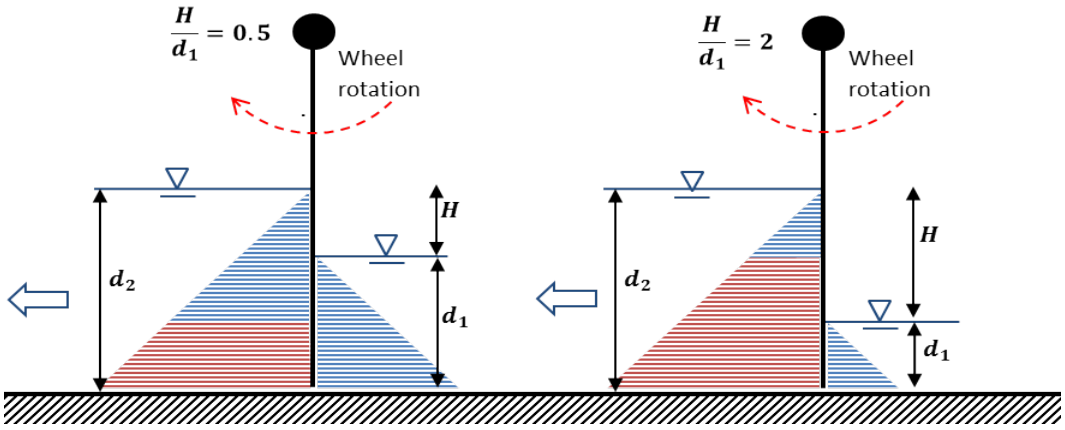

Figure 5.24. Visual comparison of the adverse pressure gradients in the fluid with a normalised head of 0.5 and 2. The light blue triangles represent the equal and opposite pressure gradients and the red quadrilaterals represent the adverse pressure gradient.

Increasing the submersion depth of the wheel, i.e. upstream depth (d_1), led to higher efficiencies. Similar results have been found by Park et al. (2014) where a rise in the submersion depth resulted in greater flow rates per unit power and was found to be more energy efficient than increasing the rotational speed. In this experiment doubling the fluid depth resulted in a more than three-fold increase in the wheel efficiency at all but the highest rotational speed. This increase in efficiency has been associated with the larger amount of fluid available for lifting, resulting in a higher discharge and increased hydraulic power (Park et al., 2014; Brown and Tucker, 2013). The amount of fluid in the system must be sufficient to meet the requirement of the wheel at the upstream side. In extremely long raceways this could become an issue as the required fluid depth at the downstream side of the wheel may become very large.

5.2.4 Length of raceway

The length of a raceway has an impact on the head loss that occurs and thus the head difference across the wheel. It has been shown above that the head difference and the efficiency are directly linked. The following set of results therefore investigated the link between the length of a race and the efficiency of the wheel.

As the length of the model raceway was limited, the weir was used to generate greater head differences and thus simulate much longer raceways. It was assumed that the majority of losses in long raceways occurred in the straight sections, therefore the simulated length can be calculated by using Manning's equation (Equation 5.11, Section 5.1.3.1) and the minor head loss equation to calculate head loss in the bends

(Equation 3.8, Section 3.2.4.). A loss coefficient of 3.0 was used to simulate end bends without deflectors (Kawamura, 2000). By using Manning's equation to calculate the length multiple different variables that affect the wheel can be taken into account. During the experiments, however, the downstream water depth varied with the flow rate and weir height. In order to compare the results, the length was therefore normalised against the downstream depth (Section 5.1.3.7.2). A wide range of normalised lengths was tested, from 100 to 50,000 m, covering the majority of standard raceway sizes.

Longer raceways require a greater head difference across the wheel, which has been shown to reduce wheel efficiencies; but they also contain a larger amount of culture for microalgal production. Therefore the traditional approach of comparing efficiencies may not be the most suitable. As algal biomass only grows in the top layer of the fluid (Section 3.1.1) it can be assumed that biomass yield is proportional to the raceway surface area. The relative shaft power (P_{S_R}), or shaft power required per unit surface area of fluid, indicates how much power is required compared to the total area available for algal growth and may thus be a more appropriate measure (Equation 5.28). A lower power to area ratio will result in a higher positive energy balance, as less energy is consumed per unit of algal biomass produced. As the calculation of the raceway length takes the fluid velocity into account this is a measure of the system efficiency that affects the design aspects of a raceway and can be used to select the optimal configuration.

$$P_{S_R} = \frac{P_S}{A_{surface}} \qquad \text{Equation 5.28}$$

where P_{S_R} is the relative shaft power (W m^{-2}), P_S is the shaft power (W) and $A_{surface}$ is the surface area of the full scale raceway (m^2).

It was found that increasing the normalised length of the raceway decreases the relative shaft power (Figure 5.25). Across the range of normalised lengths shown at the lowest rotational speed of 4 rpm the relative shaft power drops from 0.18 W m^{-2} to 0.01 W m^{-2}; while for the highest rotational speed of 18 rpm it drops from 50 W m^{-2} to 0.1 W m^{-2}. Similarly to the efficiency values there is a logarithmic decrease across the entire range of wheel speeds tested.

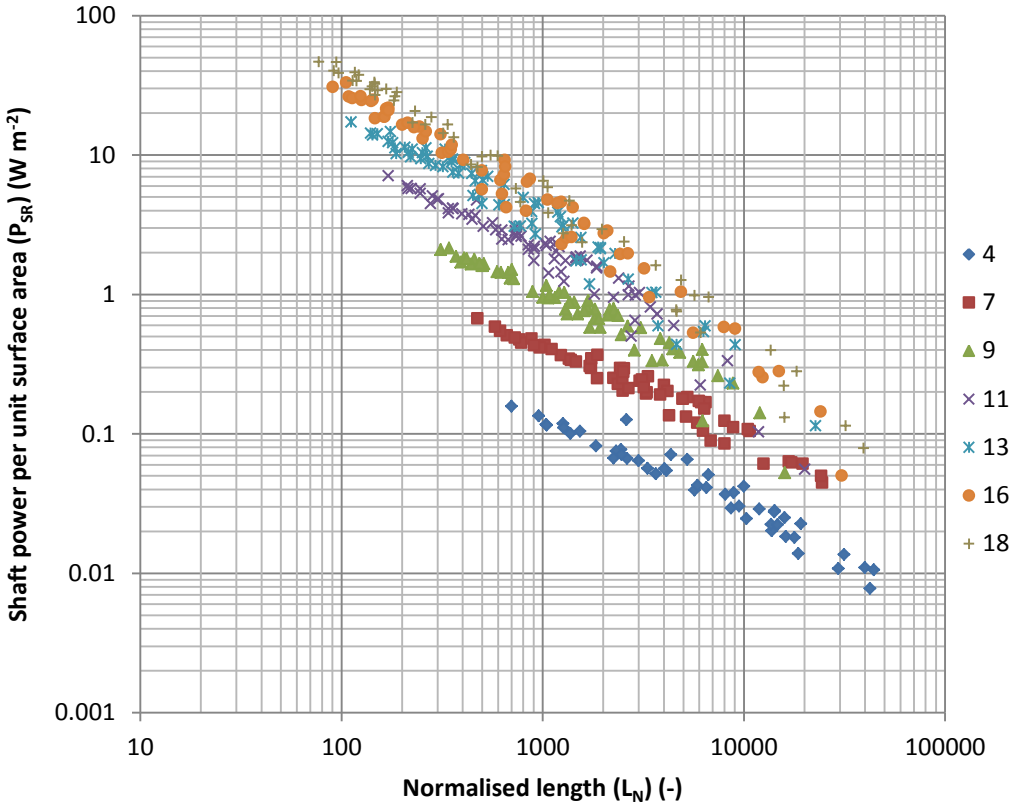

Figure 5.25. Graph showing the effects of the normalised length on the shaft power per unit volume for the 12-blade wheel. The legend indicates the full scaled wheel speed (full scale rpm).

Numerical modelling by Hadiyanto et al. (2013) and Ali et al. (2014) showed similar falls in the required power per unit area as the length to width ratio increased. This is due to the presence of more fluid in the system, which far outweighed any increase in the shaft power as a result of the greater head difference. The greater the surface area of fluid the higher the possible total yield of the system, therefore the lower relative shaft power with increased length will ultimately lead to higher biomass production.

Figure 5.26 shows a comparison of the shaft power per unit surface area and the standard measure of efficiency against the normalised wheel speed and raceway length for the 12-bladed wheel. The highest values for shaft power per unit surface area (red circles) are found at the lowest normalised lengths, whereas the highest efficiency values (largest circles) are generally found at the lowest normalised wheel speeds.

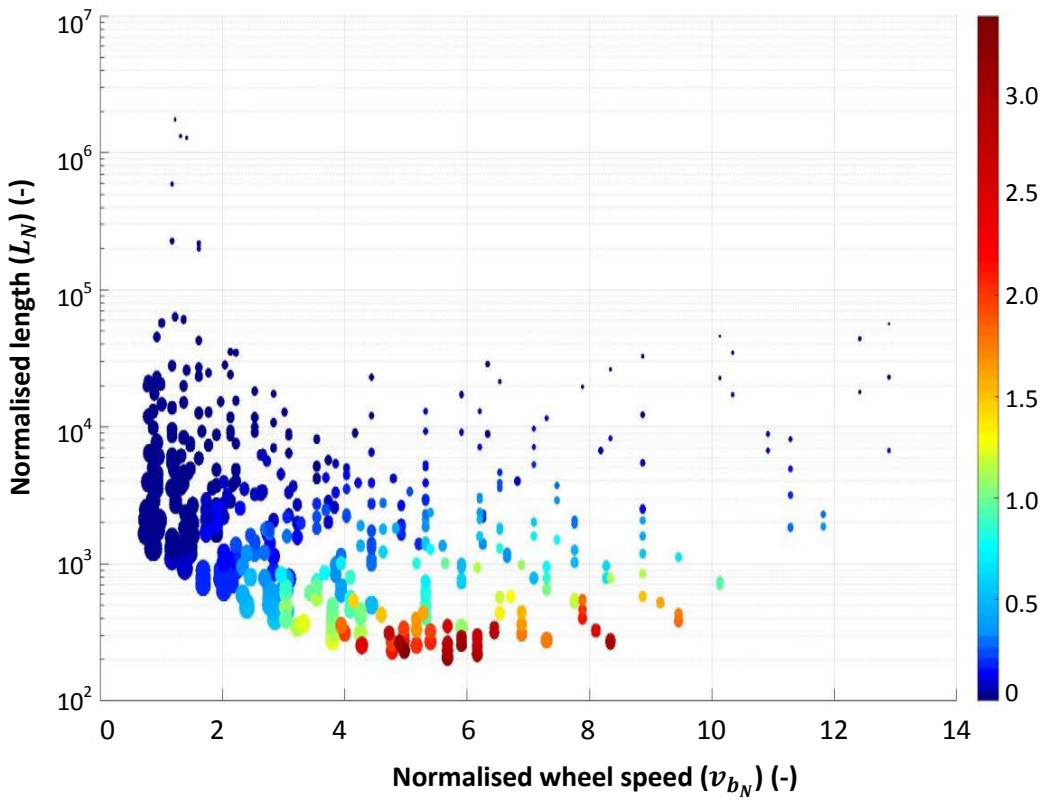

Figure 5.26. Variation of the efficiency and shaft power per unit surface area with changes in the normalised wheel speed and normalised length. The colour legend indicates the shaft power per unit surface area and the size of the data points indicates the efficiency with large points showing higher efficiencies.

The difference between the maximum efficiency and minimum relative shaft power is due to the different parameters affecting the results. Figure 5.23 showed that the head difference, which is the main factor when considering the efficiency of the wheel, rises with increased wheel speed, while Figure 5.25 shows that the shaft power per unit surface area is mainly driven by the raceway surface area or length. Therefore depending on what parameters need to be optimised ultimately will affect the operating conditions and design of the raceway.

5.2.5 Insert

The results thus far have focused on how the blade number, rotational speed or operating conditions affect the performance of the wheel. In Section 4.3.2.4.1 a platform insert was designed as a way to reduce the leakage by limiting the gap beneath the blades. The insert construction was discussed in Section 5.1.2.3. The results below present the performance of the 12-bladed wheel with and without the insert across the full range of rotational speeds. The results are shown for two weir heights of 0.175 m and 0.225 m with a base water depth of 0.125 m.

5.2.5.1 Efficiency

Figure 5.27 shows the changes in efficiency as the wheel speed increases both with and without the insert. When the insert was in place there was an improvement in the efficiency of the wheel at lower rotational speeds. This improvement declined with increasing wheel speed. For the lower weir height the insert increased the efficiency from 17 % to 36 % at the lowest rotational speed, but there was no improvement for speeds of 13 rpm or more. For the higher weir height the increase in efficiency was larger, from 4 % to 36 % at the lowest speed and 7 to 14 % at the highest. Similarly to the rotational speed results, the efficiency starts to decrease with decreasing rational speed after a peak for the 12-bladed wheel with no insert present. When the insert is used this peak does not occur and the efficiency keeps rising for the lower wheel speeds.

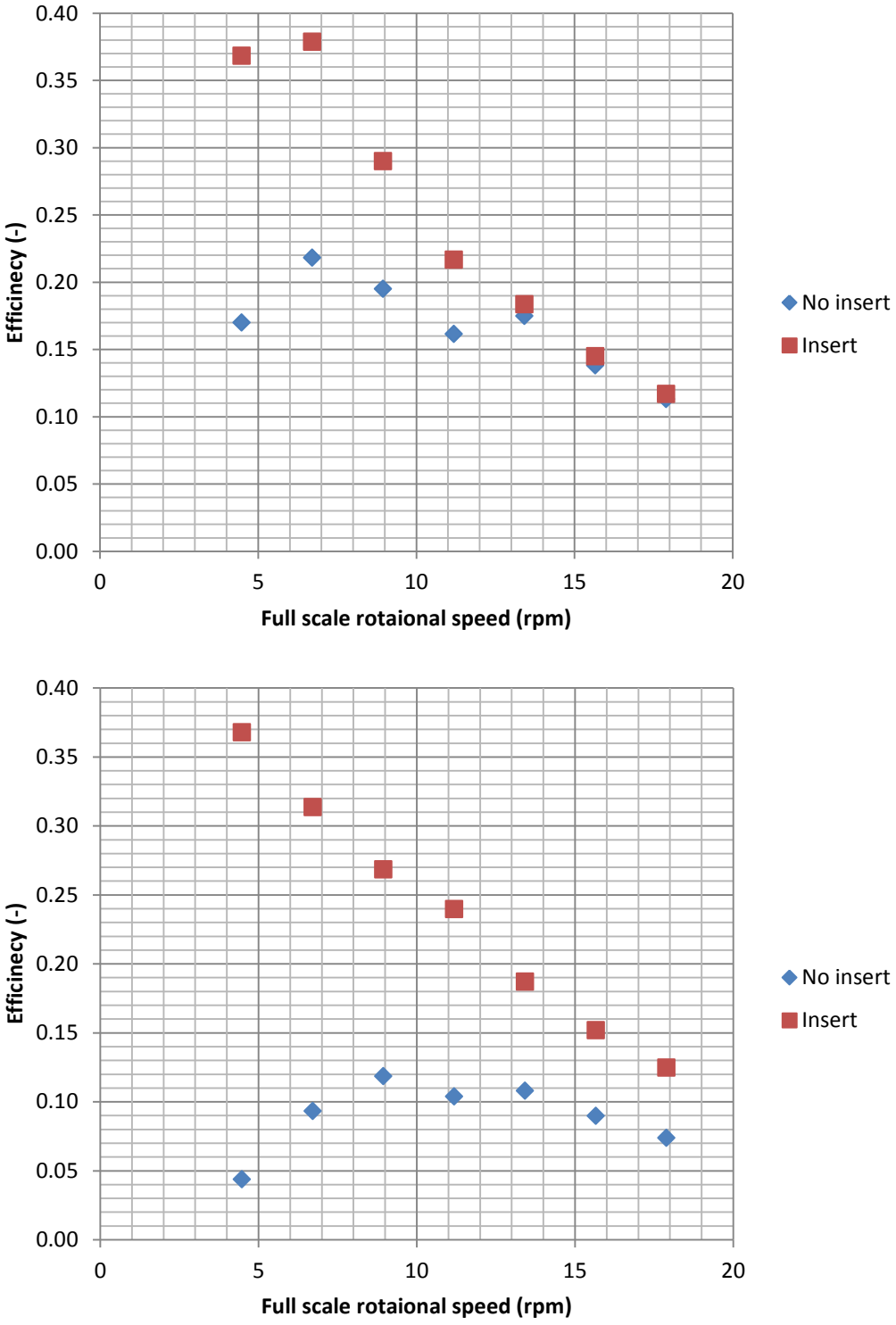

Figure 5.27. Variation in the efficiency across a range of rotational speeds. The first graph is for a weir height of 0.175 m and the second is for 0.225 m.

At the lower rotational speeds the main efficiency losses occur though the production of waves and leakage beneath the blades due to the head difference. When the insert was present there was less wave production in the system: if the raceway without an insert

shown in Figure 5.19 is compared with the insert present in Figure 5.28 it can be seen that fewer waves are formed by the wheel. The power of the waves will also be reduced as shown in Figure 4.8, as the wave height is smaller.

Figure 5.28. An image of the paddlewheel at a model wheel rotational speed of 10 rpm (4.5 rpm full scale) with the insert present.

At full scaled rotational speeds greater than 13 rpm there was little or no improvement in wheel performance with the insert. At these speeds the wheel begins to lift water with or without the insert present (Figure 5.29, Figure 5.20). This lifting of fluid becomes the dominant factor in the performance and thus the efficiency results begin to converge. A similar convergence also occurred when the number of blades was considered in Section 5.2.1.2. Alongside this the insert is able to maintain a much large head difference which will lead to a lower efficiency being recorded (Figure 5.31).

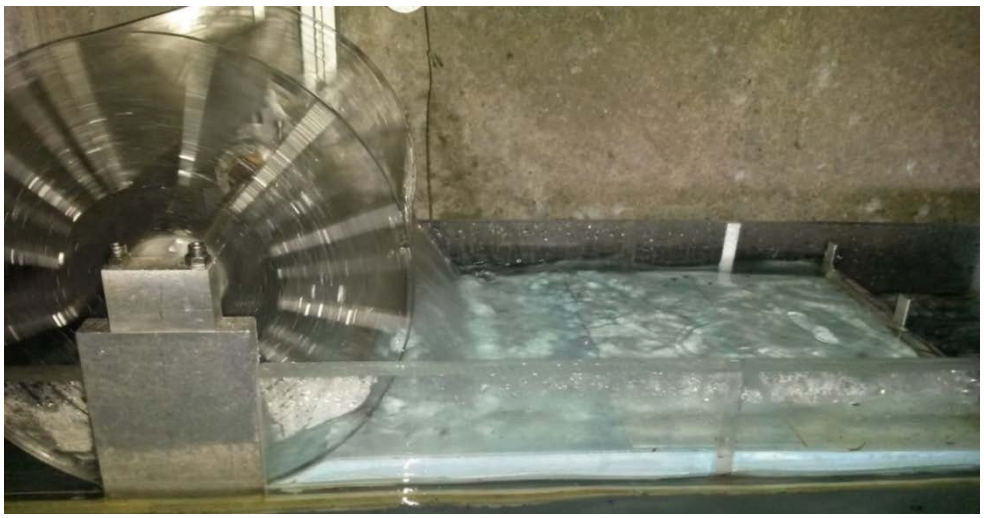

Figure 5.29. An image of the paddlewheel at a model wheel rotational speed of 30 rpm (13.4 rpm full scale) with the insert present.

5.2.5.2 Fluid discharge

The impact of the inset on the fluid discharge is an important consideration when designing an insert for use in full-scale systems. If use of the insert has a negative effect on discharge, the rotational speed of the wheel may need to be increase to ensure that the biomass stays in suspension. This would lead to lower efficiencies, as discussed in Section 5.2.1.2. Discharge was measured using the weir.

From the results in Figure 5.30 it can be seen that the use of the insert increased the discharge for both weir heights. For the higher weir height the discharge is consistently 0.15 $m^3 s^{-1} m^{-1}$ higher with the insert in place than without it. For the lower weir height, however, the increase was less pronounced at only around 0.005 $m^3 s^{-1} m^{-1}$. The higher discharge means that lower rotational speeds can be used can be used to achieve the same flow velocity. This reduces the power consumption of the wheel and generally increases its efficiency. For example if a discharge of 0.03 $m^3 s^{-1} m^{-1}$ is required at the lower weir height a rotational speed of 11 rpm is required when no insert is used, but a speed of 7 rpm can be applied if the insert is used. This corresponds to an increase in efficiency from 17 % to 37 % (Figure 5.27).

The insert works by maintaining the minimum gap beneath the blades as they rotate. This minimum gap is 17 % smaller than the average gap that occurs when the insert is not in place for a 12-bladed wheel (Table 4.1). Equation 4.62 shows that the leakage discharge is directly proportional to the size of the gap and as this is smaller when the

insert is used there will be less leakage. The reduction in the leakage discharge results in a greater forward discharge. The leakage is the main loss factor in the forward discharge and should be minimised as much as possible.

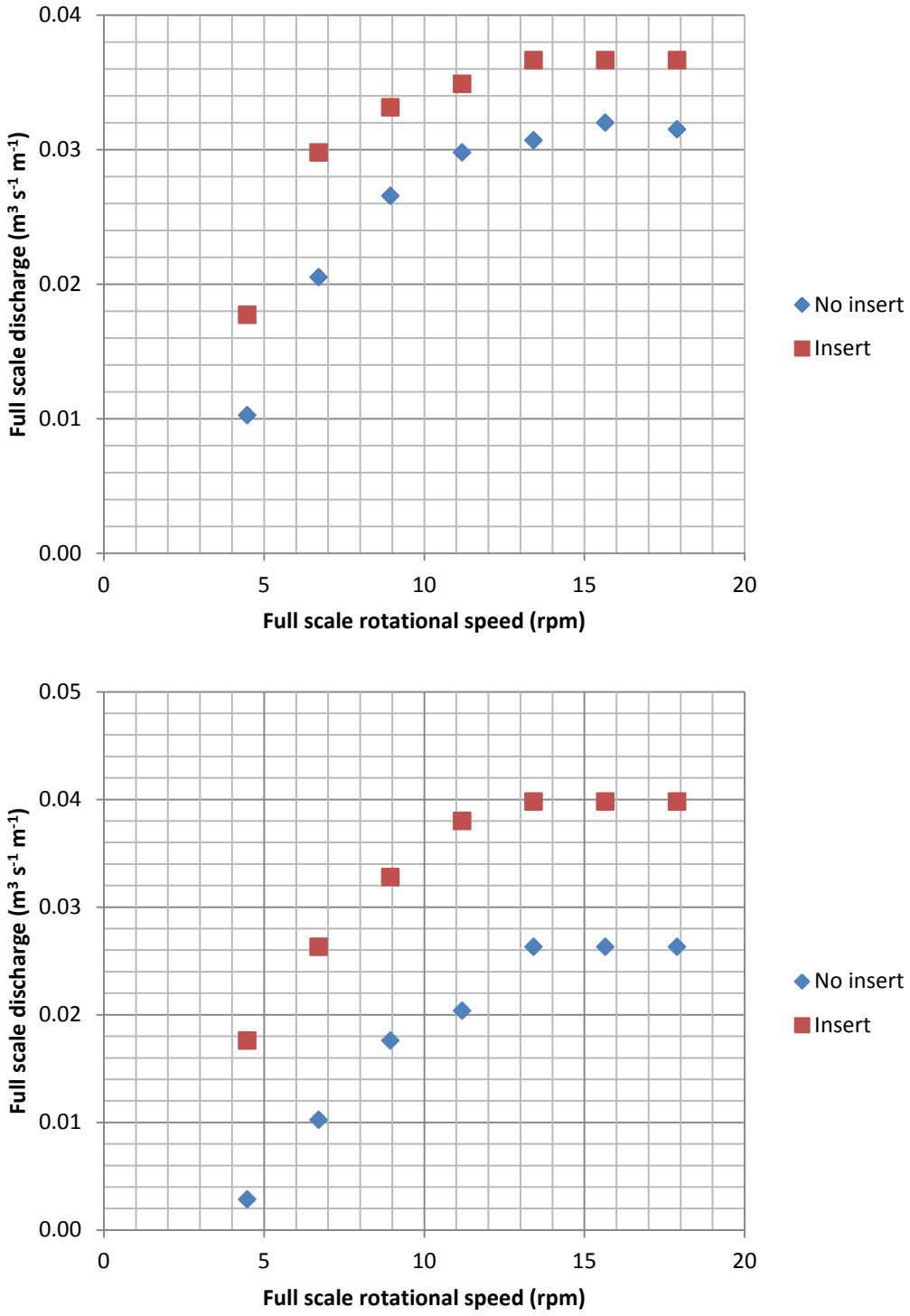

Figure 5.30. Relationship between the rotational speed and the full scaled discharge. The first graph is for a weir height of 0.175 m and the second is for 0.225 m.

5.2.5.3 Head difference

To evaluate the effect of the insert on the leakage and in raceways of different lengths the head difference across the wheel was considered. The head difference was maintained through the use of the weir and so the head difference results were normalised against the upstream depth.

For each rotational velocity there was a 50 % to 100 % rise in the normalised head across the entire range of speeds considered. The greater head differences simulate longer raceways which mean that the insert could be used in long raceways to reduce the wheel speed required to achieve the head difference needed to drive the fluid. This is an important point when trying to increase the overall efficiency of the wheel, as lower wheel speeds generally have a higher efficiency. For example at a normalised head difference of 2.0 and a weir height of 0.175 m a wheel speed of 13 rpm is required without the insert, but a speed of only 9 rpm would be sufficient with the insert for the lower weir height. This corresponds to an increase in efficiency from 17 % to 29 % when the insert is used.

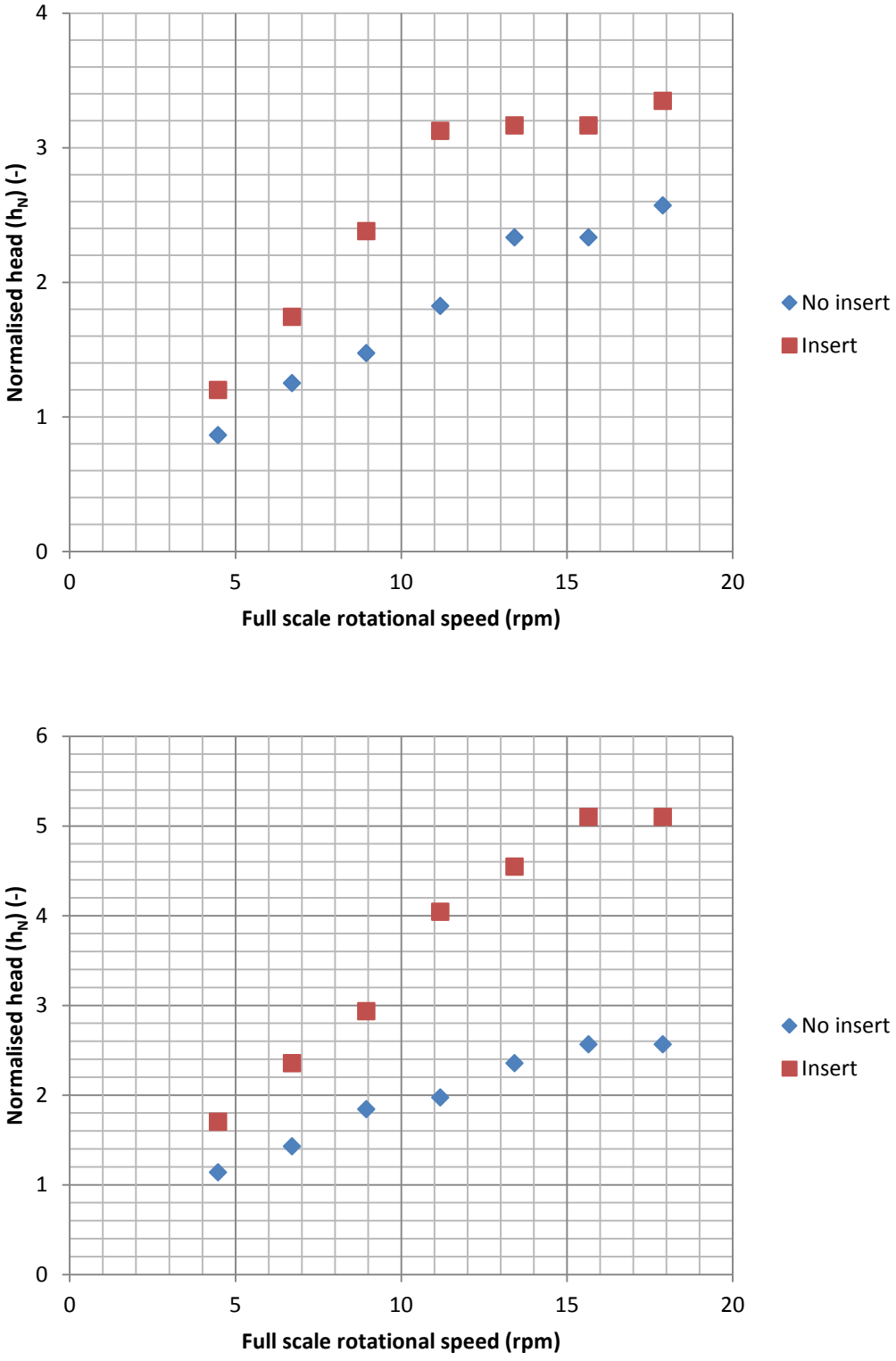

Figure 5.31. Variation in the normalised head across a range of rotational speeds. The first graph is for a weir height of 0.175 m and the second is for 0.225 m.

The reduction of the leakage was theoretically analysed in Section 4.3.2.4.1 and is reduced when the insert is present. This can be seen from Figure 5.31 where the

maximum head loss reached at any rotational speed was greater with the insert present. This shows that the wheel can hold a greater adverse pressure gradient across the wheel as less fluid is flowing backward. This is important if longer raceways are to be built with higher head differences.

5.3 Model validation

5.3.1 Theoretical model validation

The following section validates the theoretical equations set out in Section 4.3.2 against the experimental results and discusses the possible reasons for any differences.

As shown in the experimental results section the rotational speed affects all aspects of the wheel's performance, from fluid speed to head difference and efficiency. The effect of the rotational speed of the wheel (ω) on paddlewheel efficiency was investigated, keeping the number of blades, water height and weir height constant. The experimental results were then compared with values calculated using the equations set out in Section 0. The 12-bladed wheel was selected, with a full-scale base fluid height of 0.175 m and weir height of 0.185 m, to be analysed. The different parameters were scaled using the equations set out in Section 5.1.4. The depths and head differences changed depending on the rotational speed, and the base fluid depth is measured before the wheel has started.

Figure 5.32 shows the theoretical and experimental model results for the fluid velocity directly upstream of the wheel at different rotational speeds. For all wheel speeds tested a fluid velocity greater than 0.1 m s^{-1} was achieved (Figure 5.32), which is considered the minimum necessary to keep the biomass in suspension. The theoretical values increased linearly from 0.31 m s^{-1} to around 1.3 m s^{-1} at the fastest rotational velocity. This is expected as the radius is over 5 times larger than the upstream depth, and as the rotational speed increases the upstream depth decreases further: therefore the upstream depth term of Equation 4.49 becomes negligible and the fluid velocity increases linearly with rotational speed. The measured results follow a similar linear profile but start at a lower velocity of 0.16 m s^{-1} rising to just below 1.0 m s^{-1}. For these initial values, at less than 11 rpm the theoretical and measured results were very similar whereas above 11 rpm the differences increase. If leakage of the fluid is taken into account and the fluid velocity is recalculated then the increase is still linear but the

calculated results are very similar to the measured values for all rotational speeds (Figure 5.32).

The rate of increase of the measured and with-leakage values is slightly lower than the theoretical results, leading to greater differences at higher rotational speeds. This is due to energy from the blade movement going into other forms, such as turbulence and waves, which are not associated with forward movement of the fluid. At low rotational speeds this loss was minimal with only a small amount of turbulence occurring. As the wheel speed increased more energy is dissipated through turbulence and other dynamic effects as explained in Section 4.3.2.4.1.

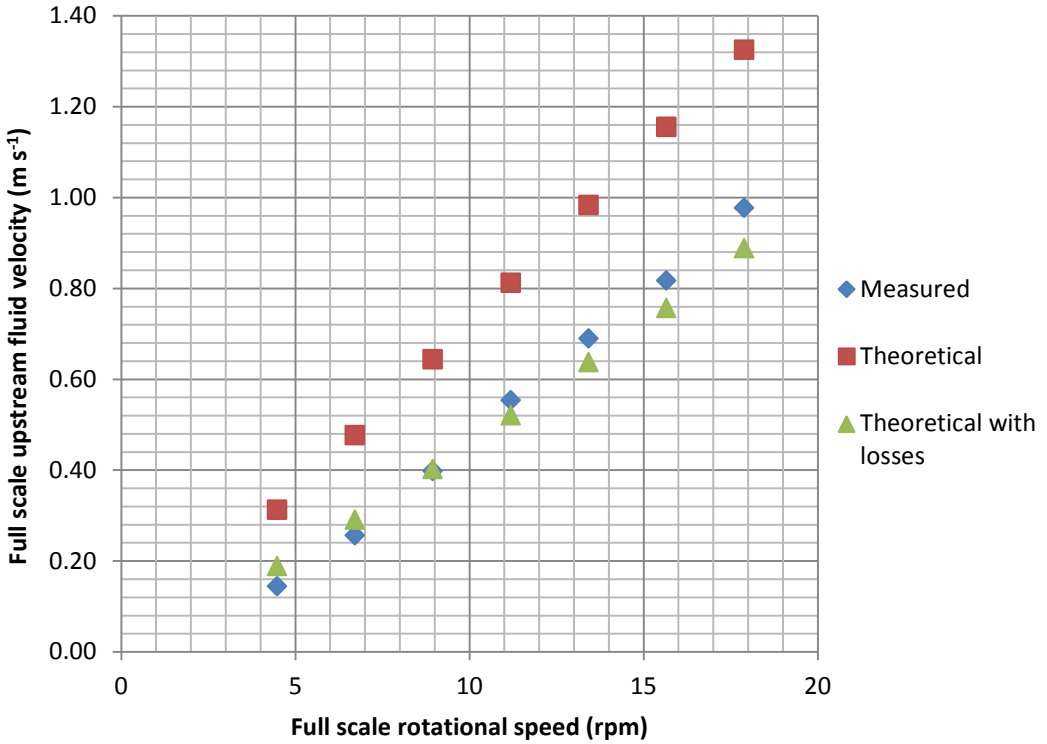

Figure 5.32. Variations in the upstream full scaled fluid velocity with changes in the full scaled rotational velocity.

Figure 5.33 compares the effect the of wheel speed on the theoretical discharge (Q_T), the measured discharge (Q_M) and the theoretical discharge with leakage (Q_{T_l}). It was found that the theoretical discharge was consistently around 0.4 $m^3 s^{-1}$ greater than the measured discharge. If leakage beneath and around the blades is accounted for this difference is minimal. The theoretical results follow a linear profile and this is again due to the upstream depth terms becoming negligible. All three sets of results showed a

similar positive relationship between the discharge and wheel speed, unlike the results for the full-scale velocity (Figure 5.32). The results with leakage show a slightly lower rate of increase compared to the non-leakage results. This is due to the leakage discharge, Equation 4.62, increasing at the greater head differences that occur at higher wheel speeds. There is a very good agreement between the measured discharge and theoretical discharge with leakage.

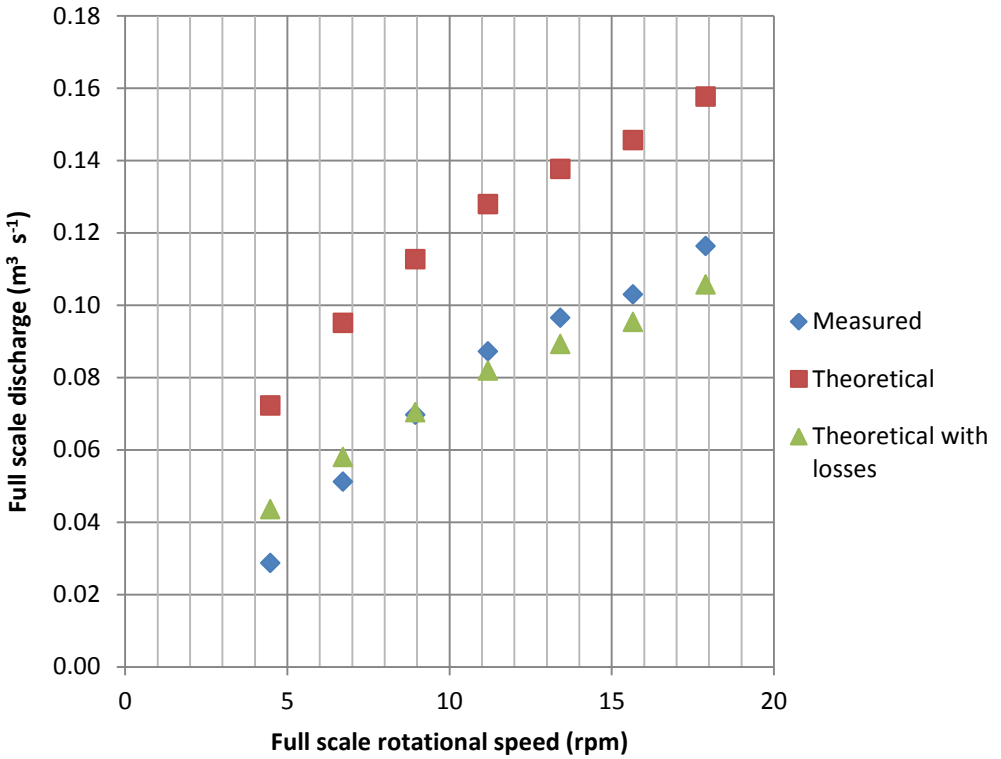

Figure 5.33. Relationship between the full scaled rotational velocity of the wheel and the discharge. The theoretical discharge was calculated using Equation 4.50 Section 4.3.2.1, the theoretical discharge with leakage was calculated using Equation 4.69, Section 4.3.2.4.

Figure 5.34 compares the theoretical and measured hydraulic power output from the wheel. The theoretical power is around twice the measured power at the lowest rational speed and around 75 % more at the highest. When leakage is taken into account the theoretical power output drops significantly to be more in line with the measured results. The power produced by the wheel is directly linked to the discharge and head difference. As the theoretical discharge values are around 60 % to 100 % greater than the measured discharge values it can be deduced that is the main factor driving the difference in hydraulic power.

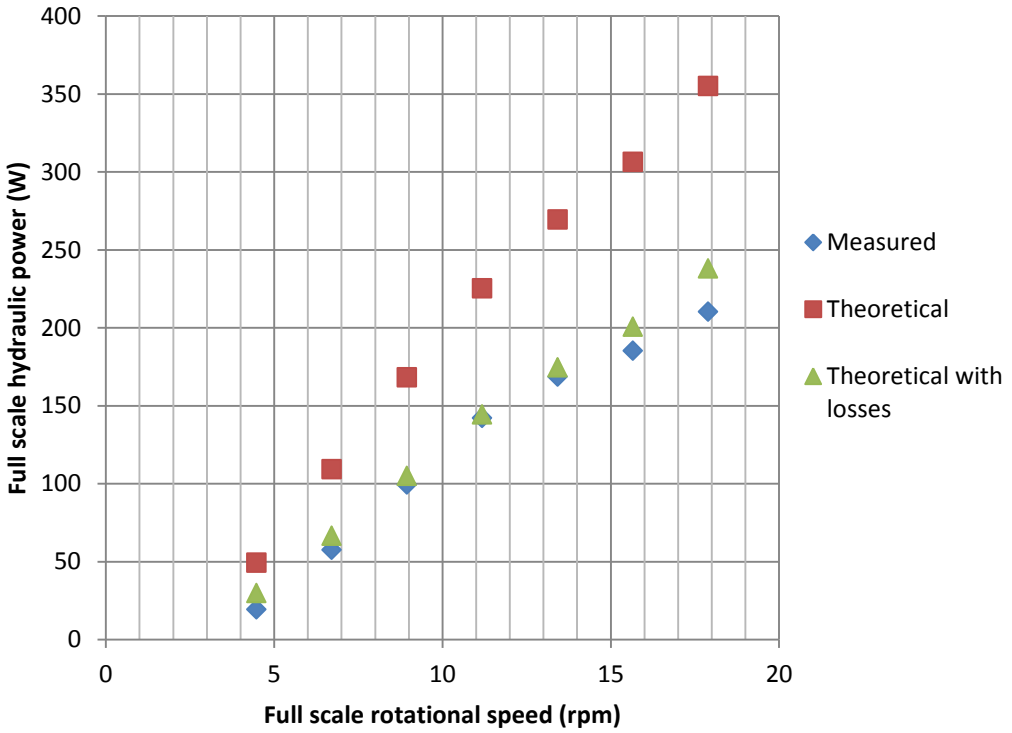

Figure 5.34. Comparison of the theoretical and measured hydraulic power.

The shaft power is the power input into the wheel and is the main focus of wheel efficiency theory devised in Equation 4.59, Section 4.3.2.2. It is therefore especially important to validate this against the experimental results. Figure 5.35 compares the theoretical shaft power calculated for the conditions when the experimental shaft power was measured. Equation 4.59 shows that the power is linearly correlated to the rotational speed, but as a result of the changes in the depths the increase in the power requirement is not linear as shown in Figure 5.35. As the downstream depth increases the $R(d_2^2 - d_1^2) - \frac{1}{3}(d_2^3 - d_1^3)$ term will increase as the depths are around 0.2 m. At very low rotational speeds the measured and theoretical results were only slightly different, and both increased with rotational speed. As the rotational speed increases, however, the difference between them grows rapidly with the measured shaft power being around 40 % greater at the highest rotational velocity measured. This increase can mainly be associated with the change in the way the blade interacts with the fluid as it begins to increase in speed. At high rotational speeds the blade starts to lift fluid out of the channel (Figure 5.20). This lifting leads to much higher shaft power requirements. In the experimental work it was observed that the amount of fluid lifted from the channel

is a function of the downstream fluid depth and wheel speed, but this was not included in the theoretical calculations as it is a purely dynamic system.

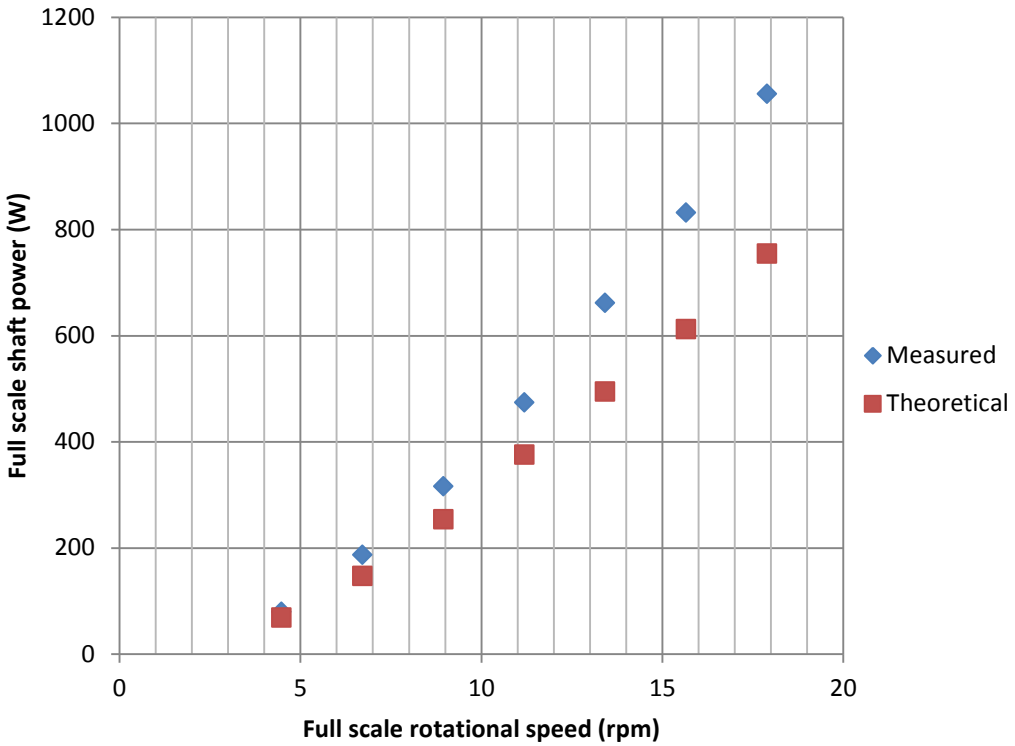

Figure 5.35. Relationship between the full scaled rotational speed of the wheel and the full scaled required shaft power.

The relative discharge is the discharge per unit power requirement. The previous paddlewheel theory used this expression for the efficiency, as the hydraulic power could not be calculated (Section 4.2.4). Figure 5.36 shows how the relative discharge changes with the speed of the wheel. It is clear that the previous theory, which works by calculating the drag force on a blade, overestimates the relative discharge at lower rotational speeds with values around eight times higher than the measured results. This is not due to the drag force coefficient, as this will cancel in the relative discharge calculation. It is mainly linked to the underestimation of the shaft power as this was around 30 % of the measured shaft power at the lowest speed rising to only 80 % at the highest. It is also partly due to calculation of the discharge using the velocity of the blade tip rather than half the upstream depth, leading to overestimation of the discharge.

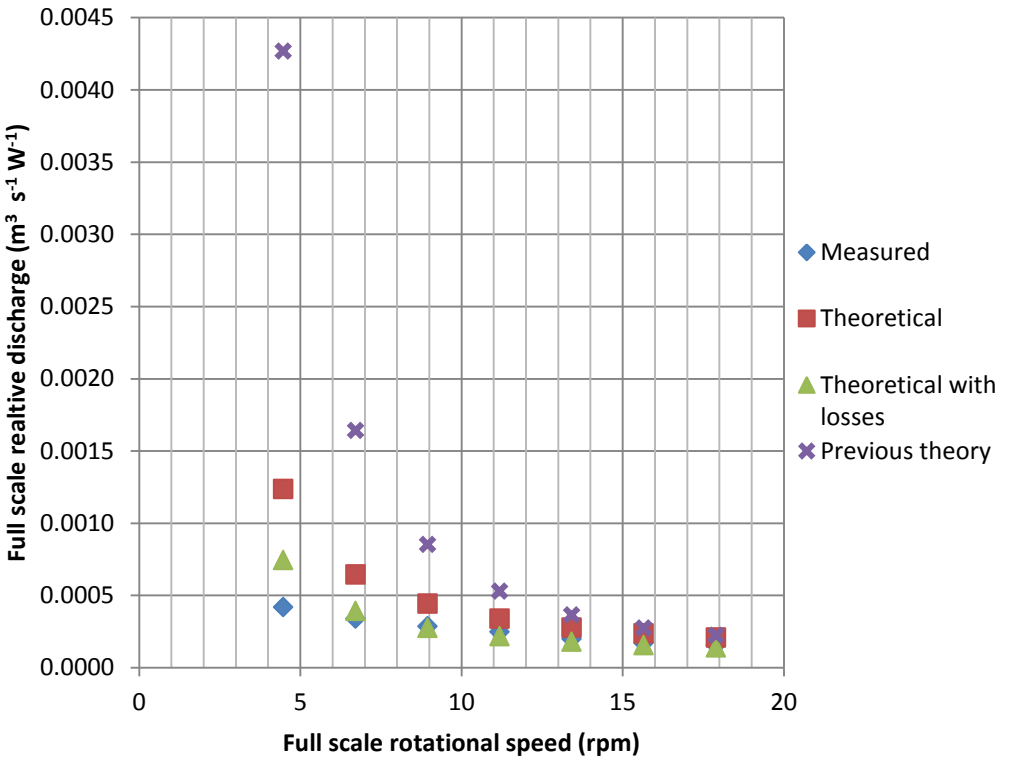

Figure 5.36. Comparison of the relative discharge and the rotational speed for the measured, new and previous theories.

The theoretical and calculated wheel efficiencies are compared in Figure 5.37. While the rotational speed is not a parameter in the efficiency in Equation 4.61, it does affect the fluid depths. As the rotational speed decreases to 0 rpm there will be no head difference across the blade and the theoretical efficiency will rise to 100 %. This is in line with the predictions shown in Figure 4.17.

The theoretical value is consistently larger than the measured values for the entire range of speeds investigated (Figure 5.37). The measured efficiency value followed a similar decreasing trend to the theoretical values with leakage as the rotational speed increased. Across the entire range of rotational speeds the theoretical values were around twice as high as the measured values. If the fluid leakage is taken into account, however, then the theoretical values are only 20 - 40 % higher than the measured values. The difference in the efficiency values is due to the theoretical shaft power being lower than the measured shaft power and the theoretical hydraulic power higher than measured hydraulic power leading. These differences between the theoretical and measured powers lead to a compounding of the errors to give a much higher theoretical efficiency (Figure 5.35).

At rotational speeds below 11 rpm the theoretical efficiency with leakage started to level off and there was a slight decrease at the lowest rpm investigated, whereas the theoretical values continued to rise towards 100 % efficiency. This indicates that a maximum possible efficiency of around 50 % is achievable for this configuration.

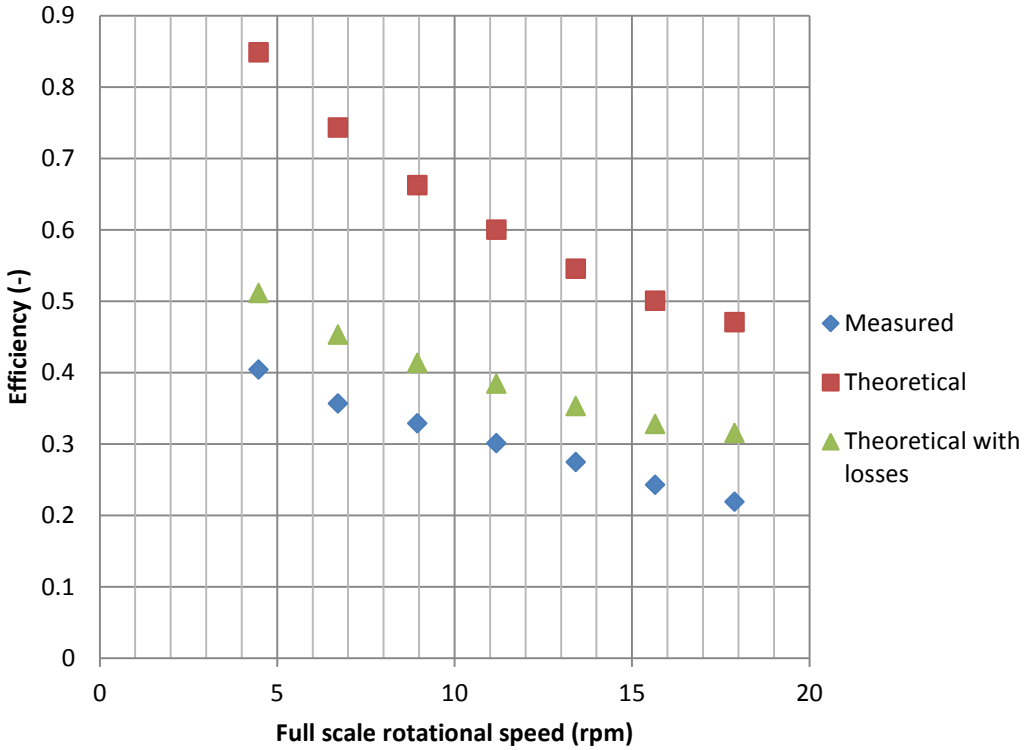

Figure 5.37. Relationship between the efficiency and the full scaled rotational velocity of the wheel.

5.3.2 Experimental model validation

In order to validate the experimental model, and to determine whether scaling affected the results, data was collected from a full sized algal raceway located in Chiclana de la Frontera, Spain (Figure 5.38).

Figure 5.38. The 500 m^2 prototype raceway reactor located in Chiclana de la Frontera.

The prototype raceway channel is 80 m long by 3 m wide, giving a total surface area of 500 m^2, and propulsion is provided by a 1 m diameter flat 8-bladed wheel (Figure 5.39). Two different operating depths of 0.3 m and 0.25 m were tested at paddlewheel speeds ranging from 3 to 10 rpm. The same method as in the experimental model was applied to the full-scale raceway to measure the head difference across the wheel using piezometers. The fluid velocity was measured by timing a semi-submerged luminous object between two marker points located 5 m apart directly downstream of the wheel. The power consumption was calculated directly from the electricity consumption of the motor: therefore the efficiency results also include the efficiency of the motor and gearbox and must be adapted when compared to the model efficiency data. The rotational speed of the motor will also impact the efficiency on it, however only a single stated figure was given for this motor which is likely to be the maximum efficiency achievable.

The results used for comparison with the experimental model were for an 8-bladed wheel where the scale length and operating conditions were similar to those in the prototype facility.

Figure 5.39. The fluid in the raceway was driven by a 1 m diameter flat 8-blade paddlewheel.

Figure 5.40 shows that the fluid velocity of the experimental model is initially 40 % lower than the velocity measured in the prototype. This can be attributed, in part, to the weather conditions at the plant when recording the velocity of the fluid, as there was a strong wind blowing parallel to the flow direction. The prototype fluid velocity also begins to level off at relatively low rotational speeds compared to those in the model. This was not expected, but could possibly be due to the fact that the tolerances in the large-scale paddlewheel are not as tight as in the model. Therefore the levelling off seen in the prototype could be due to the peak head difference being reached as in these conditions there is likely to be more leakage.

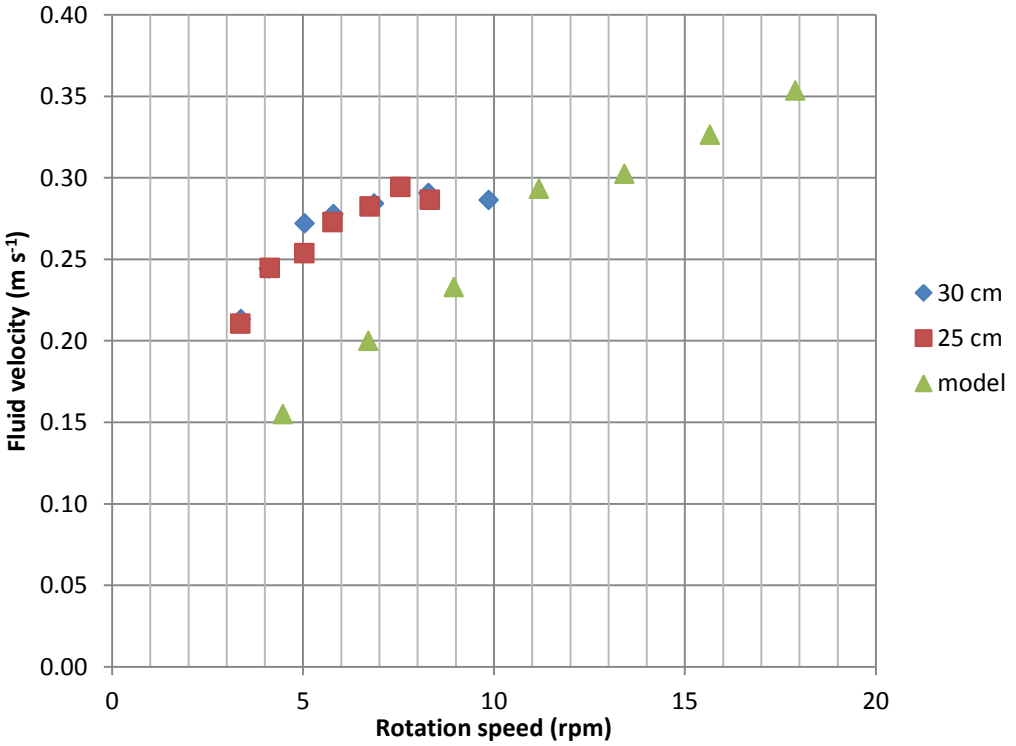

Figure 5.40. Relationship model fluid velocity and prototype fluid velocity and wheel speed. The dimensions in the legend indicate the depth of the fluid in the prototype.

Figure 5.41 shows the efficiency results for the model and the prototype. The efficiency results for the model have to be adjusted as these do not take into account the motor and gearbox efficiency losses. A combined motor and gearbox efficiency value of 40 % was applied to the model results to calculate the "adjusted power" results. When this is done the model efficiency values lie in a similar range to the prototype. It can therefore be suggested that the reverse is true, so that the actual maximum efficiency of the prototype paddlewheel is around 40 %.

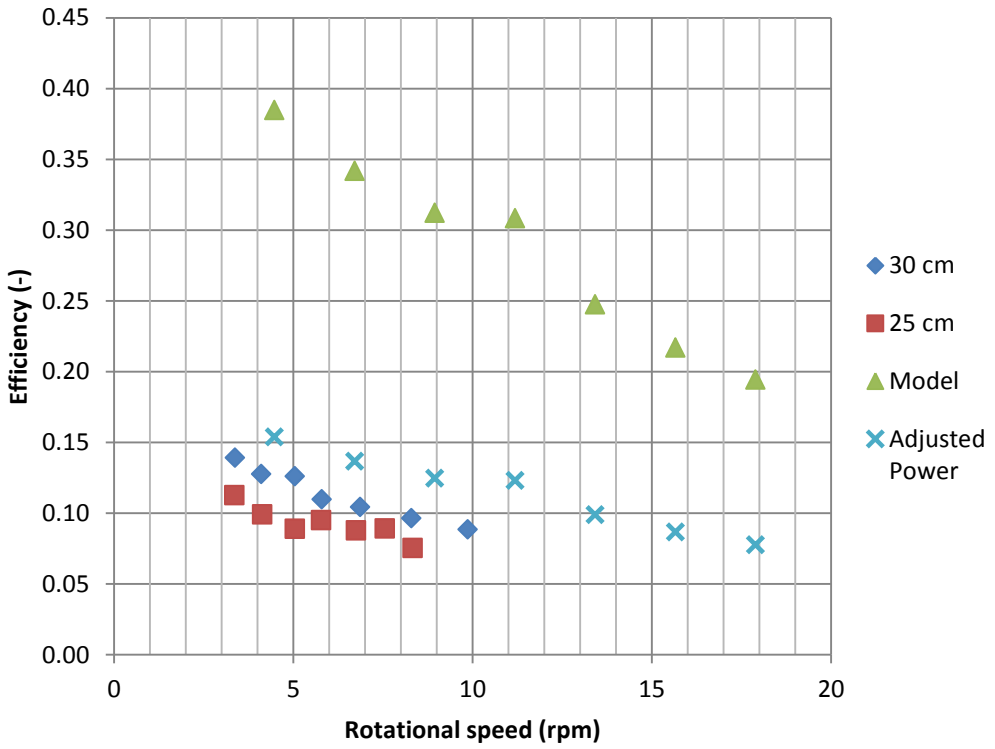

Figure 5.41. The relationship between the efficiency of the prototype and the model wheel and the rotational velocity. The dimensions in the legend indicate the depth of the fluid in the prototype and the raw and adjusted model data.

The results show that the efficiency of the prototype wheel reduced when the fluid depth decreased, as has been found in other studies and also in the experimental work. The model results are within 25 % of the results collected from the large-scale paddlewheel. The lower efficiencies in the large-scale system were expected as it is harder to get consistently good tolerances. This is indicated in the theoretical work in Section 4.3.2.4 where the larger the gap beneath the blades the higher the leakage discharge. The wheel is also likely to experience greater frictional losses from the shaft as there is considerably more weight acting on it. The difference between the adjusted power results and actual results is most likely due to this efficiency value for the motor being incorrect as this is most likely the maximum efficiency value and a lower one is expected.

5.4 Designing a paddlewheel driven system

To design the optimal system three parameters must be known: the length of the raceway, the required depth and the velocity of the fluid. These contribute to the head loss in the system and therefore the head gain that is needed from the wheel. As discussed previously the head difference is a key factor when trying to optimise the wheel and should be minimised as far as possible to limit the power required. This can be done either through reducing the fluid velocity if possible or minimising the losses, i.e. introduce deflectors around bends or a smoother channel bed.

The head loss should not be reduced by decreasing the length of the raceway if possible as longer raceways use less power per unit surface area where the biomass may grow. Therefore the length of the raceway should be maximised as much as possible. This may be limited by either the constraints of the construction site or the maximum head difference wheel can reach. In order to increase this, a wheel with more blades should be used as this limits the backflow and therefore a greater head difference can be maintained. By reducing the backflow the efficiency of the wheel is also increased as there is will be a higher discharge and therefore a higher fluid velocity.

The rotational speed of the wheel should be as low as possible to ensure that the efficiency is as high as possible. In order to do this a wheel with more blades should be used as these can maintain higher head differences at lower speeds. An additional improvement should be to use the insert design as this reduces the backflow further leading lower wheel speeds and greater efficiencies.

The final area that needs to be considered is the leakage discharge as this is the main factor for energy loss from the paddlewheel. The leakage can be reduced by in two ways: decreasing the head difference or the gap beneath the blades. The former drives the fluid through the gap and is linked to the loss of efficiency as explained earlier. The latter can be achieved by increasing the number of blades or further still by using the insert.

Figure 5.42 shows how this works in a simpler flow diagram format and how the head difference is important for all the processes that can be undertaken to reduce the pumping power. The leakage and head loss are inevitably linked such that decreasing the head loss reduces the leakage and reducing the leakage reduces the head difference required.

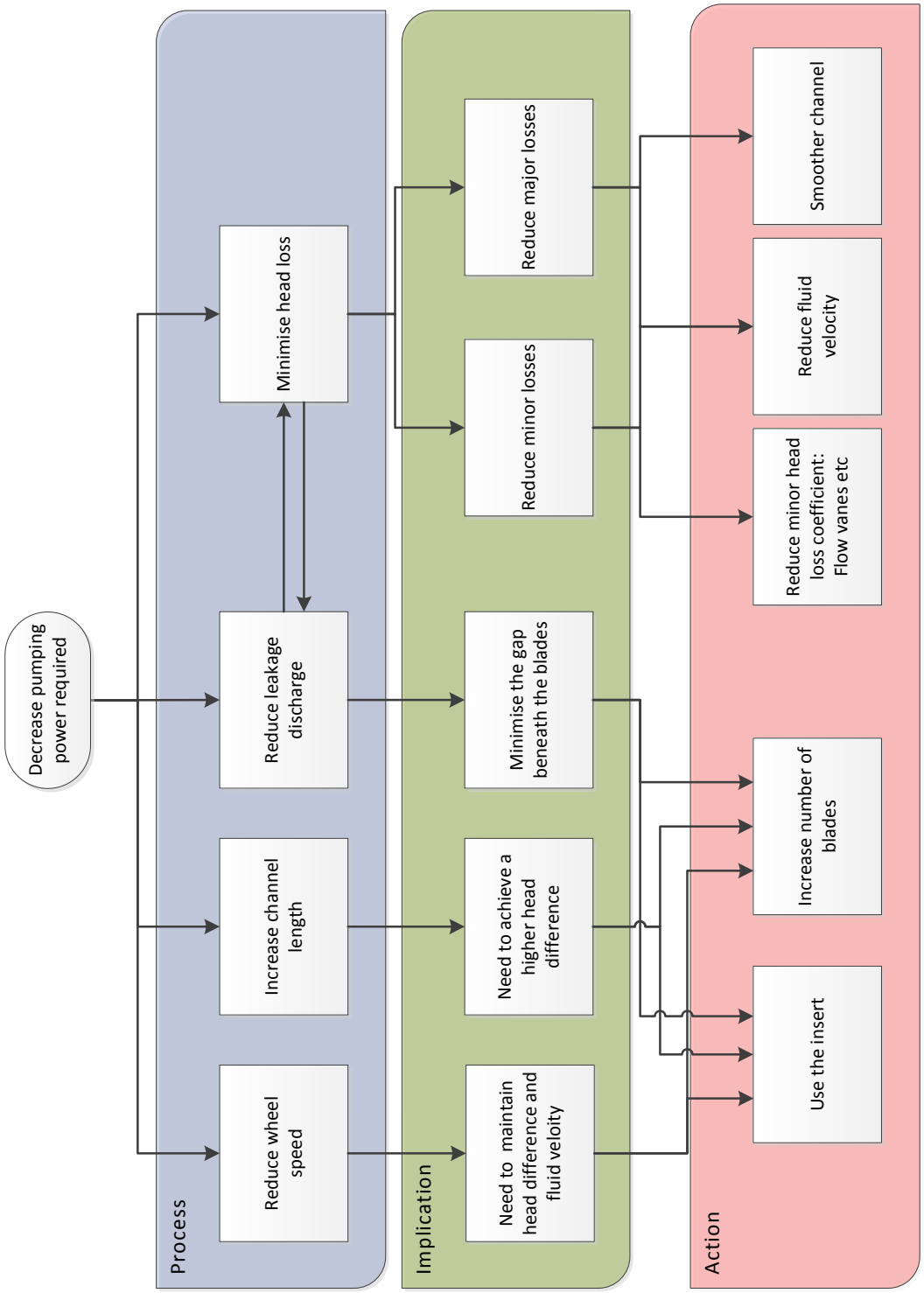

Figure 5.42. Flowchart of how to optimise the system to minimise the pumping power required. The first level is the process to reduce the power requirement, the second level is the implication and the third level is the actions that should be undertaken to/be able to achieve it.

5.5 Conclusion

The model was based on the based on the pilot-scale raceways described by Mendoza et al. (2013) and built at a scale of 1:5 with an area of 0.98 m^2. It has an internal channel width of 280 mm and a total internal length of 1820 mm. To imitate a wide range of different raceway lengths, from 50 to 10,000 m, a weir was used, therefore providing greater water head differences acting across the wheel. The weir could also be used to measure the fluid discharge from the wheel. The wheel had a diameter of 300 mm and was constructed of two 10 mm thick clear Perspex side plates, with notches for 4, 6, 8, 10 and 12 blades allowing multiple configurations to be tested.

The method used to measure the torque of the motor was developed specifically for this project. The motor was fixed in a block which is free to rotate. The block was attached to a lever arm which then applied a force at the on the force gauge. This force increased until it was equilibrium with the torque of the motor being transferred to the paddlewheel and the fluid.

The aim of the experiments was to determine the efficiency of the paddle wheel for different wheel geometries across a range of operating conditions. The parameters investigated were:

- The rotational speed of the wheel
- The number of blades in the wheel
- The fluid discharge
- The downstream fluid depth and head difference
- The length of the raceway
- The paddlewheel insert

Wheel efficiencies increased with increasing blade numbers. With the lowest efficiency was recorded for a 4-blade wheel and highest for the 8, 10 and 12-blade wheels. The effect of blade number can be attributed to the reduction in the leakage of fluid around and beneath the blades when more are present. The leakage is the amount of fluid that flows backwards against the motion of the blades. Practically all raceways have a horizontal bed therefore a gap exists between the paddlewheel's blades and the bed. During operation, the paddlewheel lifts the water upwards to the downstream side. This creates a head difference, which in turn drives a backward flow through the gap,

thereby reducing the wheel's efficiency. The gap is reduced with the higher number of blades up to 8 blades where the rate of reduction is greatly reduced.

The wheel efficiency reduces with increasing speed. At the higher rotational speeds more energy is being transferred into turbulence which will not contribute to the forward velocity of the fluid. At wheel speeds above 13 rpm, the wheel starts to lift fluid from the raceway into the air for all the blade numbers, significantly reducing its efficiency. This reduction is a result of using energy to move the fluid in an adverse direction.

The efficiency and velocity values are affected by the head difference. The increase in paddlewheel efficiency and fluid velocity as the head difference decreases is linked to the reduction in the adverse head acting against the motion of the blade. As the downstream depth tends to the upstream depth the efficiency of the wheel tends to 100%. This can be deduced from the very small amount of shaft power needed to provide the hydraulic power to overcome this head difference. At this point there will be very little energy loss or leakage in the system as the adverse pressure gradient will also be very small.

Increasing the submersion depth of the wheel, i.e. upstream depth (d_1), led to higher efficiencies. In this experiment doubling the fluid depth resulted in a more than three-fold increase in the wheel efficiency. This has been associated with the larger amount of fluid available for lifting, resulting in a higher discharge and increased hydraulic power(Park et al., 2014; Brown and Tucker, 2013). The amount of fluid in the system must be sufficient to meet the requirement of the wheel at the upstream side. In extremely long raceways this could become an issue as the required fluid depth at the downstream side of the wheel may become very large.

The power demand per unit surface area of raceway reduces with increasing raceway length despite the fact that the wheel efficiency reduces with increasing head difference. This makes longer raceways potentially more economical.

At lower rotational speeds the insert improved the efficiency of the wheel. This improvement reduces with increasing wheel speed. The use of the insert increased the maximum head difference range that the wheel could maintain. The greater head differences simulate longer raceways therefore the insert could be used in longer

raceways to reduce the wheel speed required to achieve the head difference needed to drive the fluid; further increasing the efficiency of the wheel.

In conclusion, it was found that a properly designed paddle wheel can be significantly more efficient than previously assumed with efficiencies up to 60% being recorded.

6 Case studies

This chapter explores the energy and cost savings that could be made if certain changes were implemented in real full-scale cultivation raceways. The information gathered is from a variety of sources and some assumptions have been made from literature, which are stated below.

6.1 Wastewater treatment plant of El Torno, Chiclana

As part of the FP7 All-Gas project a demonstration-sized raceways at the wastewater treatment plant of El Torno Chiclana, Spain are under construction at the time of writing. This site is used primarily for wastewater treatment with the biomass then being used for conversion to biofuels. This is a completely new plant with six paddlewheel driven reactors and one propeller driven raceway. Each raceway channel is 276 m long and 9 m wide with a total surface are of around 5200 m^2 and each has a 1 m deep carbonation sump. Each raceway utilises a single 8-bladed wheel with a rotational speed of around 6.5 rpm with a diameter of 1.5 m. It is located 17 m from one of the end bends propelling the fluid away from the end. The bends have both flow deflectors and islands to reduce head loss. This data is all from personal communications and is summarised in Table 6.1 below (Lara Corona and Arbib, 2016).

Table 6.1. Summary of dimensions and values for the raceways at the Chiclana wastewater treatment plant (Lara Corona and Arbib, 2016).

		WWTP Chiclana
Channel values	Width (m)	9
	Length (m)	276
	Depth (m)	0.3
	Number of ponds (-)	6
	Fluid velocity (m s^{-1})	0.25
	Discharge per meter (m^3 s^{-1} m^{-1})	0.075
Paddlewheel values	Number of blades (-)	8
	Rotational speed (rpm)	6.5
	Wheel diameter (m)	1.5
	Motor efficiency (-)	0.6

To estimate the raceway performance the head loss in the system must first be calculated. The major head loss can be calculated using Manning's equation (Equation 5.11, Section 5.1.3.1). The minor head loss occurs at two main locations: the bends and the carbonation sump. The minor head loss can be calculated using Equation 3.8, Section 3.2.4. For the bends with deflectors a loss coefficient of 2.0 was used (Lundquist et al., 2010). For the sump it has been calculated that the head loss coefficient with no baffle is around 0.5 (Musgrove and Heaven, 2014). Therefore the total minor head loss coefficient due to the two bends and the sump is 4.5 . The head loss that occurs in the raceway can be visualised by the changes in the total energy line as the fluid travels around the system. There is a constant decrease in energy due to friction and turbulence and then at each obstacle the head loss increases and there is a drop in the energy line (Figure 6.1).

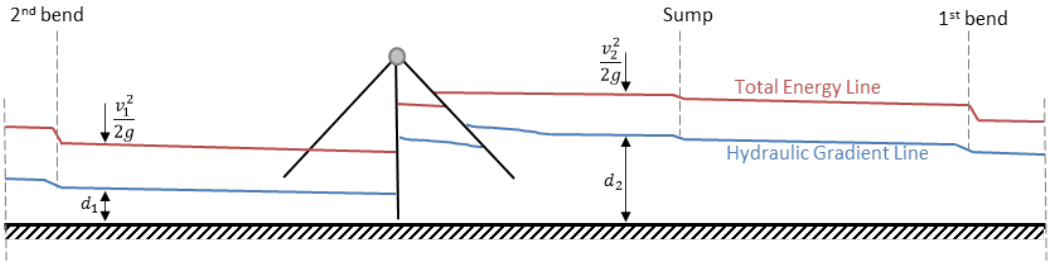

Figure 6.1. Representation of the hydraulic gradient and total energy lines as the fluid travels around the raceway.

Using the head loss data the relationship between the major and minor losses can be compared as the length is increased (Figure 6.2). As the length increases the minor head loss makes up a decreasing proportion of the total head loss in the system. Assuming smooth concrete construction with a Manning's roughness coefficient of 0.012, any channel lengths of less than 145 m the minor head losses are greater than the major head losses. As the majority of the biomass growth will occur in the straight channels it is important to maximise their area as far as possible as explained in Section 5.2.4. For the system in Chiclana the minor losses account for around a third of the total head losses so consideration should be given to minimising these when designing a system; the total head loss is around 0.043 m.

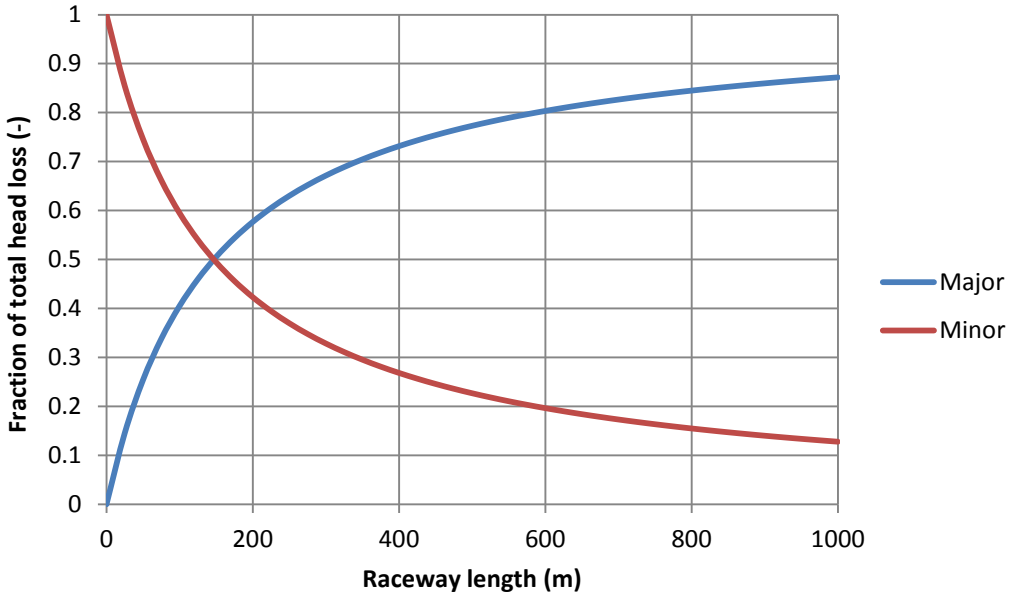

Figure 6.2. Comparison of the major and minor head loss as a fraction of the total head loss across a range of raceway channel lengths. A Manning's roughness coefficient of 0.012 and a minor loss coefficient of 2.0 were used.

Once the total head loss is calculated the hydraulic power can then be calculated. It was calculated that each pond required a hydraulic power of 294 W to drive the fluid around the raceway. When a motor efficiency of 0.6 is applied then the shaft power requirement can be calculated before any wheel losses are applied. This makes it easy to compare any energy and financial savings that are made when different wheel and raceway configurations are applied.

This method has been applied for all the following case studies: Earthrise Farm, Parry Nutraceuticals and Cyanotech Corporation. It should be noted, however, that any changes in the wheel configuration will ultimately affect the motor efficiency as different torque levels and rotational speeds will be applied.

Table 6.2. Calculation of the power and cost savings if a different blade number and rotational speed were selected instead of the current setup for continuous 24 hour and 12 hour mixing systems. A motor efficiency of 0.6 has been applied to the hydraulic power. An electrical cost of 12p kWh^{-1} has been assumed (Business Electricity Prices, 2016). All costs are in GBP.

	Current set up	12-blade	12-blade with insert	
Wheel speed (rpm)	7	4	4	7
Wheel efficiency (-)	0.50	0.60	0.70	0.55
Shaft power (W)	940	783	671	855
Total power for site (kW)	6	5	4	5
24 h continuous mixing				
Total power (MW h/y)	49	41	35	45
Cost (£/year)	5929	4941	4235	5390
Cost saving (£/year)		988	1694	539
12 h continuous mixing				
Total power (MW h/y)	25	21	18	22
Cost (£/year)	2965	2471	2118	2695
Cost saving (£/year)		494	847	270
Percentage saving (-)		17 %	29 %	9 %

This operating raceway is well optimised with a low rotational speed and 8 blades. It is unlikely that the rotational speed can be reduced with the current setup. Using the insert the rotational speed could be lowered to 4 rpm without a large impact on the fluid velocity. This would result in energy savings of around 30 % but due to the small size of the plant and its existing efficient operating mode this results in less than £1000 saving.

No information is currently available on the wave heights in the channel as a result of the paddlewheel. If a wave height of 0.05 m is assumed, based on observations of the prototype raceway at Chiclana using the same wheel set up and speed, the amount of power lost in the creation of waves can be estimated using the equations set out in Section 4.3.2.4.1. The wave power estimations are shown below in Table 6.3, with the calculated insert height of 110 mm giving a corresponding reduction in depth.

Table 6.3. Wave power estimations for the four different configurations for the Chiclana WWTP. The insert depth was calculated to be 110 mm.

	Current set up	12-blade	12-blade with insert	
Wheel speed (rpm)	7	4	4	7
Depth (m)	0.325	0.325	0.215	0.215
Wave length (m)	1.55	1.92	1.65	0.75
Wave power per unit width (W m^{-1})	3.06	3.56	3.35	1.94
Power per raceway (W)	27.53	32.02	30.13	17.42
Total wave power requirement for the entire site (kw h/day)	3.96	4.61	4.34	2.51
Total wave power requirement for the entire site (MW h/year)	1.45	1.68	1.58	0.92

The wave data shows that the amount of power per unit width is relatively low, and the total power spent creating waves in this system is only around 3 % of the total power. In larger systems this could still be a significant energy loss. The power of the wave is proportional to the square of the wave height and the assumed height here is much lower than some images of wheels operating in real systems elsewhere suggest (Figure 3.4, Figure 3.7).

If a small incline in the bed of 0.29 m is introduced then the waves would break and this energy could be utilised to provide enhanced gas transfer and forward bulk velocity. In addition to the waves created by the paddlewheel large numbers of waves are generated by wind blowing over the surface of the fluid. A raised section could also induce these waves to break and thus gain the energy.

6.2 Earthrise Farm

The Earthrise farm is one of the first large-scale production facilities for growing Spirulina (Earthrise Nutritional, 2016). Originally constructed in 1977 in Imperial Valley, California it has been expanded many times. There are currently 37 ponds each with a surface area of around 5000 m^2, which produce around 500 tons of Spirulina each year (Earthrise Nutritional, 2016). None of these raceways have carbonation sumps or end bend deflectors so the minor head loss coefficient was set to 3.4 (Kawamura, 2000; Montgomery, 1985). The propulsion mechanism is a flat 6-blade paddlewheel with a rotational velocity of 13 rpm (Henrikson, 1983). There are three paddlewheels across

the width of the channel. Each wheel is slightly out of phase so that the three wheels act similarly to a larger non-aligned wheel (Figure 6.3).

Figure 6.3. Earthrise paddlewheel system (Earthrise Nutritional, 2014).

Table 6.4. Summary of the dimensions and values for the raceways at Earthrise farms.

		Earthrise farm	Reference
Channel values	Width (m)	15	(Earthrise Nutritional, 2016)
	Length (m)	150	Calculated
	Depth (m)	0.25	Assumption (Henrikson, 1983)
	Number of ponds (-)	37	(Earthrise Nutritional, 2016)
	Fluid velocity (m s^{-1})	0.3	Calculated
Paddlewheel values	Number of blades (-)	6	(Earthrise Nutritional, 2014)
	Rotational speed (rpm)	13	(Henrikson, 1983)
	Wheel diameter (m)	1.2	Assumption (Earthrise Nutritional, 2014)
	Motor efficiency (-)	0.6	Assumption

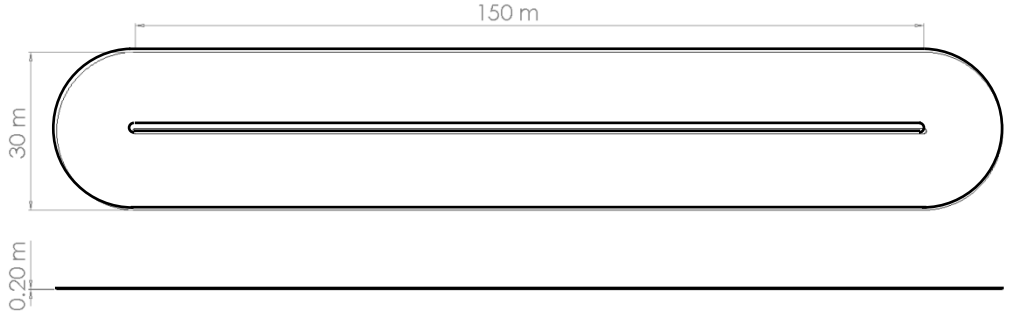

Figure 6.4. Schematic of Earthrise's raceway ponds.

Using the dimensions and values in Table 6.4 the hydraulic power can be calculated as explained previously. It was estimated that each pond system had a total head loss of 0.061 m resulting in a hydraulic power requirement of 672 W. If a motor efficiency of 0.6 is assumed then a starting power requirement of 1120 W can be used before any paddlewheel losses are applied.

Table 6.5. Calculation of the power and cost savings if a different blade number and rotational speed were selected instead of the current setup for continuous 24 hour and 12 hour mixing systems. A motor efficiency of 0.6 has been applied to the hydraulic power. An electrical cost of 12p kWh^{-1} has been assumed (Business Electricity Prices, 2016). All costs are in GBP.

	Current set up		8-blade		12-blade		12-blade with insert	
Wheel speed (rpm)	13	4	9	11	7	9	7	9
Wheel efficiency (-)	0.17	0.5	0.45	0.4	0.5	0.45	0.55	0.47
Shaft power (W)	6,591	2,241	2,490	2,801	2,241	2,490	2,037	2,384
Total power (kW)	244	83	92	104	83	92	75	88
24 h continuous mixing								
Total power (MW h/y)	2,136	726	807	908	726	807	660	773
Cost (1000's £/year)	256	87	97	109	87	97	79	93
Cost saving (1000's £/year)		169	159	147	169	159	177	164
12 h continuous mixing								
Total power (MW h/y)	1,068	363	403	454	363	403	330	386
Cost (1000's £/year)	128	44	48	54	44	48	40	46
Cost saving (1000's £/year)		85	80	74	85	80	89	82
Percentage saving (-)		66 %	62 %	58 %	66 %	62 %	69 %	64 %

The analysis shows that making small changes to the paddlewheel rotational speed can give savings of almost 70 % or around £90,000 per year for the entire facility. Reducing the rotational speed with no changes to the paddlewheel will result in a reduced fluid velocity. To ensure that the fluid velocity is maintained use of a greater number of blades is recommended as this maintains a higher velocity for a given rotational speed (Figure 5.17). Therefore it may be possible to reduce the speed to 7 rpm with 12 blades, which would result in similar savings but would not compromise the fluid velocity. Using the insert will further increase the fluid velocity and will be more successful in maintaining the current operating conditions.

As well as changing the wheel configuration and operating speed it would be beneficial if end bend deflectors were introduced to reduce the head loss in the bends. If this was

done a direct power saving of 21 % could be achieved, not including the further power savings that will occur due to the rise in the efficiency of the wheel.

6.3 Parry Nutraceuticals

The Parry Nutraceuticals production facility is located in Unaiyur, south east India. It consists of 64 ponds each 190 m long (Figure 6.5 a). The propulsion mechanism used is a flat 6-blade design with a relatively low rotational speed of 7 rpm. The design of the wheel is very simple with one wheel spanning the full width of the channel (Figure 6.5 b). This simple design leads to fewer losses as there is less area for leakage to occur. The large span, however, means that the blades must be strong enough to withstand the forces applied and thus must be made thicker. The thicker steel located away from the axle results in large moments being applied to the motor in order to rotate the wheel.

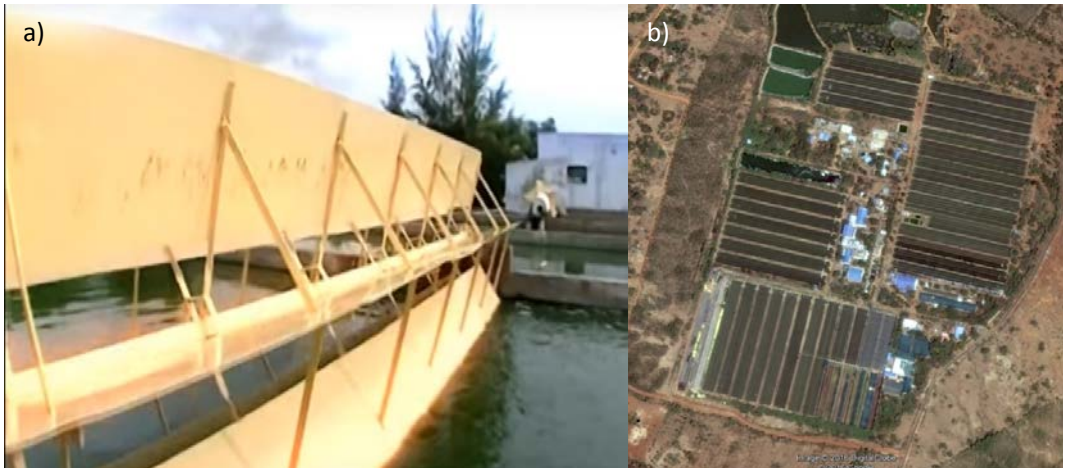

Figure 6.5. a) Parry Nutraceuticals paddlewheel system (Parry Nutraceuticals, 2011). b) Satellite image of the Parry Nutraceuticals production facility (Google Earth, 2016b).

The raceways used here have end bend deflectors but they have been poorly designed. As explained in Section 3.2.1 and shown in Figure 3.6a, if the deflectors does not start parallel to the bulk fluid velocity then small vortices are created behind the deflector. This is exactly the design that has been used by this facility as Figure 6.6a shows. Figure 6.6b shows the formation of vortices behind the deflector, which will increase the head loss around the end bends. Therefore a minor head loss coefficient of 2.5 was used instead of 2.0.

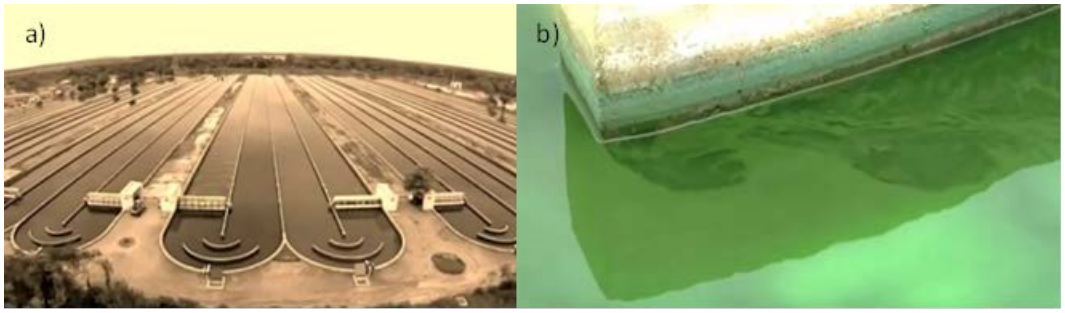

Figure 6.6. a) Parry Nutraceuticals end bend deflector system (Parry Nutraceuticals, 2011). b) Small vortices produced after the deflectors (Parry Nutraceuticals, 2011).

The data for the plant is summarised in Table 6.6 and the analysis results are shown in Table 6.7.

Table 6.6. Summary of the dimensions and values for the raceways at Parry Nutraceuticals.

		Parry Nutraceuticals	Reference
Channel values	Width (m)	5	(Google Earth, 2016b)
	Length (m)	190	(Google Earth, 2016b)
	Depth (m)	0.2	Assumption
	Number of ponds (-)	64	(Google Earth, 2016b)
	Fluid velocity (m s^{-1})	0.25	Calculation
Paddlewheel values	Number of blades (-)	7	(Parry Nutraceuticals, 2011)
	Rotational speed (rpm)	7	(Parry Nutraceuticals, 2011)
	Wheel diameter (m)	1.2	Assumption(Parry Nutraceuticals, 2011)
	Motor efficiency (-)	0.6	Assumption

Figure 6.7. Schematic of Parry Nutraceuticals' raceway ponds.

Table 6.7. Calculation of the power and cost savings if a different blade number and rotational speed were selected instead of the current setup for continuous 24 hour and 12 hour mixing systems. A motor efficiency of 0.6 has been applied to the hydraulic power. An electrical cost of 12p kWh^{-1} has been assumed (Business Electricity Prices, 2016). All costs are in GBP.

	Current set up		8-blade		12-blade		12-blade with insert	
Wheel speed (rpm)	7	4	4	7	4	7	4	7
Wheel efficiency (-)	0.40	0.60	0.70	0.50	0.65	0.45	0.70	0.50
Shaft power (W)	507	338	289	405	312	450	289	405
Total power (kW)	32	22	19	26	20	29	19	26
24 h continuous mixing								
Total power (MW h/y)	284	189	162	227	175	252	162	227
Cost (1000 £/year)	34	23	19	27	21	30	19	27
Cost saving (1000 £/year)		11	15	7	13	4	15	7
12 h continuous mixing								
Total power (MW h/y)	142	95	81	114	87	126	81	114
Cost (1000 £/year)	17	11	10	14	10	15	10	14
Cost saving (1000 £/year)		6	7	3	7	2	7	3
Percentage saving (-)		33 %	43 %	20 %	38 %	11 %	43 %	20 %

There is limited potential for large energy savings due to the low rotational speed applied. If the wheel was redesigned so that 8 blades were used instead of 6 and the rotational speed was reduced to 4 rpm then around a 40 % saving energy could be made or just under £15,000 per year. From a cost perspective this is unrealistic, as the capital

outlay for new wheels to be implemented for all 64 ponds would be high, but an improved design should be considered for new plants. If the same wheel is used in the existing plant but the rotational speed was just reduced to 4 rpm then a 30 % saving could still be made.

6.4 Cyanotech Corporation

The Cyanotech Corporation's production facility is located on the west coast of Hawaii's largest island. It is made up of 69 ponds, the majority of which are 155 m long and 9.5 m wide with some ponds almost double this (Figure 6.8). A single flat 8-blade wheel spanning the full width of the channel is used to propel the fluid around the raceway (Figure 6.9). As explained in Section 6.3 the use of a single paddlewheel spanning the width of the channel has both advantages and disadvantages. The raceways have also been designed to include islands to reduce head loss around the end bends (Figure 6.10). The data for the Cyanotech raceway is summarised in Table 6.8 and the results from the analysis is shown in Table 6.9. Due to the asymmetric island design of the end bend a minor head loss coefficient of 1.5. was applied (Kawamura, 2000).

Figure 6.8. Arial image of the Cyanotech production facility (Cyanotech Corporation, 2015).

Figure 6.9. Cyanotech paddlewheel system (Rohrer, 2011).

Table 6.8. Summary of the dimensions and values for the raceways at Cyanotech Corporation.

		Cyanotech	Reference
Channel values	Width (m)	9.5	(Google Earth, 2016a)
	Length (m)	155	(Google Earth, 2016a)
	Depth (m)	0.2	(Rohrer, 2011)
	Number of ponds (-)	69	(Google Earth, 2016a)
	Fluid velocity (m s^{-1})	0.25	Calculation
Paddlewheel values	Number of blades (-)	8	(Rohrer, 2011)
	Rotational speed (rpm)	7	(Rohrer, 2011)
	Wheel diameter (m)	1.4	Assumption (Rohrer, 2011)
	Motor efficiency (-)	0.6	Assumption

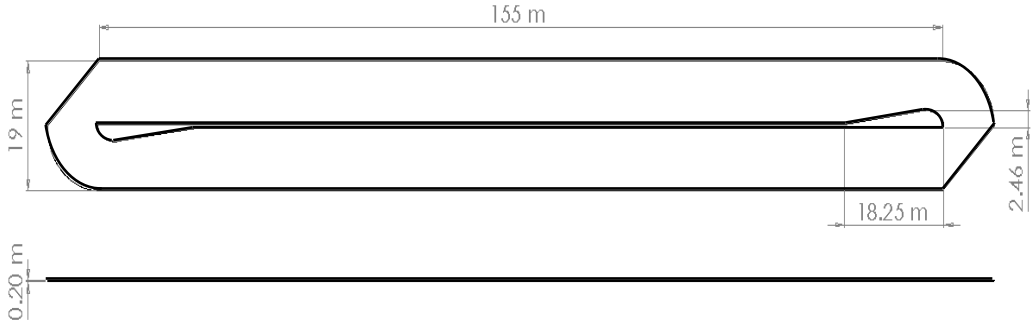

Figure 6.10. Schematic of Cyanotech's raceway ponds

Table 6.9. Calculation of the power and cost savings if a different blade number and rotational speed were selected instead of the current setup for continuous 24 hour and 12 hour mixing systems. A motor efficiency of 0.6 has been applied to the hydraulic power. An electrical cost of 12p kWh^{-1} has been assumed (Business Electricity Prices, 2016).

	Current set up		12-blade	12-blade with insert
Wheel speed (rpm)	7	4	4	4
Wheel efficiency (-)	0.50	0.65	0.65	0.70
Shaft power (W)	626	481	481	447
Total power (kW)	43	33	33	31
24 h continuous mixing				
Total power (MW h/y)	378	291	291	270
Cost (£/year)	45,392	34,917	34,917	32,423
Cost saving (£/year)		10,475	10,475	12,969
12 h continuous mixing				
Total power (MW h/y)	189	145	145	135
Cost (£/year)	22,696	17,458	17,458	16,211
Cost saving (£/year)		5,238	5,238	6,485
Percentage saving (-)		23 %	23 %	29 %

The low rotational speed of 7 rpm in conjunction with a single 8-blade paddlewheel means that there is very little potential for efficiency savings except by reducing the speed of the wheel. If the speed is reduced to just 4 rpm then savings of around 23 % would be possible or around £10,500 year. This reduced rotational speed would need to be analysed further to ensure there is still adequate fluid velocity to keep the alga in suspension.

6.5 Conclusion

Four different operational raceways have been investigated in order to evaluate the operational and design of their propulsion mechanism, paddlewheel, and see if it could be improved. If improvements could be made these were quantified in terms of energy and monetary value for the whole plant. The four sites investigated were:

1. The wastewater plant of El Torno, Chiclana, Spain
2. Earthrise Farm, California, USA
3. Parry Nutraceuticals, Unaiyur, India

4. Cyanotech Corporation, Hawaii, USA

Of these four sites the Earthrise Farms site is the largest with 37 ponds, each of these has a surface area of 5000 m^2. It was found that this site had the worst operating conditions with the rotational speed at 13 rpm. It also had the lowest number of blades on each wheel at just 6 blades. By increasing the number of blades the speed of the wheel can be reduced and the same fluid velocity can be reached. As a result it was found that by increasing the number of blades to 12 and reducing the rotational speed to 7 or 9 rpm would lead to an energy reduction of between 66 - 62 %., which equates to around £85,000 - £80,000 if the wheel is run 12 hours a day. If the insert was used for the 12-bladed wheel at 7 rpm the energy saving could be as high as 69 % which equates to a saving of £89,000.

For the other facilities investigated the energetic savings were around 30%. The lower energetic savings was mainly due to the plants running their paddlewheels at around 7 rpm and having 7 or 8 bladed wheels. The only major improvement could be made by using the insert and thus be able to reduce the paddlewheel speed.

7 Conclusion

There is a growing concern over the long term impacts of the over reliance on fossil fuels. The two main concerns are:

1. The release of greenhouse gases and the rising impact these have on global temperatures and the non-renewable aspect of fossil fuels.
2. The fuel security of nations reliant on fossil fuels.

To address both of these issues there has been an increase in alternative renewable fuel usage. Biofuels produced from terrestrial plants can be mixed with current fossil fuels to be used as a liquid fuel in the transport sector. The European Union has set a mandatory target of 10 % biofuel mix in transport fuels by 2020 for all member states. Primarily this is being met by first and second generation biofuels. While second generation fuels are from waste sources and thus will not have an impact on the production of food first generation fuels will replace food production. At the current production efficiency first generation fuels cannot replace fossil fuel usage due to the impact that the production will have on the food production.

Third generation biofuels produced from microalgae can be grown on non-arable land on saline water or wastewater; limiting its impact on food production. They are reported to give a yield of at least twice that of first generation fuels.

Currently there are two main systems to produce microalgae biomass: open and closed. Closed systems where the microalgae are not open to the atmosphere are known as photobioreactors. Open systems allow the microalgae to be in contact with the atmosphere, the most common open system is the raceway. This is characterised as a long recirculating loop where the fluid is normally driven by a paddlewheel. Open systems have been descried as the most economically feasible option to produce microalgae biomass for biofuels.

In the past there has been a great expectation of the possibilities that algal biofuels could reduce the reliance on fossil fuels. These expectations have been impacted by further research and experimentation with bigger scale prototypes where the biomass yield is greatly reduced. In recent years there has been a greater understanding that

there must be improvement to the whole system from microalgae strain selection though to cultivation to the downstream processing.

There is a large body of information and research into the growth and potential of microalgae as a possible petrochemical substitute. A large proportion of this research has not focused on energetic feasibility and the investigations into energy requirements, mainly life cycle assessments, use basic calculations and assumptions to estimate the energetic cost of production. The techno-economic assessments have shown that there is a possibility for microalgae as a fuel source to be energetically viable, however it is unlikely to be economically feasible at the current level of technology. With the cost of biodiesel derived from microalgae being $13.4 /gallon in 2012 this was three times that of terrestrial first generation biodiesel at around $4.3 /gallon. Both of biodiesels prices exceed the price of fossil fuel diesel at $3.5 /gallon. Therefore more works needs to be done in order to reduce the cost of production and processing of microalgae.

To reduce the cost of producing biofuels from microalgae the energetic performance of the system must be improved. There have been a number of numerical and experimental investigations to improve the hydrodynamic performance of raceway systems. These have mainly focussed on the bend design and carbonation of the system with little work being completed into the propulsion mechanism. Commonly this has been paddlewheels; as they are well suited to the requirements of moving a high volume of fluid with a low head difference. They are usually around 1 - 1.4 m in diameter and have four to eight blades, which can be straight, curved, inclined, aligned, non-aligned, angled or a combination of such features. There is, however, very little experimental comparison between these designs.

The work completed here has focused on the main propulsion mechanism in terms of the energetic power requirement. The analysis of the literature indicates that the reported efficiencies are very wide; with an efficiency in the 10% range is most probable. A large proportion of this research, however, has been done with differing methodologies to calculate the shaft power requirement. All methodologies used in the previous studies have been calculating the total efficiency of the whole paddlewheel system, which includes the motor and gearbox efficiencies. These can dramatically alter if the operational speed is changed then their efficiency will also change. Some of the methodologies calculate the power requirement as a difference in the electrical power

requirement when the system is run clear of fluid and when it is operational and are very unreliable. This is exposed through the results collected showing wheel efficiencies of over 100 %, which is impossible. The literature review also indicated that there is very little in terms of design guidance for paddle wheels.

The current theoretical model to calculate the shaft power and discharge of the paddlewheel was based on calculating the drag force experienced by the blades as it passed through the fluid. This method was inadequate as it did not take into account the head difference which was one of the key parameters affecting its performance. Additionally the method proposed assumed that the fluid was stationary as the blade travels through. This will lead to an overestimation of the drag force and thus the power requirement. A new theory was devised by considering the hydrostatic pressures acting on a blade as it passes through the fluid. Furthermore the main contribution to energy loss, the fluid backflow, has been incorporated.

To perform the investigation into the paddlewheel a 1:5 scale model of a raceway was constructed to accurately calculate the performance of different wheels. The geometric scaling had to be distorted as the length would have been too great, so a weir was used downstream of the wheel in order to increase the head difference to simulate a longer raceway. This weir could also be used to measure the discharge from the wheel. The head of fluid either side of the wheel was measured using piezometers in order to dampen the waves being created from the wheel. The torque on the motor shaft was measured using the newly designed Direct Torque Measurement Device (DTMD).

A number of parameters were investigated to analyse their impact on the performance of the wheel and the velocity of the fluid if appropriate. These were:

- The rotational speed of the wheel
- The number of blades in the wheel
- The fluid discharge
- The downstream fluid depth and head difference
- The length of the raceway

Further to these parameters a novel insert was designed and tested. The insert was a raised area where the curvature of the rise was the same as that of the outer wheel

diameter. By maintain a minimum clearance gap at all times with the blade the backflow beneath the wheel should be reduced.

The main contribution of the paddlewheel work is:

1. Development of theoretical paddlewheel discharge, power and efficiency formulas to accurately estimate the fluid velocity and efficiency of the wheel taking into account the leakage discharge.
2. The design and testing of a novel approach to measure the shaft power of a motor using the Direct Torque Measurement Device (DTMD).
3. The efficiency and fluid velocity changes with alterations to the parameters (Table 7.1).
4. The design and successful testing of a novel insert to reduce the backflow beneath the blades as it rotates. Showing that for wheels with a rotational speed of 13 rpm or less there was an increase in the efficiency. This improvement declined with increased discharge. At the lowest wheel speed the efficiency with the insert was over double than without. This dropped to almost no improvement at the highest wheel speeds. Furthermore the insert increased the maximum achievable head difference for any given rotational speed. Therefore a lower speed could be used while maintaining the same head difference needed to drive the fluid around the system.

Table 7.1. Summary of the findings from the paddlewheel experiments. The variables on the left are increased with the results on the two parameters shown.

	Fluid velocity	Efficiency
Rotational speed	Increase	Decrease
Blade number	Increase	Increase
Discharge	n/a	Increase
Depth	n/a	Increase
Head difference	n/a	Decrease
Raceway length	n/a	Increase in power per unit volume

When the weir height and fluid depth were kept constant just the rotational speed could be analysed. It was found that higher rotational speeds of the wheel result in higher fluid velocities. The performance was, however, reduced for the wheels with 8 or more blades. This reduction was likened to the increase in turbulence created in the system and the eventual lifting of the fluid at the very high rotational speeds. For wheels with

less than 8 blades there was an initial rise in the performance as the greater frequency of the blade entering the fluid reduced the energy spent in the creation of waves.

With a full-scale equivalent base fluid depth of 0.175 m and full-scale weir height of 0.185 m increasing the number of blades from 4 to 8 blades resulted in a rise in the fluid velocity from 0.02 m s^{-1} to 0.12 m s^{-1} at 4 rpm and from 0.25 m s^{-1} to 0.35 m s^{-1} at 18 rpm. This was due to the clearance gap beneath the wheel being significantly reduced when the number of blades is increased, thus reducing the leakage or backflow from the higher downstream head to the lower upstream head condition. Further increases to the blade number from 8 to 12 blades had a reduced impact on the flow as there was only a 0.01 m s^{-1} increase at the lowest rotational speed. This was due to there being a smaller decrease in the leakage gap between 8 and 12 blades than between 4 and 8 blades. This reduction in the gap beneath the blades also gave rise to higher efficiencies being recorded with a greater number of blades.

The increase in fluid velocity when the blade number is increased means that a lower rotational speed can be used without an impact on the fluid velocity, thus giving rise to higher efficiencies.

The higher rotational speeds and blade numbers resulted in a much greater maximum discharge being reached. This is a combination of the effects of the reduced leakage and higher fluid velocity that occurs when either of these parameters is increased.

It has been found that the head difference across the wheel was an important factor affecting its efficiency as a method of propulsion. The maximum efficiencies recorded were between 40 - 60 % at normalised head differences (head difference/upstream depth) less than 3.0 and around 20 % at higher normalised head differences of around 6.0. Increasing the head difference across the wheel was done by raising the weir downstream of the wheel, causing fluid to back up towards the wheel simulating the effect a longer raceway has on the wheel. Each rotational speed had a maximum allowable head difference where the efficiency would drop towards zero this would be the maximum normalised head that wheel speed would be able to achieve. This value increased for faster wheel speeds as more energy was transferred into the fluid, however requiring more power.

A greater head difference is normally associated with increased raceway lengths which provide a larger volume for microalgae cultivation. Therefore traditional methods of analysing efficiency may not be the most representative, with the power requirement per unit surface area possibly being more appropriate. It was found that the power per unit volume decreased with increased normalised lengths for all rotational speeds. This makes longer raceways potentially more economical.

The use of an insert resulted in higher discharge, normalised head differences and efficiency values at any given rotational speed. All of these improvements were linked to the reduction of the leakage as the gap beneath the blades is reduced to a minimum at all times as the insert curvature matches the path of the blades. Further to this the insert reduced the creation of the waves at lower rotational speeds which further improved the efficiency of the wheel. The higher maximum achievable head difference could result in a lower rotational speed being implemented. Therefore indirectly there could be a large increase in the efficiency as the lower rotational speeds have higher efficiencies.

The theory to describe the discharge and efficiency of the wheel devised matched the experimental results collected. It did not, however, give reliable estimations for the highest wheel speeds due to under estimations of the shaft power required as the blades began lifting fluid from the channel which is not taken into account by the theory. Previous models devised did not take the head difference across the wheel into account and thus cannot be employed for paddlewheels in raceways.

The main two factors that affect the performance of the wheel were the rotational speed and the head difference across the wheel. The latter cannot normally be changed by the wheel. If there are, however, any constructs or operating conditions that reduce the head loss around the raceway then not only is the power requirement to overcome the smaller head difference reduced but the efficiency of the wheel to do this increases. The rotational speed of the wheel should be kept as low as operationally possible. In very large raceways the speed required to overcome the head difference may be excessively high. If it is fast enough that there is lifting of the fluid from the surface then another approach should be considered as this dramatically decreases energetic performance. If this is the case then the number of blades should be increased or the insert should be used to reduce the back flow and head difference acting on the blades.

If either of these options are not feasible or have been done, then multiple wheels could be used located at opposite ends to reduce the effective length by half. This would, however, increase the power required per unit surface area which would be detrimental to the overall efficiency of the system.

It was found from the case studies that there can be an economic case, of up to £90,000 per year, to change the paddlewheels in use at some microalgae production facilities. The largest energetic savings can be made when the rotational speed used is greater than 10 rpm in the very large plants. In order to maintain the fluid velocity the number of blades in use would need to be increased and possibly an insert would need to designed and installed. The capital cost associated with this may outweigh the cost benefit from making the savings especially at the smaller farms.

These improvements to the paddlewheel alone will not make the algal biofuels financially viable as the techno-economic assessments have estimated that the cost of producing the biofuel must be at least halved. These improvements will however be a step towards this as a whole system wide approach is needed.

The closed system design and small scale of the experiment meant that the results from this investigation where mainly limited by the parameters that affected the wheel. If any one of the parameters changed then the others would also be affected, i.e. if the wheel speed increased then the head difference would change. This resulted in the need to use either normalised values or look at small groups of results with only one variable changing. Using normalised values can always have the possibility of misrepresenting what is really occurring in the system and using a snapshot of the results mean that the bigger picture is lost. As a result of these limitations any further work would be completed using a larger scale system to try and isolate the parameters.

7.1 Further work

The experimental work done to date has primarily been completed on a relatively small scale model. To enhance the work the scaling of the model must be investigated to see if the insert and changes made to the wheel has the benefits shown from the experimental model. To do this a full scale insert should be tested in the wastewater treatment plant in El Torno, Chiclana under the normal range of operating conditions. As the wheel at the wastewater plant has only 8 blades the insert will need to be adjusted accordingly to ensure that there is one blade on the radius of the insert at all times.

If this is not possible to test the insert or would not work due to the wheel characteristics then it is proposed that the insert be tested on a larger scale in a straight flume. This experiment should be conducted as near to full scale as possible. An additional advantage of testing it in the flume is that the fluid parameters can be adjusted to simulate a range of raceways; similar to the current model. The results can then be used can also be then used as a best practise when designing and implementing a paddlewheel in a raceway.

As discussed in Section 3.5.4.3 feathering blades which enter and exit the fluid perpendicular to the velocity result are supposedly more efficient than fixed radial wheels. These feathering blades, however, are more expensive to construct and maintain and thus fixed blade wheels are normally chosen. Fixed blade wheels with angled blades that enter or exit the surface of the fluid more perpendicular would be a cheaper option but it is unknown how these would perform. If the blade enters perpendicular it is unlikely to be more efficient as it will most likely lift more fluid from the surface. If the blade exits perpendicular, however, it should lift less fluid from the surface and thus there will be less energy spent moving the fluid in a useless direction.

To the authors knowledge the angle of the blades at the entry and exit of the fluid has not been investigated. An investigation into this should be done in order to quantify if there is any advantage of angling the blades. This would be done by the use of tangential blades instead of radial blades. The angle of blade is determined by the downstream fluid depth and wheel diameter and will be specific in every case. The optimal configuration is unlikely to be when the blade exits completely perpendicular to

the fluid as the blade will spend a considerable amount of time moving the fluid in a non-optimal direction. A more efficient configuration will possibly be when the blade exits more perpendicular to a radial blade but not fully as (Figure 7.1). This may be more optimal than a fully perpendicular blade exit as the entry angle would be less adverse.

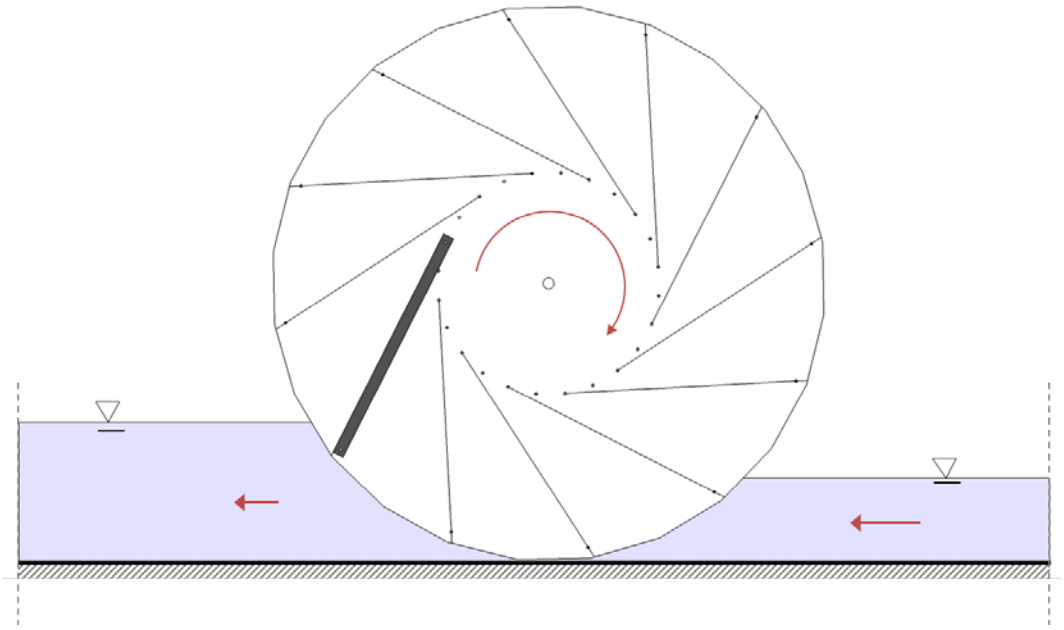

Figure 7.1. Conceptual design of the tangential blade wheel.

To the author's knowledge there have been no investigations in to the impact the wheel speed or blade number have on the height and length of the waves. As the scale of this experiment was too small this would need to be completed at the full scale operational plant. This investigation would be done in order to quantify the energy in the waves created and have a greater understanding of how to design the wheel to limit these effects and become as efficient as possible. To conduct this investigation a set of wave probes would measure the wave height immediately downstream of the wheel. The wheel would need to be operational at a range of rotational speeds and depths to fully quantify the wave creation.

During the time spent at the wastewater site in El Torno, Spain, it became apparent that the wind is a major factor to be considered when designing and orientating the raceways. When the wind blew directly along the channel the swell of fluid at the far end overtopped the side walls of the raceway with large waves. This is a problem as the site deals with raw sewage and any leakage from the raceway needs to be limited. This is normally done by raising the height of the side walls of the raceway. Doing this not

only increases the construction costs of the raceways but also the higher side walls will lead to more shading of the fluid. As well as waves created from the wind there will be a build-up of fluid at the downwind end of the raceway and a loss of fluid at the upwind end. If the upwind end of the raceway is the paddlewheel end then there would be less fluid for the wheel to lift. This has been shown to reduce the efficiency of the wheel.

A more innovative way of dealing with the wind waves would be to cause them to crest and break. If the waves were to break the energy stored in them could be utilised to increase the forward velocity of the fluid and also gas transfer as they break.

A proposed method to break the waves is shown in Figure 3.18, Section 3.5.4. This works by reducing the fluid depth and thus the wave height to depth ratio beyond the critical point where the height must not exceed:

$$H_W \leq 0.78d \qquad \text{Equation 7.1}$$

where H_W is the water wave height (m) and d the fluid depth (m).

In order to test this proposed method to control the waves produced by the wind the wave height and lengths need to be measured in the operational raceway. Alongside this the wind speed and direction should also be recorded at the same time so that a correlation between the wave height and wind speed can be deduced. The wave insert can then be tested in the flume with a range of different wave heights and fluid depths to evaluate its effectiveness at reducing the waves.

The wind may also act either positively or negatively on the wheel as it rotates. Measuring these effects would be important in the design of other sites if they located in windy areas.

The performance of the wheel studied here was based upon the power requirement and efficiency of the wheel. There is, however, an issue with this method which is that the algae require vertical mixing in order for homogenous mixing and by improving the hydrodynamic performance of the wheel and channels this might be limited. A possible improvement to the work would be measure the amount of vertical mixing per unit of energy loss for the bends, channels and wheel to evaluate which area is the most efficient mixing process and minimise the losses in the other areas.

Bibliography

ABDEL-RAOUF, N., AL-HOMAIDAN, A. A. & IBRAHEEM, I. B. M. 2012. Microalgae and wastewater treatment. *Saudi Journal of Biological Sciences,* 19**,** 257-275.

ALI, H., CHEEMA, T. & PARK, C. 2014. Effect of Paddle-Wheel Pulsating Velocity on the Hydrodynamic Performance of High-Rate Algal Ponds. *Journal of Energy Engineering,* 140**,** 1-12.

ALL-GAS 2015. ALL-GAS Newsletter 12/2015. *ALL-GAS Newsletter.*

ALL-GAS. 2017. *All-gas* [Online]. Spain. Available: http://www.all-gas.eu/ 2016].

ALL-GAS MEETING. 8/12/2016 2016.

ALTERNATIVE FUELS DATA CENTER. 2017. *Fuel Prices* [Online]. U.S. Department of Energy's Vehicle Technologies Office. Available: https://www.afdc.energy.gov/fuels/prices.html 2017].

AMINI, H., HASHEMISOHI, A., WANG, L., SHAHBAZI, A., BIKDASH, M., DUKKA, K. & YUAN, W. 2016. Numerical and experimental investigation of hydrodynamics and light transfer in open raceway ponds at various algal cell concentrations and medium depths. *Chemical Engineering Science,* 156**,** 11-23.

AQUAGY. 2010. *Wastewater Treatment and Sustainability* [Online]. Aquagy Available: http://www.aquagy.net/our_services.html 2016].

AQUALIA 2014. ALL-GAS project deliverable 4.3. New designs to decrease energy consumption and maintain biomass productivity; comparison with conventional raceway. *Raceway optimization.* Spain.

ARVANAGHI, H. & OSKUEI, N. N. 2011. Sharp-Crested Weir Discharge Coefficient.

AZOV, Y., SHELEF, G. & MORAINE, R. 1982. Carbon limitation of biomass production in high‐rate oxidation ponds. *Biotechnology and bioengineering,* 24**,** 579-594.

BARBOSA, M. J., HADIYANTO & WIJFFELS, R. H. 2003. Overcoming shear stress of microalgae cultures in sparged photobioreactors. *Biotechnology and Bioengineering,* 85**,** 78-85.

BECKER, E. W. 1994. *Microalgae: biotechnology and microbiology*, Cambridge University Press.

BEN-AMOTZ, A. 2008. Large Scale open Algal Ponds.

BENEMANN, J. R. 2003. Bio-fixation of CO2 and Greenhouse Gas Abatement with Micro-algae–Technology Roadmap. *Final report to the US Department of Energy, National Energy Technology Laboratory,* 55.

BENEMANN, J. R. & OSWALD, W. J. 1996. Systems and economic analysis of microalgae ponds for conversion of CO2 to biomass. Final report. California Univ., Berkeley, CA (United States). Dept. of Civil Engineering.

BERDALET, E., PETERS, F., KOUMANDOU, V. L., ROLDÁN, C., GUADAYOL, Ò. & ESTRADA, M. 2007. Species-specific physiological response of dinoflagellates to quantified small-scale turbulence. *Journal of Phycology,* 43**,** 965-977.

BERG-NILSEN, J. 2006. *Production of Micro algae based products,* Oslo, Nordic Innovation Centre.

BETZ, A. 1966. 60 - THE PADDLE-WHEEL. *In:* BETZ, A. (ed.) *Introduction to the Theory of Flow Machines.* Pergamon.

BITOG, J. P., LEE, I. B., LEE, C. G., KIM, K. S., HWANG, H. S., HONG, S. W., SEO, I. H., KWON, K. S. & MOSTAFA, E. 2011. Application of computational fluid dynamics for modeling and designing photobioreactors for microalgae production: A review. *Computers and Electronics in Agriculture,* 76**,** 131-147.

BLANCKAERT, K. 2003. *Flow and turbulence in sharp open-channel bends.* SECTION DE GÉNIE CIVIL POUR L'OBTENTION DU GRADE DE DOCTEUR ÈS SCIENCES PAR Burgerlijk Bouwkundig Ingenieur, Universiteit Gent.

BLANCKAERT, K. & DE VRIEND, H. 2004. Secondary flow in sharp open-channel bends. *Journal of Fluid Mechanics,* 498**,** 353-380.

BONAKDARI, H., BAGHALIAN, S., NAZARI, F. & FAZLI, M. 2011. Numerical analysis and prediction of the velocity field in curved open channel using artificial neural network and genetic algorithm. *Engineering Applications of Computational Fluid Mechanics,* 5**,** 384-396.

BOROWITZKA, M. 2005. Culturing microalgae in outdoor ponds. Academic Press, NY, USA.

BOROWITZKA, M. A. 1999. Commercial production of microalgae: ponds, tanks, tubes and fermenters. *Journal of Biotechnology,* 70**,** 313-321.

BOS, M. G. 1976. Discharge measurement structures. *NASA STI/Recon Technical Report N,* 78**,** 31395.

BOS, M. G., REPLOGLE, J. A. & CLEMMENS, A. J. 1984. Flow measuring flumes for open channel systems.

BP, BRITISH PETROLEUM 2013. BP Statistical Review of World Energy 2013. *BP Statistical Review of World Energy.* London: BP p.l.c.

BP GLOBAL, BRITISH PETROLEUM GLOBAL 2017. BP Energy Outlook - 2017 edition. *BP Energy Outlook.* London: BP p.l.c.

BRENNAN, L. & OWENDE, P. 2010. Biofuels from microalgae—A review of technologies for production, processing, and extractions of biofuels and co-products. *Renewable and Sustainable Energy Reviews,* 14**,** 557-577.

BRIGHT HUB ENGINEERING. 2016. *Real Velocity Distribution* [Online]. Bright Hub Inc. Available: http://www.brighthubengineering.com/hydraulics-civil-engineering/57703-real-velocity-distribution/ 2017].

BROWN, T. W. & TUCKER, C. S. 2013. Pumping Performance of a Slow-Rotating Paddlewheel for Split-Pond Aquaculture Systems. *North American Journal of Aquaculture,* 75**,** 153-158.

BUHR, H. O. & MILLER, S. B. 1983. A dynamic model of the high-rate algal-bacterial wastewater treatment pond. *Water Research,* 17**,** 29-37.

BUSINESS ELECTRICITY PRICES. 2016. *Business and Commercial Electricity Prices* [Online]. Available: http://www.businesselectricityprices.org.uk/ 2016].

CAMACHO, F. G. A., GOMEZ, A. C., SOBCZUK, T. M. & GRIMA, E. M. 2000. Effects of mechanical and hydrodynamic stress in agitated, sparged cultures of< i> Porphyridium cruentum</i>. *Process Biochemistry,* 35**,** 1045-1050.

CAMP, T. R. 1955. Flocculation and flocculation basins. *Transactions of the American Society of Civil Engineers,* 120**,** 1-16.

CANTRELL, K. B., DUCEY, T., RO, K. S. & HUNT, P. G. 2008. Livestock waste-to-bioenergy generation opportunities. *Bioresource technology,* 99**,** 7941-7953.

CARLTON, J. S. 2007. 2 - Propulsion systems. *Marine Propellers and Propulsion (Second Edition).* Oxford: Butterworth-Heinemann.

CELLANA INC. 2015. 8 blade paddlewheel.

CHIARAMONTI, D., PRUSSI, M., CASINI, D., TREDICI, M. R., RODOLFI, L., BASSI, N., ZITTELLI, G. C. & BONDIOLI, P. 2012. Review of energy balance in raceway ponds for microalgae cultivation: Re-thinking a traditional system is possible. *Applied Energy*.

CHISTI, Y. 2007. Biodiesel from microalgae. *Biotechnology Advances,* 25**,** 294-306.

CHISTI, Y. 2008. Biodiesel from microalgae beats bioethanol. *Trends in Biotechnology,* 26**,** 126-131.

CHISTI, Y. 2016. Large-Scale Production of Algal Biomass: Raceway Ponds. *In:* BUX, F. & CHISTI, Y. (eds.) *Algae Biotechnology: Products and Processes.* Cham: Springer International Publishing.

COMMERCIAL ALGAE PROFESSIONALS 2015a. Large Paddlewheel with Guidevain.

COMMERCIAL ALGAE PROFESSIONALS. 2015b. *Test Ponds* [Online]. Commercial Algae Professionals. Available: http://www.commercialalgae.com/products-and-services/test-ponds/#iLightbox[gallery_image_1]/1 2016].

CRAGGS, R. 2005. Advanced integrated wastewater ponds. *In:* SHILTON, A. (ed.) *Pond Treatment Technology, IWA Scientific and Technical Report Series, IWA.* London, UK.

CRAGGS, R., SUTHERLAND, D. & CAMPBELL, H. 2012. Hectare-scale demonstration of high rate algal ponds for enhanced wastewater treatment and biofuel production. *Journal of Applied Phycology,* 24**,** 329-337.

CROWE, C. T., ELGER, D. F., ROBERSON, J. A. & WILLIAMS, B. C. 2008. *Engineering Fluid Mechanics*, Wiley.

CYANOTECH CORPORATION. 2015. *Cyanotech's Facility* [Online]. Cyanotech Corporation,. Available: http://www.cyanotech.com/company/facility.html 2016].

DAVIS, R., ADEN, A. & PIENKOS, P. T. 2011. Techno-economic analysis of autotrophic microalgae for fuel production. *Applied Energy,* 88**,** 3524-3531.

DE GODOS, I., MENDOZA, J. L., ACIÉN, F. G., MOLINA, E., BANKS, C. J., HEAVEN, S. & ROGALLA, F. 2013. Evaluation of carbon dioxide mass transfer in raceway reactors for microalgae culture using flue gases. *Bioresource Technology,* 153**,** 307-314.

DELRUE, F., ÁLVAREZ-DÍAZ, P. D., FON-SING, S., FLEURY, G. & SASSI, J.-F. 2016. The environmental biorefinery: Using microalgae to remediate wastewater, a win-win paradigm. *Energies,* 9**,** 132.

DEPARTMENT FOR ENVIRONMENT, F. A. R. A. 2015. Area of Crops Grown For Bioenergy in England and the UK: 2008 - 2014. *In:* DEPARTMENT FOR ENVIRONMENT, F. A. R. A. (ed.). United Kingdom: Government Statistical Service.

DINGEMANS, M. W. 1997. *Water Wave Propagation Over Uneven Bottoms: Part 1*, World Scientific.

DODD, J. 1986. Elements of pond design and construction. *In:* A, R. (ed.) *Handbook of microalgal mass culture.* Boca Raton, Florida: CRC Press.

DOUCHA, J., STRAKA, F. & LÍVANSKÝ, K. 2005. Utilization of flue gas for cultivation of microalgae Chlorella sp.) in an outdoor open thin-layer photobioreactor. *Journal of Applied Phycology,* 17**,** 403-412.

DOYLE, C. 2013. *Slime and poo: making energy and treating waste* [Online]. ABC Environment. Available: http://www.abc.net.au/environment/articles/2013/12/02/3896391.htm 2016].

DUARTE-SANTOS, T., MENDOZA-MARTÍN, J. L., ACIÉN FERNÁNDEZ, F. G., MOLINA, E., VIEIRA-COSTA, J. A. & HEAVEN, S. 2016. Optimization of carbon dioxide supply in raceway reactors: Influence of carbon dioxide molar fraction and gas flow rate. *Bioresource Technology,* 212**,** 72-81.

EARTHRISE NUTRITIONAL. 2014. *Photograph* [Online]. Facebook. Available: https://www.facebook.com/EARTHRISE.Spirulina/photos/a.769516036415107.1073741826.769515983081779/769516023081775/?type=3&theater 2016].

EARTHRISE NUTRITIONAL. 2016. *Our Farm* [Online]. Earthrise Nutritional. Available: http://earthrise.com/about/our-farm/ 2016].

ETTEMA, R., ARNDT, R., ROBERTS, P. & WAHL, T. 2000. *Hydraulic modeling: concepts and practice,* Reston, Virginia, ASCE.

EUROPEAN COMMISSION 2011. A Roadmap for moving to a competitive low carbon economy in 2050. Brussels: European Commision.

EUROPEAN COMMISSION 2013. Smarter, greener, more inclusive: Indicators to support the Europe 2020 strategy. *In:* SAVOVA, I., HAMETNER, M., DIMITROVA, A., ENDL , A., FLIEDNER, J., SCHWAB, S., UMPFENBACH, K. & CEREZO, K. T. (eds.). Luxembourg.

EUROPEAN UNION 2009. The promotion of the use of energy from renewable sources *Directive 2009/28/EC* OJ L140/16.

EWG, ENERGY WATCH GROUP, 2007. Crude Oil: The Supply Outlook. Germany.

FAKHOORIAN, T. 2010. *Robert Vitale Reinvents the Paddlewheel* [Online]. AlgaeIndustryMagazine.com. Available: http://www.algaeindustrymagazine.com/robert-vitale-reinvents-the-paddlewheel/ 2016].

FAO, FOOD AND AGRICULTURE ORGANIZATION OF THE UNITED NATIONS, 1996. Manual on the production and use of live food for aquaculture. *In:* PATRICK LAVENS, P. S. (ed.) *FAO Fisheries technical paper.* Rome: United Nations.

FERNANDEZ, A. 2016.

FOA, FOOD AND AGRICULTURE ORGANIZATION, 2008. Biofuels: Prospects, Risks and Opportunities. . *The State of Food and Agriculture.* Rome: United Nations.

FUKUDA, H., KONDO, A. & NODA, H. 2001. Biodiesel fuel production by transesterification of oils. *Journal of Bioscience and Bioengineering,* 92**,** 405-416.

GHOSE, J. G., R.P 2004. unconventional propulsion devices. *Basic ship propulsion.* Mumbai: Allied publishers.

GLOYNA, E. F. & WHO, WORLD HEALTH ORGANIZATION, 1971. *Waste stabilization ponds,* Geneva, Switzerland, World Health Organization

GOOGLE EARTH. 2015. *Boonsom Farm 18°35'43''N 98°46'47'' E elevation 325 m*.

GOOGLE EARTH. 2016a. *Cyanotech Corporation 19°43'52''N 156°02'59''W elevation 6 m*.

GOOGLE EARTH. 2016b. *Parry Nutraceutical 10°12'34''N 78°46'56''E elevation 100 m*.

GOUVEIA, L. 2011. *Microalgae as a Feedstock for Biofuels*, Springer.

GREAT BRITAIN 2008. Climate Change Act 2008: Elizabeth II. Chapter 27. London: The Stationary Office.

GREEN DIAMOND CO. LTD 2010. Algae-Tourism at Boonsom Farm in Thailand. Earthrise Company.

GREENERLIFES. 2010. Waste Stabilization Ponds. Available: http://greenerlifes.com/1376/waste-stabilization-ponds/.

GRIMA, E. M., FERNÁNDEZ SEVILLA, J. M., ACIÉN FERNÁNDEZ, F. G. & FLICKINGER, M. C. 2010. Microalgae, Mass Culture Methods. *Encyclopedia of Industrial Biotechnology.* John Wiley & Sons, Inc.

GROBBELAAR, J. U., SOEDER, C. J. & STENGEL, E. 1990. Modeling algal productivity in large outdoor cultures and waste treatment systems. *Biomass,* 21**,** 297-314.

HADIYANTO, H., ELMORE, S., VAN GERVEN, T. & STANKIEWICZ, A. 2013. Hydrodynamic evaluations in high rate algae pond (HRAP) design. *Chemical Engineering Journal,* 217**,** 231-239.

HAN, S., RAMAMURTHY, A. & BIRON, P. M. 2011. Characteristics of flow around open channel 90 bends with vanes. *Journal of Irrigation and Drainage Engineering,* 137**,** 668-676.

HARRIS, M. J. 2011. *Venturi Meters* [Online]. Thermopedia. Available: http://www.thermopedia.com/content/1241/ 2017].

HELLER, D. V. 2012. Model-Prototype Similalrity. Available: http://www.drvalentinheller.com/Dr%20Valentin%20Heller_files/Heller_Model-Prototype%20Similarity.pdf.

HELMIZAR. 2016. *Turbine wheel - a hydropower converter for head differences between 2.5 and 5 m.* University of Southampton.

HENDRICKS, D. 2010. *Fundamentals of water treatment unit processes: physical, chemical, and biological*, CRC Press.

HENRIKSON, R. 1983. Earthrise Farms. The first commercial Spirulina Farm in the Californian Desert. Earthrise Company,.

HEUBECK, S., CRAGGS, R. & SHILTON, A. 2007. Influence of CO 2 scrubbing from biogas on the treatment performance of a high rate algal pond. *Water Science & Technology,* 55**,** 193-200.

HILL, J., NELSON, E., TILMAN, D., POLASKY, S. & TIFFANY, D. 2006. Environmental, economic, and energetic costs and benefits of biodiesel and ethanol biofuels. *Proceedings of the National Academy of Sciences,* 103**,** 11206-11210.

HILL, N., WALKER, H., CHOUDRIE, S. & JAMES, K. 2012. 2012 Guidelines to Defra / DECC's GHG Conversion Factors for Company Reporting: Methodology Paper for Emission Factors. London: Department for Environment, Food and Rural Affairs (Defra), Department of Energy and Climate Change (DECC).

HIRANO, A., HON-NAMI, K., KUNITO, S., HADA, M. & OGUSHI, Y. 1998. Temperature effect on continuous gasification of microalgal biomass: theoretical yield of methanol production and its energy balance. *Catalysis Today,* 45**,** 399-404.

HONDZO, M. & LYN, D. 1999. Quantified small-scale turbulence inhibits the growth of a green alga. *Freshwater Biology,* 41**,** 51-61.

HREIZ, R., SIALVE, B., MORCHAIN, J., ESCUDIÉ, R., STEYER, J.-P. & GUIRAUD, P. 2014. Experimental and numerical investigation of hydrodynamics in raceway reactors used for algaculture. *Chemical Engineering Journal,* 250**,** 230-239.

HSUEH, H. T., CHU, H. & YU, S. T. 2007. A batch study on the bio-fixation of carbon dioxide in the absorbed solution from a chemical wet scrubber by hot spring and marine algae. *Chemosphere,* 66**,** 878-886.

HUANG, J., QU, X., WAN, M., YING, J., LI, Y., ZHU, F., WANG, J., SHEN, G., CHEN, J. & LI, W. 2015. Investigation on the performance of raceway ponds with internal structures by the means of CFD simulations and experiments. *Algal Research,* 10**,** 64-71.

HUISMAN, J., MATTHIJS, H. C., VISSER, P. M., BALKE, H., SIGON, C. A., PASSARGE, J., WEISSING, F. J. & MUR, L. R. 2002. Principles of the light-limited chemostat: theory and ecological applications. *Antonie van Leeuwenhoek,* 81**,** 117-133.

IEA, INTERNATIONAL ENERGY AGENCY, 2006. *World Energy Outlook 2006*, OECD Publishing.

INTERNATIONAL WATER MANAGEMENT INSTITUTE 2008. *Water for food, water for life a comprehensive assessment of water management in agriculture,* London, Earthscan.

JAMES, S. C. & BORIAH, V. 2010. Modeling algae growth in an open-channel raceway. *J Comput Biol,* 17**,** 895-906.

JAOUEN, P., VANDANJON, L. & QUÉMÉNEUR, F. 1999. The shear stress of microalgal cell suspensions (Tetraselmis suecica) in tangential flow filtration systems: the role of pumps. *Bioresource Technology,* 68**,** 149-154.

JIMÉNEZ, C., COSSı, B. R. & XAVIER NIELL, F. 2003. Relationship between physicochemical variables and productivity in open ponds for the production of Spirulina: a predictive model of algal yield. *Aquaculture,* 221**,** 331-345.

JOHNSON, M. C. 2000. Discharge coefficient analysis for flat-topped and sharp-crested weirs. *Irrigation Science,* 19**,** 133-137.

KADAM, K. L. 2002. Environmental implications of power generation via coal-microalgae cofiring. *Energy,* 27**,** 905-922.

KAO, C.-Y., CHEN, T.-Y., CHANG, Y.-B., CHIU, T.-W., LIN, H.-Y., CHEN, C.-D., CHANG, J.-S. & LIN, C.-S. 2014. Utilization of carbon dioxide in industrial flue gases for the cultivation of microalga Chlorella sp. *Bioresource Technology,* 166**,** 485-493.

KAWAMURA, S. 2000. *Integrated design and operation of water treatment facilities*, John Wiley & Sons.

KETHEESAN, B. & NIRMALAKHANDAN, N. 2011. Development of a new airlift-driven raceway reactor for algal cultivation. *Applied Energy,* 88**,** 3370-3376.

KINDSVATER, C. E. & CARTER, R. W. 1957. Discharge characteristics of rectangular thin-plate weirs. *Journal of the Hydraulics Division,* 83**,** 1-36.

LAMONT, J. C. & SCOTT, D. 1970. An eddy cell model of mass transfer into the surface of a turbulent liquid. *AIChE Journal,* 16**,** 513-519.

LARA CORONA, E. & ARBIB, Z. 2016. *RE: Spain data.* Type to MUSGROVE, E.

LARDON, L., HÉLIAS, A., SIALVE, B., STEYER, J.-P. & BERNARD, O. 2009. Life-Cycle Assessment of Biodiesel Production from Microalgae. *Environmental Science & Technology,* 43**,** 6475-6481.

LAWS, E., TERRY, K., WICKMAN, J. & CHALUP, M. 1983. A simple algal production system designed to utilize the flashing light effect. *Biotechnology and bioengineering,* 25**,** 2319-2335.

LI, S., LUO, S. & GUO, R. 2013. Efficiency of CO2 fixation by microalgae in a closed raceway pond. *Bioresource Technology,* 136**,** 267-272.

LI, Y., ZHANG, Q., WANG, Z., WU, X. & CONG, W. 2014. Evaluation of power consumption of paddle wheel in an open raceway pond. *Bioprocess and Biosystems Engineering,* 37**,** 1325-1336.

LI, Z., YUAN, H., YANG, J. & LI, B. 2011. Optimization of the biomass production of oil algae Chlorella minutissima UTEX2341. *Bioresource Technology,* 102**,** 9128-9134.

LIFFMAN, K., PATERSON, D. A., LIOVIC, P. & BANDOPADHAYAY, P. 2012. Comparing the energy efficiency of different high rate algal raceway pond designs using computational fluid dynamics. *Chemical Engineering Research and Design,* 91**,** 221-226.

LINTON, P. N. 2014. *Field Trials and Development of a Hydrostatic Pressure Machine.*, University of Southampton.

LUNDQUIST, T. J., WOERTZ, I. C., QUINN, N. & BENEMANN, J. R. 2010. A realistic technology and engineering assessment of algae biofuel production. *Energy Biosciences Institute***,** 1-178.

MACDONALD, D. & STREICHER, L. 1977. Water treatment plant design is cost-effective. *Public Works,* 108.

MALLICK, N. 2002. Biotechnological potential of immobilized algae for wastewater N, P and metal removal: A review. *Biometals,* 15**,** 377-390.

MALONE, T. R. & PARR, A. D. 2008. *Bend Losses in Rectangular Culverts,* Kansas, Kansas Department of Transportation.

MCCOWAN, J. 1891. VII. On the solitary wave. *The London, Edinburgh, and Dublin Philosophical Magazine and Journal of Science,* 32**,** 45-58.

MCGINN, P., DICKINSON, K., BHATTI, S., FRIGON, J.-C., GUIOT, S. & O'LEARY, S. B. 2011. Integration of microalgae cultivation with industrial waste remediation for biofuel and bioenergy production: opportunities and limitations. *Photosynthesis Research,* 109**,** 231-247.

MENDOZA, J. L., GRANADOS, M. R., DE GODOS, I., ACIÉN, F. G., MOLINA, E., BANKS, C. & HEAVEN, S. 2013a. Fluid-dynamic characterization of real-scale raceway reactors for microalgae production. *Biomass and Bioenergy,* 54**,** 267-275.

MENDOZA, J. L., GRANADOS, M. R., DE GODOS, I., ACIÉN, F. G., MOLINA, E., HEAVEN, S. & BANKS, C. J. 2013b. Oxygen transfer and evolution in microalgal culture in open raceways. *Bioresource Technology,* 137**,** 188-195.

METTING JR, F. 1996. Biodiversity and application of microalgae. *Journal of industrial microbiology,* 17**,** 477-489.

MICHELL, J. H. 1893. XLIV. The highest waves in water. *The London, Edinburgh, and Dublin Philosophical Magazine and Journal of Science,* 36**,** 430-437.

MILLEDGE, J. J. 2013. *Energy balance and techno-economic assessment of algal biofuel production systems.* University of Southampton.

MILLEDGE, J. J. & HEAVEN, S. 2014. Methods of energy extraction from microalgal biomass: a review. *Reviews in Environmental Science and Bio/Technology,* 13**,** 301-320.

MILLEDGE, J. J. & HEAVEN, S. 2015. Energy balance of biogas production from microalgae: development of an energy and mass balance model. *Current Biotechnology,* 4**,** 554-567.

MIRÓN, A. S., GARCíA, M. C. C., GÓMEZ, A. C., CAMACHO, F. G. A., GRIMA, E. M. & CHISTI, Y. 2003. Shear stress tolerance and biochemical characterization of Phaeodactylum tricornutum in quasi steady-state continuous culture in outdoor photobioreactors. *Biochemical Engineering Journal,* 16**,** 287-297.

MOFJELD, H. O. & LAVELLE, J. W. 1988. Formulas for velocity, sediment concentration and suspended sediment flux for steady uni-directional pressure-driven flow. Seattle. Washington: Pacific Marine Environmental Laboratory.

MOLINA, E., FERNÁNDEZ, J., ACIÉN, F. G. & CHISTI, Y. 2001. Tubular photobioreactor design for algal cultures. *Journal of biotechnology,* 92**,** 113-131.

MONTGOMERY, J. M. 1985. *Water treatment: principles and design*, John Wiley & Sons.

MOOG, D. B. & JIRKA, G. H. 1999. Air-water gas transfer in uniform channel flow. *Journal of hydraulic engineering,* 125**,** 3-10.

MUSGROVE, E. & HEAVEN, S. 2014. Investigating the hydrodynamic performance of carbonation sumps in High Rate Algal Pond (HRAP)raceways using computational fluid dynamics (CFD). *Biofuels,* 5**,** 1-17.

NAJI-ABHARI, M., GHODSIAN, M., VAGHEFI, M. & PANAHPUR, N. 2010. Experimental and numerical simulation of flow in a 90°bend. *Flow Measurement and Instrumentation,* 21**,** 292-298.

NARALA, R. R., GARG, S., SHARMA, K. K., THOMAS-HALL, S. R., DEME, M., LI, Y. & SCHENK, P. M. 2016. Comparison of Microalgae Cultivation in Photobioreactor, Open Raceway Pond, and a Two-Stage Hybrid System. *Frontiers in Energy Research,* 4.

NEENAN, B., FEINBERG, D., HILL, A., MCINTOSH, R. & TERRY, K. 1986. Fuels from Microalgae: Technology Status, Potential, and Research Requirements. Golden, Colorado (USA): Solar Energy Rsearch Institute.

NEZU, I. & NAKAGAWA, H. 1993. *Turbulence in Open Channel Flows*, Taylor & Francis.

NOCK, W. J. 2015. *An investigation into gas transfer from bubbles into water.* University of Southampton.

OLAIZOLA, M., DUERR, E. O. & FREEMAN, D. W. 1991. Effect of CO2 enhancement in an outdoor algal production system usingTetraselmis. *Journal of applied phycology,* 3**,** 363-366.

OSWALD, W. J. 1988. Large-Scale Algal Culture Systems (Engineering Aspects). *In:* BOROWITZKA, M. A. & BOROWITZKA, L. J. (eds.) *Micro-Algal Biotechnology.* Cambridge: Cambridge University Press.

OWEN, N. A., INDERWILDI, O. R. & KING, D. A. 2010. The status of conventional world oil reserves—Hype or cause for concern? *Energy Policy,* 38**,** 4743-4749.

PACHECO-CEBALLOS, R. 1983. Energy losses and shear stresses in channel bends. *Journal of Hydraulic Engineering,* 109**,** 881-896.

PACKER, M. 2009. Algal capture of carbon dioxide; biomass generation as a tool for greenhouse gas mitigation with reference to New Zealand energy strategy and policy. *Energy Policy,* 37**,** 3428-3437.

PARK, J., HEIKES, D., RECSETAR, M. & ROY, L. A. 2014. Performance evaluation and engineering considerations for a modular- and culvert-based paddlewheel circulator for split-pond systems. *Aquacultural Engineering,* 61**,** 1-8.

PARK, J. B. K., CRAGGS, R. J. & SHILTON, A. N. 2011. Wastewater treatment high rate algal ponds for biofuel production. *Bioresource Technology,* 102**,** 35-42.

PARRY NUTRACEUTICALS 2011. Organic Spirulina Manufacturing process. Parry Nutraceuticals,.

PERSOONE, G., MORALES, J., VERLET, H. & DE PAUW, N. 1980. Air-lift pumps and the effect of mixing on algal growth. *Algal Biomass. Elsevier/North Holland Biomedical Press, Amsterdam***,** 505-522.

PITTMAN, J. K., DEAN, A. P. & OSUNDEKO, O. 2011. The potential of sustainable algal biofuel production using wastewater resources. *Bioresource Technology,* 102**,** 17-25.

POSTEN, C. & SCHAUB, G. 2009. Microalgae and terrestrial biomass as source for fuels—A process view. *Journal of Biotechnology,* 142**,** 64-69.

PRUSSI, M., BUFFI, M., CASINI, D., CHIARAMONTI, D., MARTELLI, F., CARNEVALE, M., TREDICI, M. R. & RODOLFI, L. 2014. Experimental and numerical investigations of mixing in raceway ponds for algae cultivation. *Biomass and Bioenergy,* 67**,** 390-400.

PRUVOST, J., CORNET, J.-F. & PILON, L. 2016. Large-scale production of algal biomass: photobioreactors. *Algae Biotechnology.* Springer.

PUTT, R., SINGH, M., CHINNASAMY, S. & DAS, K. C. 2011. An efficient system for carbonation of high-rate algae pond water to enhance CO2 mass transfer. *Bioresource Technology,* 102**,** 3240-3245.

QUINN, J., DE WINTER, L. & BRADLEY, T. 2011. Microalgae bulk growth model with application to industrial scale systems. *Bioresource technology,* 102**,** 5083-5092.

RAES, E. J., ISDEPSKY, A., MUYLAERT, K., BOROWITZKA, M. A. & MOHEIMANI, N. R. 2014. Comparison of growth of Tetraselmis in a tubular photobioreactor (Biocoil) and a raceway pond. *Journal of Applied Phycology,* 26**,** 247-255.

RAJU, S. P. 1937. Resistance to Flow in Curved Open Channels. *Abridged Translations of Hydraulic Papers, Proceedings, American Society of Civil Engineers,,* 63**,** 49-55.

RAMAMURTHY, A., HAN, S. & BIRON, P. 2012. Three-dimensional simulation parameters for 90° open channel bend flows. *Journal of Computing in Civil Engineering,* 27**,** 282-291.

RICHARDSON, J. W., JOHNSON, M. D. & OUTLAW, J. L. 2012. Economic comparison of open pond raceways to photo bio-reactors for profitable production of algae for transportation fuels in the Southwest. *Algal Research,* 1**,** 93-100.

RICHARDSON, J. W., JOHNSON, M. D., ZHANG, X., ZEMKE, P., CHEN, W. & HU, Q. 2014. A financial assessment of two alternative cultivation systems and their contributions to algae biofuel economic viability. *Algal Research,* 4**,** 96-104.

RODOLFI, L., CHINI ZITTELLI, G., BASSI, N., PADOVANI, G., BIONDI, N., BONINI, G. & TREDICI, M. R. 2009. Microalgae for oil: Strain selection, induction of lipid synthesis and outdoor mass cultivation in a low‐cost photobioreactor. *Biotechnology and bioengineering,* 102**,** 100-112.

ROHRER, M. 2011. Spirulina. Cyanotech Corporation.

SAPPHIRE ENERGY. 2009. *A gem in the desert* [Online]. The Business Journals. Available: http://www.bizjournals.com/albuquerque/stories/2009/06/08/story1 2016].

SCHENK, P., THOMAS-HALL, S., STEPHENS, E., MARX, U., MUSSGNUG, J., POSTEN, C., KRUSE, O. & HANKAMER, B. 2008. Second Generation Biofuels: High-Efficiency Microalgae for Biodiesel Production. *BioEnergy Research,* 1**,** 20-43.

SCHWARTZ, D. 2012. *A.I.M. Interview: Waterwheel Factory's Bob Vitale* [Online]. AlgaeIndustryMagazine.com. Available: http://www.algaeindustrymagazine.com/aim-interview-waterwheel-factorys-bob-vitale/ [Accessed 07/09/2014 2014].

SCOTT, S. A., DAVEY, M. P., DENNIS, J. S., HORST, I., HOWE, C. J., LEA-SMITH, D. J. & SMITH, A. G. 2010. Biodiesel from algae: challenges and prospects. *Current Opinion in Biotechnology,* 21**,** 277-286.

SEARCHINGER, T., HEIMLICH, R., HOUGHTON, R. A., DONG, F., ELOBEID, A., FABIOSA, J., TOKGOZ, S., HAYES, D. & YU, T.-H. 2008. Use of U.S. Croplands for Biofuels Increases Greenhouse Gases Through Emissions from Land-Use Change. *Science,* 319**,** 1238-1240.

SEMAT, H. & KATZ, R. 1958. Chapter 20: Wave Motion. *Physics.* New York: Rinehart & Company Inc., .

SENIOR, J. A. 2009. *Hydrostatic pressure converters for the exploitation of very low head hydropower potential.* University of Southampton.

SHAMS GHAHFAROKHI, G. R., VRIJLING, J. K. & VAN GELDER, P. H. A. J. M. Evaluation of Superelevation in Open Channel Bends with Probabilistic Analysis Methods. World Environmental and Water Resources Congress 2008@ sAhupua'A, 2008. ASCE, 1-14.

SHEN, Y., YUAN, W., PEI, Z., WU, Q. & MAO, E. 2009. Microalgae mass production methods. *Transactions of the ASABE,* 52**,** 1275-1287.

SHUKRY, A. 1950. Flow around bends in an open flume. *Transactions of the American Society of Civil Engineers,* 115**,** 751-779.

SINGH, A. & OLSEN, S. I. 2011. A critical review of biochemical conversion, sustainability and life cycle assessment of algal biofuels. *Applied Energy,* 88**,** 3548-3555.

SOBCZUK, T. M., CAMACHO, F. G., GRIMA, E. M. & CHISTI, Y. 2006. Effects of agitation on the microalgae Phaeodactylum tricornutum and Porphyridium cruentum. *Bioprocess and Biosystems Engineering,* 28**,** 243-250.

SOMPECH, K., CHISTI, Y. & SRINOPHAKUN, T. 2012. Design of raceway ponds for producing microalgae. *Biofuels,* 3**,** 387-397.

SONIN, A. 2002. Basics of Turbulent Flow. *Turbulent Flow and Transport.* Massachusetts: Massachusetts Institute of Technology.

SPOLAORE, P., JOANNIS-CASSAN, C., DURAN, E. & ISAMBERT, A. 2006. Commercial applications of microalgae. *Journal of bioscience and bioengineering,* 101**,** 87-96.

STEPHENSON, A. L., KAZAMIA, E., DENNIS, J. S., HOWE, C. J., SCOTT, S. A. & SMITH, A. G. 2010. Life-cycle assessment of potential algal biodiesel production in the United Kingdom: a comparison of raceways and air-lift tubular bioreactors. *Energy & Fuels,* 24**,** 4062-4077.

STURM, B. S. M. & LAMER, S. L. 2011. An energy evaluation of coupling nutrient removal from wastewater with algal biomass production. *Applied Energy,* 88**,** 3499-3506.

SUBHADRA, B. G. 2010. Sustainability of algal biofuel production using integrated renewable energy park (IREP) and algal biorefinery approach. *Energy Policy,* 38**,** 5892-5901.

SULLIVAN, J. M. & SWIFT, E. 2003. Effects of small-scale turbulence on net growth rate and size of ten species of marine dinoflagellates. *Journal of Phycology,* 39**,** 83-94.

SULLIVAN, J. M., SWIFT, E., DONAGHAY, P. L. & RINES, J. E. B. 2003. Small-scale turbulence affects the division rate and morphology of two red-tide dinoflagellates. *Harmful Algae,* 2**,** 183-199.

SUZUKI, T., MATSUO, T., OHTAGUCHI, K. & KOIDE, K. 1995. Gas‐Sparged bioreactors for CO2 fixation by Dunaliella tertiolecta. *Journal of chemical technology and biotechnology,* 62**,** 351-358.

SWAN, C. 2011. *Pitot Tube* [Online]. Thermopedia. Available: http://www.thermopedia.com/content/1032/ 2017].

TEVATA, A. & INPRASIT, C. 2011. The Effect of Paddle Number and Immersed Radius Ratio on Water Wheel Performance. *Energy Procedia,* 9**,** 359-365.

TEXAS A&M AGRILIFE RESEARCH. 2016. *Communications Resources Section* [Online]. Texas A&M AgriLife Research - Bioenergy Program. Available: http://algaeforfuel.agrilife.org/communications/media/ 2016].

THAJUDDIN, N. 2016. *Algal biomass production at Micro Algal raceway faclility at Bharathidasan University* [Online]. Bharathidasan Universit. Available: http://thajuddin.com/index.html 2016].

THEIN, M. 2011. Lake Harvest Production System in Myanmar.: Algae Competition.

THEOFANOUS, T. G., HOUZE, R. N. & BRUMFIELD, L. K. 1976. Turbulent mass transfer at free, gas-liquid interfaces, with applications to open-channel, bubble and jet flows. *International Journal of Heat and Mass Transfer,* 19**,** 613-624.

THOMAS, W. & GIBSON, C. 1990. Effects of small-scale turbulence on microalgae. *Journal of Applied Phycology,* 2**,** 71-77.

THUNG PI, M. W. 2016. *Boonsom farm* [Online]. Bangkok Post. Available: http://www.bangkokpost.com/business/companies%20in%20thailand/45548/boonsom-farm 2016].

TRANSPORT, D. F. 2014. Renewable Transport Fuel Obligation statistics: obligation period 7, 2014/15, report 1 *In:* TRANSPORT, D. F. (ed.). United Kingdom: Department for Transport.

TRIBAL ENERGY AND ENVIRONMENTAL INFORMATION CLEARINGHOUSE. 2016. *Biomass Energy Project Phases and Activities* [Online]. Available: http://teeic.indianaffairs.gov/er/biomass/activities/act/ 2016].

VANDANJON, L., ROSSIGNOL, N., JAOUEN, P., ROBERT, J. & QUÉMÉNEUR, F. 1999. Effects of shear on two microalgae species. Contribution of pumps and valves in tangential flow filtration systems. *Biotechnology and bioengineering,* 63**,** 1-9.

VARGAS E SILVA, F. & MONTEGGIA, L. O. 2015. PYROLYSIS OF ALGAL BIOMASS OBTAINED FROM HIGH RATE ALGAE PONDS APPLIED TO WASTEWATER TREATMENT. *Frontiers in Energy Research,* 3.

VAUGHAN, G. 2013. *Experimental studies of vertical mixing patterns in open channel flow generated by two delta wings side-by-side*.

VITALE, R. 2012. *Paddlewheel apparatus*. United States patent application US 13/401,186.

VOLETI, R. S. 2012. *Experimental Studies of Vertical Mixing in an Open Channel Raceway for Algae Biofuel Production.*

VOLPICH, H. & BRIDGE, I. 1956. Paddle Wheels Part II: Systematic Model Experiments. *Transactions of the Institution of Engineers and Shipbuilders in Scotland,* 99**,** 467-510.

VUNJAK-NOVAKOVIC, G., KIM, Y., WU, X., BERZIN, I. & MERCHUK, J. C. 2005. Air-Lift Bioreactors for Algal Growth on Flue Gas: Mathematical Modeling and Pilot-Plant Studies. *Industrial & Engineering Chemistry Research,* 44**,** 6154-6163.

WALLER, P., RYAN, R., KACIRA, M. & LI, P. 2012. The algae raceway integrated design for optimal temperature management. *Biomass and Bioenergy***,** 1-8.

WARNAARS, T. A. & HONDZO, M. 2006. Small-scale fluid motion mediates growth and nutrient uptake of Selenastrum capricornutum. *Freshwater Biology,* 51**,** 999-1015.

WATERS, R. 2008. *Energy from ocean waves: full scale experimental verification of a wave energy converter.* Uppsala University.

WEISSMAN, J. C. & GOEBEL, R. P. 1987. *Design and analysis of microalgal open pond systems for the purpose of producing fuels: A subcontract report,* Golden, Colorado (USA), Midwest Research Institute.

WEISSMAN, J. C., GOEBEL, R. P. & BENEMANN, J. R. 1988. Photobioreactor design: mixing, carbon utilization, and oxygen accumulation. *Biotechnology and bioengineering,* 31**,** 336-344.

WEISSMAN, J. C., TILLET, D. M. & GOEBEL, R. P. 1989. *Design and Operation of an Outdoor Microalgae Test Facility,* Golden, Colorado, Midwest Research Institue.

WORLD ENERGY COUNCIL 2013. World Energy Resources 2013 Survey. *World Energy Resources* London: World Energy Council.

WRAY, G. A. & STARRETT, J. A. 1970. A Model Study of the Hydrodynamic Characteristics of a series of Paddle-wheel Propulsive Devices for High-Speed Craft. DTIC Document.

YANG, A. 2011. Modeling and evaluation of CO2 supply and utilization in algal ponds. *Industrial & Engineering Chemistry Research,* 50**,** 11181-11192.

ZENG, F., HUANG, J., MENG, C., ZHU, F., CHEN, J. & LI, Y. 2015. Investigation on novel raceway pond with inclined paddle wheels through simulation and microalgae culture experiments. *Bioprocess and Biosystems Engineering***,** 1-12.

ZHANG, Q., MA, J., QIU, G., LI, L., GENG, S., HASI, E., LI, C., WANG, G. & LI, X. 2012. Potential energy production from algae on marginal land in China. *Bioresource Technology,* 109**,** 252-260.

ZHANG, Q., XUE, S., YAN, C., WU, X., WEN, S. & CONG, W. 2015. Installation of flow deflectors and wing baffles to reduce dead zone and enhance flashing light effect in an open raceway pond. *Bioresource Technology,* 198**,** 150-156.

Appendix A – Journal papers and conferences

Journal papers published

Musgrove, E., & Heaven, S. (2014). Investigating the hydrodynamic performance of carbonation sumps in High Rate Algal Pond (HRAP) raceways using computational fluid dynamics (CFD). *Biofuels*, 1-17.

Journal papers pending

Investigating the performance of paddlewheels used in High Rate Algal Ponds (HRAPs)

E. Musgrove, S. Heaven & G. Muller

Conferences attended

1. Poster presented at The 4th UK microalgae Conference 2014 in Cambridge. Title: Title: Improving the efficiency of paddlewheels
2. Poster presented at microalgae Around the World Symposium 2015 in Malta. Title: Improving the efficiency of paddlewheels in microalgae production
3. Session chair and presented at Marine Biomass for Renewable Energy 2016 in Glasgow. Title: Investigating the performance of paddlewheels used in high rate algal ponds (HRAPs)

Appendix B – Paddlewheel experiment technical drawings

Specification drawings for all parts used in the construction of the model raceway. All dimensions are in millimetres unless stated otherwise.

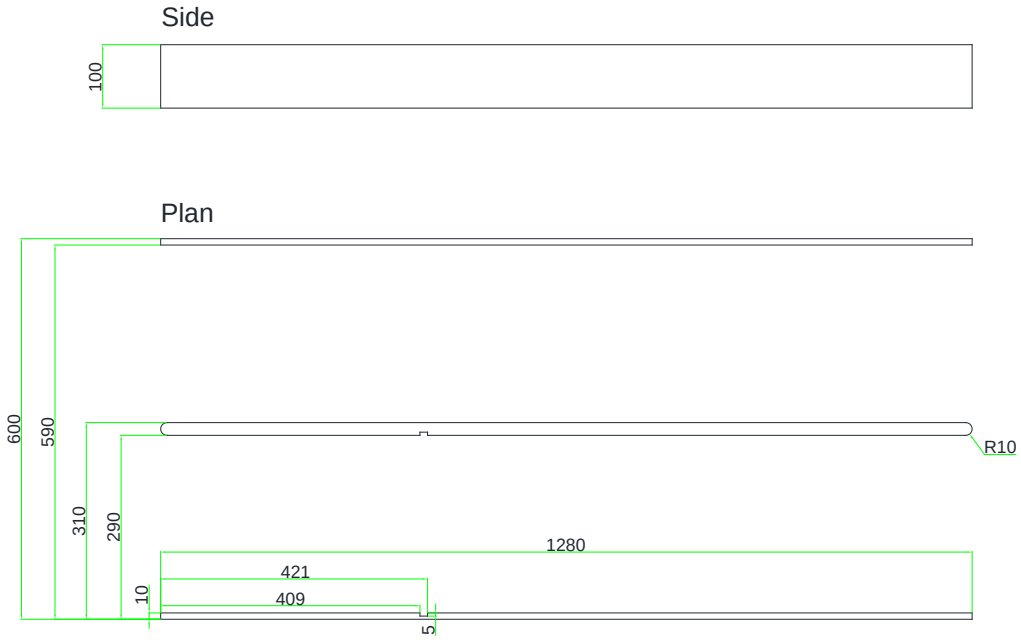

Figure B 1.Raceway walls specification drawing

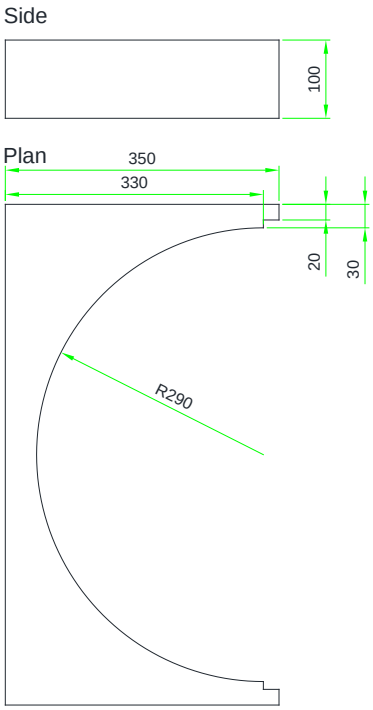

Figure B 2. End bend specification drawing

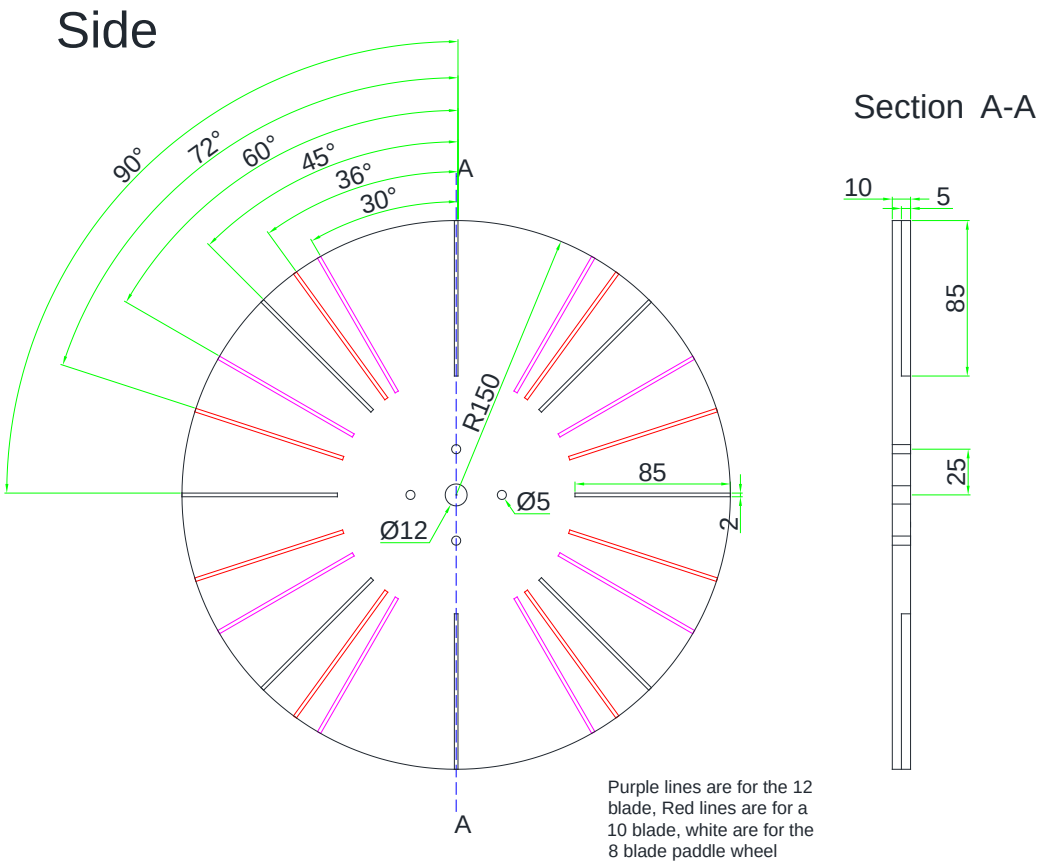

Figure B 3. Wheel plate specification drawing

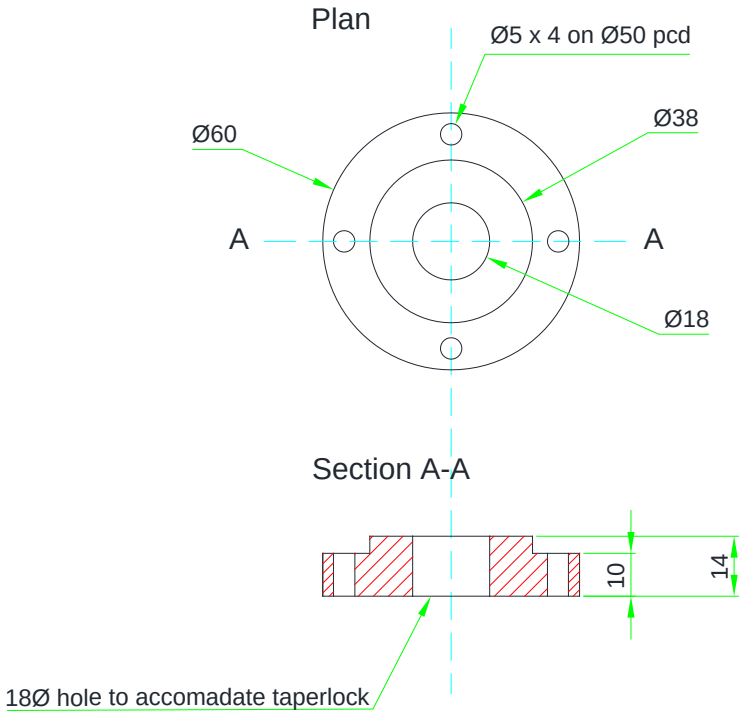

Figure B 4. Wheel collar specification drawing

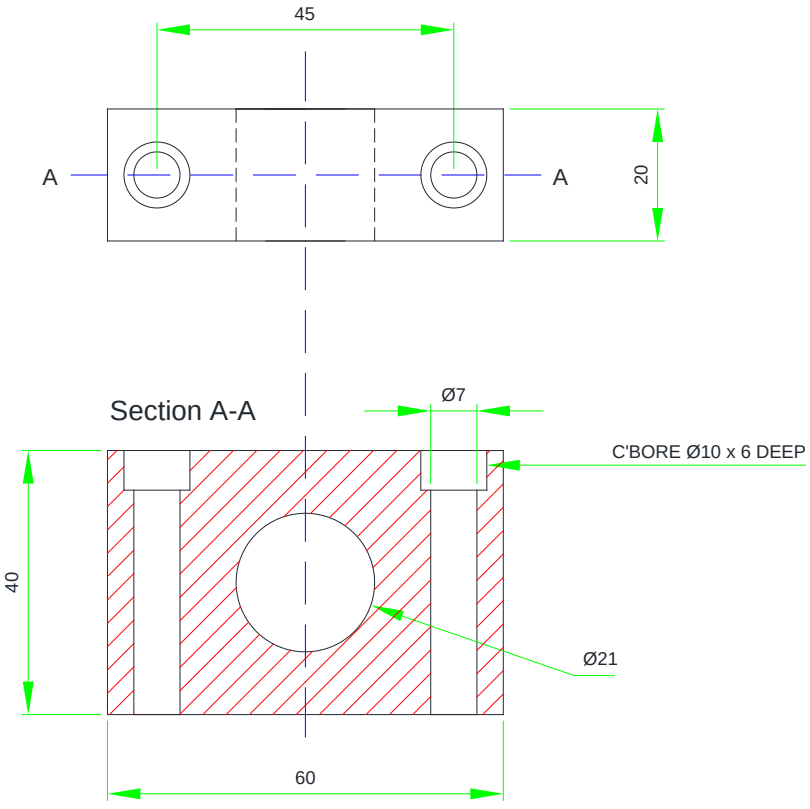

Figure B 5. Bearing block specification drawing

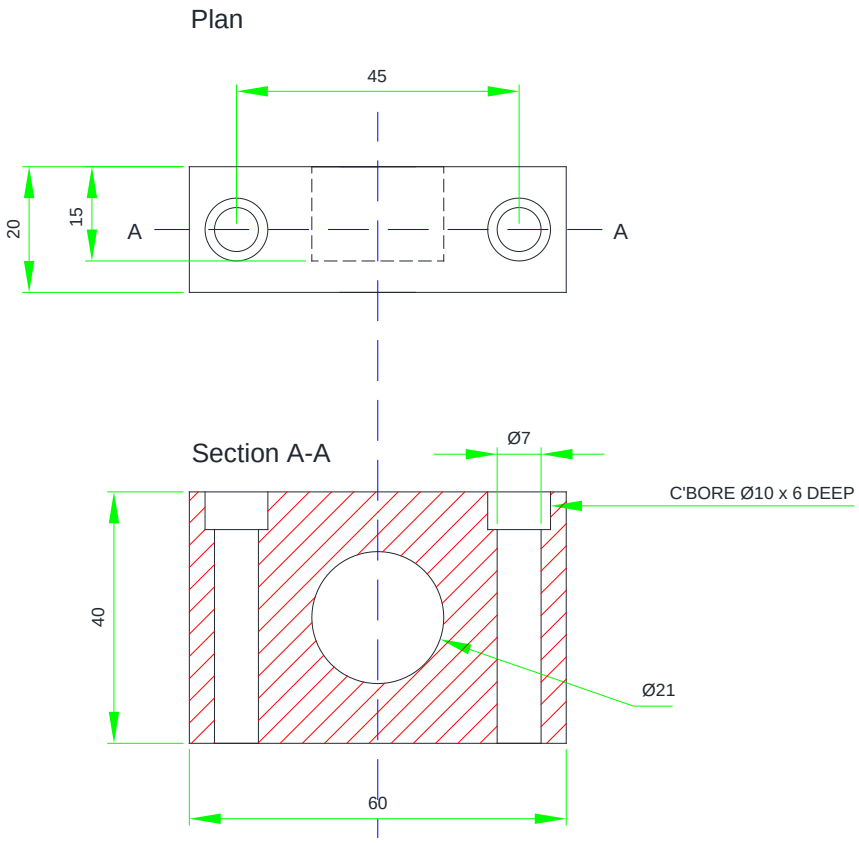

Figure B 6. Counter bore bearing block specification drawing

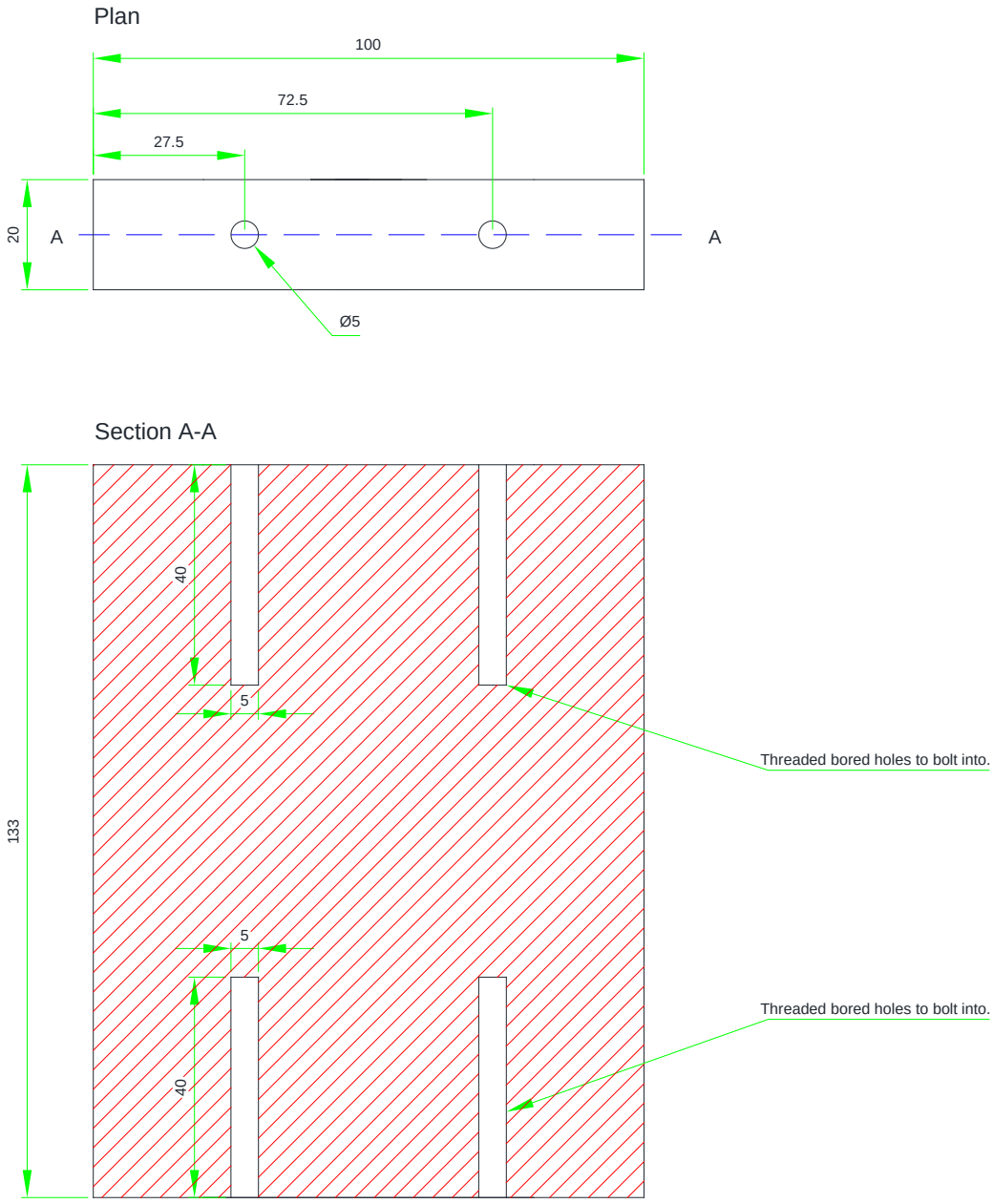

Figure B 7. Bearing block support specification drawing

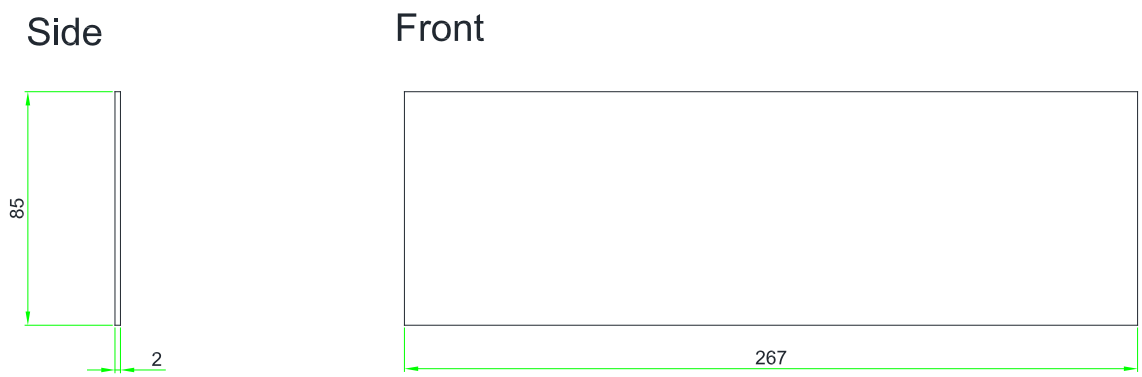

Figure B 8. Blade specification drawing

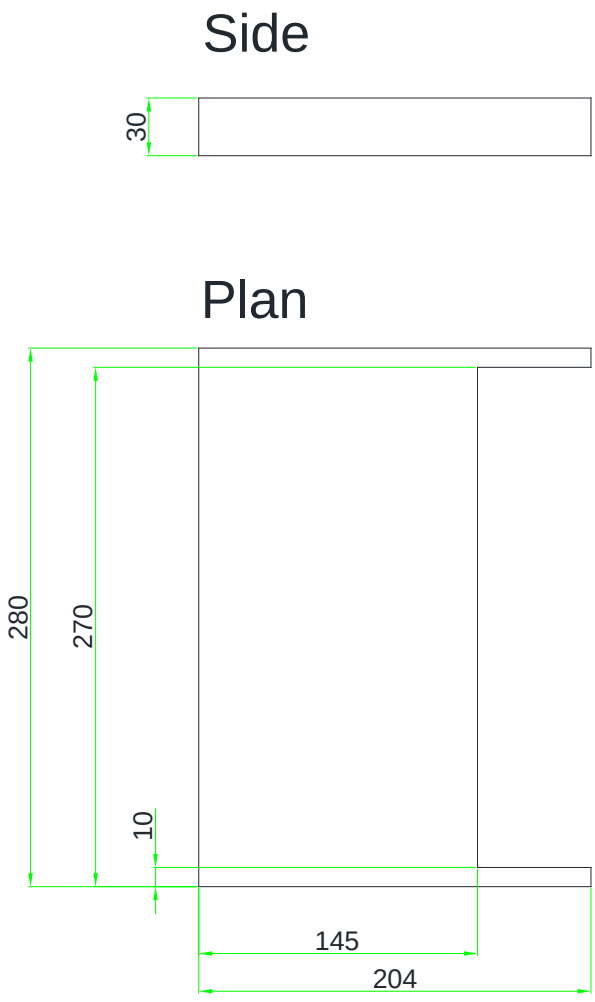

Figure B 9. Downstream insert specification drawing

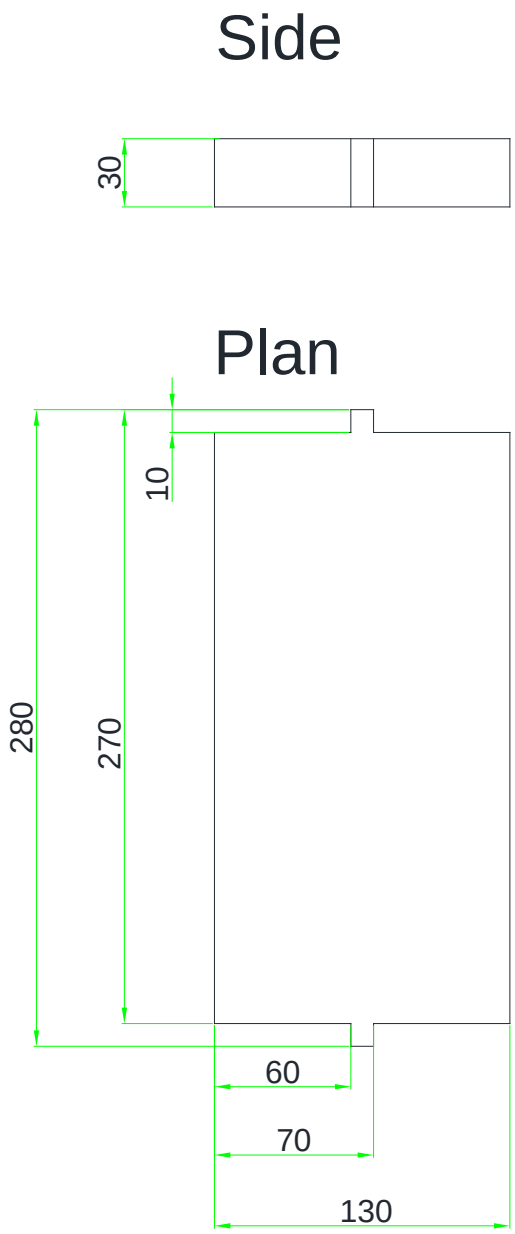

Figure B 10. Centre insert specification drawing

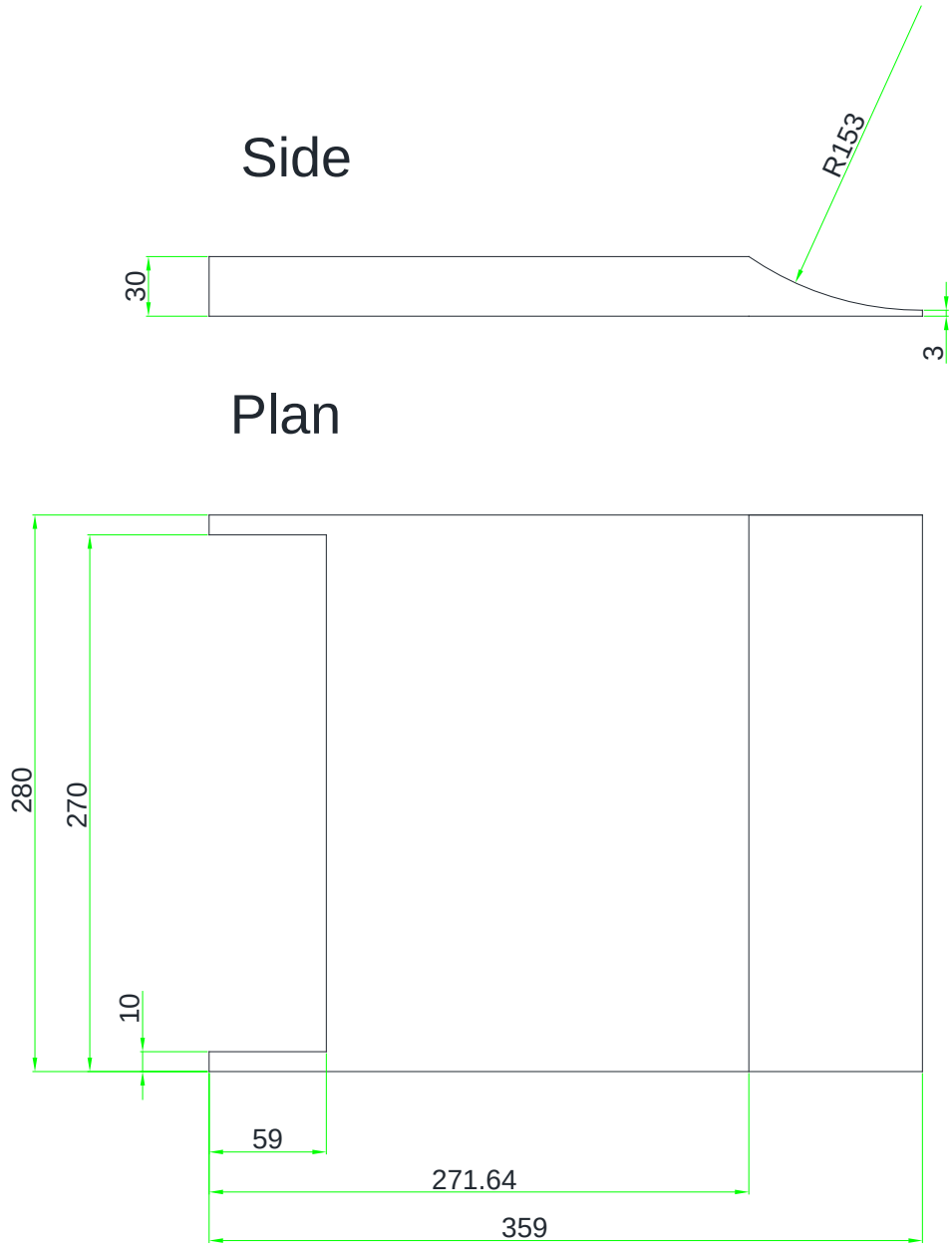

Figure B 11. Upstream insert specification drawing

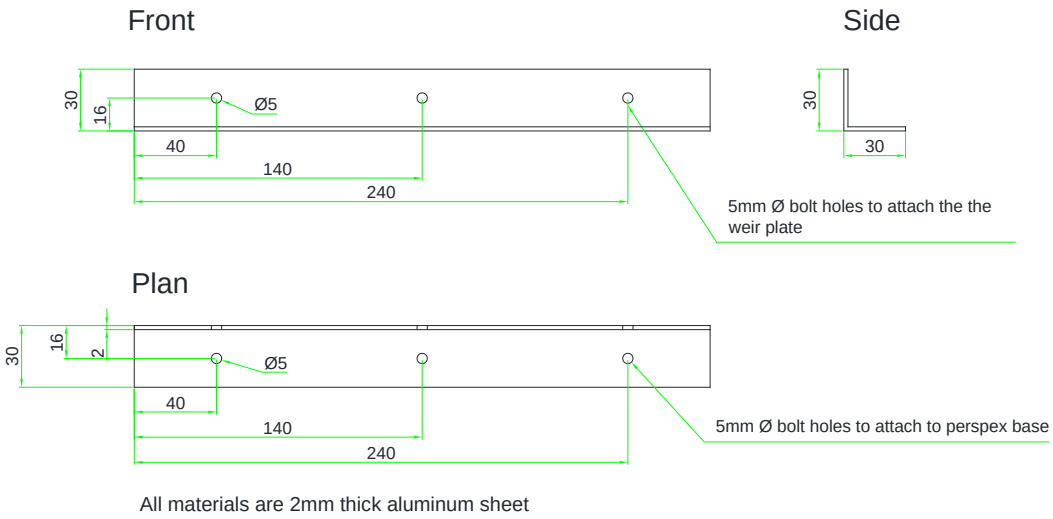

Figure B 12. Weir base plate specification drawing

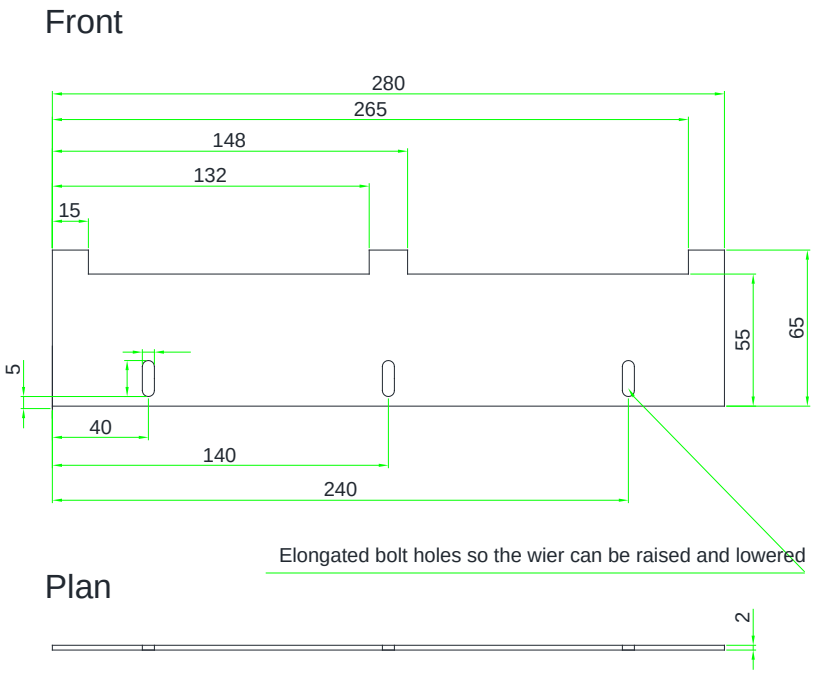

Figure B 13. Weir adjustment plate specification drawing

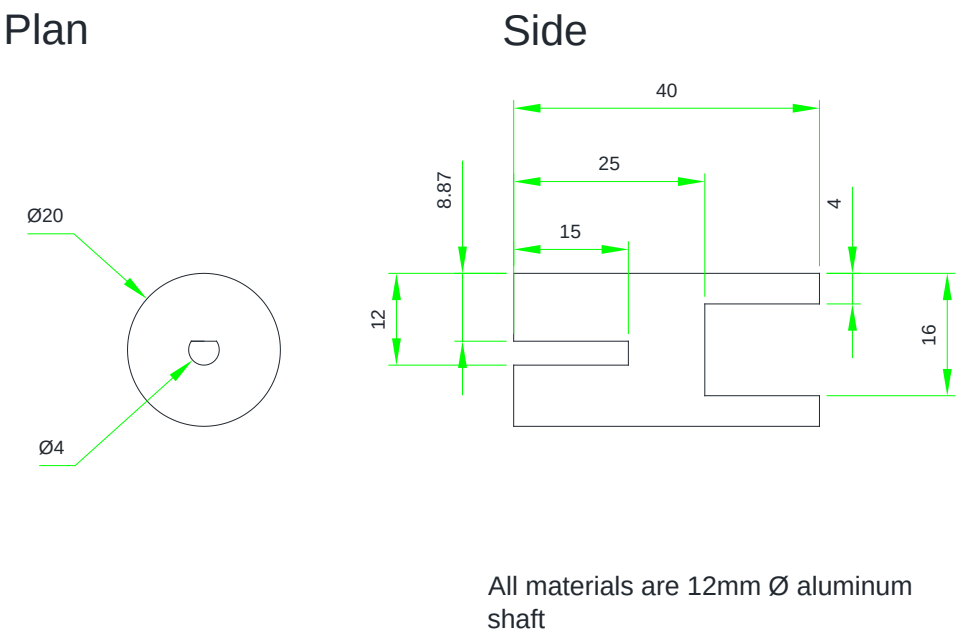

Figure B 14. Shaft sleeve specification drawing

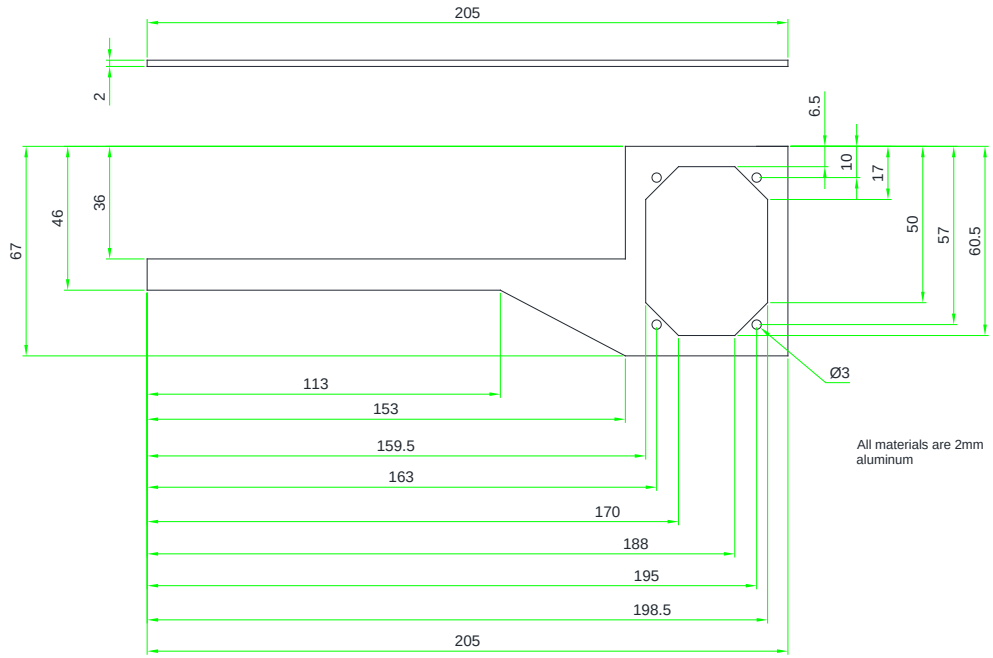

Figure B 15. Torque measurement device specification drawing